© 2012 by Lee D. Cremar. All rights reserved.

INSIGHTS FOR DESIGNING MECHANOCHROMIC SPIROPYRANS FROM FIRST PRINCIPLES DYNAMICS AND MINIMUM ENERGY PATHWAYS

BY

LEE D. CREMAR

DISSERTATION

Submitted in partial fulfillment of the requirements
for the degree of Doctor of Philosophy in Chemistry
in the Graduate College of the
University of Illinois at Urbana-Champaign, 2012

Urbana, Illinois

Doctoral Committee:

Professor Todd J. Martínez, Chair
Professor Jeffrey S. Moore
Professor Dana D. Dlott
Professor So Hirata

Abstract

The energy needed for a chemical reaction usually comes in the form of heat or light, which may alter the arrangement of reactant molecules on the ground state or place them on an excited state to surmount an energy barrier. An alternative and less well-explored way of initiating a chemical reaction is to use an applied force to distort the reactant molecules along a specific reaction coordinate. Recent experiments have demonstrated that the nature of the applied force can have a significant effect on the distribution of reaction products. This may allow the development of novel stress-responsive materials. In this work, we use first principles dynamics and constrained optimization approaches to investigate the mechanochemical activity of a spiropyran molecule. When a particular bond is broken, the spiropyran changes color. In combination with an understanding of the specific reaction products enhanced by applied forces, this can be exploited to create a mechano-chromophore, which changes color according to the distribution of stress in a polymeric material. Our simulations explore the amount of applied force required to induce bond rupture and the specific mechanism of bond rupture for different directions and magnitude of the applied force. We use the steered molecular dynamics method in combination with on the fly solution of the electronic structure problem, allowing arbitrary bond rearrangement in response to the applied force. The nature of the minimal energy pathway (MEP) on the force modified potential energy surface (FMPES) was investigated and utilized to determine reaction rate expressions within the context of transition state theory.

Weeping may endure for a night, but joy cometh in the morning.
-Psalm 30:5

Acknowledgments

My graduate experience at Urbana-Champaign has been a welcoming one to say the least. I am grateful for having the opportunity to be exposed to many people from various backgrounds and cultures, which has provided much insight. I am happy to have had the privilege to work with Todd J. Martínez, who encouraged and motivated me to pursue graduate research in his group. My initial discussions with Todd concerning mechanochemistry modeling were/are truly engaging, and I can think of no other project that excited me. I would like to express my gratitude to my professors at the University of Texas Pan-American, especially Phillip DeLassus and Christina VillaLobos who both stressed the importance of higher education in my life. In addition, I am grateful to the MERGE and pre-doctoral programs, which provided me the opportunity to visit University of Illinois to meet various graduates and professors from different research backgrounds; this sparked my interest for graduate study at Illinois. I would also like to thank Jeffrey S. Moore for allowing me to conduct undergraduate research in his lab, which exposed me to several research themes in his group including those within the AMS group at Beckman Institute.

I believe a large part of my success and survival in graduate school came from the support of my research group. I thank Ben Levine for advising me for the first few months in the Martínez group regarding my initial research. His patience and positive outlook was a source of my motivation. Chaehyuk Ko, who expressed much interest in answering numerous questions regarding directions in research. Guishan Zheng, for constantly sharing his guidance, wisdom, and all those late night food runs. Hanneli Hudock, for her keen outlook on life and work, and those morning chats with Ben that I found so much fun. I appreciate Jiahao Chen for mentoring me, providing me research advice, and for listening to my graduate school dilemmas. Sandy Yang for his jolly attitude, his consideration for my future prospects in research, and for making my transition in the Bay area much more manageable. I am grateful to Joshua Coe, Alexis Thompson, and Chutintorn Punwong for making the lab feel more like home. Taras Pogorelov for those research discussions which included tea and chocolate. I thank Aaron Virshup, Beth Lindquist, and especially Jeff Leiding for guidance, support, and his humble persona in and outside work. I would also like

to acknowledge Hongli Tao and Mitchell Ong for their support during our transition to the Bay. I appreciate Sergey Varganov for his mentoring and discussions on electronic structure. I acknowledge Ivan Ufimtsev and Nathan Luehr for their contributions towards computing and performance on GPUs, which made my last chapter possible. Additionally, I would like to express my gratitude to Christian R. Evenhuis for mechanocemistry related discussions and the following post-doctoral researchers: William Glover, Christine Isborn, Hyeon-Deuk Kim, Shungo Miyabe, Toshifumi Mori, and Alex Witt. Finally, I would like to express my gratitude to my undergraduate student Jennifer Kim for her hard work in assisting me, and her perseverance for research in mechanochemistry related topics. Thanks goes to Jade Shi for his summer research on spiropyran modeling, which assisted in the completion of my final chapter.

I acknowledge my collaborators Doug Davis and Stephanie Potisek for their hard efforts, patience, and assistance regarding spiropyran mechanochemistry. I truly enjoyed the exciting research collaboration within the Moore and AMS groups during my stay at Illinois. I believe this has greatly fueled my passion for completing my dissertation regarding the theoretical aspects of spiropyran mechanochemistry.

Table of Contents

Chapter 1

Introduction

Since the advent of quantum mechanics in the mid-1920's[1] and the application of ab initio quantum chemistry in the 1970's[2, 3]considerable progress has been made towards describing thermal and photo-chemical reactions.[4, 5] Within theoretical chemistry, the potential energy surface (PES) paradigm has been used to describe the possible molecular pathways for the canonical routes of chemical transformations. An alternate means of chemical reactivity comes through mechanical force, which is exhibited in know biological process,[6, 7] whereby mechanical forces are exerted to surmount energy barriers that are otherwise unattainable.

The investigation of mechano-chemical processes such as protein unfolding and polymer chain rupture has been facilitated by the development of atomic scale manipulation techniques such as the scanning tunneling microscope,[8] atomic force microscope (AFM),[9, 10] and single molecule force probes.[11, 12] The theoretical framework for describing molecular systems subject to a mechanical force surfaced in the context of polymers, and has been extended mostly to protein unfolding and polymer chain rupture.[13–15]

The ability to selectively break bonds, via macroscopic forces, by inserting mechanically reactive molecules called mechanophores within the polymer backbone has driven the need to design stress-sensing and self-healing polymers. However, the design of mechanophores that can efficiently and controllably respond to mechanical deformation is a complex task. With molecular modeling, mechanophore tailoring can be guided to predict the outcome of mechano-chemical reactions, which would confirm the possible reaction products formed, therefore determining material properties. These simulations would address questions regarding the nature of the potential energy surface for the mechanophore under a myriad of applied forces. The force site selectivity relationship is a theme explored herein to assist with the design of novel stress-sensing mechanophores with extension to reaction rate models incorporating mechanical force.

Mechanophore design also requires understanding the relationship between force, chain length, and site attachment onto the mechanophore. Modeling the effect of a mechanical force translating from the polymer chain to the mechanophore would provide insightful design rules. This will provide the permissible mechanophore architectures that will enable optimal

mechanical activation.

1.1 Covalent Mechanochemistry

The concept of a mechanical force deforming the PES was discussed theoretically by Eyring and Kauzmann in the 1930's[13] in the context of polymer viscosity, which suggested barrier lowering in the presence of an exergonic force. Modeling with Density Functional Theory (DFT) employed constraint optimization[16–23] schemes to determine the constrained energy of an elongated polymer chain[16, 24] which showed barrier lowering of the PES under applied force. Although this successfully demonstrated that applied force deforms the PES by decreasing the activation energy, however, this was restricted to single bond rupture models that required analytical potentials.[14, 25] The strain energy of bulk-like and polymer knot chains were investigated using ab initio molecular dynamics simulations (AIMD)[26] which provided clues to the dynamical evolution of homolytic bond cleavage.[27–33] The barrier lowering under force relationship was further studied, using AIMD, for a polymer chain undergoing cis-trans isomerization subject to tensile stress and allowed the quantification of bond rupture forces which ranged in nano-Newtons (nN).[19] Thus AIMD methods, which typically modeled AFM experiments, employed constant velocity pulling schemes to provide mechanistic information for bond rupture[34] and constrained optimization studies indicated this was due to external forces that resulted in barrier lowering.[35–38]

The advent of polymers incorporating mechanophores presented new theoretical challenges.[39] Unlike previous external force simulations which were confined to protein unfolding or polymer chain rupture, external force can be transmitted at numerous sites on the mechanophore which may result in the breaking of any particular bond. To effectively scan and design a mechanically active mechanophore required not only a suitable AIMD method, however, also a description of the potential energy landscape with direct incorporation of mechanical force, of great interest in the Martínez group.

1.2 Mechanochemistry with Mechanophores

Recent studies have explored the development of smart polymeric materials incorporating reactive functional groups or "Mechanophores", whereby macroscopic mechanical forces are harnessed to induced localized molecular reactivity at the mechanophore resulting in specific bond cleavage.[40–47] The mechanophore is coupled to the polymer backbone, in the middle of the chain, where forces are maximal allowing directed covalent bond cleavage. This is in contrast to non-specific covalent bond cleavage such as the grinding and milling of polymers.[12]

Mechanochemical activation has demonstrated the acceleration of chemical reactions and reaction pathway bias, illustrating a novel approach for exploring chemical reactivity.[39]

Hickenboth *et al.* first demonstrated non-random bond cleavage of a benzocyclobutene mechanophore-linked polymer, using ultrasound to induce a solvodynamic shear.[39] The product formed a reactive diene that underwent a Diels-Alder cycloaddition with a pyrene fluorescent-labeled dienophile trap, forming one unique product regardless of the cis or trans linkages to benzocyclobutene. According to Woodward and Hoffmann,[48] under thermal conditions, they predicted that the ring-opening of a cis or trans benzocyclobutene would proceed through either a conrotatory or a disrotatory motion to form two different stereoisomers. However, sonication of both cis and trans benzocylcobutene linked polymers formed one stereoisomer, indicating how mechanical force can alter and bias reaction pathways. Calculations using constrained optimizations indicated that cis and trans forms underwent disrotatory and conrotatory motion towards one stereoisomer complementing experimental observations.

Molecular dynamics simulations of protein unfolding by Schulten *et al.* has provided a framework for mechanical force pulling schemes[49–51] , however, to describe chemical processes that undergo covalent bond rupture requires a quantum mechanical or *ab initio* treatment of the PES. A Born-Oppenheimer molecular dynamics approach under external force, termed Ab Initio Steered Molecular Dynamics (AISMD), was adopted in the Martínez group for describing mechanochemical reactions.[52] For the first time, this allowed the reaction dynamics for the ring-opening of cyclobutene under external force to be followed. The simulations indicated two different pathways, which formed one stereoisomer. For cis-pulling the ring-opening of cyclobutene proceeded through a disrotatory motion, whereas for trans pulling ring opening occurred via a conrotatory motion, supporting experimental observations.[39]

Although earlier work mapped the PES, this was subject to a constraint rather than displaying the PES as a function of applied mechanical force. The PES under the presence of applied force was formulated simultaneously in the Martínez group termed "Force Modified Potential Energy Surface" (FMPES)[52] and the Marx group coined "External Force is Explicitly Included" (EFEI).[53–57] The FMPES of cyclobutene and benzocyclobutene studied in the Martínez group indicated that at increasing forces the activation barrier was lower for cis-pulling which displayed a disrotatory motion. For trans-pulling the energy barrier was relatively lower for the conrotatory motion at increasing forces. Similar conclusions have been reached whereby the disrotatory process for cis is allowed when mechanical force is applied.[54, 58] The FMPES concept not only demonstrates barrier lowering as a function of applied force, but also how tuning the force can bias a particular reaction route. Other mechanophores such as cyclopropanes and cyanoacrylates have been explored, which have

potential use in self-healing applications.[43, 59, 60]

The present focus herein is the rationale design of self-sensing materials, which requires a novel mechanophore displaying colored properties upon mechanical stress. A mechano-chromophore would be beneficial since it not only allows the stress distribution in a material to be visualized and mapped, it can guide the tuning of mechanical force within the polymer architecture.[61]

1.3 Spiropyrans as Mechanophores

Mechanochromic polymers are attractive stress-sensing materials, whereby an induced mechanical strain results in change of the absorption and/or fluorescence of the polymer.[62, 63] Molecules such as spiropyrans (SPs) are known to be mechanochromic which result in color change upon grinding at low temperatures and show promise as mechano-chromophores.[12]

SPs are thermo- and photochromic compounds that undergo 6-π electrocyclic ring opening to form colored species in solution when heated or irradiated with ultraviolet light.[64, 65] The spiro-heterocyclic compounds are composed of two orthogonal indole and benzopyran rings, linked by an unusually weak Spiro C-O bond, which exist in equilibrium between two thermodynamically stable states: a colorless closed form SP and a highly colored open form trans merocyanine (MC) isomer. The observed color change is due to the planarity and π-conjugation of the open MC form (Figure 1.1). The conversion of SP to MC has been verified experimentally with fluorescence and UV/Vis absorption spectroscopy. Photochemical experiments have indicated rupture of the Spiro C-O bond is followed by formation of a transient cis-cisoid MC and a stable trans MC isomer.[66–70] The existence of an unstable cis-cisoid intermediate was confirmed through metal chelation trapping of the cis-cisoid conformer, which produced a unique absorption band verified by experimental and theoretical studies.[69, 71–76] The reverse process to the closed form, SP, is induced by visible light or heat through a reaction pathway on the ground state. The facile Spiro bond and optical switching properties of SPs are therefore desirable for stress sensing mechano-chromophores in polymeric materials.[77]

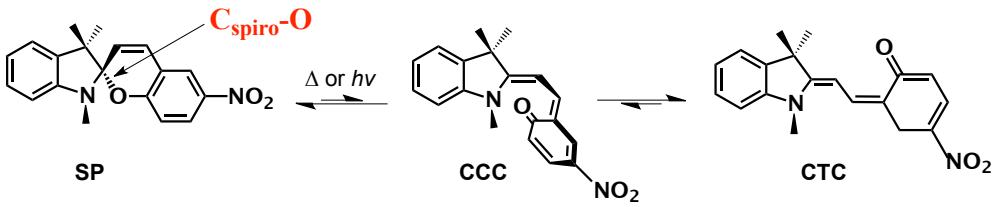

Figure 1.1: Spiropyran thermal and photochemical reaction mechanism. SP is the closed formed reactant, which undergoes cleavage at the Spiro C-O bond under heat or light. The cis-cisoid intermediate, CCC, is formed following bond breaking, however, rapidly converts to the stable MC trans isomer CTC. The trans isomer is highly colored with an absorption wavelength that peaks between 500-600 nm.

1.4 Designing Mechanochromic Spiropyrans

The Moore group at the University of Illinois first incorporated SP mechanophore linked polymers with the linkage sites lying approximately along the plane of the Spiro C-O bond. The effect of a mechanical force was induced by solvodynamic shear via ultrasound experiments, shown by Potisek *et al.*,[78] demonstrating SP mechanochromism[12] and indicating the potential stress-sensing capabilities of SP mechanophores. The observed color changed was presumed to be from mechanical forces directed to SP, however, the nature of the reaction mechanism with respect to applied force and SP attachment sites remained unclear.

Doug Davis, from the Moore group, discussed and experimented with different polymer chain linkages to the SP molecule to determine the modes of force that resulted in cleavage of the Spiro C-O bond. Unlike some mechanophores, where the polymer chain is coupled closely to the breaking bond of interest, the Spiro C-O bond is further away from the polymer attachment sites. Thus, numerous attachment sites are possible on the indole and the benzopyran rings, and the mode of attachment is expected to alter chemical reactivity due to the way force is transmitted from the rings to the Spiro C-O bond. To synthesize and test the numerous possible attachment sites on SP, including other mechanophores, would be cumbersome. Thus, a primary goal is to rationally design and effectively screen potentially mechanically active mechano-chromophores, like SP, with respect to linkage sites using computational methods presented herein.

Two modes of force transmission to the Spiro C-O bond under consideration are the stretching and torsional motion. The stretching motion of the Spiro C-O bond may be

achieved by applied force at the atom sites located on the benzene ring of the indole and benzopyran portion (Figure 1.2). For instance, external force at the atom labeled 5' or 6' and any atom from 5 through 8 would correspond to the stretched induced pulling motion. Pulling at atom sites within the indole ring connected to the Spiro C-O bond and on the benzopyran would illustrate a twist like motion. N or 3' and atoms 5 though 8 are attachment sites of interest for twist induced pulling. The stretching motion across the spiropyran molecule is coined "Stretched Induced Mechanophore" or SIM, whereas the twisting motion is referred to as "Twist Induced Mechanophore" or TIM, as discussed by Davis.[79]

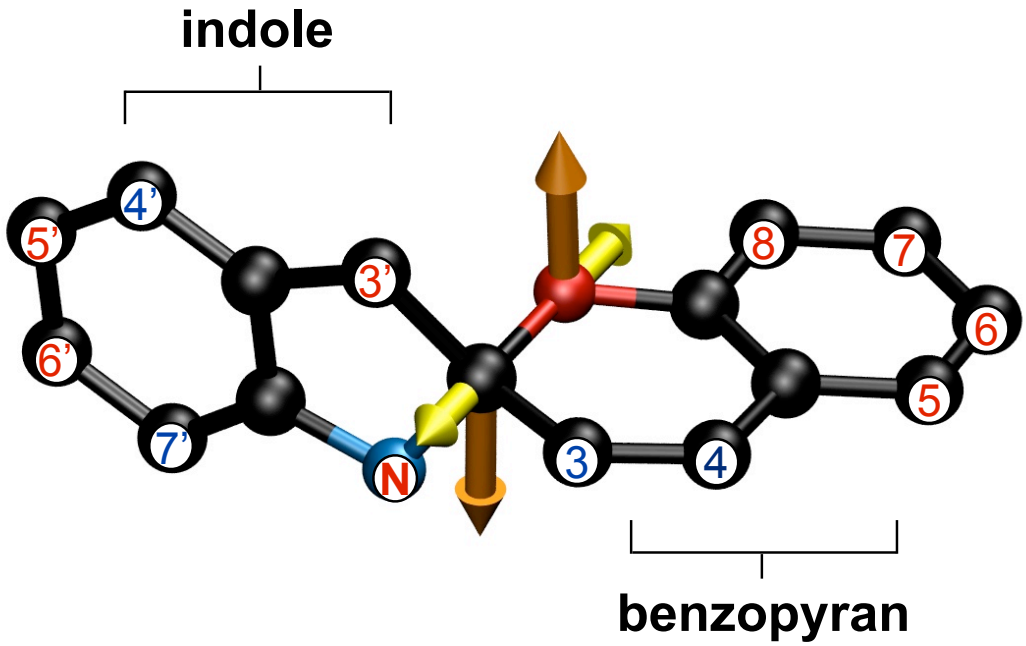

Figure 1.2: Spiropyran stretching and torsional modes. The yellow arrows display the stretching motion whereas the orange arrows illustrate a twist-pulling mode. The possible attachments sites that may lead to mechanical activation are labeled in red numbering, while the atoms indicated by blue numbering are pulling sites less likely to channel the force to the Spiro C-O bond effectively.

1.5 Concluding Remarks

Current theoretical contributions for describing mechano-chemical reactions allow the screening of potential mechano-chromophores such as SP, which may undergo ring-opening to a colored product if force is transferred efficiently. Design of a polymeric material that changes color due to the application of stress to the polymer chain resulting in covalent bond rupture at the mechanophore requires careful consideration. The relationship between attachment site and the magnitude of the force on a SP mechanophore is presented herein and will aid the design of polymeric materials incorporating novel mechano-chromophores.

1.6 References

[1] Dirac, P. A. M. *Proc. R. Soc. Lond. A* **1929**, *123*, 714.

[2] Kolos, W.; Roothaan, C. *Rev. Mod. Phys.* **1960**, *32*, 219.

[3] Kolos, W. *J. Chem. Phys.* **1968**, *49*, 404.

[4] Bender, C. F.; Schaefer, Henry F., I. *J. Am. Chem. Soc.* **1970**, *92*, 4984.

[5] Ben-Nun, M.; Martínez, T. J. *Adv. Chem. Phys.* **2002**, *121*, 439.

[6] Puchner, E. M.; Alexandrovich, A.; Kho, A. L.; Hensen, U.; Schäfer, L. V.; Brandmeier, B.; Gräter, F.; Grubmüller, H.; Gaub, H. E.; Gautel, M. *Proc. Natl. Acad. Sci. USA* **2008**, *105*, 13385.

[7] Wiita, A. P.; Perez-Jimenez, R.; Walther, K. A.; Gräter, F.; Berne, B. J.; Holmgren, A.; Sanchez-Ruiz, J. M.; Fernandez, J. M. *Nature* **2007**, *450*, 124.

[8] Eigler, D. M.; Schweizer, E. K. *Nature* **1990**, *344*, 524.

[9] Custance, O.; Perez, R.; Morita, S. *Nature Nanotech.* **2009**, *4*, 803.

[10] Wu, D.; Lenhardt, J. M.; Black, A. L.; Akhremitchev, B. B.; Craig, S. L. *J. Am. Chem. Soc.* **2010**, *132*, 15936.

[11] Yang, Q.-Z.; Huang, Z.; Kucharski, T. J.; Khvostichenko, D.; Chen, J.; Boulatov, R. *Nature Nanotech.* **2009**, *4*, 302.

[12] Beyer, M. K.; Clausen-Schaumann, H. *Chem. Rev.* **2005**, *105*, 2921.

[13] Kauzmann, W.; Eyring, H. *J. Am. Chem. Soc.* **1940**, *62*, 3113.

[14] Evans, E.; Ritchie, K. *Biophys. J.* **1997**, *72*, 1541.

[15] Crist, B.; Oddershede, J.; Sabin, J. R.; Perram, J. W.; Ratner, M. A. *J. Polymer Sci. Polymer Phys. Ed.* **1984**, *22*, 881.

[16] Beyer, M. K. *J. Chem. Phys.* **2000**, *112*, 7307.

[17] Garnier, L.; Gauthier-Manuel, B.; van der Vegte, E. W.; Snijders, J.; Hadziioannou, G. *J. Chem. Phys.* **2000**, *113*, 2497.

[18] Buldum, A.; Ciraci, S.; Fong, C. Y.; Nelson, J. S. *Phys. Rev. B* **1999**, *59*, 5120.

[19] Rohrig, U. F.; Frank, I. *J. Chem. Phys.* **2001**, *115*, 8670.

[20] Pérez, R.; Štich, I.; Payne, M.; Terakura, K. *Phys. Rev. B* **1998**, *58*, 10835.

[21] Pérez, R.; Payne, M.; Štich, I.; Terakura, K. *Phys. Rev. Lett.* **1997**, *78*, 678.

[22] Novaes, F. D.; da Silva, A. J.; da Silva, E. Z.; Fazzio, A. *Phys. Rev. Lett.* **2006**, *96*, 016104.

[23] Vélez, P.; Dassie, S. A.; Leiva, E. P. M. *Phys. Rev. Lett.* **2005**, *95*, 045503.

[24] Grandbois, M.; Beyer, M.; Rief, M.; Clausen-Schaumann, H.; Gaub, H. E. *Science* **1999**, *283*, 1727.

[25] Izrailev, S.; Stepaniants, S.; Balsera, M.; Oono, Y.; Schulten, K. *Biophys. J.* **1997**, *72*, 1568.

[26] Car, R.; Parrinello, M. *Phys. Rev. Lett.* **1985**, *55*, 2471.

[27] Saitta, A. M.; Soper, P. D.; Wasserman, E.; Klein, M. L. *Nature* **1999**, *399*, 46.

[28] Saitta, A. M.; Klein, M. L. *J. Chem. Phys.* **1999**, *111*, 9434.

[29] Saitta, A. M.; Klein, M. L. *J. Am. Chem. Soc.* **1999**, *121*, 11827.

[30] Saitta, A. M.; Klein, M. L. *J. Phys. Chem. B* **2000**, *104*, 2197.

[31] Saitta, A. M.; Klein, M. L. *J. Phys. Chem. B* **2001**, *105*, 6495.

[32] Saitta, A. M.; Klein, M. L. *J. Chem. Phys.* **2002**, *116*, 5333.

[33] Kim, E.-G.; Klein, M. L. *Macromolecules* **2004**, *37*, 1674.

[34] Aktah, D.; Frank, I. *J. Am. Chem. Soc.* **2002**, *124*, 3402.

[35] Krüger, D.; Fuchs, H.; Rousseau, R.; Marx, D.; Parrinello, M. *Phys. Rev. Lett.* **2002**, *89*, 186402.

[36] Krüger, D.; Rousseau, R.; Fuchs, H.; Marx, D. *Angew. Chem. Int. Ed.* **2003**, *42*, 2251.

[37] Konôpka, M.; Turanský, R.; Reichert, J.; Fuchs, H.; Marx, D.; Štich, I. *Phys. Rev. Lett.* **2008**, *100*, 4.

[38] Konôpka, M.; Turanský, R.; Dubecký, M.; Marx, D.; Štich, I. *J. Phys. Chem. C* **2009**, *113*, 8878.

[39] Hickenboth, C. R.; Moore, J. S.; White, S. R.; Sottos, N. R.; Baudry, J.; Wilson, S. R. *Nature* **2007**, *446*, 423.

[40] Caruso, M. M.; Davis, D. A.; Shen, Q.; Odom, S. A.; Sottos, N. R.; White, S. R.; Moore, J. S. *Chem. Rev.* **2009**, *109*, 5755.

[41] Black, A. L.; Lenhardt, J. M.; Craig, S. L. *J. Mater. Chem.* **2011**, *21*, 1655.

[42] Black, A. L.; Orlicki, J. A.; Craig, S. L. *J. Mater. Chem.* **2011**, *21*, 8460.

[43] Kryger, M. J.; Ong, M. T.; Odom, S. A.; Sottos, N. R.; White, S. R.; Martínez, T. J.; Moore, J. S. *J. Am. Chem. Soc.* **2010**, *132*, 4558.

[44] Lenhardt, J. M.; Ong, M. T.; Choe, R.; Evenhuis, C. R.; Martínez, T. J.; Craig, S. L. *Science* **2010**, *329*, 1057.

[45] Lenhardt, J. M.; Black, A. L.; Beiermann, B. A.; Steinberg, B. D.; Rahman, F.; Samborski, T.; Elsakr, J.; Moore, J. S.; Sottos, N. R.; Craig, S. L. *J. Mater. Chem.* **2011**, *21*, 8454.

[46] Brantley, J. N.; Wiggins, K. M.; Bielawski, C. W. *Science* **2011**, *333*, 1606.

[47] Piermattei, A.; Karthikeyan, S.; Sijbesma, R. P. *Nature Chem.* **2009**, *1*, 133.

[48] Woodward, R. B.; Hoffmann, R. *Angew. Chem. Int. Ed.* **1969**, *8*, 781.

[49] Isralewitz, B.; Gao, M.; Schulten, K. *Curr. Opin. Struct. Biol.* **2001**, *11*, 224.

[50] Isralewitz, B.; Baudry, J. B.; Gullingsrud, J. G.; Kosztin, D.; Schulten, K. *J. Mol. Graphics. Modell.* **2001**, *19*, 13.

[51] Sotomayor, M.; Schulten, K. *Science* **2007**, *316*, 1144.

[52] Ong, M. T.; Leiding, J.; Tao, H.; Virshup, A. M.; Martínez, T. J. *J. Am. Chem. Soc.* **2009**, *9*, 6377.

[53] Ribas-Arino, J.; Shiga, M.; Marx, D. *Angew. Chem. Int. Ed.* **2009**, *48*, 4190.

[54] Ribas-Arino, J.; Shiga, M.; Marx, D. *Chem.-Eur. J.* **2009**, *15*, 13331.

[55] Ribas-Arino, J.; Shiga, M.; Marx, D. *J. Am. Chem. Soc.* **2010**, *132*, 10609.

[56] Dopieralski, P.; Anjukandi, P.; Rückert, M.; Shiga, M.; RibasArino, J.; Marx, D. *J. Mater. Chem.* **2011**, *21*, 8309.

[57] Dopieralski, P.; Ribas-Arino, J.; Marx, D. *Angew. Chem. Int. Ed.* **2011**, *50*, 1.

[58] Friedrichs, J.; Lüssmann, M.; Frank, I. *ChemPhysChem* **2010**, *11*, 3339.

[59] Lenhardt, J. M.; Ogle, J. W.; Ong, M. T.; Choe, R.; Martínez, T. J.; Craig, S. L. *J. Am. Chem. Soc.* **2011**, *133*, 3222.

[60] Kryger, M. J.; Munaretto, A. M.; Moore, J. S. *J. Am. Chem. Soc.* **2011**, *133*, 18992.

[61] Kingsbury, C. M.; May, P. A.; Davis, D. A.; White, S. R.; Moore, J. S.; Sottos, N. R. *J. Mater. Chem.* **2011**, *21*, 8381.

[62] Bruns, N.; Pustelny, K.; Bergeron, L. M.; Whitehead, T. A.; Clark, D. S. *Angew. Chem. Int. Ed.* **2009**, *48*, 5666.

[63] Crenshaw, B. R.; Weder, C. *Macromolecules* **2006**, *39*, 9581.

[64] Minkin, V. I. *Chem. Rev.* **2004**, *104*, 2751.

[65] Flannery, J. B. *J. Am. Chem. Soc.* **1968**, *90*, 5660.

[66] Chibisov, A. K.; Görner, H. *J. Phys. Chem. A* **1997**, *101*, 4305.

[67] Chibisov, A. K.; Görner, H. *J. Photochem. Photobiol. A: Chem.* **1997**, *105*, 261.

[68] Chibisov, A. K.; Görner, H. *Chem. Phys.* **1998**, *237*, 425.

[69] Görner, H.; Chibisov, A. K. *J. Chem. Soc., Faraday Trans.* **1998**, *94*, 2557.

[70] Görner, H. *Phys. Chem. Chem. Phys.* **2001**, *3*, 416.

[71] Wojtyk, J. T. C.; Wasey, A.; Kazmaier, P. M.; Hoz, S.; Buncel, E. *J. Phys. Chem. A* **2000**, *104*, 9046.

[72] Wojtyk, J. T. C.; Kazmaier, P. M.; Buncel, E. *Chem. Mater.* **2001**, *13*, 2547.

[73] Cottone, G.; Noto, R.; Manna, G. L. *Chem. Phys. Lett.* **2004**, *388*, 218.

[74] Day, P. N.; Wang, Z.; Pachter, R. *J. Phys. Chem.* **1995**, *99*, 9730.

[75] Maurel, F.; Aubard, J.; Rajzmann, M.; Guglielmetti, R.; Samat, A. *J. Chem. Soc., Perkin Trans. 2* **2002**, 1307.

[76] Horii, T.; Abe, Y.; Nakao, R. *J. Photochem. Photobiol. A: Chem.* **2001**, *144*, 119.

[77] Seefeldt, B.; Kasper, R.; Beining, M.; Mattay, J.; Arden-jacob, J.; Kemnitzer, N.; Drexhage, K. H.; Heilemann, M.; Sauer, M. *Photochem. Photobiol. Sci.* **2010**, *9*, 213.

[78] Potisek, S. L.; Davis, D. A.; Sottos, N. R.; White, S. R.; Moore, J. S. *J. Am. Chem. Soc.* **2007**, *129*, 13808.

[79] Davis, D. A.; PhD dissertation; University of Illinois at Urbana-Champaign; 2010.

Chapter 2

Theory*

Mechanochemistry experiments incorporating mechanophore linked polymers demonstrate specific covalent bond cleavage within the weak chemical bond on the mechanophore, which lies approximately in the middle of the polymer chain.[1] The nonrandom process highlights the potential of substituting various mechanophores to tailor the polymer for desired material properties. Thus, the question then is to determine what mechanophore is suitable for a desired material response. Considering the process of mechanophore incorporation in recent experiments, it is practical to carry out quantum mechanical calculations, with respect to an applied force, to determine mechanochemical reactivity. In addition, a quantum mechanical treatment is necessary to account for electron correlation for the dissociation of covalent bonds, as opposed to using molecular mechanic descriptions.[2] A thorough description of mechanophore reactivity necessitates a dynamical and static picture, which will provide a glimpse of mechanophore reaction mechanisms and reaction energetics.

2.1 The Born-Oppenheimer Approximation

The time independent Schrödinger equation for a given molecule or system is

$$\mathbf{H}\Psi(\mathbf{r},\mathbf{R}) = E\Psi(\mathbf{r},\mathbf{R}) \tag{2.1}$$

The wavefunction ψ(r,R) describes the motion of the electrons and nuclei which depend on the electron coordinates $\mathbf{r}$ and the nuclear coordinates $\mathbf{R}$. The nonrelativistic Hamiltonian $\mathbf{H}$ is

$$\mathbf{H} = T_N + T_e + V_{eN} + V_{ee} + V_{NN} \tag{2.2}$$

where T_N, T_e, V_{eN}, V_{ee}, and V_{NN} correspond to the nuclear kinetic energy, electronic kinetic energy, electron-nuclear attractive Coulomb potential, electron-electron repulsive

*Some of the material contained within this chapter has been published in the following references: Ortiz, C.; Hadziioannou, G. *Macromolecules* 1999, 32, 780, Copyright 1999 American Chemical Society.

Coulomb potential, and the nuclear-nuclear repulsive Coulomb potential respectively. The Schrödinger equation can be parametrically separated into an electronic and nuclear term represented by the following product:

$$\mathbf{\Psi}(\mathbf{r},\mathbf{R}) = \psi(\mathbf{r};\mathbf{R})\chi(\mathbf{R}) \tag{2.3}$$

This is known as the Born-Oppenheimer approximation where ψ(r;R) is a wavefunction associated with solving the electronic component for a fixed nuclear configuration and χ corresponds to the nuclear wavefunction. Of interest herein is the solution of the electronic Schrödinger equation which depends explicitly on the electronic coordinates:

$$(T_e + V_{eN} + V_{ee})\psi = E_{el}(\mathbf{R})\psi \tag{2.4}$$

Addition of V_{NN} to E_{el} gives the electronic potential energy surface (PES), $V_{ab\ initio}$, which governs nuclear motion:

$$V_{ab\ initio}(\mathbf{R}) = V_{NN} + E_{el} \tag{2.5}$$

The description of mechanochemical reactions are treated with respect to the ground state formalism so corrections to the Born-Oppenheimer approximation in terms of the kinetic energy coupling between multiple electronic states are not accounted for.

2.2 First Principles Steered Molecular Dynamics Simulations

Mechanistic information for a molecule on the PES can be acquired through molecular dynamics simulations, whereby Newton's equation of motion are solved:

$$\mathbf{F}_i = -\frac{dV_{ab\ initio}(\mathbf{R}_i)}{d\mathbf{R}_i} = m_i\ddot{\mathbf{R}}_i \tag{2.6}$$

The differential equation involves time and is solved by propagating an initial state through a series of finite time steps, via numerically using a velocity verlet algorithm. The internal forces (left hand side of equation 2.6) for a molecule are obtained by solving the time-independent Schrödinger equation. Simulations are carried out within a micro-canonical ensemble requiring that the total energy be conserved. The energy of the molecule is distributed between the kinetic and potential energy, allowing the molecule to surmount energy barriers provided that the kinetic energy is greater than the barrier height. The amount

of energy is related to the temperature, which is provided in the simulation (hundreds to thousands in Kelvin), and will allow the system to surmount relatively small barriers within a local area near the starting point. Small time steps are used when integrating Newton's equation, so simulations may span from femto-seconds (fs) to several pico-seconds (ps) using quantum mechanical potentials. Initial conditions herein are sampled from a Boltzmann distribution, using a force free optimized starting configuration or geometry.

To simulate the effects of a mechanical force breaking a covalent bond we employed Ab Initio Steered Molecular Dynamics (AISMD),[3, 4] whereby the PES is calculated on the fly by solving the electronic Schrödinger equation at each time step. Internal forces (left hand side of equation 2.6) are calculated at each point in the dynamics, which allow complete flexibility for any of the bonds in the molecule to break. The position and momentum of the atoms are propagated according to the classical equations of motion. Several reports for the treatment of mechanical force pulling have focused on constant velocity pulling schemes,[5] however, external forces here are modeled using a constant force fixed pulling scheme. External force is applied at two atoms in the molecule reflecting the polymer chain attachments to the mechanophore (Figure 2.1).

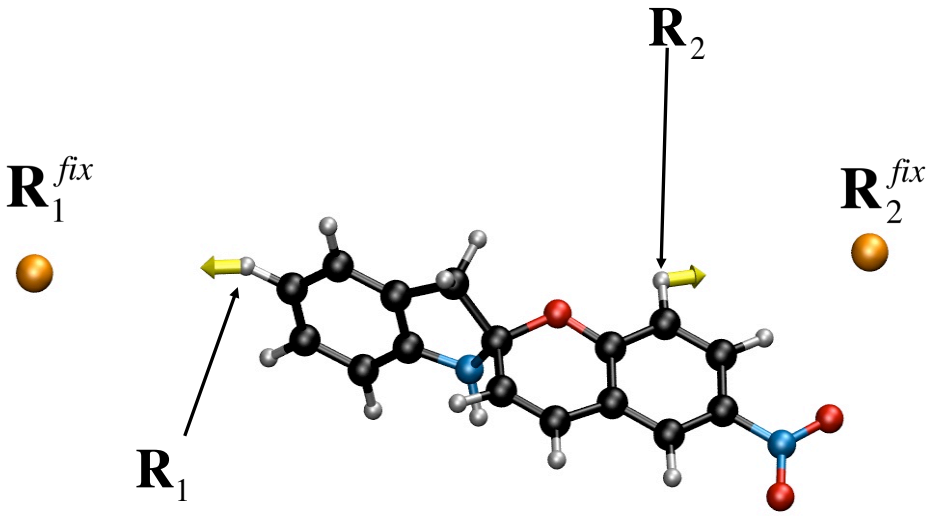

Figure 2.1: Spiropyran SIM model showing two attachments sites on the indole ring (C-H) and on the benzopyran ring (C-H). The fixed points define (orange sphere) the direction of pulling with respect to the attachement sites (yellow arrows).

Each atom or attachment point is pulled towards a fixed pulling point at constant force, defined for each atom in cartesian space, reflecting the direction of force for a stretched polymer chain. The external force, $\mathbf{F}_{ext}$, acting on each atom is defined as

$$\mathbf{F}_{ext} = \sum_{i}^{N_{attach}} F_0 \mathbf{n}_i \tag{2.7}$$

,which sums over the number of the attachment points, N_{attach}, with F_0 as the magnitude of the constant external force and the unit vector, $\mathbf{n}_i$, designating the pulling direction towards the fixed pulling point. The pulling direction is defined as follows:

$$\mathbf{n}_i = \frac{\mathbf{R}_i^{fix} - \mathbf{R}_i}{\parallel \mathbf{R}_i^{fix} - \mathbf{R}_i \parallel} \tag{2.8}$$

$\mathbf{R}_i^{fix}$ represents the position of the i^{th} fixed point and $\mathbf{R}_i$ is the i^{th} attachment site or atom respectively. The mechanical force pulling schemes, herein, involve two atoms under

applied force, in accordance with the attachment points of the mechanophore to the polymer backbone. The terminal atoms connected to these chains define one of many points to apply external force. The total force, $\mathbf{F}_{total}$ is the vector sum of the *ab initio* internal forces, $\mathbf{F}_{ab\ initio}$, and external forces, $\mathbf{F}_{ext}$:

$$\mathbf{F}_{total} = \mathbf{F}_{ab\ initio} + \mathbf{F}_{ext} \tag{2.9}$$

$\mathbf{F}_{ab\ initio}$ is the sum of the internal forces for each atom:

$$\mathbf{F}_{ab\ initio} = \sum_{i}^{N_{atoms}} \mathbf{F}_i \tag{2.10}$$

The total force is adjusted at each time step through out dynamics and accounts for the external forces applied to each attachment site respectively. To ensure the total energy is conserved the electronic potential energy is corrected to account for the presence of an applied force. The energy correction due to force is a work integral denoted as:

$$V_{ext}(\mathbf{R}) = -\int \mathbf{F}_{ext} d\mathbf{R} = -F_0 \parallel \mathbf{R}_i - \mathbf{R}_j \parallel \tag{2.11}$$

$\mathbf{R}_i$ and $\mathbf{R}_j$ are the two attachment sites respectively. The total electronic potential energy becomes:

$$V_{total}(\mathbf{R}) = V_{ab\ initio}(\mathbf{R}) - V_{ext}(\mathbf{R}) \tag{2.12}$$

2.3 Constrained optimizations for external force simulations

A constrained optimization approach is used to model the effect of an applied force by optimizing the molecular geometry subject to a distance constraint between two atoms that represent the attachment points. This is also referred to as the COnstrained Geometries simulate External Force (COGEF),[6] which is a simple method for probing mechanochemical reactivity trends. The COGEF procedure is also used in combination with the solution of the electronic Schrödinger equation for different geometries which allows complete flexibility regarding which bond is ultimately broken. The COGEF electronic potential energy, $V_{COGEF}(\mathbf{R})$, is shown as follows:

$$V_{COGEF}(\mathbf{R}, q) = V_{ab\ initio}(\mathbf{R}) - \lambda(q(\mathbf{R}) - q_o) \tag{2.13}$$

λ is referred to as the Lagrange multiplier and $q(\mathbf{R})$ is the distance constraint defined as:

$$q(\mathbf{R}) = |\mathbf{R}_i - \mathbf{R}_j| \tag{2.14}$$

$\mathbf{R}_i$ and $\mathbf{R}_j$ are the two attachment sites or atoms that are constrained while the remaining atoms are allowed to relax. $V_{COGEF}(\mathbf{R}, \mathbf{q})$ provides the energy profile for each of the distorted geometries.

2.4 Force Modified Potential Energy Surface

Guided by the idea that nuclei move on the PES, solutions to the electronic Schrödinger equation, the description of a starting geometry subject to a mechanical force on the PES can be accounted for directly. Kauzmann and Eyring introduced the concept of a tilted PES in the presence of a constant linear force.[7] A constant force adaptive pulling formalism was adopted to account for an external mechanical force, $\mathbf{F}_{ext}$, which acts on each atom defined by

$$\mathbf{F}_{ext,i} = F_0\mathbf{n}_i \; ; \quad \mathbf{F}_{ext,j} = F_0\mathbf{n}_j \tag{2.15}$$

F_0 is the magnitude of the constant external force where $\mathbf{n}_i$ and $\mathbf{n}_j$, designate the pulling directions for two attachment sites i and j which are opposite in direction along a line.

$$\mathbf{n}_i = \frac{\mathbf{R}_i - \mathbf{R}_j}{\parallel \mathbf{R}_i - \mathbf{R}_j \parallel}; \quad \mathbf{n}_j = \frac{\mathbf{R}_j - \mathbf{R}_i}{\parallel \mathbf{R}_j - \mathbf{R}_i \parallel} \tag{2.16}$$

$\mathbf{R}_i$ and $\mathbf{R}_j$ are the two attachment sites respectively. The electronic potential energy is corrected for external force as follows:

$$V_{FMPES}(\mathbf{R}) = V_{ab\ initio}(\mathbf{R}) - F_0 \parallel \mathbf{R}_i - \mathbf{R}_j \parallel \tag{2.17}$$

To demonstrate that force 'tilts' the PES, the previous expression is applied to the dissociation of an H_2 molecule at constant force (Figure 2.2). The resulting energy barrier is lowered under applied forces, which was similarly shown in earlier work by Kauzmann and Eyring. For a geometry at a stationary point, when the gradient for the corrected potential energy under force becomes zero, $\bigtriangledown_R V_{FMPES}$=0 , the ab initio forces are equal to the applied external forces. The distorted geometry now becomes a function of external force for the corresponding stationary point. So the reactant and transition states geometries can now be obtained in the context of a FMPES allowing the direct determination of activation barriers. A similar formalism by Marx and coworkers was reported.[2]

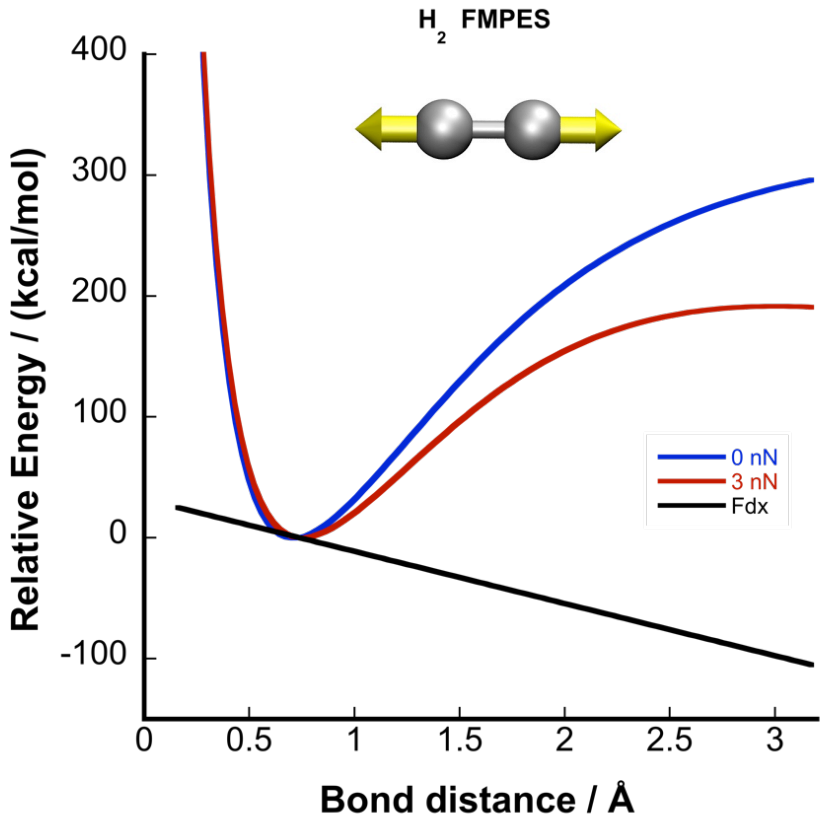

Figure 2.2: Tilting of the PES. The dissociation energy of an H_2 molecule calculated using a STO-3G basis at the Hartree Fock (HF) level.[8] The linear curve is the constant force correction, Fdx, which is the work added to the PES resulting in a lowering of the dissociation energy.

2.4.1 Nudged Elastic Band under External Force

The Nudged Elastic Band (NEB) algorithm is used to optimize a reaction path and locate a transition state between the reactant and product on the PES.[9, 10] This requires knowledge of the endpoints, which are typically the stationary points or reactant and product geometries. A string of M images $(\mathbf{R}^1,..,\mathbf{R}^I,\mathbf{R}^M)$, or geometries in cartesian coordinate space, between the endpoints are acquired through a linear or internal coordinate interpolation. The total force, $\mathbf{F}(\mathbf{R^I})$, acting on each I^{th} image is the sum of the spring force, $\mathbf{F}(\mathbf{R})^{\mathbf{I}}{}_{S_{||}}$, on the tangent path and the true force, $\mathbf{F}(\mathbf{R^I})_{T_\perp}$, perpendicular to the tangent path:

$$\mathbf{F}(\mathbf{R^I}) = \mathbf{F}(\mathbf{R^I})_{S_{||}} + \mathbf{F}(\mathbf{R^I})^{FMPES}_{T_\perp} \tag{2.18}$$

The projection of the true force ensures that the spring forces do not interfere with convergence of the total force. The spring force ensures equal spacing along the path and prevents any image from sliding down towards the endpoints:

$$\mathbf{F}(\mathbf{R^I})_{S_{||}} = k(|\mathbf{R}^{I+1} - \mathbf{R}^I| - |\mathbf{R}^I - \mathbf{R}^{I-1}|)\hat{\boldsymbol{\tau}}_I \tag{2.19}$$

The perpendicular component of the force is the true force defined by the following projection:

$$\mathbf{F}(\mathbf{R^I})^{FMPES}_{T_\perp} = (1 - \hat{\boldsymbol{\tau}}_I \hat{\boldsymbol{\tau}}_I^T)\mathbf{F}(\mathbf{R^I})^{FMPES} \tag{2.20}$$

For each nuclear configuration along the path, ($\mathbf{R}_1$,..,$\mathbf{R}_I$,$\mathbf{R}_N$), the energy correction with applied force at each point becomes:

$$V(\mathbf{R_1}, .., \mathbf{R_N})^{FMPES} = V(\mathbf{R_1}, .., \mathbf{R_N})_{ab\ initio} - F_0 \parallel \mathbf{R}_i - \mathbf{R}_j \parallel \tag{2.21}$$

$V(\mathbf{R_1}, .., \mathbf{R_N})^{FMPES}$ is the objective function that is minimized and $\mathbf{R}_i$, $\mathbf{R}_j$ are the two attachment sites respectively for each configuration.

2.4.2 Transition State Search and Intrinsic Reaction Pathways under External Force

After optimization of the reaction path and location of the approximate transition state (TS) using NEB, it is appropriate to determine if the endpoints are connected to the correct TS. The first step employs a TS algorithm for finding a first-order saddle point on the PES, where calculation of the second derivative or Hessian matrix has only one negative eigenvalue. The first-order TS is located using a partitioned rational function optimization (P-RFO) method, which takes a step upward along the mode corresponding to the negative eigenvalue of the Hessian matrix and a step downward along other higher modes. The P-RFO method is described in the DL-FIND library and elsewhere.[11–15] When searching for first-order saddle points under external force, the FMPES can be expressed equivalently like equation 2.17. Thus, at each optimization step the external forces are simply added to the internal forces to locate the stationary point. The step, $\mathbf{h}$, taken towards the first order TS can be expressed as:

$$\mathbf{h_k} = \frac{\boldsymbol{\nu}_k^+ \mathbf{F}_{total} \boldsymbol{\nu}_k}{b_k - \lambda_p} \quad ; \quad \mathbf{h_i} = \frac{\boldsymbol{\nu}_i^+ \mathbf{F}_{total} \boldsymbol{\nu}_i}{b_i - \lambda_n} \quad i = (1, ..., 3N) \;\; and \;\; i \;\; \neq \;\; k \tag{2.22}$$

$$\mathbf{h} = \sum_{j}^{3N} \mathbf{h}_j$$

Here, $\boldsymbol{\nu}$ and $\mathbf{F}_{total}$ are the eigenvectors and the total force vector, which is expressed in equation 2.9. In addition, b_k and b_i are eigenvalues and λ_p and λ_n are shift parameters that are solutions to a quadratic equation. These are the modes where the energy is maximized and minimized.

The second step requires a rigorous proof for determination of the Minimal Energy Path (MEP) from the TS to the minima in mass-weighted coordinates also known as the Intrinsic Reaction Coordinate (IRC).[16] The IRC reflects the reaction dynamics since the nuclei will tend to stay close to the IRC, the lowest energy path connecting the reactant and product. The nuclear configuration composed of N nuclei is represented by a point in 3N configuration space with 3N Cartesian coordinates X_i, Y_i, and Z_i (i=1,2,...N). At a stationary point, the electronic potential energy is:

$$\bigtriangledown_{\mathbf{X_i}} V_{ab\ initio} = \bigtriangledown_{\mathbf{Y_i}} V_{ab\ initio} = \bigtriangledown_{\mathbf{Z_i}} V_{ab\ initio} = 0 \quad (i = 1, 2, ...N) \tag{2.23}$$

IRC is based on the classical equations of motions:

$$\frac{d}{dt}(m_i \dot{\mathbf{X}}_\mathbf{i}) = -\bigtriangledown_{\mathbf{X_i}} V... \tag{2.24}$$

Assuming the nuclei move at infinitesimal velocity at a small time interval, we have the following expression after integration:

$$m_i \dot{\mathbf{X}}_\mathbf{i} = -\bigtriangledown_{\mathbf{X_i}} V_{ab\ initio} t + C, ... \tag{2.25}$$

C is the constant of integration, which is zero if the nuclei move infinitesimally. From the previous equation we obtain the following simplified expression:

$$\frac{m_i d\mathbf{X}_i}{\bigtriangledown_{\mathbf{X_i}} V_{ab\ initio}} = \frac{d\tilde{\mathbf{X}}}{\bigtriangledown_{\tilde{\mathbf{X}}_\mathbf{i}} V_{ab\ initio}} = \frac{d\mathbf{s}}{\bigtriangledown_{\mathbf{s_i}} V_{ab\ initio}} \tag{2.26}$$

$\tilde{\mathbf{X}}_\mathbf{i}(\mathbf{s})$=$\sqrt{m_i}$ $\mathbf{X_i}(\mathbf{s})$ is the mass-weighted cartesian coordinates applied to the L.H.S and, d$\mathbf{s}$, is the infinitesimal distance of the mass-weighted cartesian configuration space shown on the R.H.S. Fukui's IRC concept, under the presence of an external force, may be defined by the following differential equation:

$$\frac{d\tilde{\mathbf{X}}_i(s)}{ds} = -\frac{\nabla_{\tilde{\mathbf{X}}_\mathbf{i}} V(\tilde{\mathbf{X}}_i(s))^{FMPES}}{|\nabla_{\tilde{\mathbf{X}}_\mathbf{i}} V(\tilde{\mathbf{X}}_i(s))^{FMPES}|} \tag{2.27}$$

where s is the path length or steps taken from the transition state downward via a steepest descent path. The expression is identical to that of Marx and coworkers.[17] The IRC algorithm utilized is described in GAMESS,[18–23] and was modified such that each step accounts for corrections to the force vector (equation 2.9).

2.5 Transition State Theory

Considering the following chemical reaction A + B $\rightarrow$ C +D the rate of reaction may be defined as

$$-\frac{d[X]}{dt} = k[A]^n[B]^m \tag{2.28}$$

where X = A or B and k is the rate constant. At the molecular level k is a function of the quantum states (the electronic, translational, rotational, and vibrational quantum numbers) of A, B, C, and D. The average of the microscopic k's provides the macroscopic rate constant which is weighted by a Boltzmann distribution of velocities for a given quantum state. At equilibrium, the probability of finding a molecule at a certain state depends on its energy and so the macroscopic k becomes a function of temperature.[24–27]

Within Transition State Theory (TST) it is assumed that a chemical reaction proceeds through a reaction coordinate, which leads from an energy minima, the reactant, to another minima or the product along a MEP where the TS is the intermediate energy maxima.[28] Of interest in chemical reactions is the first-order saddle point on the PES, which is a local maxima on the reaction coordinate and a minima along other coordinates. Assuming an equilibrium energy distribution at the TS and the reactant, the rate may be expressed as

$$k(\mathbf{T}) = \frac{k_b T}{h} \frac{Q(T)_{TS}}{Q(T)_{React}} \exp\left(\frac{-E_a}{k_b T}\right) \tag{2.29}$$

where $Q(T)_{TS}$, $Q(T)_{React}$ are the partition functions for the TS, T is the temperature, h is Planck's constant, and k_b is Boltzmann's constant. E_a is the energy difference or activation barrier, including the zero point energy correction, between the TS and the reactant.[29–31] If the rate of reaction does not depend on how the molecule is activated, but rather from the vibrational modes of the molecule, the expression becomes a microcanonical rate constant or a Rice-Ramsperger-Kassel-Marcus (RRKM) rate expression.[32–35]

With respect to reaction rates under mechanical force, E_a, would be the barrier height

corresponding to a chemical transition on the FMPES. In addition since the partition function is dependent on the vibrational partition function, which accounts for all the molecular vibrational energies, corrections to the vibrational frequencies under applied force must be accounted for. Therefore, the force corrected Hessian matrix is represented as the partial derivative of $V(\mathbf{R_1}, .., \mathbf{R_N})^{FMPES}$. The Hessian matrix can be constructed using a forward finite differencing method, which requires that 3N displacements of the geometry be taken with a specified step.[11]

2.6 Entropic Statistical Chain Models

Statistical chain models have determined the types of forces that are likely exerted upon a single polymer chain. The qualitative estimates are used as a rationale for choosing minimal forces for simulations herein. A statistical chain approach was formulated to determine the magnitude of forces exerted on a single poly(methyl acrylate) (PMA) chain. Figure 2.3 illustrates the freely jointed chain (FJC) model and force extension curves, for a polymer, determined by atomic force microscopy (AFM). The theoretical curves are in good agreement with the AFM data points.[36]

On this basis, an FJC model was applied to a SP PMA chain, which corresponds to the chains used in recent experiments.[37, 38] The following equation is used to calculate the entropic force at full polymer elongation:[39]

$$F_s = \left(\frac{3kT}{na^2}r\right)\left\{1 + \frac{3}{5}\left(\frac{r}{na}\right)^2 + ...\right\} \tag{2.30}$$

F_s is the entropic force to elongate a polymer chain, k_b is Boltzmanns constant, T is the temperature at 298 K, r is the end to end chain length in Å, and n is the number of repeating monomer units in PMA which spans a length a in Å. The parameters (r, n, and a) were obtained from the SP PMA bulk experiment. A poly dispersity index (PDI) of 1.3 was measured for the SP PMA polymer chain, corresponding to an average molecular weight of 80 kilo-Daltons (kDa). The length for each chain is about the same and is roughly (fully extended):

$$r = na = \left(\frac{80 \times 10^3 \text{ g/mol}}{86.09 \text{ g/mol}}\right)\left(2.8 \text{ Å}\right) \sim 2600 \text{ Å} \tag{2.31}$$

The denominator in the first term is the molecular weight for PMA and 2.8 Å is an approximate estimate of the monomer length at full elongation. The calculated entropic force is 550 pN. Considering the latter value, it seems reasonable that the minimal forces

felt by a chain are several hundred pNs. Similar values have recently been reported.[40]

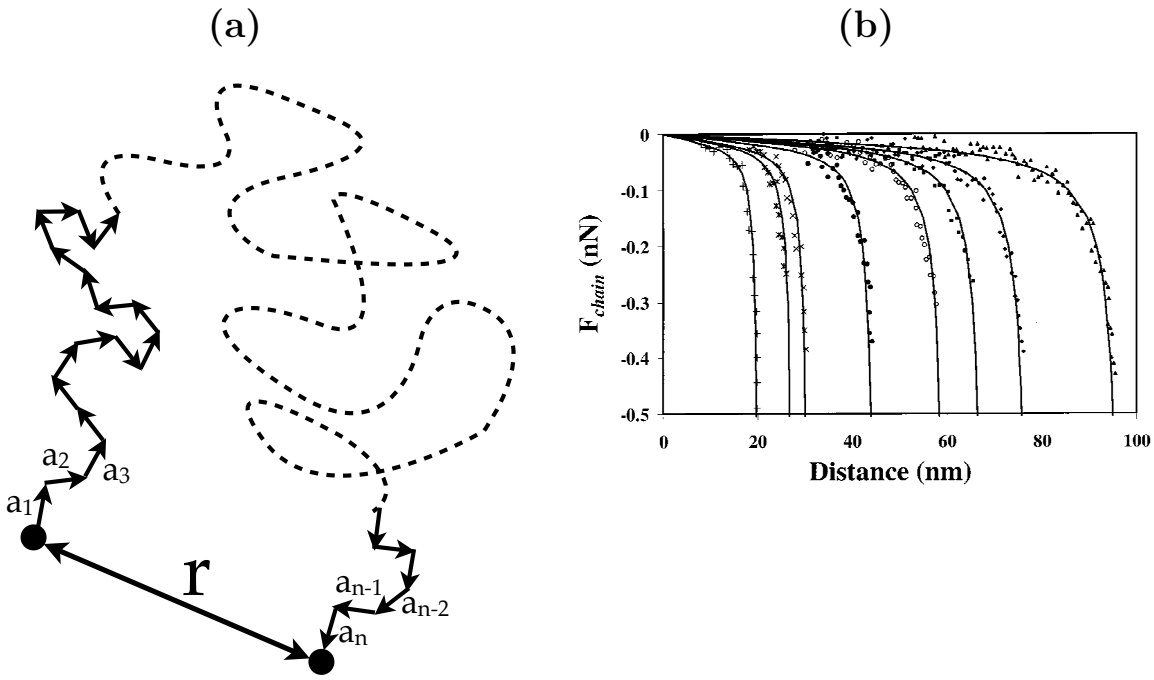

Figure 2.3: **a**, Freely jointed chain model (FJC) **b**, AFM, force vs distance, data points for several PMA chains of different lengths. The solid lines are the FJC curves, corresponding to different chain lengths, determined by an entropic chain formulation. The curves calculated from the FJC model predict the correct force extension profiles from AFM. Reprinted (adapted) with permission from Reference 35. Copyright 1999 American Chemical Society.

2.7 References

[1] Potisek, S. L.; Davis, D. A.; Sottos, N. R.; White, S. R.; Moore, J. S. *J. Am. Chem. Soc.* **2007**, *129*, 13808.

[2] Ribas-Arino, J.; Shiga, M.; Marx, D. *Angew. Chem. Int. Ed.* **2009**, *48*, 4190.

[3] Ong, M. T.; Leiding, J.; Tao, H.; Virshup, A. M.; Martínez, T. J. *J. Am. Chem. Soc.* **2009**, *9*, 6377.

[4] Sotomayor, M.; Schulten, K. *Science* **2007**, *316*, 1144.

[5] Friedrichs, J.; Lüssmann, M.; Frank, I. *ChemPhysChem* **2010**, *11*, 3339.

[6] Beyer, M. K. *J. Chem. Phys.* **2000**, *112*, 7307.

[7] Kauzmann, W.; Eyring, H. *J. Am. Chem. Soc.* **1940**, *62*, 3113.

[8] Szabo, A.; Ostlund, N. S. *Modern Quantum Chemistry: Introduction to Advanced Electronic Structure Theory, New Ed.*; Dover, 1996.

[9] Henkelman, G.; Jónsson, H. *J. Chem. Phys.* **2000**, *113*, 9978.

[10] Henkelman, G.; Uberuaga, B. P.; Jónsson, H. *J. Chem. Phys.* **2000**, *113*, 9901.

[11] Kästner, J.; Carr, J. M.; Keal, T. W.; Thiel, W.; Wander, A.; Sherwood, P. *J. Phys. Chem. A* **2009**, *113*, 11856.

[12] Baker, J. *J. Comput. Chem.* **1986**, *7*, 385.

[13] Banerjee, A.; Adams, N.; Simons, J.; Shepard, R. *J. Phys. Chem.* **1985**, *89*, 52.

[14] Cerjan, C. J.; Miller, W. H. *J. Chem. Phys.* **1981**, *75*, 2800.

[15] Simons, J.; Jø rrgensen, P.; Taylor, H.; Ozment, J. *J. Phys. Chem.* **1983**, *87*, 2745.

[16] Fukui, K. *Acc. Chem. Res.* **1981**, *14*, 363.

[17] Ribas-Arino, J.; Shiga, M.; Marx, D. *J. Am. Chem. Soc.* **2010**, *132*, 10609.

[18] Schmidt, M. W.; Baldridge, K. K.; Boatz, J. A.; Elbert, S. T.; Gordon, M. S.; Jensen, J. H.; Koseki, S.; Matsunaga, N.; Nguyen, K. A.; Shyjun, S. U.; Dupuis, M.; Montgomery, J. A. *J. Comput. Chem.* **1993**, *14*, 1347.

[19] Ishida, K.; Morokuma, K.; Komornicki, A. *J. Chem. Phys.* **1977**, *66*, 2153.

[20] Schmidt, M. W.; Gordon, M. S.; Dupuis, M. *J. Am. Chem. Soc.* **1985**, *107*, 2585.

[21] Gonzalez, C.; Schlegel, H. B. *J. Chem. Phys.* **1989**, *90*, 2154.

[22] Gonzalez, C.; Schlegel, H. B. *J. Phys. Chem.* **1990**, *94*, 5523.

[23] Gonzalez, C.; Schlegel, H. B. *J. Chem. Phys.* **1991**, *95*, 5853.

[24] Eyring, H. *J. Chem. Phys.* **1935**, *3*, 107.

[25] Eyring, H. *Trans. Faraday Soc.* **1938**, *34*, 41.

[26] Eyring, H. *Trans. Faraday Soc.* **1938**, *34*, 3.

[27] Wigner, E. *Trans. Faraday Soc.* **1938**, *34*, 29.

[28] Evans, M. G.; Polanyi, M. *Trans. Faraday Soc.* **1938**, *34*, 11.

[29] Miller, W. H. *J. Chem. Phys.* **1974**, *61*, 1823.

[30] Miller, W. H.; Schwartz, S. D.; Tromp, J. W. *J. Chem. Phys.* **1983**, *79*, 4889.

[31] Yamamoto, T. *J. Chem. Phys.* **1960**, *33*, 281.

[32] Baer, T.; Mayer, P. M. *J. Am. Soc. Mass. Spectrom.* **1997**, *8*, 103.

[33] Marcus, R. A.; Rice, K. *J. Phys. Colloid Chem.* **1951**, *55*, 894.

[34] Kassel, L. S. *J. Phys. Chem.* **1928**, *32*, 225.

[35] Rice, O. K.; Ramsperger, H. C. *J. Am. Chem. Soc.* **1927**, *49*, 1617.

[36] Ortiz, C.; Hadziioannou, G. *Macromolecules* **1999**, *32*, 780.

[37] Hickenboth, C. R.; Moore, J. S.; White, S. R.; Sottos, N. R.; Baudry, J.; Wilson, S. R. *Nature* **2007**, *446*, 423.

[38] Davis, D. A.; Hamilton, A.; Yang, J.; Cremar, L. D.; Gough, D. V.; Potisek, S. L.; White, S. R.; Moore, J. S.; Sottos, N. R.; Ong, M. T.; Braun, P. V.; Martínez, T. J. *Nature* **2009**, *459*.

[39] Mark, J. E.; Erman, B. *Rubberlike Elasticity: A molecular Primer, 2nd ed.*; UK, 2007.

[40] Black, A. L.; Orlicki, J. A.; Craig, S. L. *J. Mater. Chem.* **2011**, *21*, 8460.

Chapter 3

First Principles Dynamics and Constrained Optimization Models for Mechanical Activation[†]

3.1 Introduction

Spiropyran (SP) mechanophore linked functionalized polymers (LFPs) were first reported by Moore and co workers.[1, 2] Hydrodynamic forces applied to a polymeric solution containing SP LFPs resulted in a color change attributed to cleavage of a specific bond on the SP mechanophore. The nature of the color change was presumed to be brought about by the formation of merocyanine (MC), a planar trans isomer (Figure 3.1) with extensive π conjugation which is visibly active displaying a peaked absorption band between 500-600 nm (Figure 3.2).[3]

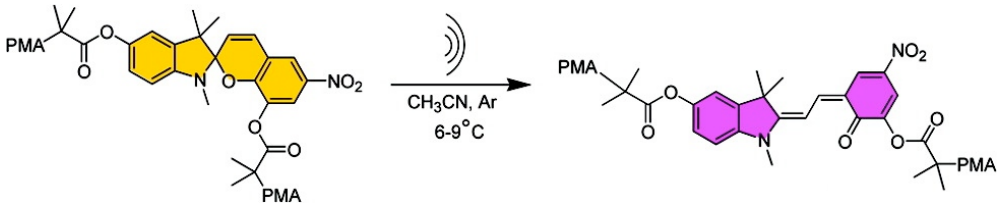

Figure 3.1: Spiropyran SIM linked polymer illustrating mechanical ring opening to the colored MC product. Reprinted (adapted) with permission from Reference 2. Copyright 2007 American Chemical Society.

The hypothesis presented was that mechanical forces, applied at the terminal ends of the polymer chain, assisted in the non-random cleavage of the Spiro C-O bond, which facilitated isomerization of SP to the colored MC isomer (Figure 3.2). Signifying the potential of SP

[†]Some of the material contained within this chapter has previously been published in the following references: Potisek, S. L.; Davis, D. A.; Sottos, N. R.; White, S. R.; Moore, J. S. *J. Am. Chem. Soc.* 2007, 129, 13808, Copyright 2007 American Chemical Society; Davis, D. A.; Hamilton, A.; Yang, J.; Cremar, L. D.; Van Gough, D.; Potisek, S. L.; Ong, M. T.; Braun, P. V.; Martínez, T. J.; White, S. R.; Moore, J. S.; Sottos, N. R. *Nature* 2009, 459, 68.

LFPs as stress-sensing indicators, this motif was extended to bulk polymeric materials.[1] The bulk tensile testing of SP LFPs proved specific site cleavage on SP evident by the localized color change (Figure 3.3). In addition, the transduction of mechanical forces from the polymer chain to various sites on SP were investigated, indicating the sensitivity of polymer -SP attachment sites which may result in the lack of color formation in the bulk material. With the aid of previously defined theoretical methods outlined in chapter 2, the aim is to clarify whether mechanical force, at specific SP sites corresponding to initial studies, enhances bond cleavage.

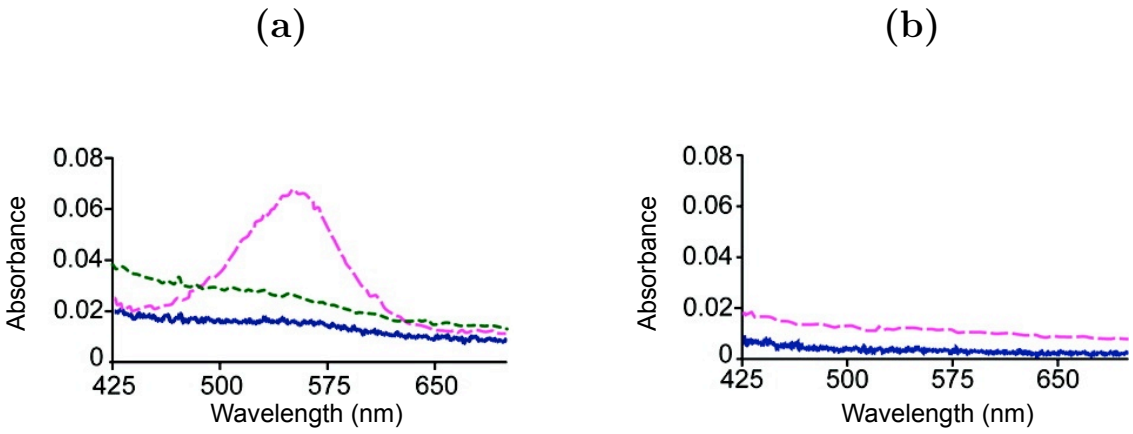

Figure 3.2: **a**, The UV spectrum of PMA-SP-PMA corresponding to the SIM attachment sites. The blue trace is before sonication, the dashed pink trace is after 18 min of pulsed sonication, and the dotted green trace is after 40 min of exposure to ambient light **b**, UV spectrum of end-functionalized PMA-SP control, the blue trace is before sonication and the dashed pink trace is after 18 min of pulsed sonication. Reprinted (adapted) with permission from Reference 2. Copyright 2007 American Chemical Society.

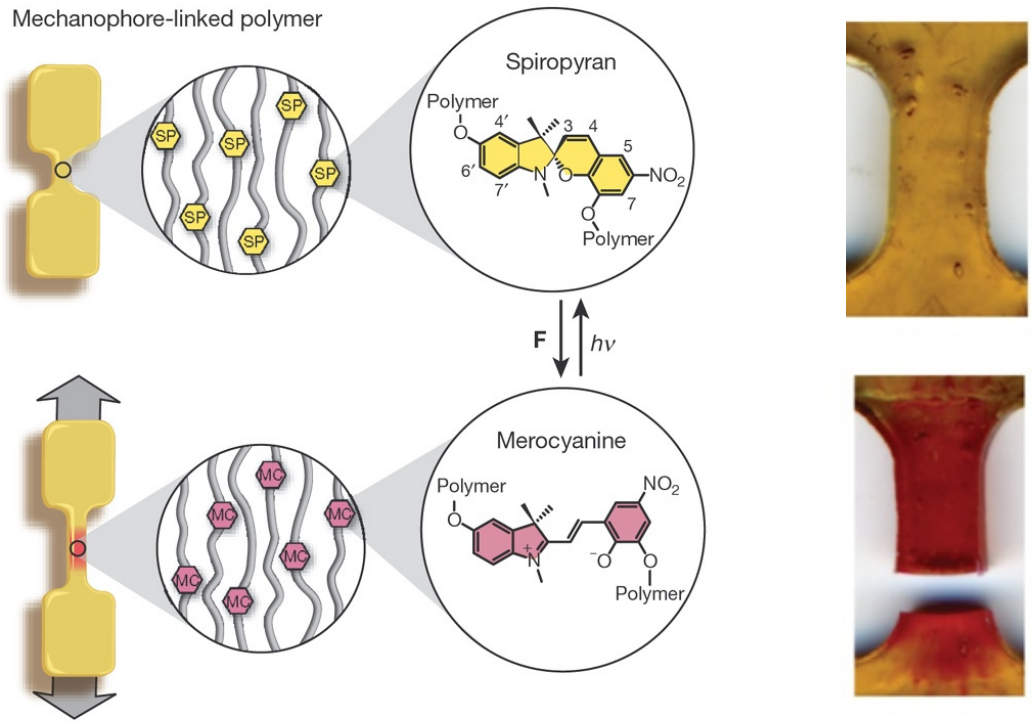

Figure 3.3: Polymeric material incorporating SP linked polymers. A tensile stress, with the applied direction shown, on the dog bone polymer illustrates the induced color change, indicative of a mechano-chemical reaction in which SP undergoes mechanical ring opening to the MC isomer.

The effect of external force was modeled on the SP mechanophore with both Ab Initio Steered Molecular Dynamics (AISMD) simulations[4–6, 6–9] and constrained optimization (CO-GEF) methods[10] and using truncated (t) (Figure 3.4) as well as extended (e) models of the SP mechanophore (Figure 3.8). Two different modes of applied force were investigated for the (t) and (e) SP models, whereby the modes correspond to mechanically active and difunctional control mechanical pulling. The mechanically active pulling has polymer linkages (red arrows, Figure 3.4) that would enable force transmission across the spiro-junction, whereas the difunctional control has polymer chains that are linked to one side of the spiro-junction or the indole ring (blue arrows, Figure 3.4 and 3.5). Experimental observations indicated that the color change was dependent on the linking geometry, across the spiro-junction, ruling out the possibility of localized heating and radical generation for the observed color change for mechanically active pulling.

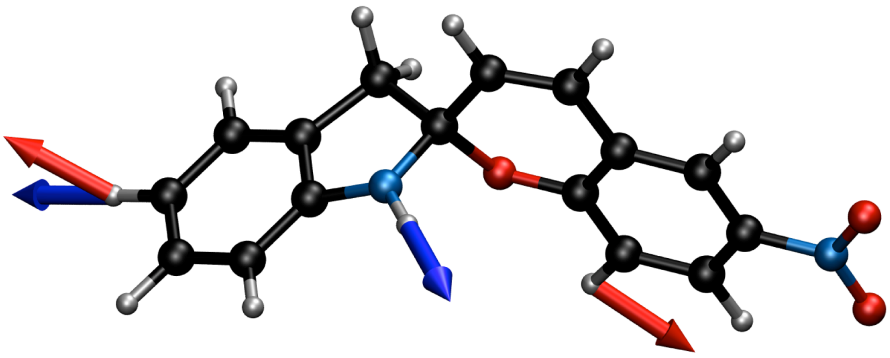

Figure 3.4: Truncated model of spiropyran showing the pulling directions (mechanophore 1t, red arrows; control 3t, blue arrows). The extended model includes ester chains in place of the H atoms.

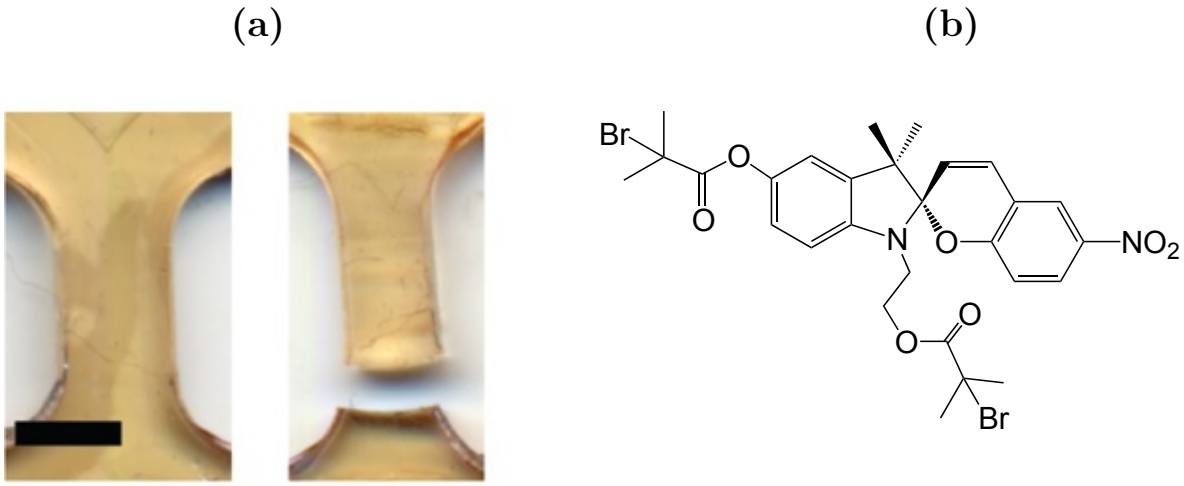

Figure 3.5: Difunctional control bulk polymer. **a**, Tensile forces results in no visible color change. **b**, SP with polymer chain attachments corresponding to the difunctional control.

3.2 Truncated Spiropyran Mechanophore Models

AISMD simulations were performed on the truncated mechanophore model 1t and difunctional control model 3t using density functional theory (DFT)[11, 12] within a modified version of AIMS- MolPro code.[13] The 6-31G basis was used in conjunction with the Perdew, Burke, and Ernzerhof density functional (PBE).[14–16] Initial conditions for position and momentum

were chosen randomly from a Boltzmann distribution at 298 K. The simulations were followed for at least 500 fs, with a time step of 0.5 fs or until bond rupture occurred (Figure 3.6), whereby at each step the electronic structure was solved to compute the intramolecular forces during dynamics.

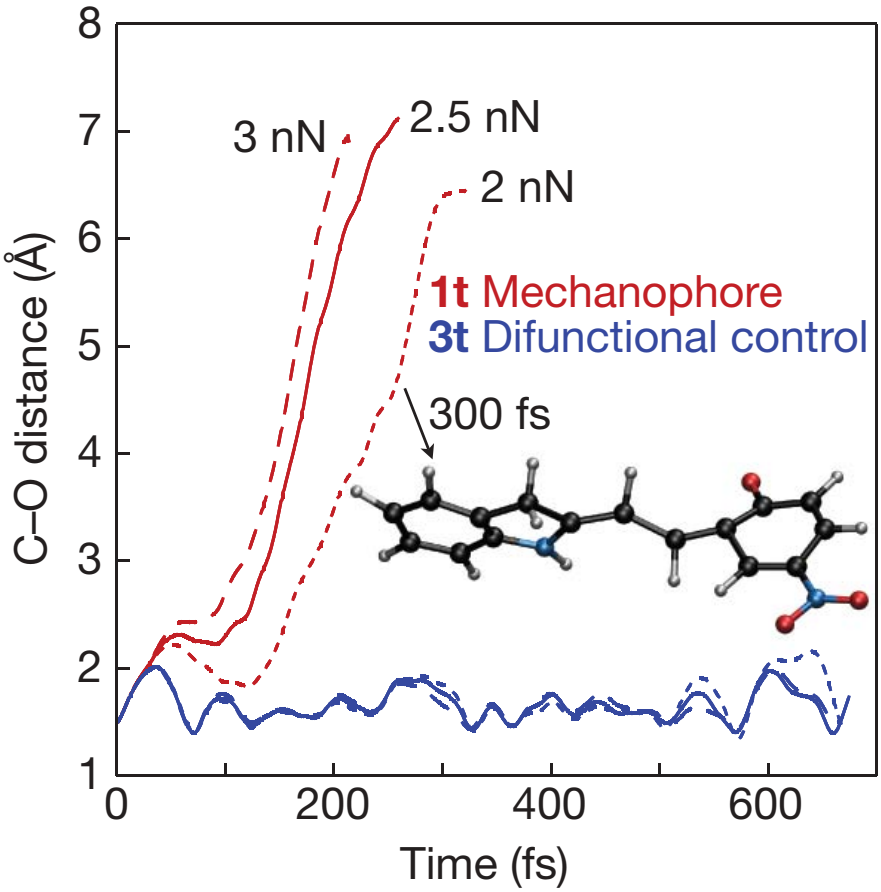

Figure 3.6: Steered molecular dynamics for the truncated mechanophore and control. The C-O bond distance is plotted versus time at 2, 2.5 and 3 nN, as shown.

At first, one trajectory was pulled at different forces (1-3 nN) and different attachment sites (1t and 3t) to determine if covalent bond rupture would occur. The results of dynamics simulations are shown in figure 3.6 and 3.7 for mechanophore model 1t and difunctional control model 3t. For 1t, scission occurred exclusively at the C-O bond for all applied forces investigated within this range. For 3t, no C-O bond rupture was observed on the indicated timescale.[1] The C-O distance at the Spiro bond is plotted as a function of time for a variety of applied forces, ranging from 2 to 3 nN. Since 2 nN was sufficient to break the C-O Spiro bond for 1t, ten additional trajectories at this force were run for both the 1t mechanophore and 3t control. Results for the control indicated no bond breakage within 500 fs for any of

the ten trajectories. However, all ten trajectories for the mechanophore showed the Spiro C-O bond breaking.

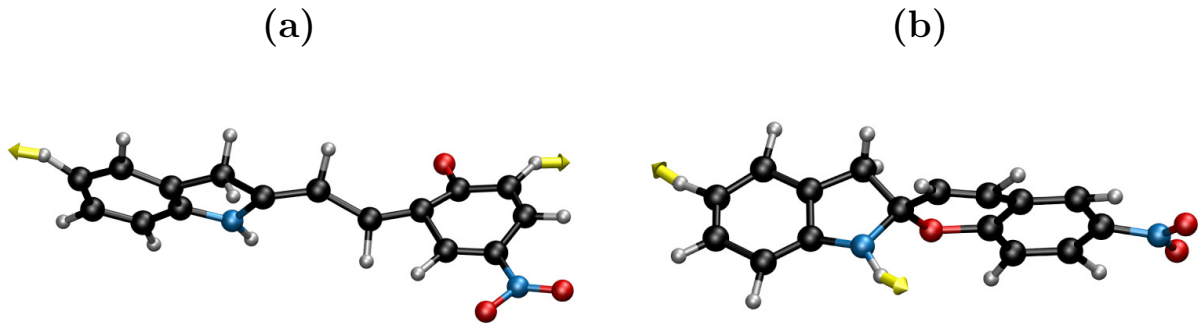

Figure 3.7: SMD snapshopts of truncated SP models at 2 nN where the yellow arrows indicate the direction of pulling. **a**, Simulation of 1t mechanophore shows C-O Spiro bond rupture. **b**, Simulation of 3t difunctional control indicates no rupture at the C-O Spiro bond.

The origin of this behavior was further explored using the COGEF procedure (Figure 3.8) in which the initial equilibrium structure for the truncated mechanophore unit was obtained through simulated annealing techniques with subsequent optimization at the DFT levels. From the truncated model, the mechanophore and control were extended in increments of 0.2 Å from the equilibrium structures to generate COGEF potentials. For 1t, the potential energy of the molecule rose as the distance between the attachment points increased, leading to a reaction activation barrier of 2.3 eV at an elongation of 17 percent; further elongation of the molecule to 20 percent ruptured the Spiro C-O bond. In contrast, 3t showed no C-O bond rupture at 20 percent elongation and the activation barrier increased to 3.7 eV at an elongation of 24 percent; further elongation finally caused rupture of the N-H bond.

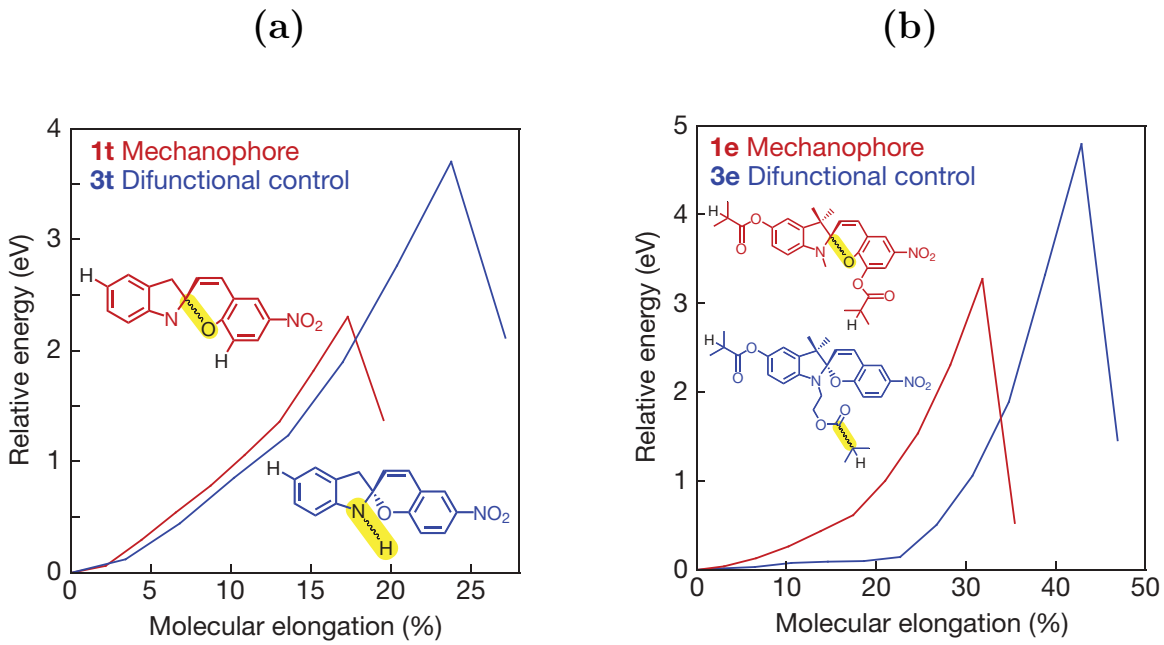

Figure 3.8: **a**, Potential energy versus percentage elongation for the truncated models (1t and 3t) calculated at the DFT level. Elongation, the distance between the pulled H atoms, is increased systematically and all other geometric coordinates are optimized at each point. Bond rupture occurs at the highlighted Spiro C-O and N-H bonds for 1t and 3t, respectively. **b**, Potential energy for the extended models (1e and 3e) calculated with DFT. Elongation is the distance between the terminal H (instead of Br in Figure 3.5b) atoms on the side chains. Rupture for 1e and 3e occurs at the highlighted C-O Spiro and C-C ester bonds, respectively.

As shown in figure 3.9, the results of multi-reference semi-empirical methods, implemented in a developmental version of MOPAC[17] software package, are in reasonable agreement with DFT results. For the electronic structure, the PM3 Hamiltonian was used with the fractional occupation molecular orbital (FOMO) method[17–19] and a complete active space configuration interaction (CASCI) wavefunction. The chosen active space consists of two electrons in two orbitals (CAS(2,2)). For the 1t mechanophore, the potential energy along the reaction path increases with an activation barrier of 2.35 eV at 17 percent elongation. Continued elongation leads to bond rupture of the C-O Spiro bond at 20 percent. In contrast, the reaction path for 3t difunctional control has an activation barrier of 4.2 eV at 24 percent elongation. Unlike the mechanophore, continued elongation induces bond rupture at the N-H bond. For the mechanophore, the absorption wavelength and oscillator strength for the lowest electronic transition were calculated using time-dependent density functional theory (TDDFT) with the B3LYP functional at the optimized force-free equilibrium geometry and at 20 percent elongation after bond rupture (Figure 3.10). A large red shift of 4.75 eV (261 nm) to 2.76 eV (450 nm) is observed due to the increased conjugation length after Spiro

bond rupture (Figure 3.11). The red shift is expected to increase to longer wavelengths if solvent interactions with the mechanophore are accounted for.

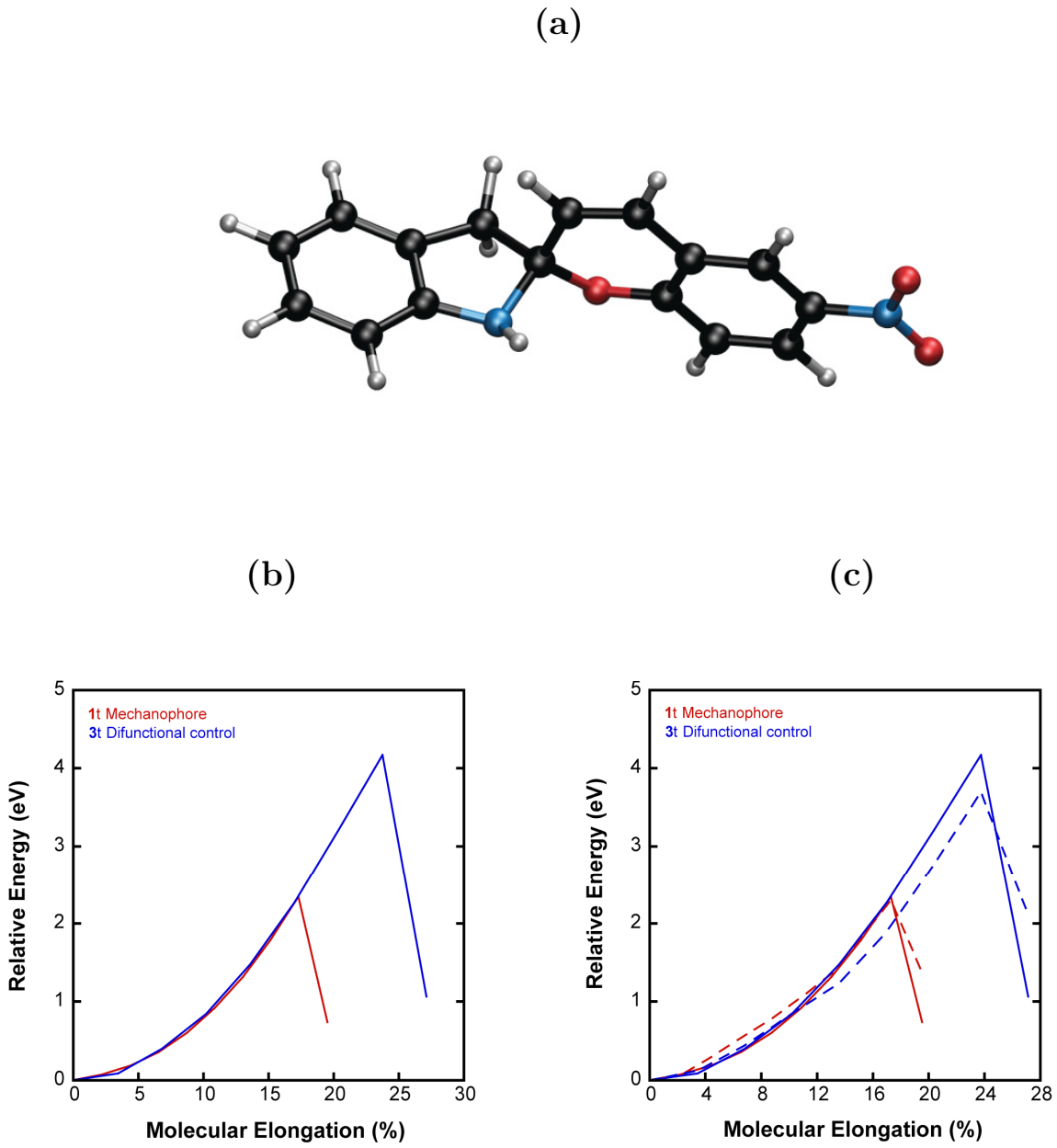

Figure 3.9: COGEF electronic potential calculated at the PM3 level. **a**, Equilibrium molecular geometry of truncated spiropyran. **b**, The relative activation barrier as a function of molecular elongation is shown for both 1t and 3t. **c**, DFT (- -) results are compared to PM3 (-); the potential energy surface is similar with bond breaking also occurring at the C-O Spiro and N-H bonds for the 1t and 3t models.

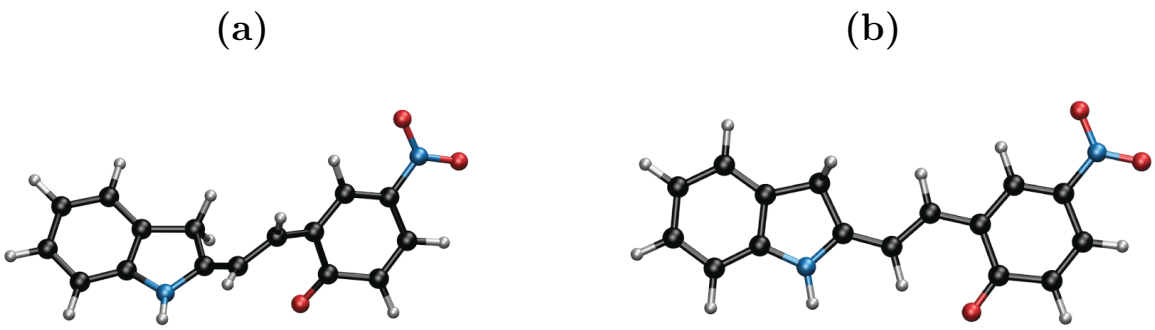

Figure 3.10: DFT optimized molecular geometries of 1t after bond rupture. **a**, Constrained 1t molecular geometry at 20 percent elongation. **b**, Equilibrium molecular geometry of 1t, which was obtained by relaxing the constraints from part a. TDDFT with the B3LYP functional was used to calculate the absorption wavelength.

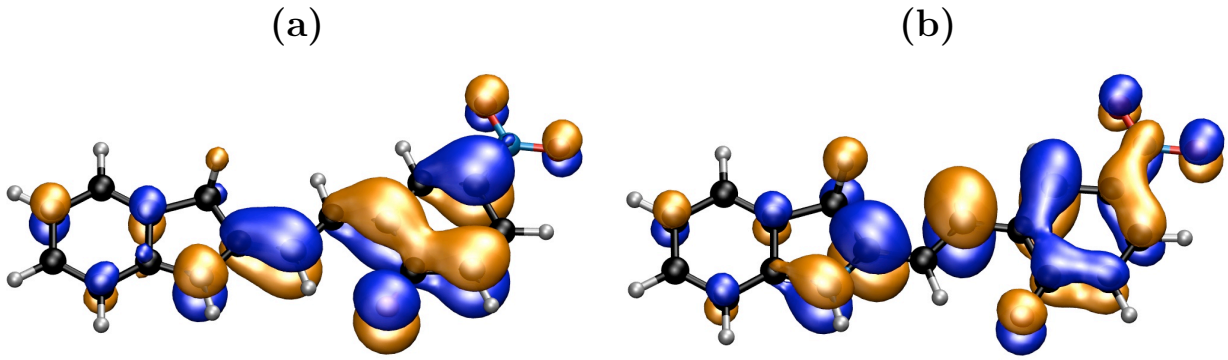

Figure 3.11: **a**, LUMO for the equilibrium trans MC conformer. **b**, HOMO for the equilibrium trans MC conformer.

3.3 Simulation of Extended Spiropyran Mechanophore Models

In the experimentally-studied mechanophore, the external force is transmitted through the polymer backbone to attachment points that are further removed from the mechanophore unit than the ones used in the truncated model. Therefore, the effect of more distant attachment points were investigated by carrying out AISMD and COGEF simulations of the 1e mechanophore and 3e difunctional control containing the ester side chains. Equilibrium structures for the extended mechanophore and difunctional control were obtained through simulated annealing techniques and x-ray crystal structures (Figure 3.12).

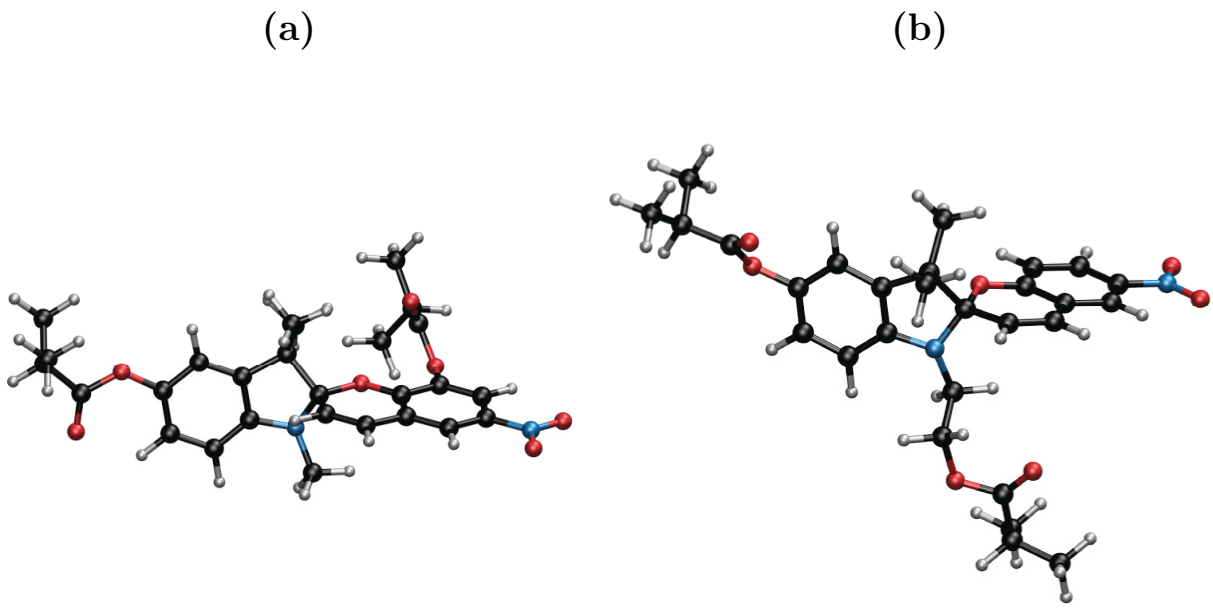

Figure 3.12: Equilibrium molecular geometries for extended SP models. **a**, The initial structure for the 1e mechanophore was obtained from simulated annealing algorithms followed by optimization at the DFT level. **b**, The equilibrium structure for the 3e difunctional control was provided by x-ray crystallography information.

AISMD simulations were conducted for the extended models 1e and 3e (Figure 3.13) at similar force ranges (1-3 nN) using multi-reference semi-empirical methods described previously. These simulations ran for at least 50 ps or until bond rupture with a time step of 0.5 fs. Initial conditions were sampled randomly from a finite temperature Boltzmann distribution at 298 K. For the 1e mechanophore, 3 nN was sufficient to break the C-O Spiro bond. Twenty additional trajectories at this force were simulated for both the 1e mechanophore and 3e control. Results for 3e indicated no C-O Spiro bond breaking for any of the 20 trajectories. However, rupture occurred either at a side C-C chain (11 trajectories) or a side C-O ester chain (9 trajectories). For 1e, we observed 12 trajectories rupture at the C-O Spiro bond with the remaining 8 trajectories rupturing at a side C-O ester bond, indicating mechanoselectivity may not be complete. One might be able to leverage this by determining the precise force, which was applied to generate a particular color change, if one could quantify the fraction of mechanophores undergoing color change.

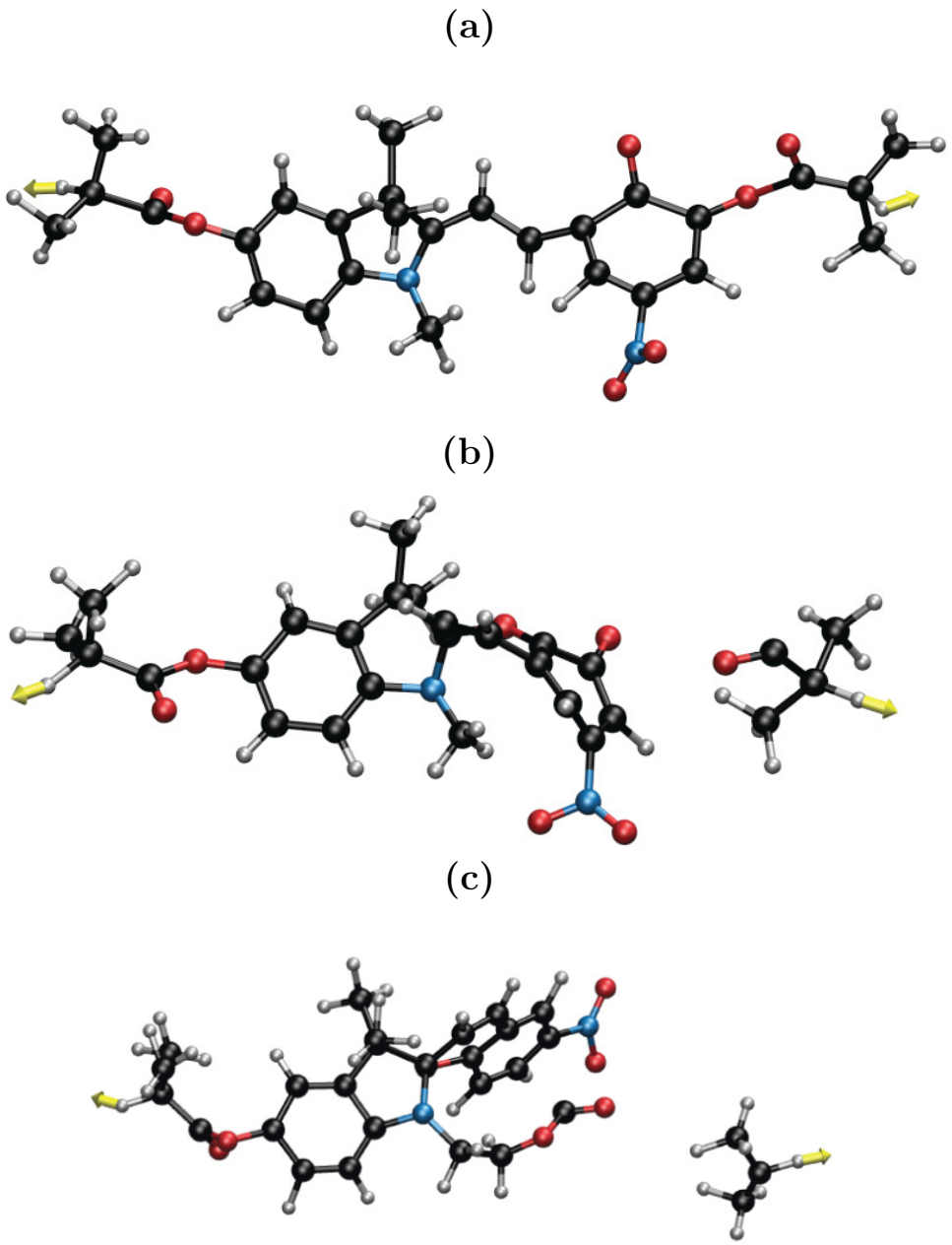

Figure 3.13: SMD snapshots of extended SP models at 3 nN where the yellow arrows show direction of pulling. **a**, Simulation of 1e mechanophore shows bond rupture at the C-O Spiro bond. **b**, A different trajectory of 1e mechanophore results in bond rupture at a side C-O ester bond. **c**, Simulation of 3e difunctional control indicates rupture at the terminal C-C bond.

The DFT COGEF energy profiles were generated, for the equilibrium structures of the extended models 1e and 3e, by elongating the distance along the reaction path in 0.5 Å increments with optimization at each step (Figure 3.12). 1e again showed Spiro C-O bond

rupture, whereas the difunctional control molecule 3e underwent a bond rupture at one of the side chains that does not lead to color change.

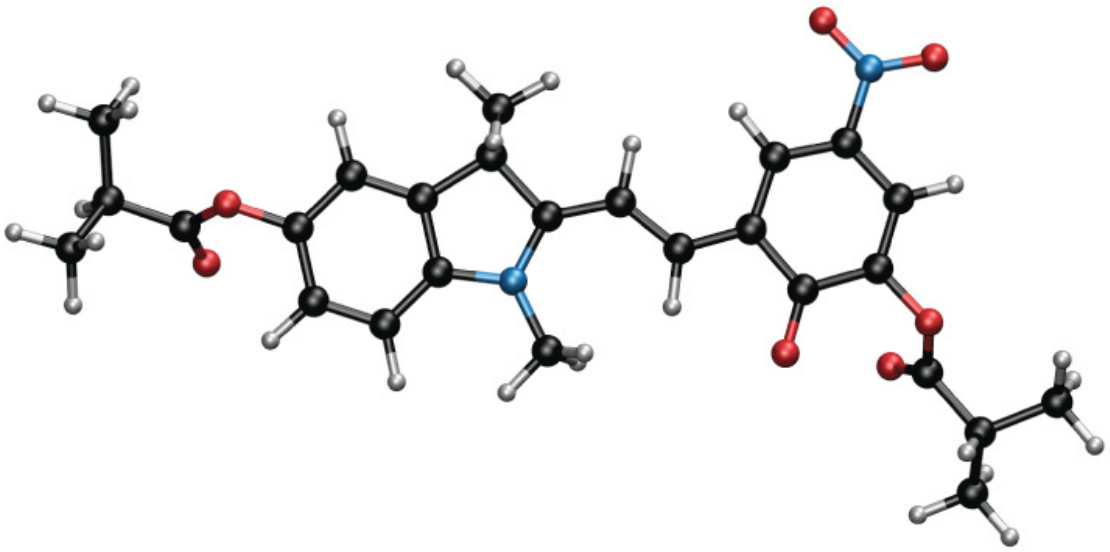

Figure 3.14: Equilibrium molecular geometry of open form 1e calculated at the DFT level. The structure was obtained by optimizing the 1e geometry at 35 percent elongation without any constraints.

Thus, like the truncated model, the reaction activation barrier is significantly higher for the 3e difunctional control (4.8 eV barrier at 43 percent elongation) compared to the 1e mechanophore (3.2 eV barrier at 32 percent elongation) at the DFT level (Figure 3.15). This is due to the rupture of the side chain which requires more energy than that needed to activate 1e. For the latter case, we also observe distinct bond rupture; the Spiro C-O bond breaks at 35 percent elongation for the 1e mechanophore which forms an MC isomer (Figure 3.14). Thus, the COGEF calculations predicted selective Spiro C-O bond rupture for the 1t as well as the 1e models. In contrast, one of the C-C bonds in the alkyl chain breaks at 47 percent elongation for the 3e difunctional control. As shown in figure 3.15, DFT and semi-empirical methods are again in reasonable agreement concerning the COGEF energy profile for both extended models, justifying their use in longer-lasting dynamics simulations to explore the effects of lower applied forces. The semi-empirical method indicates an activation barrier of 2.9 eV at 32 percent elongation for the 1e mechanophore with bond rupture of the C-O Spiro bond at 35 percent elongation. In contrast, the reaction path for the 3e difunctional control resulted in a barrier of 4.7 eV at 43 percent elongation with bond rupture of the C-C ester bond at 47 percent elongation.

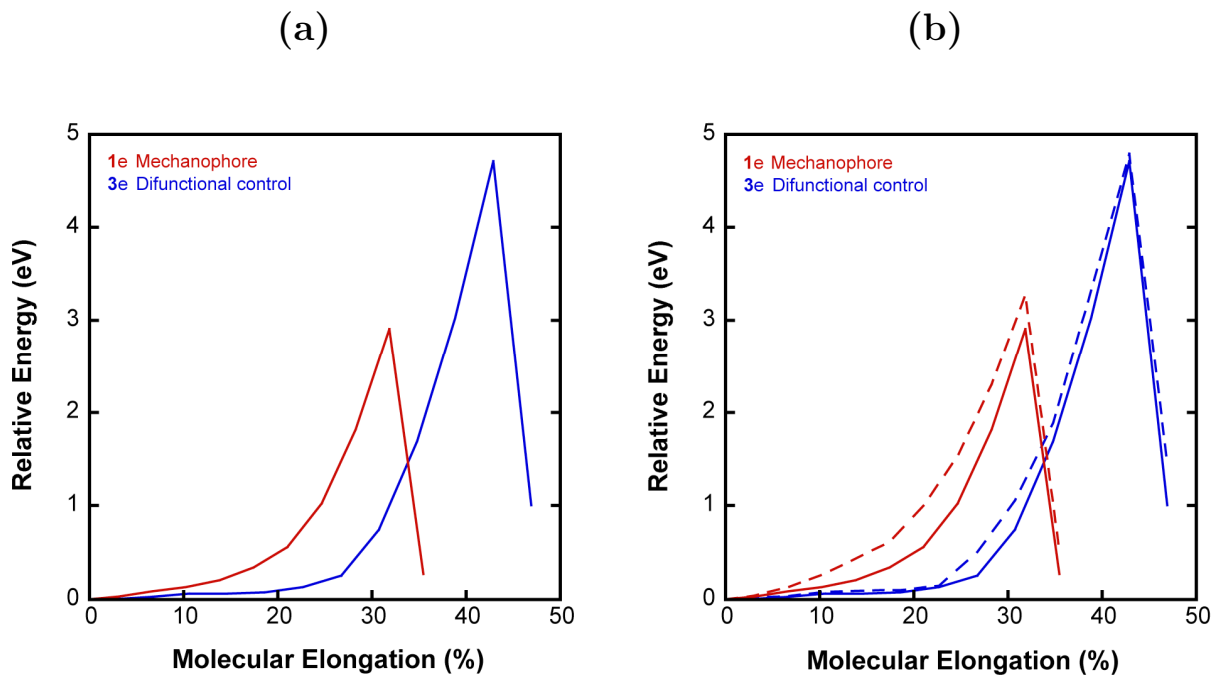

Figure 3.15: COGEF electronic potentials calculated at the PM3 level. **a**, The reaction path for the extended models are shown at the PM3 (-) level only. **b**, Potential surfaces are shown at the DFT (- -) level. Like the PM3 potentials, bond breaking occurs at the C-O Spiro and C-C ester bonds for the 1e and 3e models, respectively.

3.4 References

[1] Davis, D. A.; Hamilton, A.; Yang, J.; Cremar, L. D.; Gough, D. V.; Potisek, S. L.; White, S. R.; Moore, J. S.; Sottos, N. R.; Ong, M. T.; Braun, P. V.; Martínez, T. J. *Nature* **2009**, *459*.

[2] Potisek, S. L.; Davis, D. A.; Sottos, N. R.; White, S. R.; Moore, J. S. *J. Am. Chem. Soc.* **2007**, *129*, 13808.

[3] Flannery, J. B. *J. Am. Chem. Soc.* **1968**, *90*, 5660.

[4] Ong, M. T.; Leiding, J.; Tao, H.; Virshup, A. M.; Martínez, T. J. *J. Am. Chem. Soc.* **2009**, *9*, 6377.

[5] Ben-Nun, M.; Martínez, T. J. *Adv. Chem. Phys.* **2002**, *121*, 439.

[6] Sotomayor, M.; Schulten, K. *Science* **2007**, *316*, 1144.

[7] Saitta, A. M.; Klein, M. L. *J. Phys. Chem. B* **2001**, *105*, 6495.

[8] Isralewitz, B.; Gao, M.; Schulten, K. *Curr. Opin. Struct. Biol.* **2001**, *11*, 224.

[9] Phillips, J. C.; Braun, R.; Wang, W.; Gumbart, J.; Tajkhorshid, E.; Villa, E.; Chipot, C.; Skeel, R. D.; Kalé, L.; Schulten, K. *J. Comput. Chem.* **2005**, *26*, 1781.

[10] Beyer, M. K. *J. Chem. Phys.* **2000**, *112*, 7307.

[11] Hohenberg, P.; Kohn, W. *Phys. Rev.* **1964**, *136*, B864.

[12] Kohn, W.; Sham, L. J. *Phys. Rev.* **1965**, *140*, A1133.

[13] Levine, B. G.; Coe, J. D.; Virshup, A. M.; Martínez, T. J. *Chem. Phys.* **2008**, *347*, 3.

[14] Perdew, J. P.; Burke, K.; Ernzerhof, M. *Phys. Rev. Lett.* **1996**, *77*, 3865.

[15] Perdew, J. P.; Ernzerhof, M.; Burke, K. *J. Chem. Phys.* **1996**, *105*, 9982.

[16] Perdew, J. P.; Burke, K.; Ernzerhof, M. *Phys. Rev. Lett.* **1997**, *78*, 1396.

[17] Stewart, J. J. P. *J. Comput. Chem.* **1989**, *10*, 209.

[18] Granucci, G.; Toniolo, A. *Chem. Phys. Lett.* **2000**, *325*, 79.

[19] Toniolo, A.; Thompson, A. L.; Martínez, T. J. *Chem. Phys.* **2004**, *304*, 133.

Chapter 4

Simulation of a Mechanically Active Spiropyran

4.1 Introduction

The effect of an applied force at various attachment sites on a spiropyran (SP) mechanophore, as reported by Davis *et al.*, will change the mechanochemical reaction outcome, ultimately determining the response of the bulk material.[1] The mode of force transmission, induced via bulk tensile forces or ultrasound, from the terminal polymer chains to the mechanically active attachment sites on SP indicates Spiro C-O bond cleavage. This is evident by a visible color change due to merocyanine (MC) formation. The specific mechanism following Spiro C-O cleavage is reported herein for the mechanically active sites discussed in chapter 2, which correspond to a stretched induced mechanophore (SIM) pulling motion at at atoms 5' and 8 (Figure 1.2). Additional SIM pulling schemes are investigated to explore the mechanochemical reactivity, which may change the global nature of the reactants, transition states, and products on the force modified potential energy surface (FMPES).

4.2 Ab Initio Steered Molecular Dynamics of SIM1

Molecular dynamics simulations were carried out with a modified version of the AIMS-GAMESS[2, 3] program using a 6-31G basis set and the B3LYP[4, 5] functional. The initial geometry reflects the force free optimized SP. Initial positions and momenta are acquired from a Boltzmann distribution at 298 K corresponding to the force free SP vibrational modes with frequencies greater than 100 cm^{-1}. Ab initio steered molecular dynamics (AISMD) simulations were performed, at the SIM1 attachment points (APs) 5' and 8 (figure 1.2), with an applied force ranging from 1-5 nN to confirm the minimal forces for bond rupture. For one trajectory a minimal force of 2.5 nN was sufficient to break the Spiro C-O within a 500 fs timescale, figure 4.1a. It is expected that forces less than 2.5 nN will follow a similar outcome, however, at much longer timescales that are not computationally feasible. Forces greater than 2.5 nN also show C-O dissociation, although, at these forces the amount of work placed into the system may result in the loss of energy conservation due to the formation of

unphysical structures. As shown in figure 4.1b, for one trajectory at an applied force of 2.5 nN, when the APs are pulled towards the fixed pulling points (PPs), the C-O breaks. Thirty additional trajectories for the SIM1 pulling scheme were followed to quantify the frequency of C-O breaking. A summary of the reaction outcome is shown in figure 4.6.

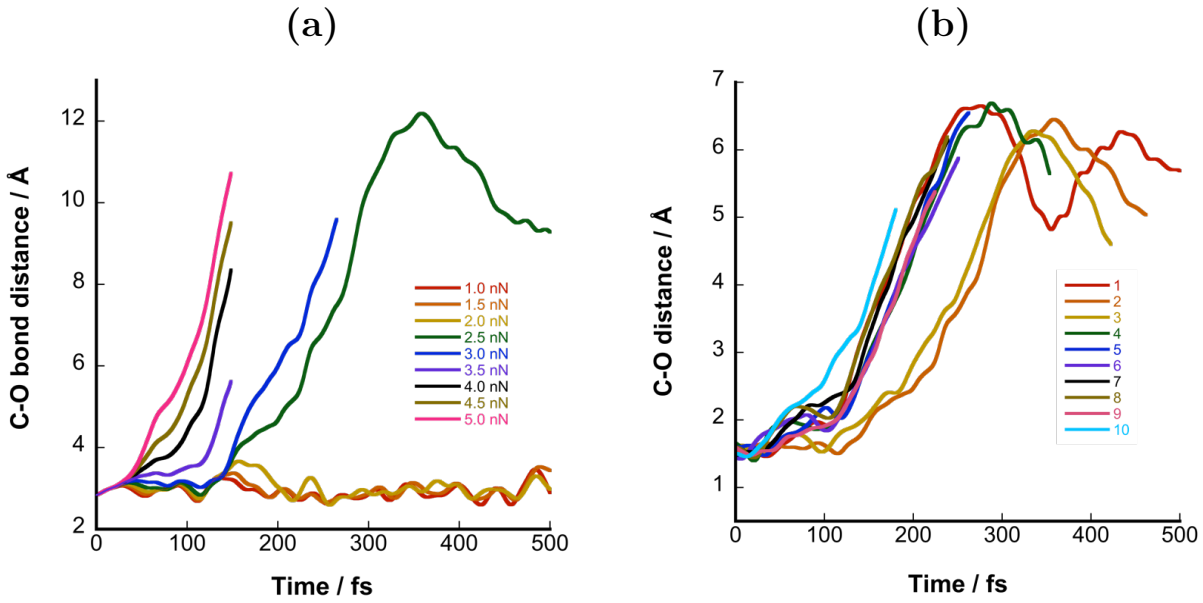

Figure 4.1: **a**, External force between 1-5 nN is applied for one trajectory, SIM1, whereby the C-O bond distance is monitored as a function of time. The colored lines denote different forces. Within 500 fs the C-O bond breaks with a minimal force of 2.5 nN. **b**, The C-O distance is plotted as a function of time for ten different trajectories (labeled 1-10) at an applied force of 2.5 nN. All trajectories show bond breakage at the Spiro C-O bond.

Further analysis of the reaction products indicates the formation of two distinct MC isomers (Figures 4.2-4.5). The number of MC isomers formed was quantified by monitoring two dihedral angles, which reflect a bond dissociation ($\boldsymbol{\alpha}$) and isomerization ($\boldsymbol{\beta}$) coordinate. Figure 4.2 depicts a 2-D dihedral angle plot where $\boldsymbol{\alpha}$ is the abscissa and $\boldsymbol{\beta}$ the ordinate, which illustrates two competing reaction routes whereby SP can ring-open to either a CTC or TTC MC isomer. The isomer labels (e.g. SP) on the plot correspond to the force free optimized geometries. For one pulling trajectory, when the C-O bond breaks $\boldsymbol{\alpha}$ decreases and $\boldsymbol{\beta}$ increases simultaneously. Following bond rupture, the $\boldsymbol{\beta}$ C-C bond isomerizes to trans CTC. There is no indication that the CCC isomer is an intermediate along the reaction path since the angles are initially localized at SP, which then pass to CTC. This suggests the absence of the CCC intermediate at applied forces near 2.5 nN.

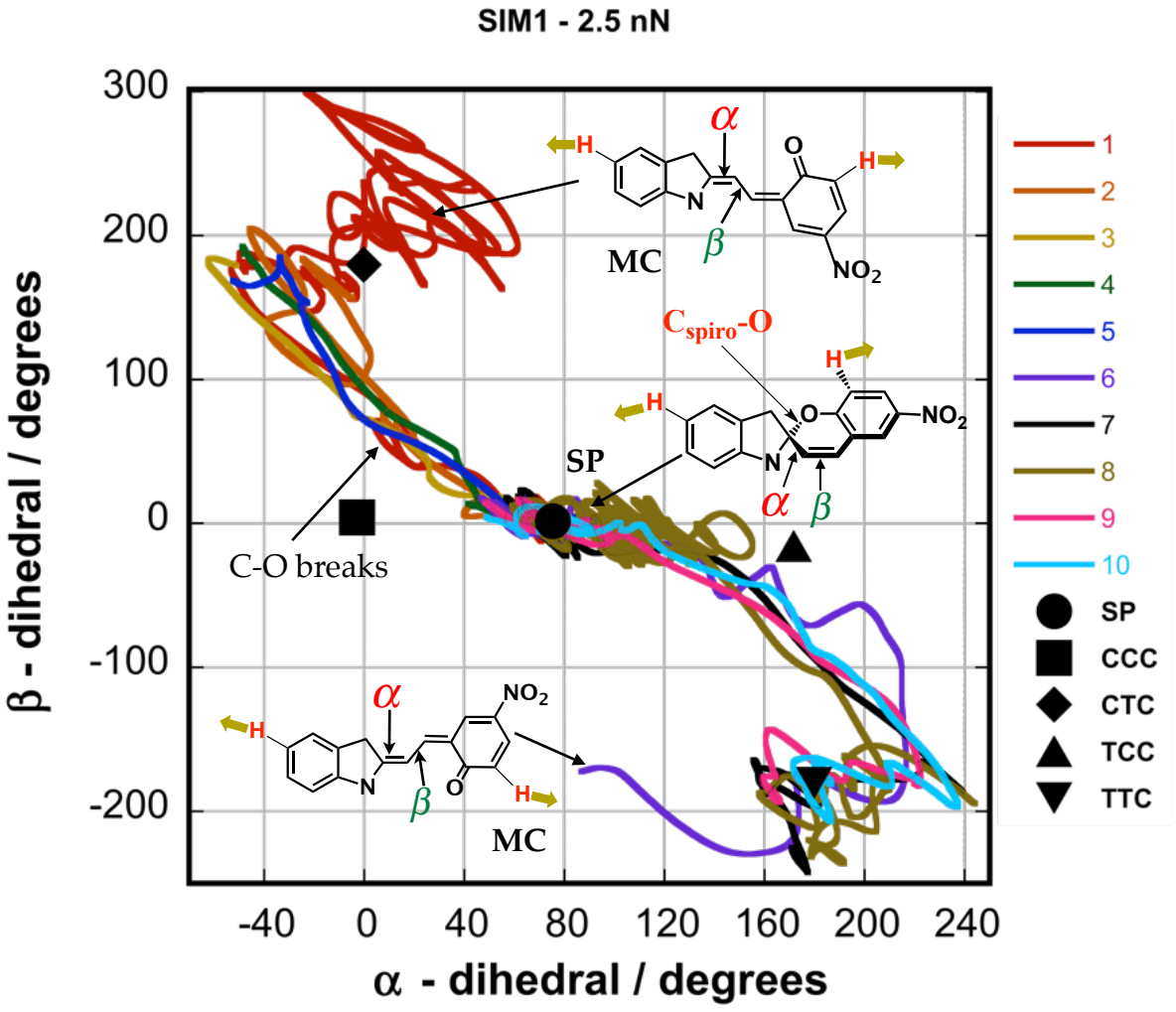

Figure 4.2: SIM1 2-D dihedral angle plot. The equilibrium bond angles for the SP, CCC, CTC, TCC, and TTC isomers are indicated by the black markers. The colored lines indicated different reaction trajectories and are labeled 1-10. The $\boldsymbol{\alpha}$ and $\boldsymbol{\beta}$ angles are shown for all ten trajectories. Starting at the SP, two reaction routes exist towards a particular trans MC isomer. For five trajectories, the $\boldsymbol{\alpha}$ angle decreases while the $\boldsymbol{\beta}$ angle increases simultaneously which corresponds to both C-O bond cleavage and C-C isomerization to CTC. There is no indication of any CCC formation. For the remaining five trajectories, $\boldsymbol{\alpha}$ increases while $\boldsymbol{\beta}$ decreases concurrently towards the TTC conformer, with no evidence of TCC formation.

For another particular trajectory shown in figure 4.2 and 4.4, the C-O breaks with an increasing $\boldsymbol{\alpha}$ and decreasing $\boldsymbol{\beta}$ dihedral angle, which then isomerizes to the MC isomer TTC. Like the reaction pathway that ring opens to CTC, there is no indication of any intermediate or TCC cis-cisoid formation. This suggests there is only one barrier along the reaction pathway at 2.5 nN. All thirty trajectories resulted in bond rupture of the C-O, where eleven trajectories resulted in the formation of TTC and nineteen towards the CTC

product. The remaining four trajectories, however, ring-opened to the CCC conformer, which required slightly longer timescales to isomerize to CTC (Figure 4.5). Time dependent density functional theory (TDDFT) calculations were carried out to determine the optical properties for the unconstrained MC isomers. The ten lowest singlet excitations and oscillator strengths were calculated at the B3LYP level of theory. As shown in table 4.1, The CTC and TCC isomers both have similar values for the absorption wavelength, which are red shifted with respect to SP.

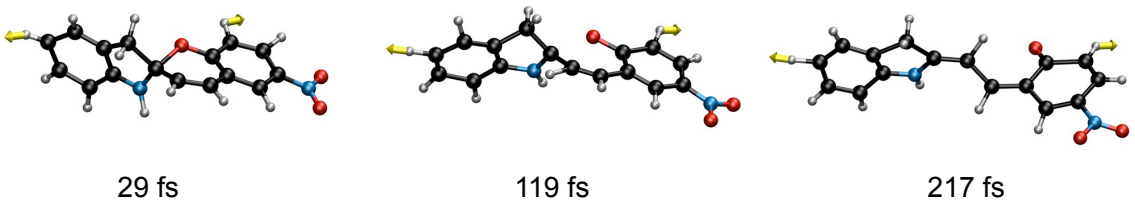

Figure 4.3: AISMD of SIM1 for one trajectory at 2.5 nN, which represents the reaction path SP → CTC. The yellow arrows designate applied force at the H atoms. From the initial SP geometry, the Spiro C-O bond cleaves near 119 fs followed by the C-C isomerization to the trans MC CTC at 217 fs.

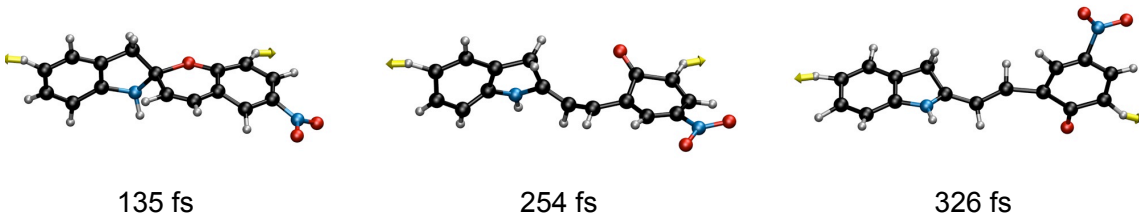

Figure 4.4: Snapshot of a SIM1 trajectory from SP → TTC at an applied force of 2.5 nN. Eleven of thirty trajectories follow this reaction route without any indication of an intermediate.

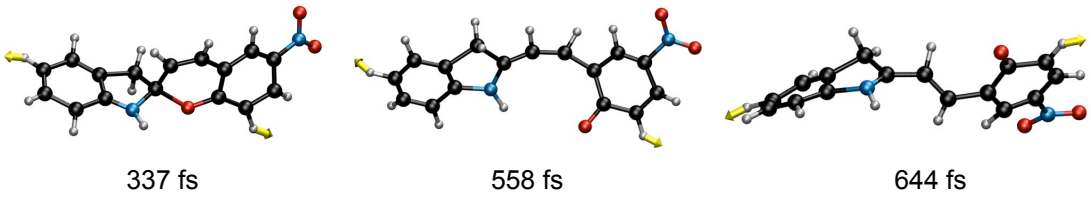

Figure 4.5: SIM1 trajectory snapshot at 2.5 nN which follows an unfavorable reaction route from the cis-cisoid, CCC $\rightarrow$ CTC.

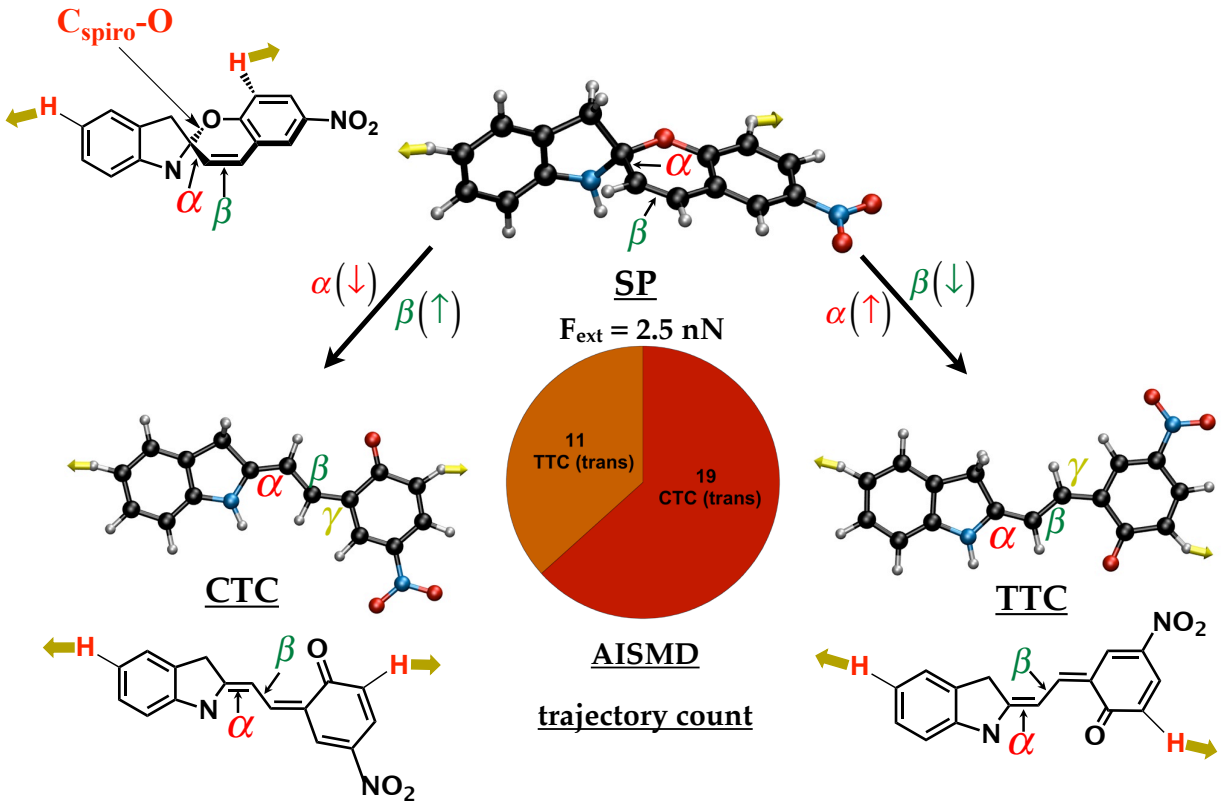

Figure 4.6: SIM1 conformer breakdown for thirty trajectories at 2.5 nN. Two possible reaction paths exist: SP → CTC and SP → TTC. Within 1 ps, eleven trajectories ring open to the trans TTC isomer while the other nineteen simulations provide evidence of the CTC product. Additionally, there is no indication that the cis-cisoid conformers are stabilized or formed.

Table 4.1: Predicted absorption wavelength for the trans MC isomers.

MC isomer	Transition dipole	Oscillator strength	Wavelength / nm
CTC	-3.13349 -0.01188 1.87688	0.90497	448
TTC	-3.31621 0.21154 1.61046	0.91797	451

4.3 SIM1 Reaction Pathways on the Force Modified Potential Energy Surface

Understanding mechanophore reactivity is incomplete without discussing transition state theory, especially in the limit of low force mechanochemical dynamics simulations where computational limitations are imposed. As discussed in chapter 2, Eyring and Kauzmann conceptualized a constant force correction to the potential energy surface (PES) which resulted in barrier lowering.[6] The reaction activation barrier now becomes explicitly dependent on the applied force and the stationary points on the PES are the force-perturbed geometries. The rate of bond breaking as a function of force is now exponentially proportional to the activation barrier. The activation barrier is derived by knowledge of the stationary points on the force modified potential energy surface (FMPES). The possible reactants, intermediates, and products at a specified force may be provided from molecular dynamics. To search for transitions along the reaction pathway, a modified nudged elastic band (NEB) under external force was used to locate approximate transition states. In addition, NEB provides the minimal energy pathway (MEP) on the FMPES, which connects the transition to the reactant and product or endpoints. The MEP is modified by external force and is a function of applied force on the FMPES.

For both reaction pathways, SP $\rightarrow$ CTC and SP $\rightarrow$ TTC, the endpoints were obtained from molecular dynamics simulations and optimized at forces between 0-2.5 nN. The modified NEB algorithm was used to locate the transition between SP and the MC at the specified forces. After convergence of the band, the first order saddle points were located using TS search methods discussed in chapter 2. The order of the TS is determined by carrying out a frequency analysis. This requires that the mass-weighted Hessian be calculated via finite differencing following diagonalization to obtain the eigenvalues. To confirm that the TS does indeed connect to the reactants and products found in dynamics and optimizations, an extended intrinsic reaction coordinate (IRC) algorithm under force was utilized. From the TS, a steepest descent direction towards the reactant or product is followed respectively. Figure 4.7 shows the energy profile for the two reaction paths on the FMPES, where SP is the reference point in mass-weighted distance (MWD). Table 4.2 lists the relative energy barriers for transitions between each isomer under applied force.

With respect to figure 4.7, the y-axis indicates the relative barrier height for the energy profile under application of external forces between 0 and 2.5 nN. On the force free reaction pathway, five minima are present as labeled in figure 4.2. Starting at the reference point, SP can convert to either the CCC or TCC cis-cisoid conformers, which are intermediates along the pathway. Transitions over the reaction barrier to these intermediates reflect cleavage

of the Spiro C-O bond. Figure 4.8a plots the C-O barrier heights between SP and a TS along the pathway. In addition, the C-C isomerization barriers are also plotted, and reflect the transition from the cis-cisoid conformer to another TS along each pathway. Figure 4.8b shows the relative distance in MWD from one minimum to the designated TS on the MEP. A noticeable distinction between the relative barrier heights for bond breaking and isomerization can be pointed out. For example, the isomerization barriers become absent at forces of 1.5 nN in contrast to the C-O barriers, which change relatively less. The force free reaction barrier height to TS1 for the SP $\rightarrow$ CCC transition is 13.65 kcal/mol at a MWD of 10.77 Å*amu$^{1/2}$. Similarly, the force free barrier height to TS3 for the SP $\rightarrow$ TCC transition is 13.09 kcal/mol at 20.9 Å*amu$^{1/2}$ (Figure 4.8). The TCC minima is less stable (9.26 kcal/mol) with respect to the CCC isomer (1.08 kcal/mol) which may be due to the electronic repulsion between the oxygen orbital with the two hydrogen orbitals on the indole ring. With respect to the MEP on the PES, the CCC isomer undergoes isomerization about the β C-C bond to TS2 with a reaction barrier equal to 30.72 kcal/mol at 55.92 Å*amu$^{1/2}$, yielding the CTC isomer (5.63 kcal/mol). Similarly, TCC under goes isomerization to TS4 with a reaction barrier equal to 30.69 kcal/mol at 45.87 Å*amu$^{1/2}$, forming the TTC isomer (3.79 kcal/mol). The relative energies, MEP, and geometries of various stationary points at several forces are reported in table 4.2, appendix D and E.

With an increase in applied force, from 0 to 0.5 nN, the C-O bond breaking barrier and MWD may increase. For instance, the SP $\rightarrow$ TS1 barrier is 13.90 kcal/mol at 12.72 Å*amu$^{1/2}$ compared to SP $\rightarrow$ TS3 which lowers to 12.67 kcal/mol at 17.44 Å*amu$^{1/2}$ respectively. The application of external forces greater than 0.5 nN, for both pathways not only lowers the energy barrier, it may also shift the TS geometry closer to SP along the reaction path (Figure 4.8). Thus, the decrease in barrier height is followed by a decrease in MWD distance from the starting geometry to the transition state.

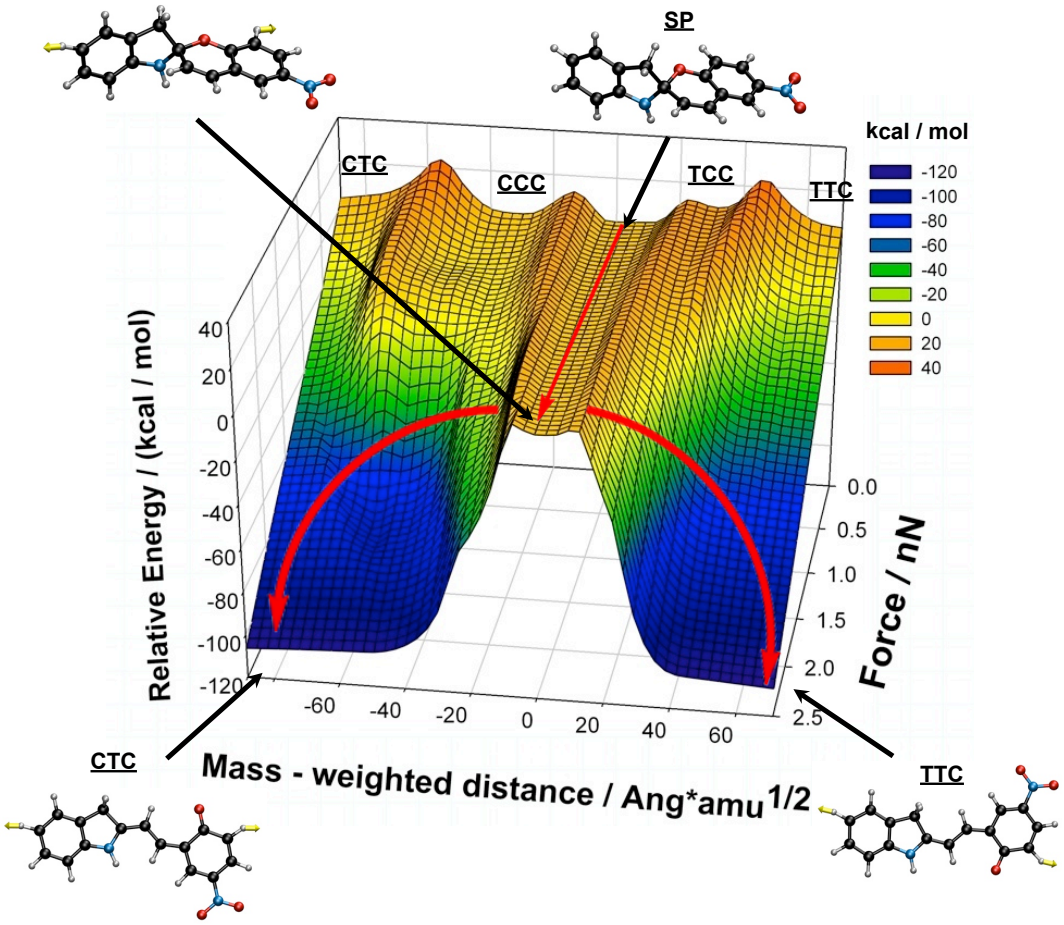

Figure 4.7: SIM1 FMPES. The zero force barrier heights for C-O cleavage and C-C isomerization to any of the respective cisoid and trans conformers are approximately equal. At 0.5 nN the C-O barrier height for both pathways increases marginally, while the barrier corresponding to the CCC → CTC or TCC decreases respectively. At forces of 1.5 nN or lower the cis-cisoid minima are present for both pathways, however, increased forces comparable to AISMD, result in the disappearance of the cis-cisoid intermediates. Only a single barrier, reflecting concerted dissociation and isomerization remains for each pathway whereby the MC isomers are increasingly stabilized with respect to SP. The latter complements dynamics since the SP → CTC or TTC transition is primarily seen without any indication of cis-cisoid stability.

A three dimensional interpretation of the FMPES, portrayed in figure 4.7, illustrates how the cis-cisoid minima and the TS corresponding to C-C isomerization disappear. These geometries change as a function of force (Figure 4.9), demonstrating how applied force can alter the reaction mechanism. Although in the absence of force, the SP geometry is relatively stable with respect to the MC geometries (table 4.2 and 4.3). With an increase in

applied force SP becomes less stable with respect to MC and the cis-cisoid to trans isomerization barriers decrease (Figure 4.8). The trans MC isomers, however, become increasingly stabilized with respect to SP.

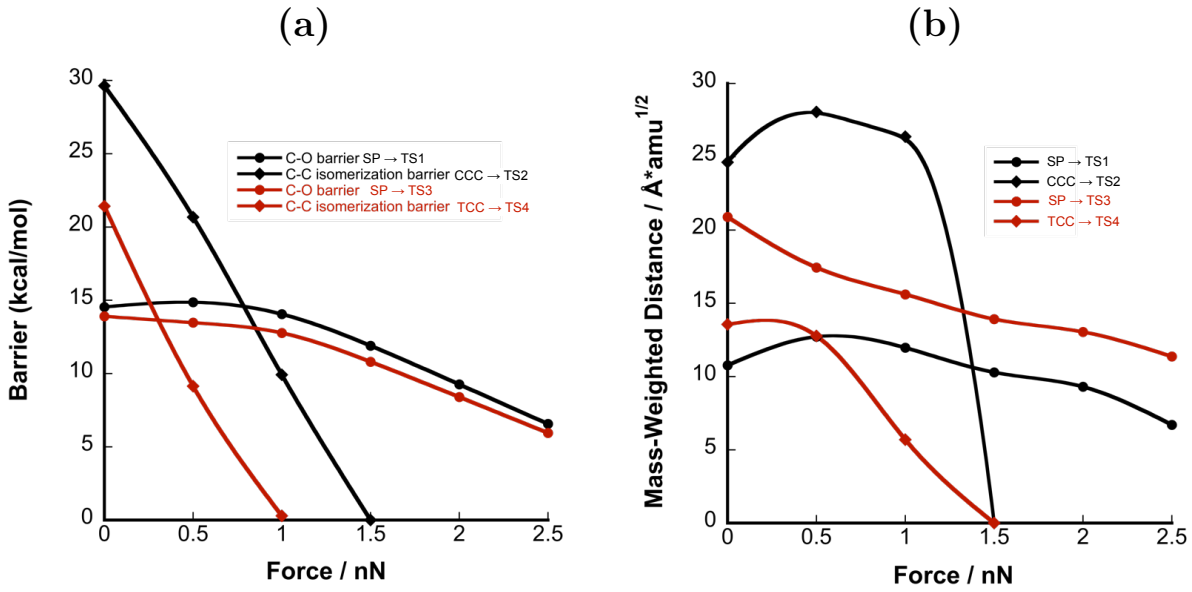

Figure 4.8: TS1 and TS3 are transitions states for the C-O barriers corresponding to the following transitions: SP → CCC and SP →TCC. TS2 and TS4 are the transitions states for the following C-C isomerization barriers: CCC → CTC and TCC → TTC. **a**, For the SP → CCC transition at 0.5 nN, the C-O barrier increases within 1 kcal/mol before lowering at larger forces. The SP → TCC barrier decreases monotonically. At 1 nN, the C-C isomerization barrier for TCC → TTC transition disappears in contrast to the CCC → CTC transition which disappears at 1.5 nN. **b**, the mass weighted distance on the MEP to the specified transition state with respect to SP or the cis-cisoid conformer.

The pathway towards the CTC isomer has an intermediate or cis-cisoid CCC conformer that is present up to a force of 1.5 nN. The barriers corresponding the C-O cleavage up to this force range are within 3 kcal/mol apart, unlike the transition over the isomerization barrier, which decreases relatively more so (Figure 4.8). With respect to the second pathway towards the TTC isomer, the cis-cisoid intermediate TCC is present up to forces of 1.0 nN. The C-C isomerization barriers decrease more so than the C-O barriers with respect to applied force. At forces of 1.5 nN, the C-C isomerization barriers for both pathways are negligible and the cis-cisoid conformers, CCC or TCC, are no longer minima on the FMPES. There is a single barrier on the FMPES at forces exceeding 1.5 nN, which are primarily attributed to the C-O bond breakage. The barriers now reflect the following transitions: SP → CTC and SP → TTC which are nearly energetically equivalent or within 1 kcal/mol (Table 4.2 and 4.3) apart. The MEP bypasses the cis-cisoid intermediates, and the reaction path may be described by

C-O bond breakage with C-C bond isomerization occurring simultaneously. Under applied force, the root mean square deviation (RMSD) values for the MC isomers changes less so with respect to other geometries. This indicates greater stabilization at increasing forces. This is in accord with the AISMD results where C-O bond rupture, at 2.5 nN, was followed by formation of the trans MC isomer. Interestingly, the reactant and transition state geometries on the FMPES (Figure 4.9) are more perturbed with increasing external force compared to the MC products. The effect of an applied force on SP is therefore stabilized by conversion to the trans isomers, which are color generating. Therefore, one would expect a mixture of both trans CTC and TTC products at increasing forces for the SIM1 APs, which is expected to enhance absorption.

Corissa *et al.*[7] incorporated SP mechanophores within a polyurethane backbone, reflecting the SIM1 APs, in order to investigate the kinetic mechanochemical bulk polymer response to fluorescence and absorbance measurements. The absorbance was shown to increase with strain and at constant strain the colored MC did not revert back to SP. An applied light source on the strain material resulted in loss of color, however, this color returned only when the bulk material remained strained. Thus, the experiment demonstrates stabilization of the colored trans MC under applied force, as predicted by modeling.

Table 4.2: Relative energies in kcal/mol (with respect to SP) for minima and transition states along the SP $\rightarrow$ CCC $\rightarrow$ CTC reaction path.

Force	TS1	CCC	TS2	CTC
0	14.54	1.08	30.72	5.63
0.5	14.86	-6.39	14.30	-19.58
1.0	14.05	-11.70	-1.78	-40.99
1.5	11.90	-19.54	-18.65	-62.03
2.0	9.26	n/a	n/a	-83.09
2.5	6.56	n/a	n/a	-104.04

Table 4.3: Relative energies of minima and transition states along the SP → TCC → TTC reaction path.

Force	TS3	TCC	TS4	TTC
0	13.91	9.26	30.69	3.79
0.5	13.46	7.44	16.59	-21.81
1.0	12.77	2.45	2.75	-43.07
1.5	10.81	n/a	n/a	-63.76
2.0	8.40	n/a	n/a	-84.23
2.5	5.95	n/a	n/a	-104.61

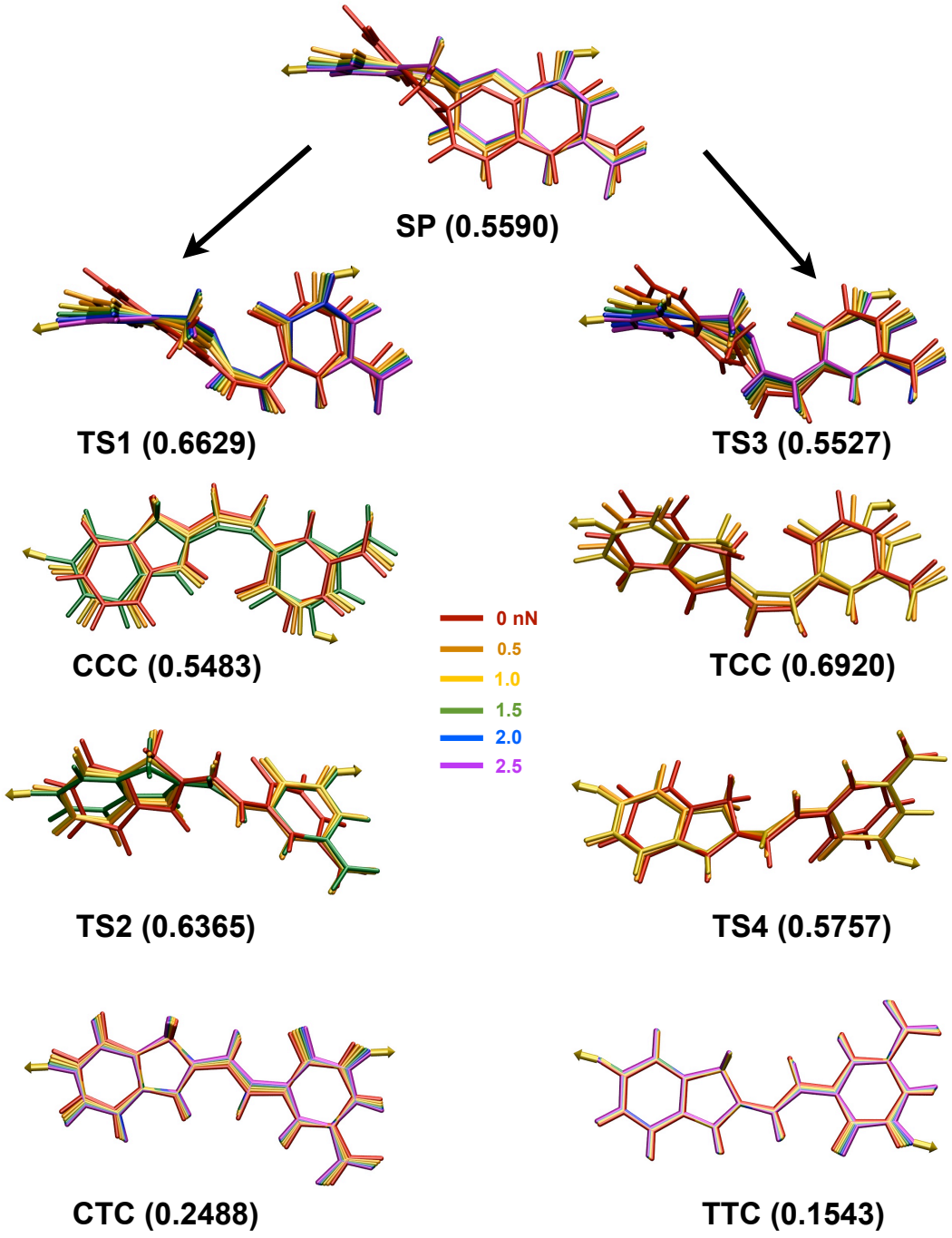

Figure 4.9: SIM1 Reactant, transition state, and product geometries on the FMPES at forces ranging 0-2.5 nN along the SP → CCC → CTC and SP → TCC → TTC reaction route. The force free geometries are denoted in red, which deviate under applied force. The root mean square deviation (RMSD) with respect to the zero force geometry is indicated in parentheses.

Further TDDFT calculations of both the cis-cisoid and trans MC minima were determined at various forces. Figure 4.10 plots the calculated absorption wavelength as a function of the conformer along the reaction path. In the absence of force the absorption wavelength of SP is 339 nm, which increases to 488 nm and 417 nm for CCC and TCC respectively. The trans MC conformers have equal values of 448 nm. At applied forces of 1 nN, the wavelength for SP is blue shifted to 265 nm, remaining unchanged at increasing forces. Interestingly, the cis-cisoid conformers have wavelengths at 475 nm and 435 nm, which are in range of the MC isomers with wavelengths of 446 nm and 448 nm. However, the excitation energies for the cis-cisoid isomers have transition probabilities that are roughly half compared to the MC conformers. Appendix B provides further information regarding the wavelengths and oscillator strengths for these conformers at forces between 0-2.5 nN. In addition, the cis-cisoid conformers have transition probabilities at lower wavelengths. The lower conformer stability with respect to the trans MC indicates that the cis-cisoid conformers may elude spectroscopic characterization at timescales corresponding to experimental visible absorption measurements.

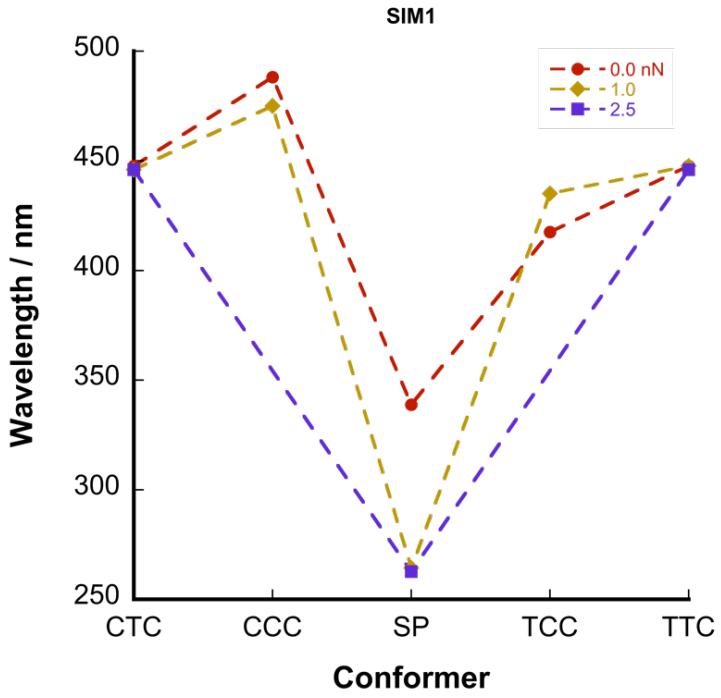

Figure 4.10: SIM1 calculated absorbance wavelength as a function of the conformer. The wavelength for SP at zero force is blue shifted at forces of 1 and 2.5 nN. The wavelengths for the trans MC isomers CTC and TTC corresponds to the $\pi \rightarrow \pi^*$ transition. The cis-cisoid conformers, CCC and TCC, have wavelengths similar to the trans MC isomers, although with transition probabilities that are a factor of two less.

The hyper-dimensionality of the PES indicates that several modes of activation (e.g. bond stretching) may exist for a reaction pathway. The nature of the reactants and products in addition to the information provided by AISMD, suggested two possible torsional modes ,$\boldsymbol{\alpha}$ and $\boldsymbol{\beta}$, which correspond to Spiro C-O cleavage and C-C isomerization respectively. To better explore and visualize the local topography about the SP, cis-cisoid, and trans minima, a set of interpolated geometries between each minima were generated by varying the dihedral angles, $\boldsymbol{\alpha}$ and $\boldsymbol{\beta}$, within a specified range (see Appendix C for further discussion). A grid of isotropic points or geometries was generated via the interpolation scheme, and the force free interaction energy was calculated for each point. The force free 2-D PES is shown in figure 4.11. To visualize how the contours change under applied force, an energy correction due to force was added to each point. A 2-D representation of the FMPES (Figure 4.11) in addition to the angles extracted from the MEP for a specified force, illustrates how force alters the reaction pathway by altering the energy landscape.

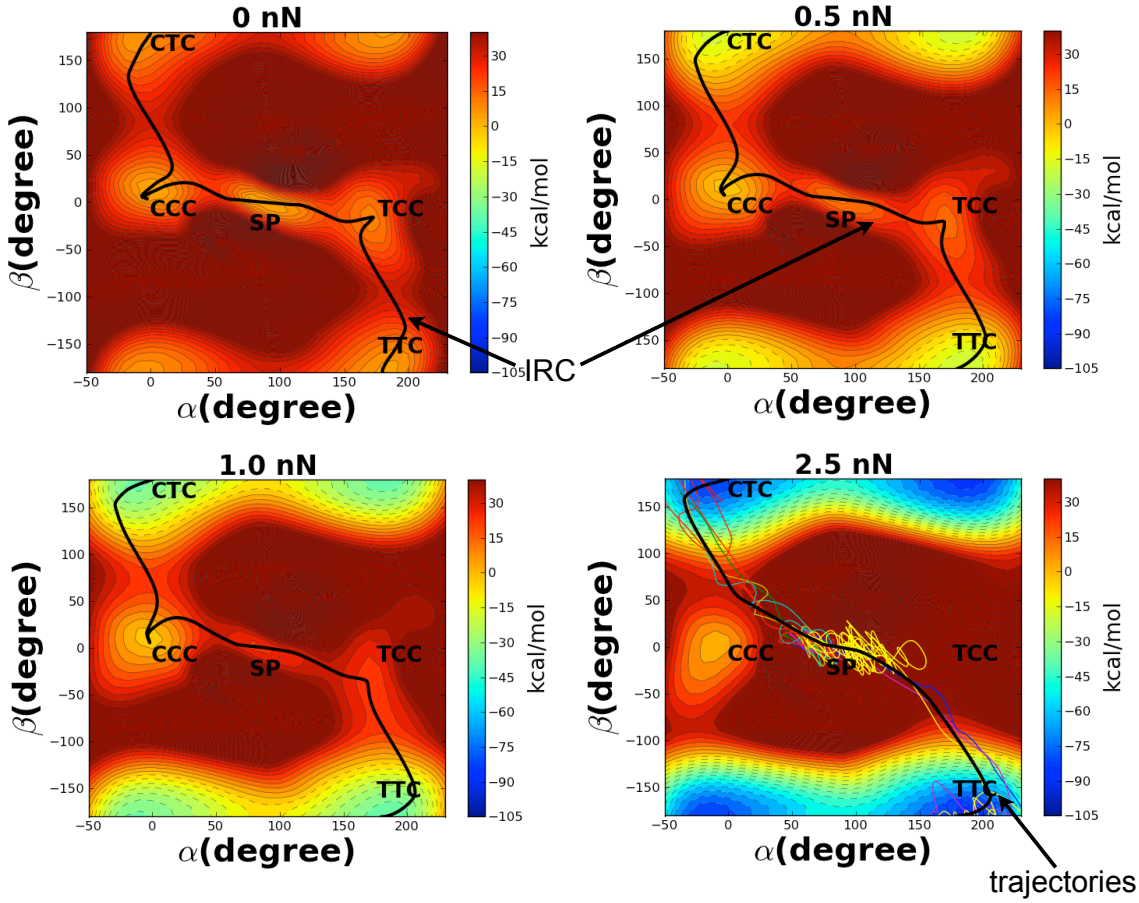

Figure 4.11: SIM1 2-D FMPES contour plot. The solid black line corresponds to the IRC pathway. A 0.5 nN force results in destabilization of the CCC and TCC conformers, which increase in energy with respect to SP while the trans CTC and TTC isomers lower in energy, respectively. The reaction path towards the TTC isomer at 1 nN indicates an energetically unstable flat region near TCC. In contrast, the CCC minima is slightly more stable and about 10 kcal/mol below SP. At 1 nN, The trans minima lie about 40 kcal/mol below SP. Steered molecular dynamics trajectories are shown at 2.5 nN indicating how reaction dynamics stay close to the minimal energy pathway.

At no force, it is evident from the local minima that SP may pass through one of two transition states (TS1 or TS3) whereby the $\boldsymbol{\alpha}$ angle decreases or increases. One of the two cis-cisoid conformers may form, since other regions around SP are highly unstable. The latter transitions reflect the breakage of the C-O bond. From any of the cis-cisoid conformers, isomerization may proceed by increasing or decreasing the $\boldsymbol{\beta}$ angle to the trans MC isomers, CTC or TTC. With the external force correction at 0.5 nN, there is added stability to the trans MC isomers whereas the well around the cis-cisoid conformers becomes broader and

unstable. At 1 nN, the energy well about the CCC conformer remains with an evident barrier to the trans MC CTC. However, the TCC minimum at 1 nN is noticeably flat and the contorted MEP still passes across the shallow barrier (Figure 4.9). Forces exceeding 1 nN, indicate that the MEP for both pathways will bypass the intermediate minima.

SIM1 AISMD simulations show how applied force can selectively cleave the Spiro C-O bond resulting in the formation of the trans MC isomers, CTC and TTC. Trajectory analysis indicates that both pathways are equally likely at forces exceeding 1.5 nN. As figure 4.8 suggests, this is attributed to the nearly equal Spiro C-O barriers. The MEP on the FMPES at 2.5 nN clearly indicates that the trans isomers are relatively more stable with respect to SP. These results are in accord with SP bulk experiments, whereby a macroscopic stress was applied to a bulk polymer containing polymer chains linked at the SIM1 APs, which resulted in a localized color change.[1, 7] Although, dynamics simulations predict color generation, the range of applied forces accessed in experiment is unclear. The force-barrier relationship, in the limit of no force, is further studied to better understand the mechano-chemical reaction rates for color generation.

4.4 SIM1 Reaction Rates under External Force

Various studies have exploited the relationship between applied force and barrier heights, which have led to the development of rate models for chemical processes.[6, 8–17] In the context of the recent experimental and theoretical studies, the effect of an applied force has been shown to result in increased reaction rates. Concerning the mechanochemical activation of mechanophores, canonical transition state theory is utilized (Chapter 2.5) to provide the reaction rates as a function of force. The rate requires information on the activation barrier height, which can be extracted by obtaining the absolute energies of the reactant connected to the transition state on the FMPES. The SP reaction mechanism involves transitions over multiple barriers, which may diminish with applied force (Table 4.2 and 4.3), necessitating the importance of accounting for the activation barriers, which determine the rate-determining step. This is apparent for forces less than 1 nN, where the absolute energy of the TS corresponding to the C-C isomerization barriers may be relatively greater than the Spiro C-O barriers.

Figure 4.12 plots the activation barrier heights, with zero point energy correction, as a function of force for both pathways. At no force, the barrier heights correspond to the TS that reflect C-C isomerization (Figures 4.13 and 4.14) as opposed to the TS with modes for C-O dissociation. Therefore, the activation barriers energies are the difference between SP $\rightarrow$ TS2 and SP $\rightarrow$ TS4. The activation barrier heights are 28.49 and 28.17 kcal/mol

towards the CTC and TTC product. These are in good agreement with the experimentally determined activation energies of 26.8 and 27.8 kcal/mol for thermal coloration.[18] However, an applied force at 0.5 nN reverses the order of the activation barriers for the SP → CCC → CTC pathway only. The activation barrier is the difference from SP → TS1 which reflects the C-O dissociation (Figures 4.15 and 4.16, Tables 4.2 and 4.3) equal to 13.90 kcal/mol. With respect to the SP → TCC → TTC pathway at 0.5 nN, the activation barrier is the difference between SP → TS4. The TS is the C-C isomerization mode and the relative barrier is 14.25 kcal/mol. At 1 nN, TS1 and TS3 are the C-O activation barriers for both pathways and therefore rate determining. As figure 4.15 and 4.16 suggest, the frequencies for the TS referring to the C-C isomerization modes, have reduced considerably by hundreds of wavenumbers. Forces greater than 1 nN indicate only single barrier transitions corresponding to C-O dissociation, figure 4.17.

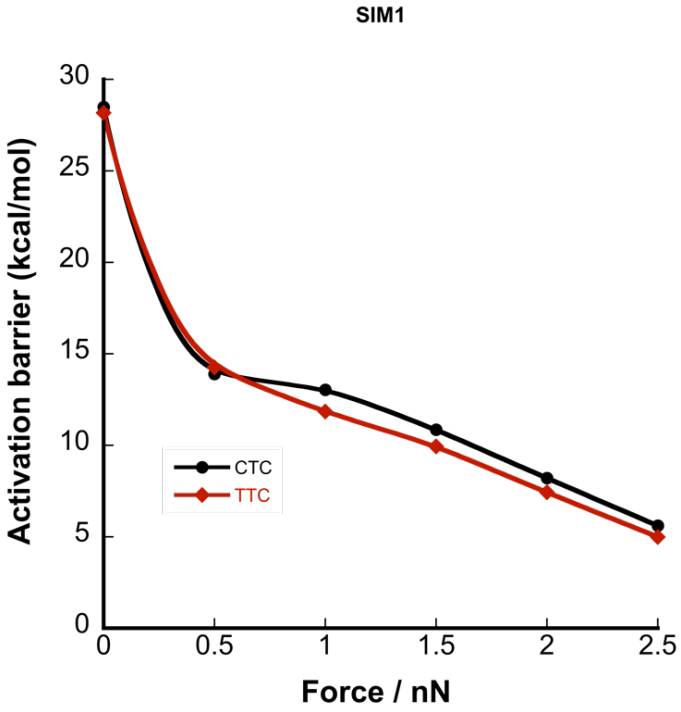

Figure 4.12: SIM1 activation barrier heights as a function of applied force. The force free barrier is the energy difference between SP and the TS for C-C isomerization for both reaction pathways. However, at applied forces equal to 0.5 nN or greater, the activation barrier for each process is now the difference in energy between SP and the TS for C-O bond dissociation.

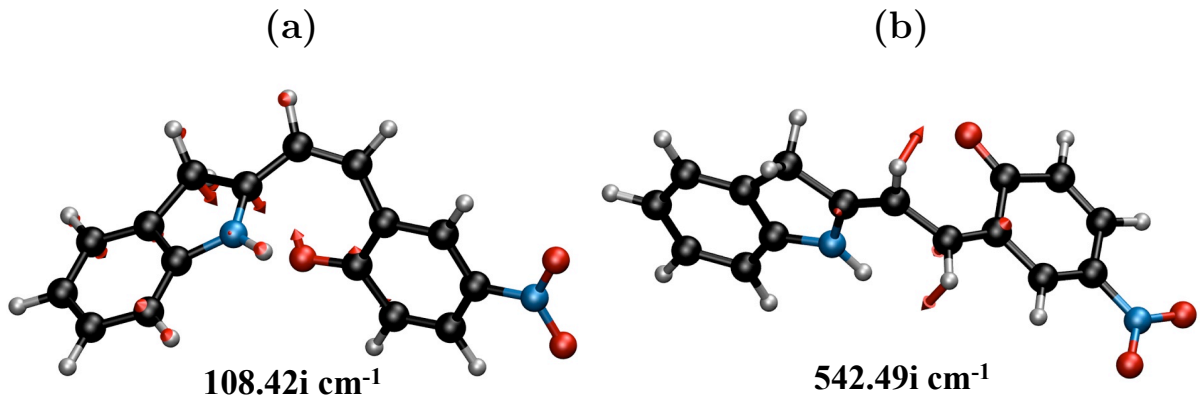

Figure 4.13: Transition state geometries at zero force showing the normal modes (red arrows) for transitions states along the SP → CCC → CTC pathway. The imaginary frequencies are denoted by (i) **a**, TS1 reflects the Spiro C-O cleavage mode while **b**, TS2 is the C-C isomerization mode towards the CTC isomer.

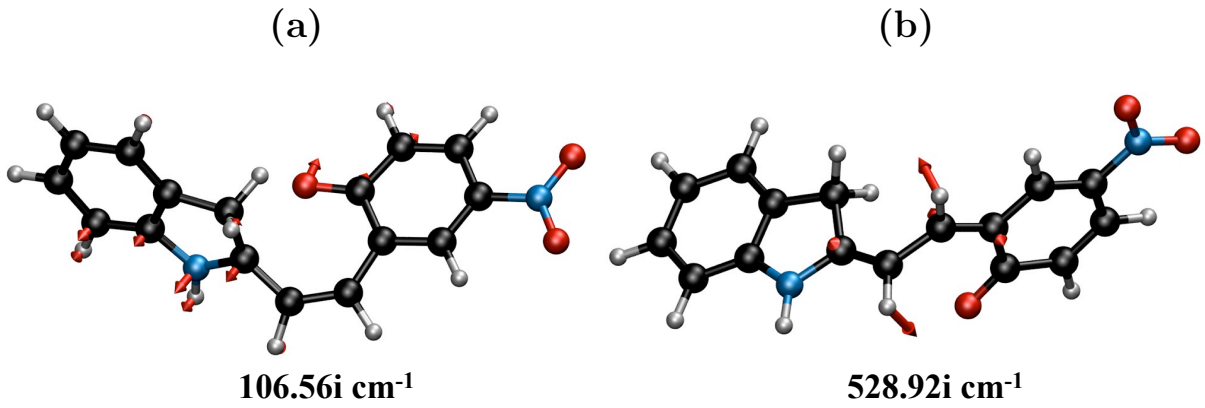

Figure 4.14: Transition state geometries at zero force showing the normal modes (red arrows) for transitions states along the SP → TCC → TTC pathway. **a**, TS3 reflects the Spiro C-O cleavage mode towards TCC and **b**, TS4 is the C-C isomerization mode towards the TTC isomer.

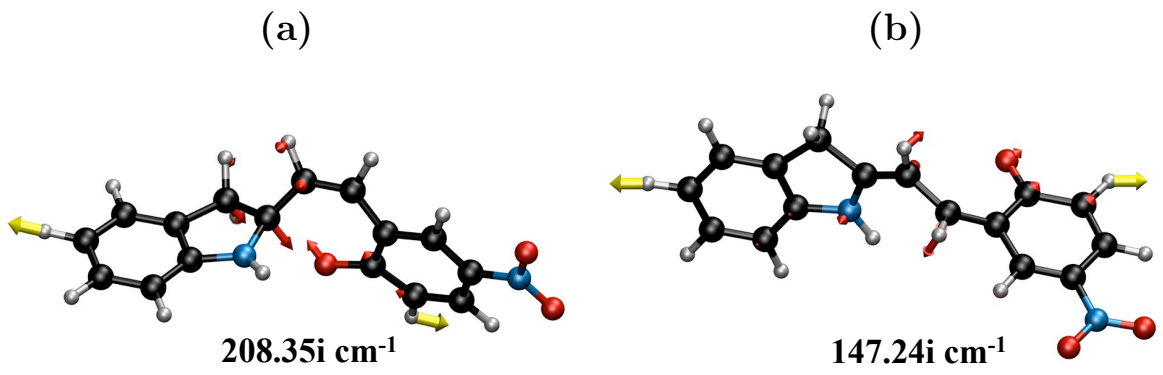

Figure 4.15: 1 nN normal modes for transitions states along the SP → CCC → CTC pathway. The normal modes are indicated by the red arrows and with applied force at the H atoms (yellow arrows). **a**, TS1 reflects the Spiro C-O cleavage mode while **b**, TS2 is the C-C mode towards the CTC isomer. With respect to the zero force pathway, there is a reduction in the frequency and magnitude of the normal mode vector.

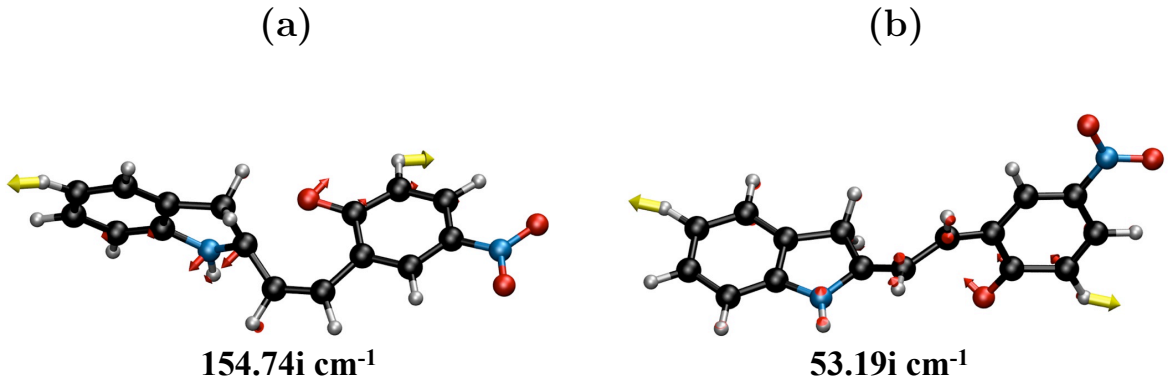

Figure 4.16: 1 nN normal modes (red arrows) for transitions states along the SP → TCC → TTC pathway. The yellow arrows denote applied force at the H atoms. **a**, TS3 reflects the Spiro C-O cleavage mode towards TCC and **b**, TS4 is the C-C isomerization mode towards the TTC isomer. With respect to the zero force pathway, there is a reduction in the frequency and magnitude of the normal mode vector.

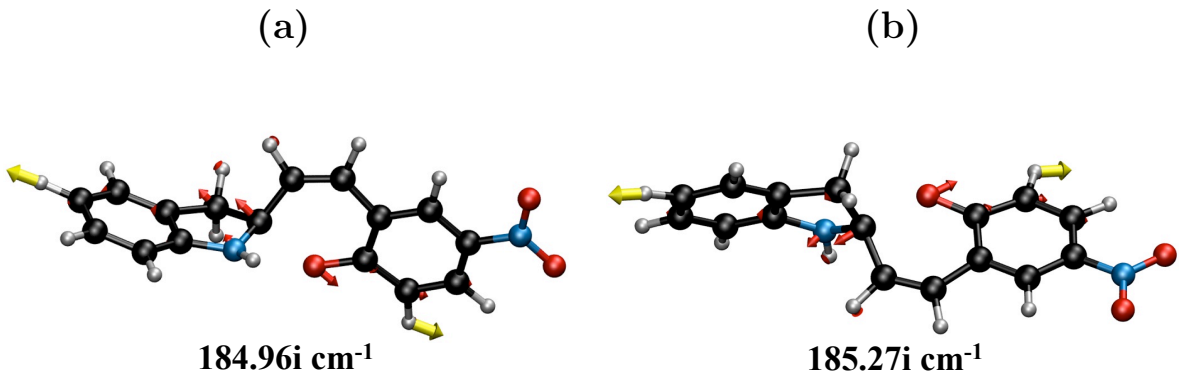

Figure 4.17: Transition states at 2.5 nN along the SP → CTC and the SP → TTC pathway. The normal modes are indicated by the red arrows and with applied force at the H atoms (yellow arrows). **a**, TS1 reflects the Spiro C-O cleavage mode while **b**, TS3 is the C-O mode towards the TTC isomer.

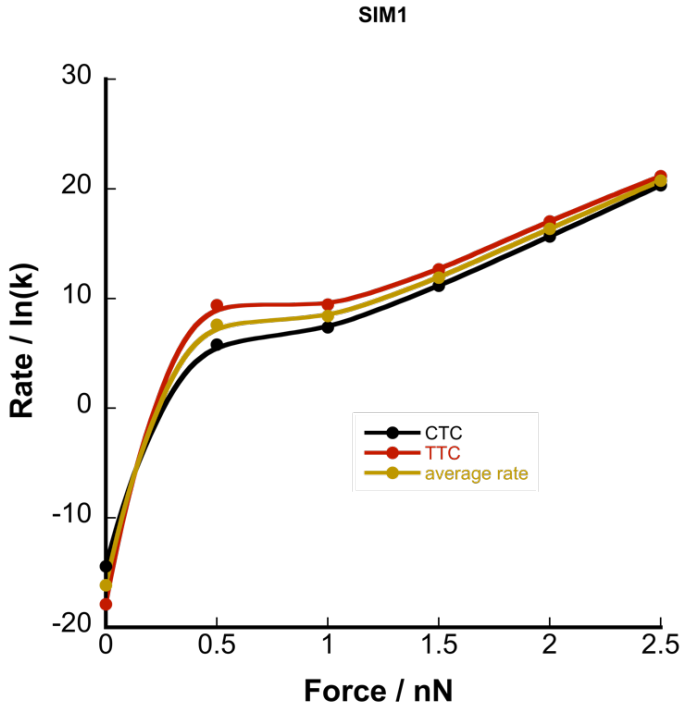

Figure 4.18: SIM1 reaction rate as a function of applied force. The reaction rate is dependent on the activation barrier height, which is shown in figure 4.12. The solid black line is the rate of ring opening towards the CTC isomer, whereas the solid red line reflects opening to the TTC isomer. The solid yellow line is the average rate for ring opening of CTC and TTC. The relationship between rate and force is linear at forces of 1 nN or greater, where the rate is dependent on the C-O barrier height.

Table 4.4: SIM1 lifetime of color formation in units of seconds.

Force	CTC	TTC	average
0	1.84e+06	5.85e+07	1.04e+07
0.5	3.04e-03	8.28e-05	5.02e-04
1.0	6.25e-04	7.85e-05	2.21e-04
1.5	1.43e-05	3.18e-06	6.73e-06
2.0	1.56e-07	3.99e-08	7.89e-08
2.5	1.47e-09	6.49e-10	9.78e-10

The rate of coloration as a function of force at 298 K is shown in figure 4.18 for both reaction pathways corresponding to formation of the CTC and TTC products. It is evident that the force free rate for ring opening to CTC is one order of magnitude less than the TTC transition (Table 4.4). The calculated rate for color formation towards the CTC isomer is $5.44e^{-7}$ sec^{-1}, which is in reasonable agreement with the experimental value of $3.2e^{-6}$ sec^{-1}. The calculated rate for TTC formation is one order of magnitude smaller at $1.71e^{-8}$ sec^{-1}. This is consistent with experimental studies that support the stabilization of SP, however, these studies account for an SP with methyl groups on the indole ring, which results in the absence of the TCC minima as discussed in chapter 6. For the experimentally studied SP mechanophore, which includes methyl groups, it is expected the force free rate would be similar (Chapter 6) since the activation barrier at zero force still depends on the TS along the C-C isomerization mode. At an applied force of 0.5 nN the average rate increases substantially and the rate of color formation is predicted to occur within 0.5 milli-seconds. As discussed in chapter 2, 0.5 nN is the minimal entropic force required to elongate a polymer chain. These forces are enough to induce color generation, however, only a fraction of the chains may experience this force due to the nature of the polymer network (e.g. chain entanglements and cross-linking).[19] The lifetimes of CTC and TTC formation at various forces are shown in table 4.4. The rate increase is attributed to the decreasing C-C isomerization barriers where at forces of 1-1.5 nN they are nearly absent. The C-O barriers decrease linearly between forces of 1.5-2.5 nN and consequently the rate for both pathways increase linearly.

4.5 Ab Initio Steered Molecular Dynamics of SIM2

AISMD simulations were followed for the SIM2 pulling scheme, which have the APs at 5' and 7 in figure 1.2. This differs from SIM1 where the pulled H atom is one bond further away from the Spiro C-O bond. An applied force of 1-4 nN was used for the simulations to explore the mechanochemical reactivity as shown in figure 4.19a. The minimal force for C-O bond rupture within a 500 ps timescale is 2.5 nN, similar to that of SIM1. However, the rupture distribution is broader compared to SIM1 and forces at 3 nN or greater result in cleavage of the C-O at timescales less than 200 fs. At forces equal to or less than 2.5 nN, longer timescales are required to break the C-O, e.g. 300-600 fs.

The C-O bond distance was monitored as a function of time for thirty trajectories at an applied force of 2.5 nN, shown in figure 4.19b. SIM2 shows C-O bond breakage at 400 fs, in contrast to SIM1 which occurs approximately at 200 fs. The $\boldsymbol{\alpha}$ and $\boldsymbol{\beta}$ angles were monitored for all trajectories, shown in figure 4.20, which like SIM1 exhibits the competition of two reaction pathways where two different MC trans isomers may form. With respect to the reaction path that leads to the CTC isomer, following C-O bond cleavage, SP proceeds to the cis-cisoid CCC conformer whereby the $\boldsymbol{\alpha}$ dihedral angle decreases. Unlike SIM1, the stabilization of the cis-cisoid minima is apparent for a few trajectories where the dihedral angles are equivalent to the force free CCC. Figure 4.21, illustrates C-O bond cleavage followed by formation of the CCC conformer and subsequent isomerization to CTC. One trajectory was able to bypass the CCC minima and complete C-C isomerization to the CTC trans isomer, analogous to SIM1 (Figure 4.22). The 2-D trajectory plot would suggest that the C-C isomerization from CCC $\rightarrow$ CTC is the preferred pathway at lower forces. The alternate reaction path to TTC did not indicate TCC stabilization, since $\boldsymbol{\alpha}$ increases and $\boldsymbol{\beta}$ decreases simultaneously, like SIM1, suggesting a concerted ring-opening process (Figure 4.23). The distribution of CTC and TTC products is shown in figure 4.24. Of the thirty trajectories, seventeen followed the pathway to CTC; however, five trajectories remained trapped at CCC and one trajectory was unable to undergo ring-opening. Figure 4.24, illustrates the suggested mechanism for the simulations at 2.5 nN along with the trajectory breakdown. Since the SIM2 simulations indicate CCC stabilization, a CCC $\rightarrow$ CTC isomerization barrier is present even at forces of 2.5 nN. The cis-cisoid trapping may likely inhibit the rate of color formation at lower forces.

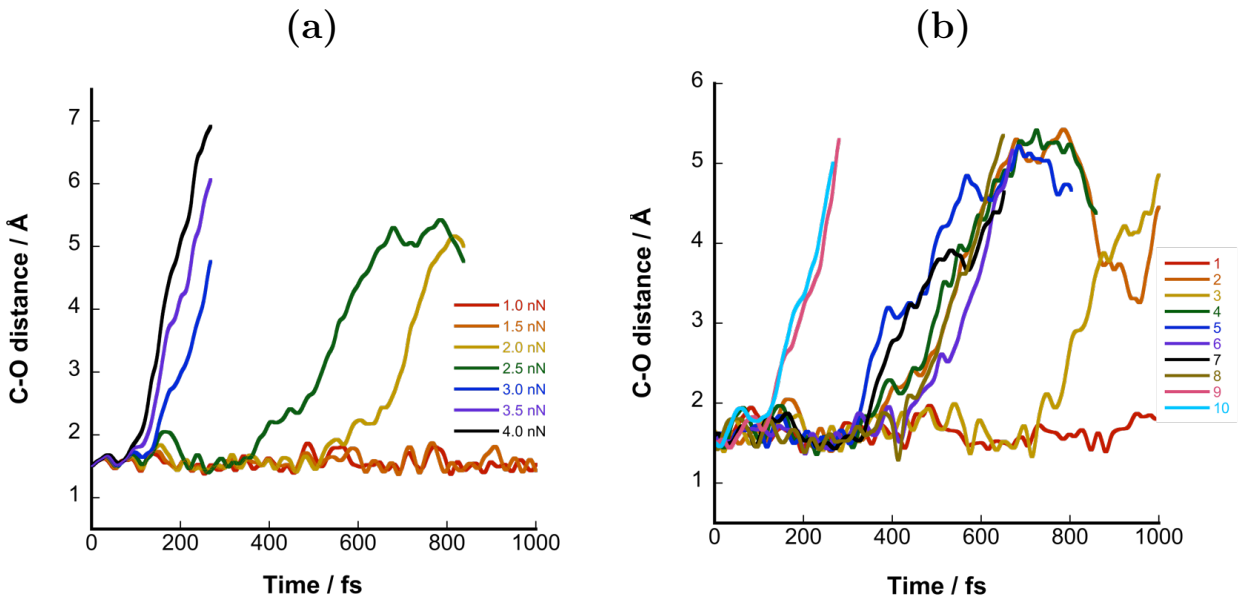

Figure 4.19: SIM2 reaction outcome **a**, External force between 1-4 nN (colored lines) is applied for one SIM2 trajectory in which the C-O bond distance is monitored as a function of time. Within 1 ps the Spiro C-O bond breaks with a minimal force of 2 nN. **b**, The C-O distance is plotted as a function of time for ten different trajectories (labeled 1-10) at 2.5 nN which all exhibit C-O bond dissociation.

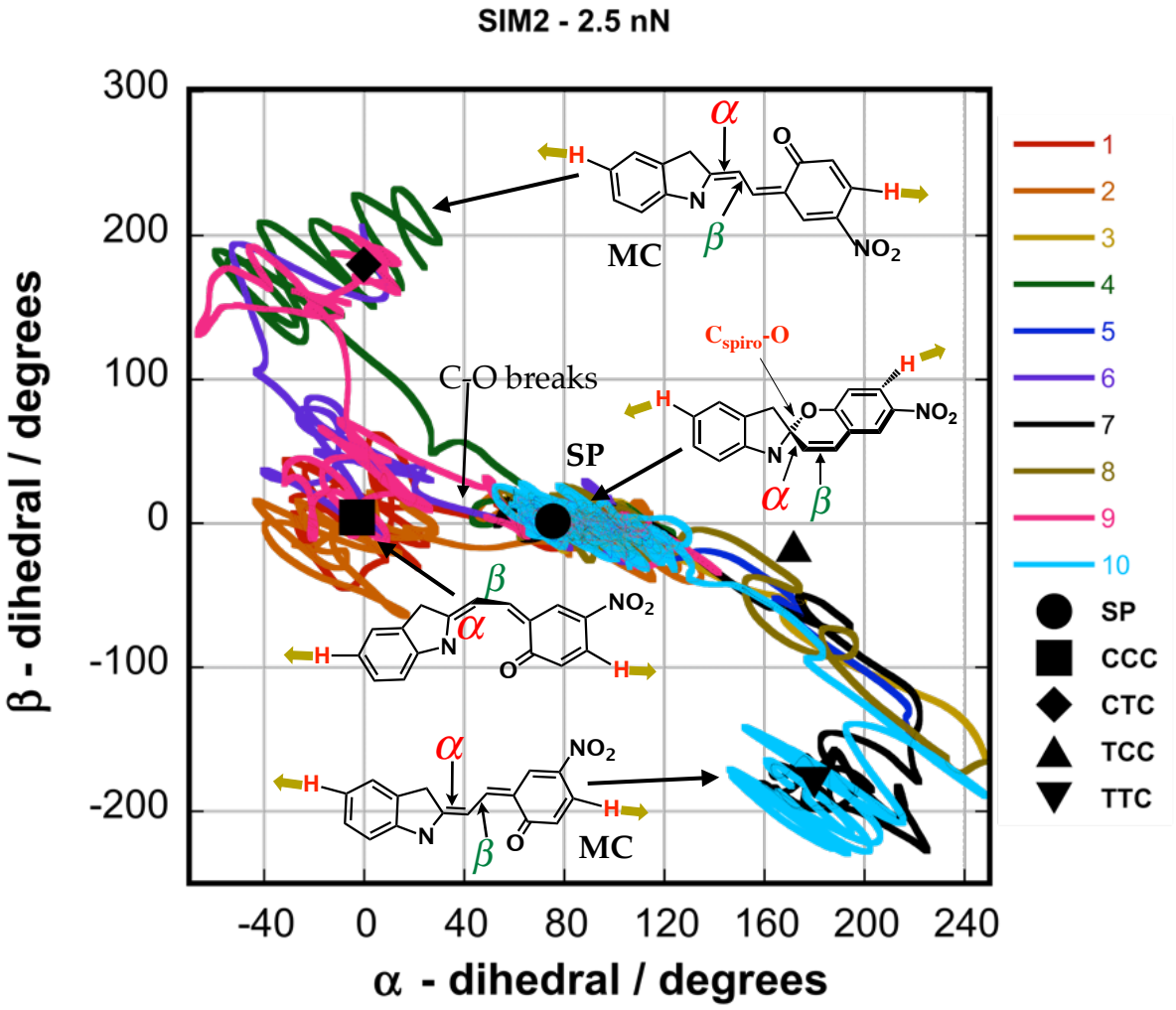

Figure 4.20: SIM2 2-D dihedral angle plot. The equilibrium angles for each minimum (e.g. SP) are indicated by the black markers. The $\boldsymbol{\alpha}$ and $\boldsymbol{\beta}$ angles are shown for ten trajectories (colored lines). Beginning at SP, there are two possible reaction routes towards a particular trans MC isomer, CTC and TTC. Five trajectories reflect the SP $\rightarrow$ CCC $\rightarrow$ CTC whereby most trajectories decreases at the $\boldsymbol{\alpha}$ angle followed by an increase in the $\boldsymbol{\beta}$ angle. Unlike SIM1, C-O bond cleavage and C-C isomerization to CTC do not necessarily occur concurrently since there is indication of CCC stabilization. For the remaining five trajectories, $\boldsymbol{\alpha}$ increases while $\boldsymbol{\beta}$ decreases concurrently towards the TTC conformer, with no evidence of TCC formation.

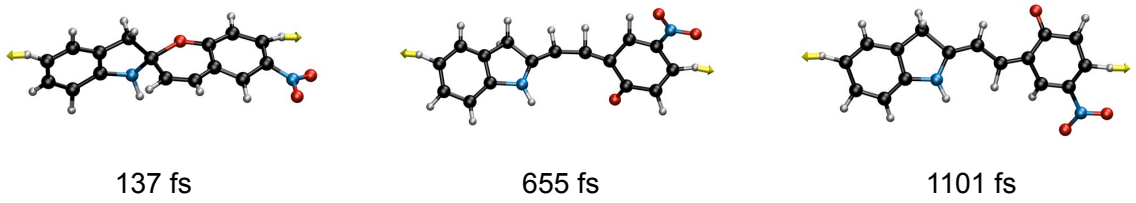

Figure 4.21: SIM2 SP → CCC → CTC reaction path. External force is applied to the H atoms indicated by the yellow arrows. Once the C-O bond is broken the cis-cisoid CCC intermediate is formed at 655 fs and follows C-C bond isomerization to CTC at 1101 fs.

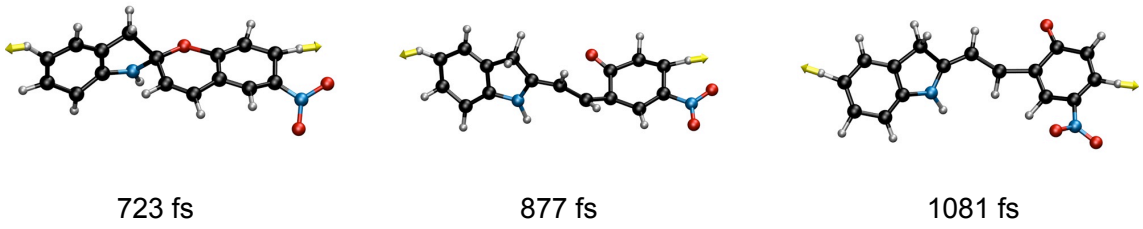

Figure 4.22: SIM2 SP → CTC reaction path. A higher energy reaction route can bypass the CCC intermediate as shown here. The intermediate at 877 fs reflects a pathway where C-O cleavage and C-C isomerization can occur concurrently.

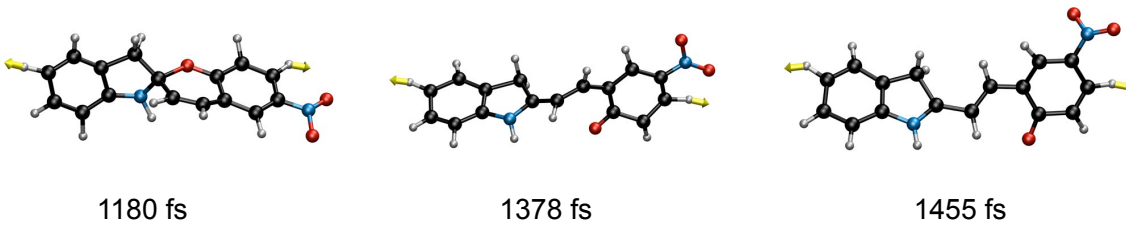

Figure 4.23: SIM2 SP → TTC is the alternate reaction route analogous to SIM1. There is no evidence of any cis-cisoid intermediate, TCC.

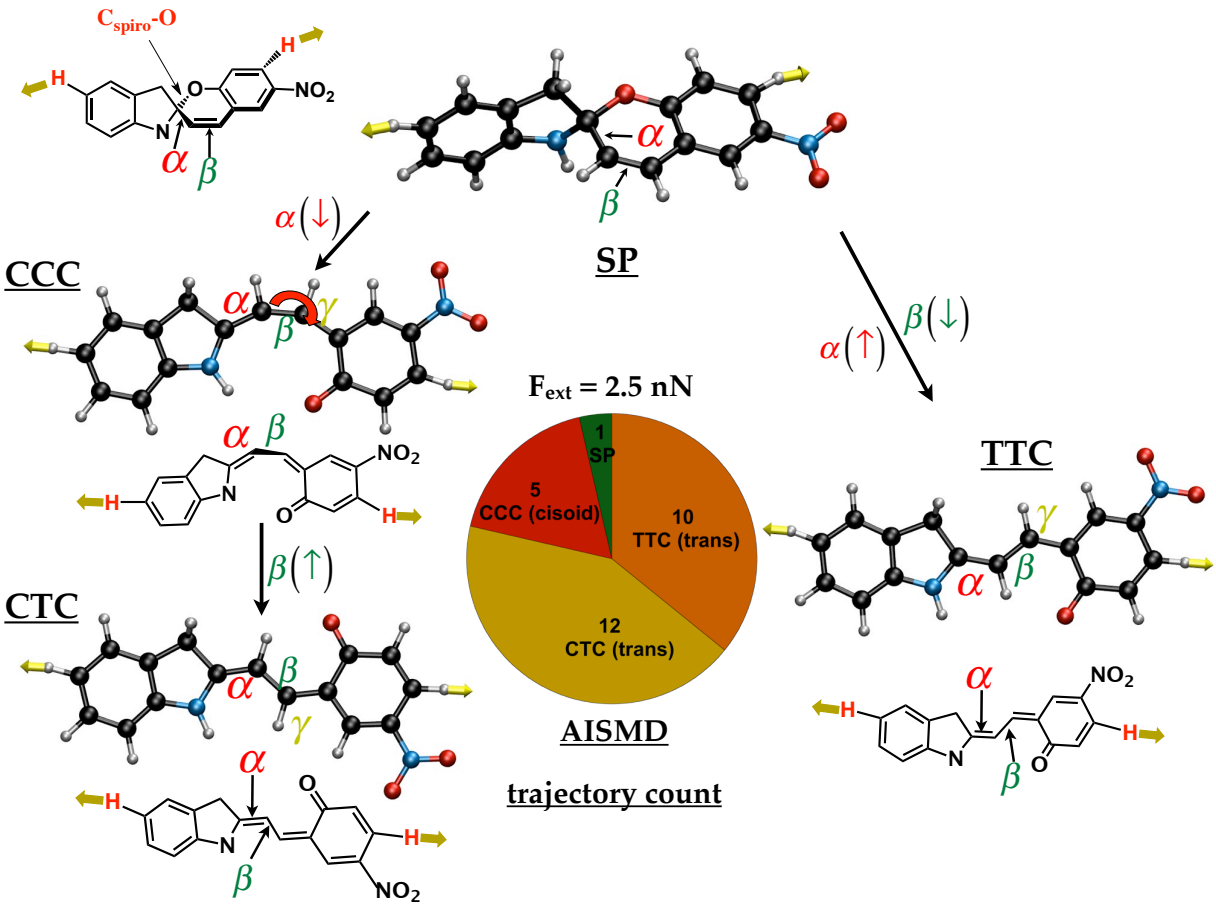

Figure 4.24: SIM2 conformer breakdown for thirty trajectories at 2.5 nN. Two reaction paths are shown: SP → CCC → CTC and SP → TTC. Within 1 ps, seventeen trajectories ring open to the cis-cisoid CCC, however, only twelve isomerize about the C-C bond. Ten simulations follow the alternate pathway to the TTC product, which bypass the cisoid TCC conformer. The six trajectories that did not undergo C-O cleavage or C-C isomerization likely require simulations at longer timescales to observe the trans MC products.

4.6 SIM2 Reaction Pathways on the Force Modified Potential Energy Surface

As discussed previously, the force free energy profile for spiropyran contains five minima (SP, CCC, TCC, CTC, and TTC) and four TSs that lie in between each isomer. The effect of an applied force at the SIM2 APs will not necessarily remove the same stationary points (e.g. CCC minima) on the FMPES (Figure 4.25) like SIM1. This is notable for the reaction pathway to the CTC isomer, whereby the CCC intermediate is present even at forces up

to 2.5 nN (Figure 4.27). Unlike SIM1, the barrier for the CCC → CTC isomerization does not disappear and is 5 kcal/mol at 2.5 nN (Figure 4.26). These results are consistent with AISMD, whereby several trajectories formed the CCC, which was present for over 100 fs before undergoing isomerization. The TCC → TTC isomerization barrier decreases more so with respect to force and is less than 5 kcal/mol at 1.5 nN and barrierless at 2 nN. A similar decreasing trend for the C-O barrier heights is evident for each pathway, like SIM1, which converge to nearly similar values at forces equal and greater than 1.5 nN (Figure 4.26a). Unlike the isomerization barriers, which decrease several kcal/mol at 0 and 0.5 nN, the bond breaking barriers increase slightly from 13.65 to 14.17 kcal/mol towards the CCC transition and 13.03 to 13.32 kcal/mol for the TCC transition (Tables 4.5 and 4.6, Figure 4.26). Figure 4.26b represents the MWD as a function of force where each point reflects the MWD from a given minimum to a respective TS. At forces of 0 and 0.5 nN, the MWD from SP → TS1 decreases from 10.71 to 8.98 Å*amu$^{1/2}$ compared to the SP → TS3 transition which decreases more from 20.89 to 13.21 Å*amu$^{1/2}$. With respect to C-C isomerization the trend is opposite whereby the relative MWD increases slightly from 24.63 to 24.95 Å*amu$^{1/2}$ towards CTC and 13.56 to 13.91 Å*amu$^{1/2}$ for the TTC pathway. Forces greater than 0.5 nN show decreasing barrier heights for all bond breaking and isomerization transitions, which are paralleled by decreasing MWD of the TS states to the respective minima. At 2.5 nN the distance to the TS for both bond breaking pathways are the same, in contrast to isomerization, which differ by as much as 20 Å*amu$^{1/2}$.

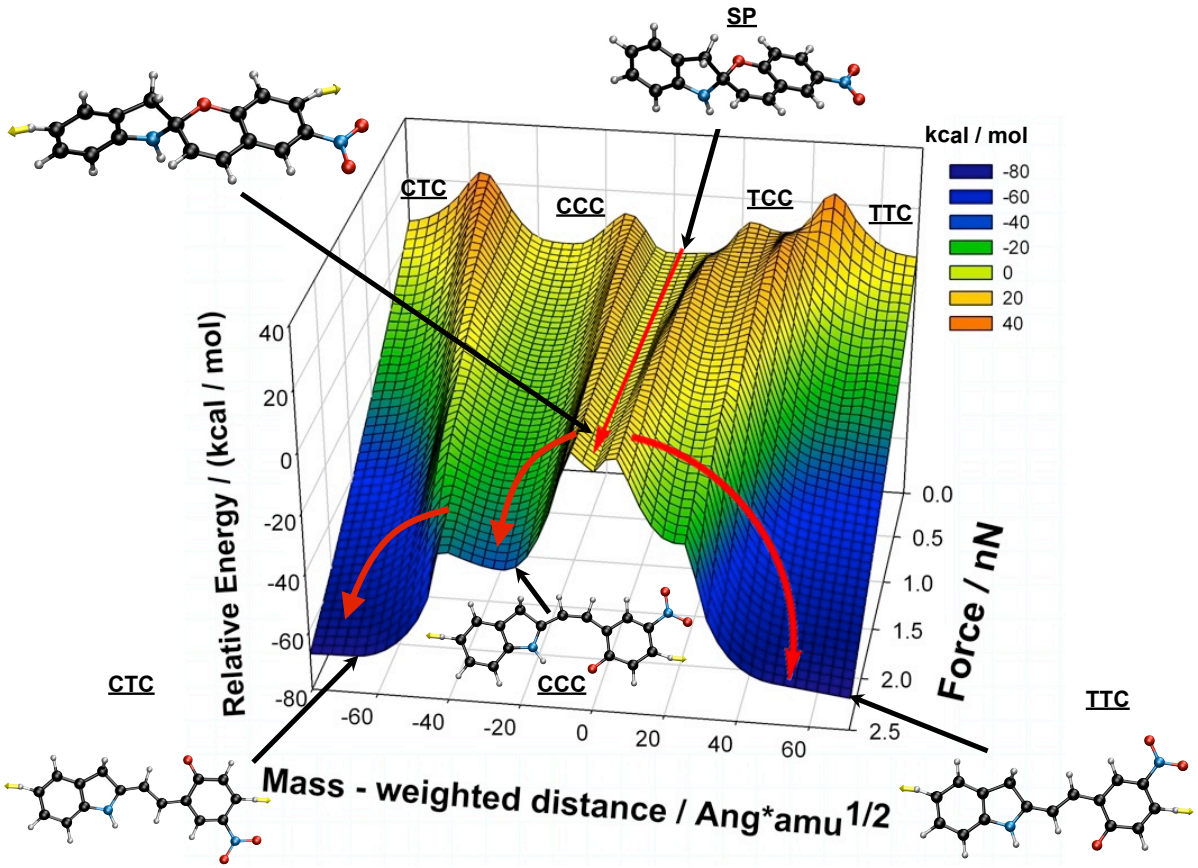

Figure 4.25: SIM2 FMPES. At zero force SP must surmount one of two possible C-O barriers to reach one of the cis-cisoid conformers. Although the latter barriers are approximately equal, the CCC conformer is more stable than TCC. As a result, C-C isomerization to the CTC conformer is greater compared to TTC. Both trans MC isomers are approximately equal in energy with respect to SP. At 0.5 nN the distance to the transition state for the CCC ← SP → TCC transition decreases. The C-O barrier heights for both pathways increase marginally whereas the isomerization barriers decrease respectively. Increased forces gradually results in disappearance of the TCC → TTC barrier and hence the TCC cis-cisoid intermediate. This in contrast to the CCC → CTC barrier that remains even at large applied forces explaining the observed intermediate in AISMD. For transition towards the CTC isomer, there is a double barrier reflecting the dissociation and isomerization steps. The isomerization barrier for the alternate path TCC → TTC is barrier-less at 2 nN and there is only a single barrier pertaining to SP → TTC.

Table 4.5: Relative energies in kcal/mol (with respect to SP) for minima and transition states along the SP → CCC → CTC reaction path.

Force	TS1	CCC	TS2	CTC
0	14.54	1.08	30.72	5.63
0.5	15.14	-5.82	19.72	-11.85
1.0	14.16	-10.72	8.87	-25.99
1.5	12.03	-16.54	-2.89	-39.83
2.0	9.30	-24.02	-15.45	-53.55
2.5	6.15	-34.06	-28.61	-67.24

Table 4.6: Relative energies of minima and transition states along the SP → TCC → TTC reaction path.

Force	TS3	TCC	TS4	TTC
0	13.91	9.26	30.69	3.79
0.5	14.07	8.94	22.28	-12.53
1.0	13.38	6.33	13.20	-25.94
1.5	11.54	0.33	2.79	-39.25
2.0	9.04	-9.15	-8.74	-52.57
2.5	6.36	n/a	n/a	-65.97

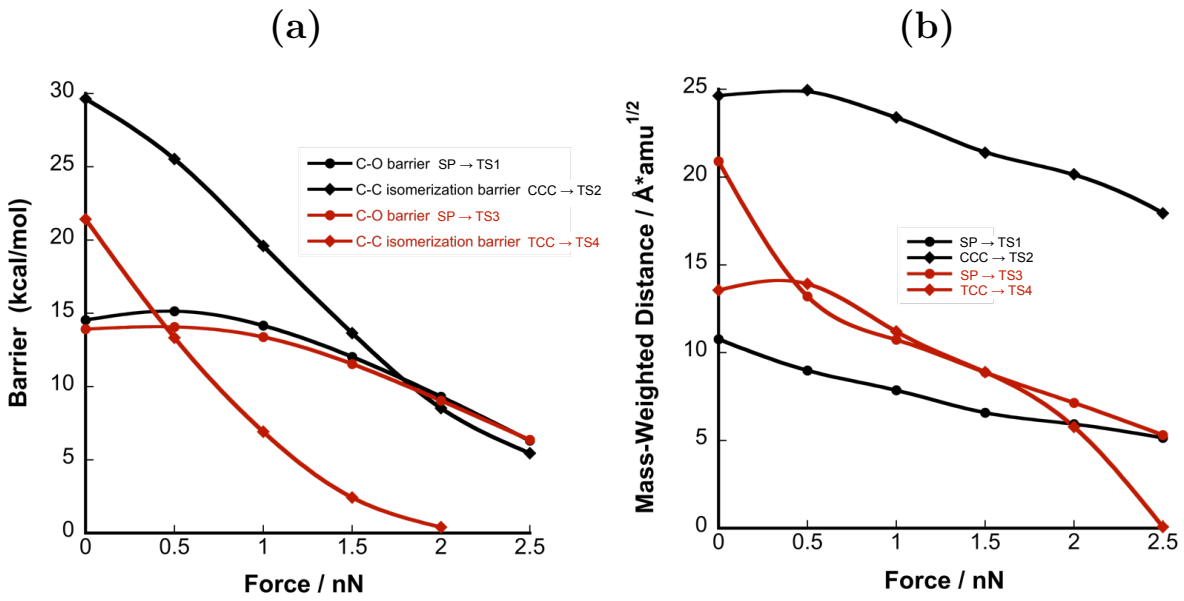

Figure 4.26: SIM2 conformer barrier heights and mass-weighted distance along the MEP with respect to force **a**, The C-O barriers reflect the following transitions: SP → TS1 → CCC and SP → TS3 → TCC cis-cisoid. The C-C isomerization barriers are the following transitions on the MEP: CCC→ TS2 → CTC and TCC → TS4 → TTC trans. The C-O barrier to CCC or TCC increases within 1 kcal/mol at 0.5 nN before lowering at larger forces. The C-C isomerization barrier to TTC is negligible near 2 nN whilst that for CTC lowers to within 5 kcal/mol. **b**, The mass weighted distance (MWD) along the MEP to the transition state with respect to SP or the cisoid conformer. The TCC cis-cisoid minima disappears by 2.5 nN, however, the CCC minima is still present as indicated by the MWD from CCC → TS2.

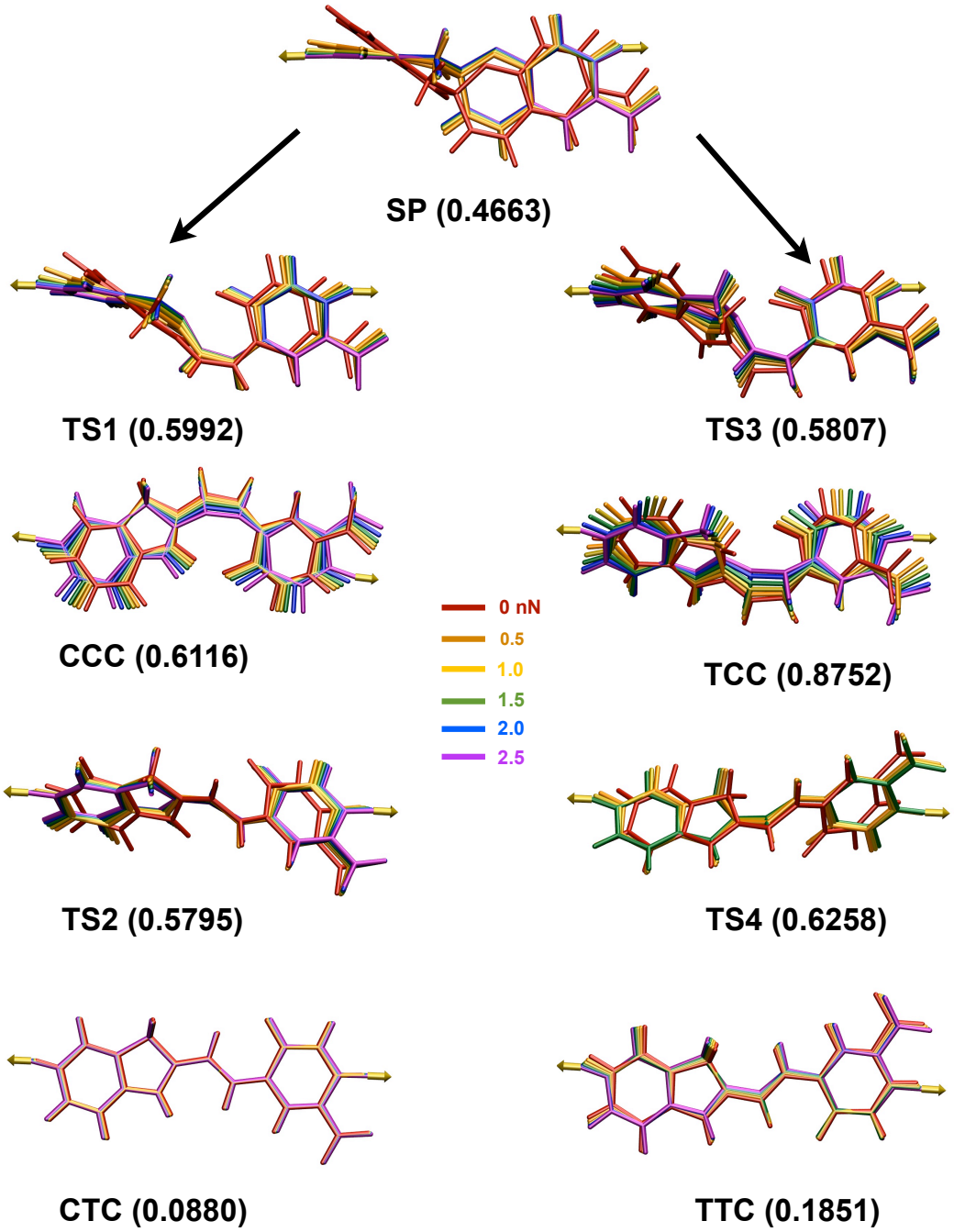

Figure 4.27: Figure 4.27 SIM2 Reactant, transition state, and product geometries at forces ranging 0-2.5 nN along the SP → CCC → CTC and SP → TCC → TTC reaction route. The force free geometries are denoted in red, which are perturbed under applied force. The root mean square deviation (RMSD) with respect to the zero force geometry is indicated in parentheses for each geometry.

The excitation energy for all conformers along both reaction pathways is shown in figure 4.28. The SP wavelength decreases from 339 to 266 nm when the force is increased from 0 to 0.5 nN, and remains constant throughout at increasing forces. The wavelengths for the CCC conformer increases slightly from 488 to 494 nm at 0 and 0.5 nN, however, is blue shifted to 486 and 459 nm at forces of 1.0 and 2.5 nN. In contrast, the TCC isomer becomes increasingly red shifted as the force is ramped upward, from 418 nm at 0 nN to 451 nm at 1.5 nN (see appendix B). The cis-cisoid transition probabilities, however, are half that of the MC isomers since another transition exists at higher energies. The force free MC isomer excitation energy for CTC and TTC is 448 nm which reflects the $\pi \rightarrow \pi^*$ transition. At forces of 2.5 nN, this value is slightly red shifted from 448 nm to wavelengths of 456 nm for CTC and 459 nm for TTC.

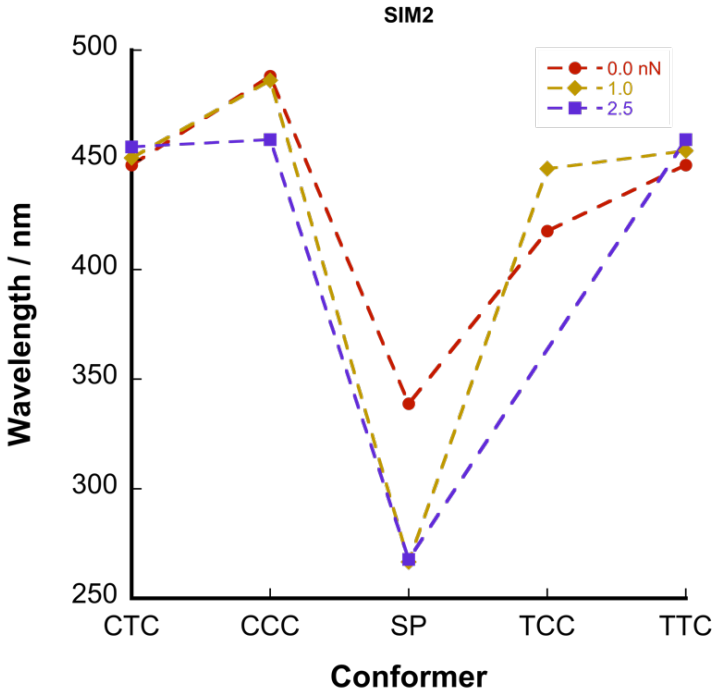

Figure 4.28: SIM2 calculated absorbance wavelength as a function of the conformer. The wavelength for SP at zero force is reduced at forces of 1 and 2.5 nN. The wavelengths for the trans MC isomers CTC and TTC are slightly red shifted, and corresponds to the $\pi \rightarrow \pi^*$ transition. The cis-cisoid conformers, CCC and TCC, have wavelengths similar to the trans MC isomers, however, the transition probabilities are a factor of two less.

A 2-D contour representation of the FMPES is illustrated in figure 4.29, which bears resemblance to SIM1 where the trans MC isomers also become increasingly stabilized with applied force. At 1 nN the ring-opening reaction to trans TTC also shows destabilization of the TCC conformer, shown by the flat region on the FMPES. The TCC minimum becomes

unstable at increased forces as indicated by the higher energy regions near TCC on the contour plot and is absent at 2 nN. Regarding the reaction pathway towards CTC, the CCC minimum is evident even up to forces of 2.5 nN like SIM1, however, the region about the CCC minima is stabilized with respect to SP. The MEP is shown by the $\boldsymbol{\alpha}$ and $\boldsymbol{\beta}$ dihedral angles (solid black line) for both reaction pathways at several forces, which follows along the respective minima and TS. As shown in figure 4.29, reaction dynamics at 2.5 nN follows the MEP on the FMPES for both reaction pathways where the $\boldsymbol{\alpha}$ and $\boldsymbol{\beta}$ dihedral angles are taken at every time step for each trajectory.

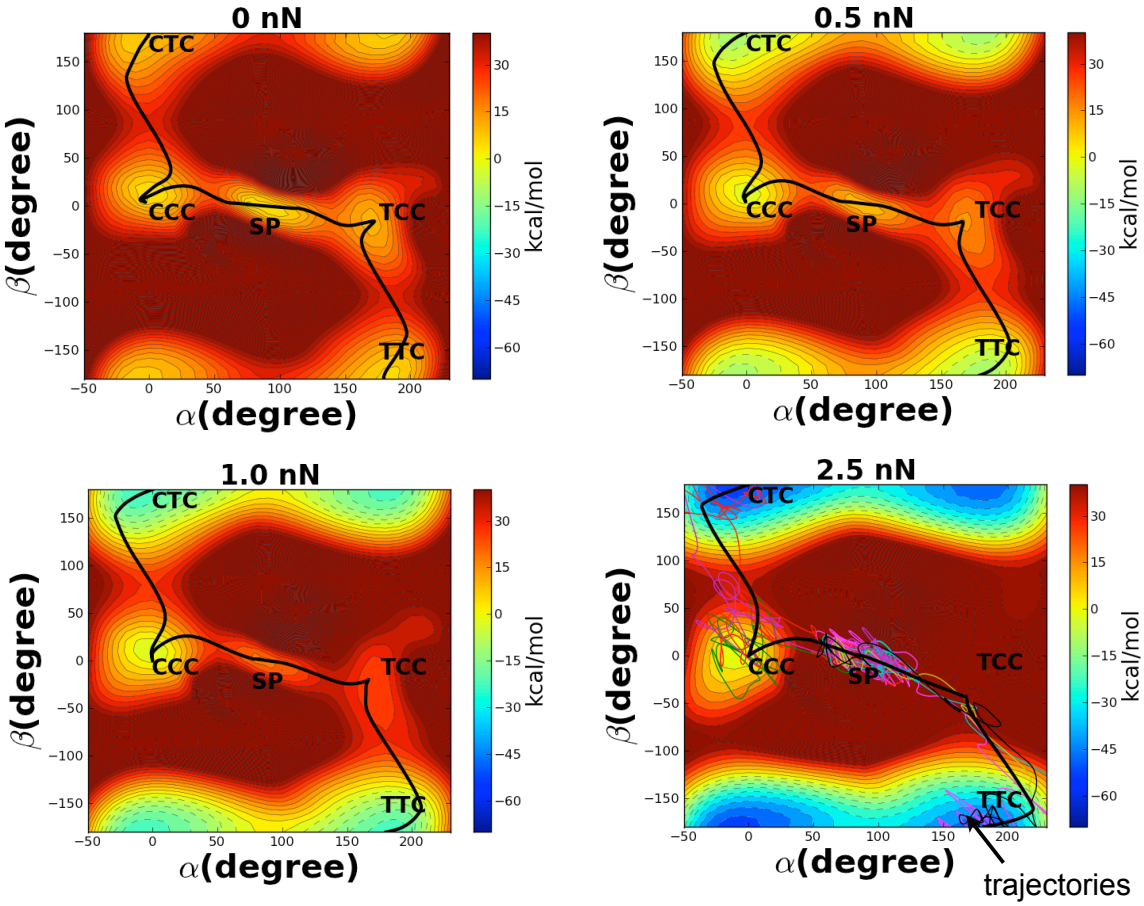

Figure 4.29: SIM2 2-D FMPES contour plot. The solid black line corresponds to the IRC pathway. A 0.5 nN force results in destabilization of the TCC conformer in contrast to CCC which decreases in energy with respect to SP. The trans isomer, CTC and TTC, are stabilized more so than CCC. At 1 nN, the reaction path towards the TTC isomer shows a flat high energy region around TCC. As the force is ramped upward the TCC minima vanishes resulting in a single barrier transition for SP $\rightarrow$ TTC at 2.5 nN. In contrast to the reaction pathway towards CTC, the CCC minima at 1 nN is further stabilized which lies about 11 kcal/mol below SP. Even at 2.5 nN the CCC minima is present and AISMD trajectories indicate this (colored lines) from SP $\rightarrow$ CCC $\rightarrow$ CTC which follow along the MEP. The CTC and TTC minima trans isomers lie about 65 kcal/mol below SP.

4.7 SIM2 Reaction Rates under External Force

The activation barrier heights for both reaction pathways ring-opening to either CTC or TTC, with zero point energy corrections, are shown in figure 4.30. The zero force barriers reflect the C-C isomerization barrier as reported in section 4.4. Applied forces of 0.5 nN

reduced the activation barrier to 17.45 and 20.13 kcal/mol for the CTC and TTC reaction pathway. These barriers reflect C-C isomerization to the MC isomers. The C-O barrier heights are 14.17 and 13.32 kcal/mol for the SP $\rightarrow$ CCC and SP $\rightarrow$ TCC transition, and are not the rate-determining step at 0.5 nN. However, the order of the activation barrier heights reverses at 1 nN. The TS geometries along with the normal modes are shown in figures 4.31 and 4.32. The C-C isomerization barriers are 6.61 and 11.02 kcal/mol towards the CTC and TTC products, which are relatively lower than the C-O barriers at 13.27 and 12.58 kcal/mol. External forces exceeding 1 nN have activation barriers corresponding to the TS that reflect the C-O modes, shown in figures 4.33 and 4.44. The barriers for both transitions are within 1 kcal/mol apart and decrease linearly between 1.0 and 2.5 nN.

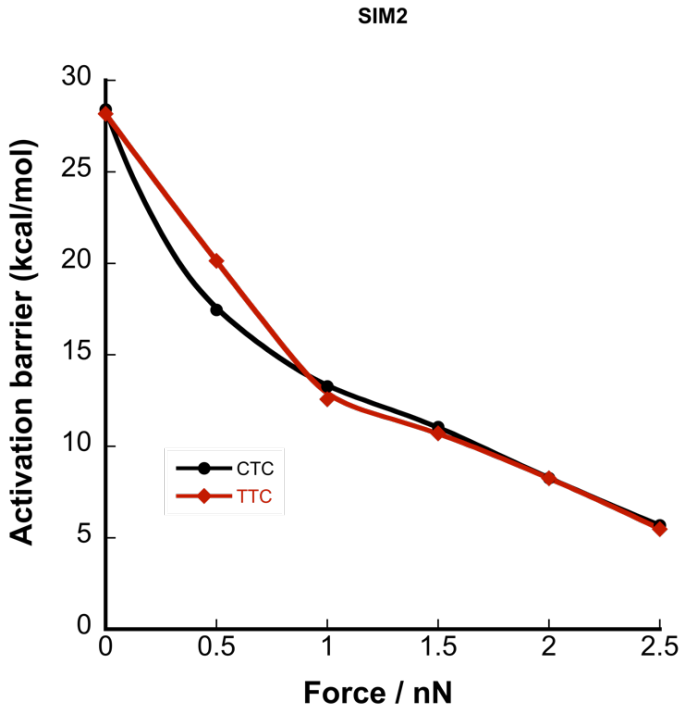

Figure 4.30: SIM2 activation barrier height as a function of applied force. The force free barrier is the energy difference between SP and the TS for C-C isomerization for both reaction pathways. However, at applied forces equal to 1 nN and greater, the activation barrier for each process is now the difference in energy between SP and the TS for C-O bond dissociation.

The rate as a function of force at 298 K (Figure 4.35) for applied forces ranging from 0-2.5 nN is shown for both reaction pathways towards the CTC and TTC products. At applied forces of 0.5 nN, the average rate for color formation increases, with predicted timescales of 0.16 and 16 seconds for ring opening to CTC and TTC respectively. Although the timescales

for ring opening are longer with respect to SIM1 at 0.5 nN, this force would be sufficient to observe color formation at experimental timescales. The reaction rates for CTC and TTC formation for forces exceeding 0.5 nN are shown in table 4.7.

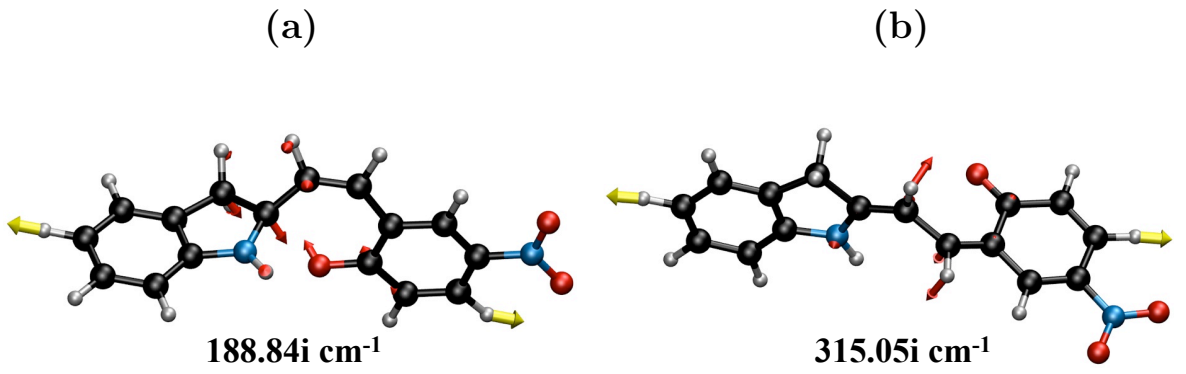

Figure 4.31: 1 nN normal modes (red arrows) for transitions states along the SP → CCC → CTC pathway. The yellow arrows are the external force vectors which are applied to the H atoms. The imaginary frequency is designated by (i). **a**, TS1 reflects the Spiro C-O reaction mode while **b**, TS2 is the C-C isomerization mode.

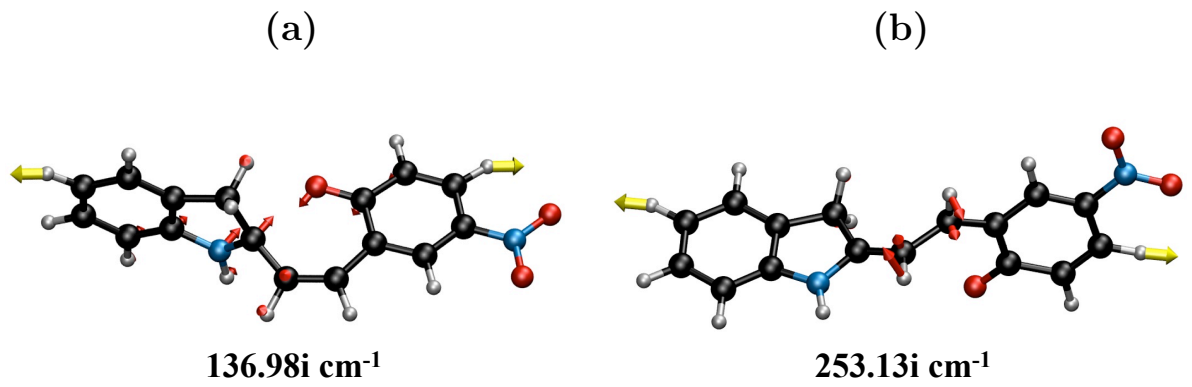

Figure 4.32: 1 nN normal modes (red arrows) for transitions states along the SP → TCC → TTC pathway. **a**, TS3 reflects the Spiro C-O reaction mode while **b**, TS4 is the C-C isomerization mode.

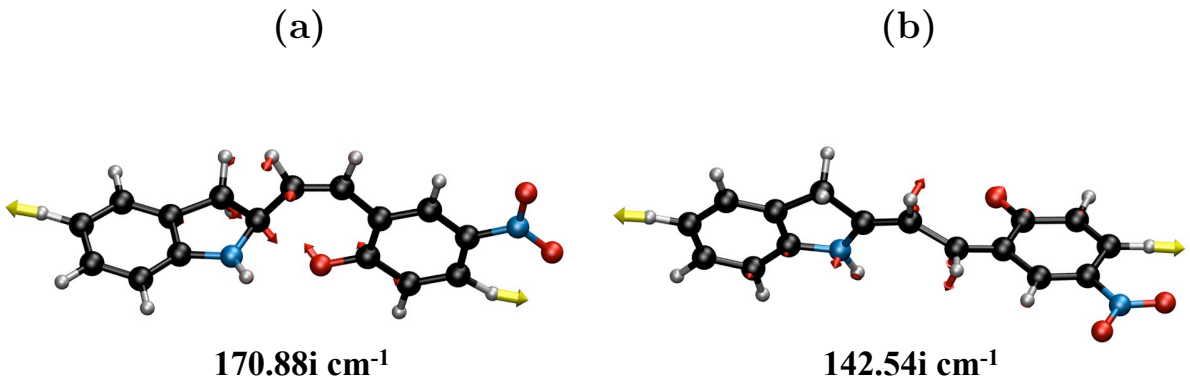

Figure 4.33: 2.5 nN normal modes (red arrows) for transitions states along the SP → CCC → CTC pathway. **a**, TS1 reflects the Spiro C-O reaction mode while **b**, TS2 is the C-C isomerization mode. There is a considerable reduction with respect to the frequency and magnitude of normal mode vector for TS2.

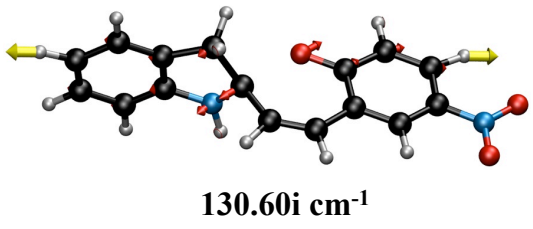

Figure 4.34: 2.5 nN normal modes (red arrows) for transitions states along the SP → TTC pathway. The yellow arrows indicate the points where external force is applied. The geometry shown is the only TS along the TTC pathway, which shows modes that reflect Spiro C-O bond cleavage.

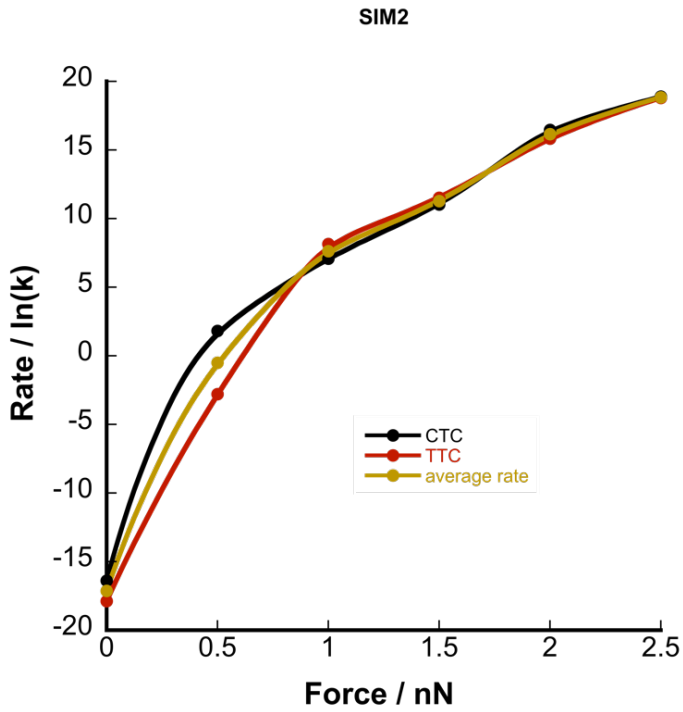

Figure 4.35: SIM2 reaction rate as a function of force. The reaction rate is dependent on the activation barrier height, which is shown in figure 4.30. The solid black line is the rate of ring opening towards the CTC isomer, whereas the solid red line reflects opening to the TTC isomer. The solid yellow line is the average rate for ring opening to CTC and TTC.

Table 4.7: SIM2 lifetime of color formation in units of seconds (s).

Force	CTC	TTC	average
0	1.29e+07	5.85e+07	2.75e+07
0.5	1.64e-01	1.63e+01	1.63e+00
1.0	8.40e-04	2.86e-04	4.90e-04
1.5	1.61e-05	9.94e-06	1.26e-05
2.0	7.07e-08	1.32e-07	9.66e-08
2.5	6.26e-09	6.83e-09	6.54e-09

4.8 Ab Initio Steered Molecular Dynamics of SIM3

AISMD simulations of SP with external force applied to the H atoms connected to the C5' and C5 sites (figure 1.2), called SIM3, was investigated for mechanochemical reactivity. A range of relatively large applied forces from 4-7 nN, with respect to SIM1 and SIM2, were necessary to observe bond cleavage within 500 fs for one trajectory. For this pulling trajectory, a minimal force of 5 nN resulted in cleavage of the terminal C-H bond located on the benzopyran ring (Figure 4.36a and 4.38). Ten trajectories were followed at a force of 5 nN to determine if bond cleavage occurred at any of the terminal C-H bonds. Figure 4.36b indicates approximately eight of ten trajectories underwent C-H cleavage. As shown in figure 4.37, the $\boldsymbol{\alpha}$ and $\boldsymbol{\beta}$ dihedral angles indicate that three trajectories underwent C-O cleavage to form either the CCC or TCC cis-cisoid conformer. However, after formation of the cis-cisoid conformer, bond rupture followed at the terminal C-H bond located on the benzopyran ring (Figures 4.39 and 4.40). Twenty additional trajectories were followed to determine if any of the trans MC isomers were present. Figure 4.41 illustrates the suggested SIM3 reaction mechanism, which shows the respective isomer distribution for all thirty trajectories. Nineteen trajectories did not undergo C-O bond cleavage or ring opening and instead resulted in bond rupture at a terminal C-H bond located either on the indole or benzopyran ring. In addition, figure 4.41 indicates that C-O bond rupture occurred for nine representative trajectories. Two trajectories formed the CCC conformer and subsequently cleaved at the terminal C-H bond at the benzopyran ring. However, seven trajectories underwent TCC formation whereby only two trajectories broke about the terminal C-H bond. The remaining five trajectories underwent C-C bond isomerization from TCC $\rightarrow$ TTC. Given the fraction of trans MC isomers formed and the excessive force applied in the simulation, it is anticipated SIM3 would not transmit force across the C-O bond effectively. The applied force would likely result in cleavage at the C-C bond on the polymer chain or at the terminal end of the mechanophore. Thus mechanochromaticity is not expected for SIM3 and the nature of FMPES is expected to disfavor the pathway towards the MC isomers.

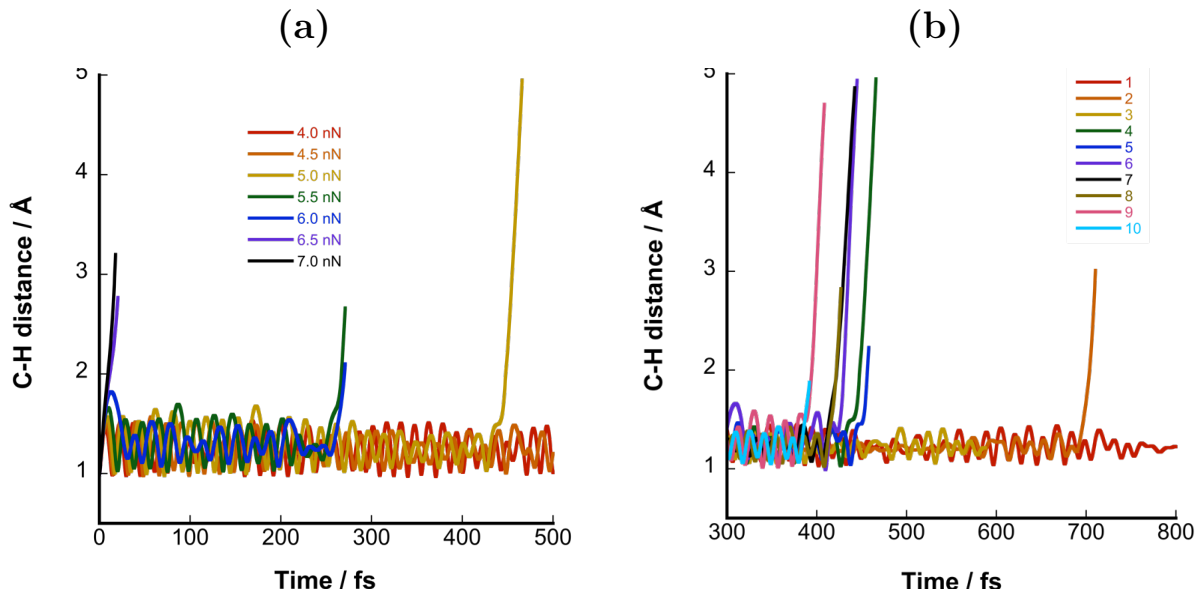

Figure 4.36: The C-H bond, located on the benzopyran ring, is plotted as function of time. **a**, Applied forces between 4-7 nN for one trajectory showed C-H bond rupture at the benzopyran ring. **b**, An analysis of eight of the ten trajectories (colored lines) at a force of 5 nN which indicate bond rupture at the terminal C-H bond.

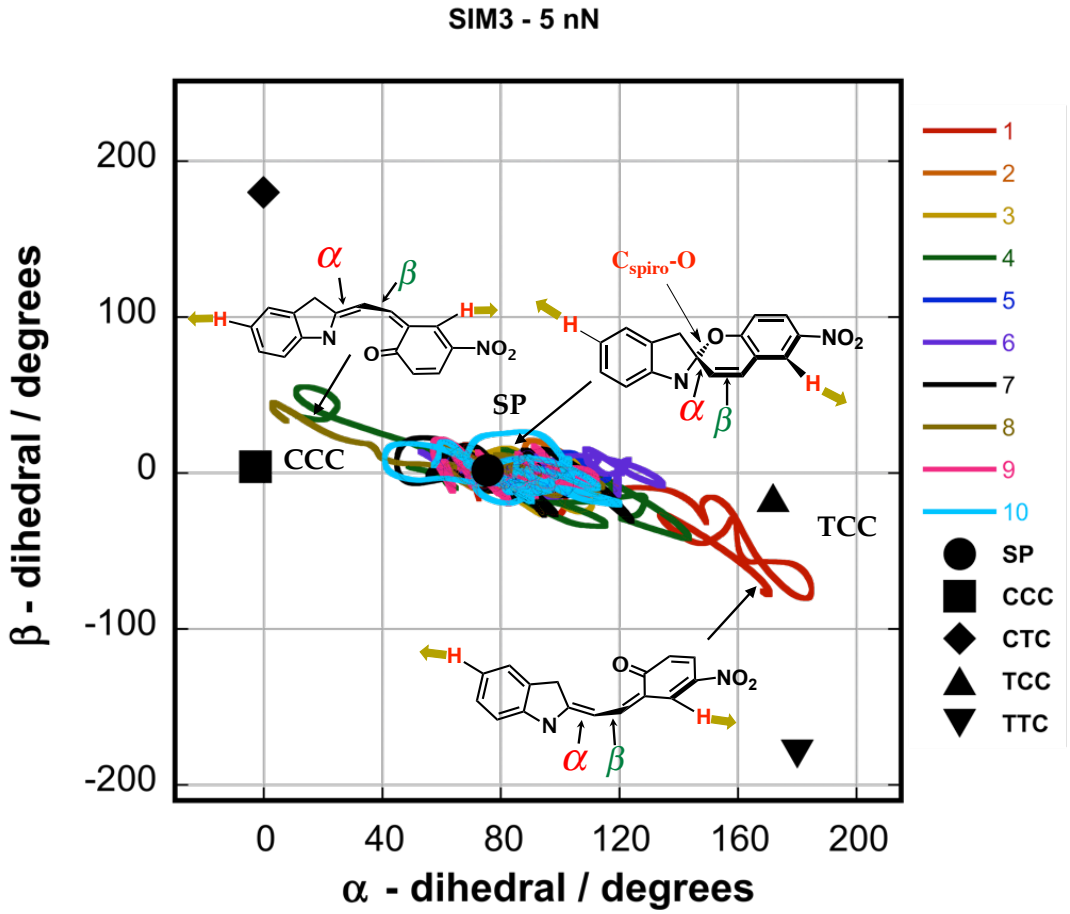

Figure 4.37: SIM3 2-D dihedral angle plot. The equilibrium angles for each isomer is indicated by the black markers. The $\boldsymbol{\alpha}$ and $\boldsymbol{\beta}$ angles are shown for ten trajectories (colored lines labeled 1-10) of which only three open to a cis-cisoid form. Thus, from SP, there are two possible reaction routes towards a particular cis-cisoid MC conformer, CCC and TCC. Two trajectories reflect the SP $\rightarrow$ CCC transition, which decreases at the $\boldsymbol{\alpha}$ angle, followed by an increase in the $\boldsymbol{\beta}$ angle. One trajectory transitions from SP $\rightarrow$ TCC, where $\boldsymbol{\alpha}$ increases and the $\boldsymbol{\beta}$ angle decreases concurrently. The remaining trajectories indicate no ring opening. Unlike SIM1 or SIM2, there is no indication of C-C isomerization to CTC or TTC.

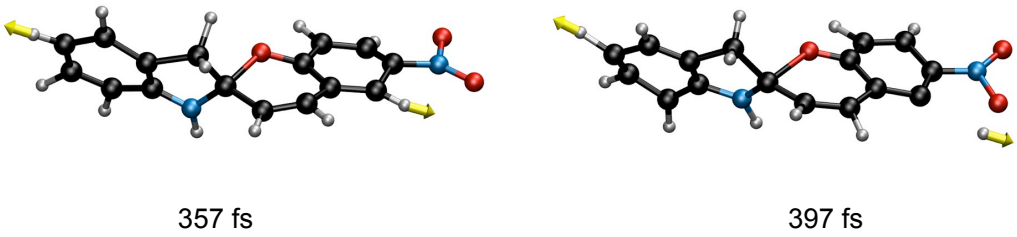

Figure 4.38: AISMD of SIM3 at 5 nN . For nineteen of thirty trajectories the terminal C-H bond located on the benzopyran ring ruptures before any ring opening is observed.

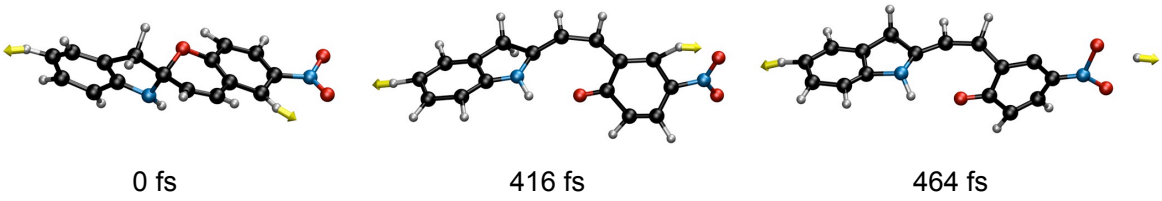

Figure 4.39: SIM3 at 5 nN. Of thirty trajectories only two followed Spiro C-O cleavage with the following order of the reaction path, SP → CCC. After formation of the cis-cisoid conformer CCC, the terminal C-H bond located on the benzopyran ring breaks.

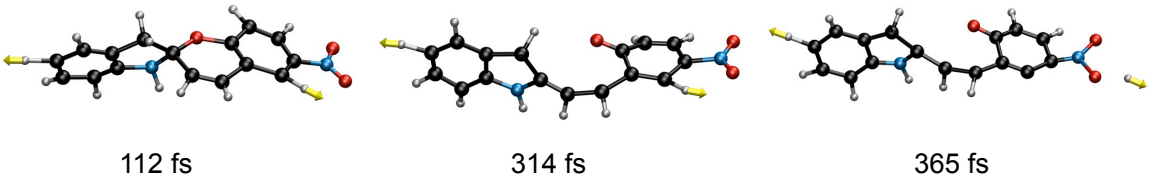

Figure 4.40: SIM3 at 5 nN. Two of thirty trajectories follow the reaction route SP → TCC which is followed by C-H bond rupture at the benzopyran ring.

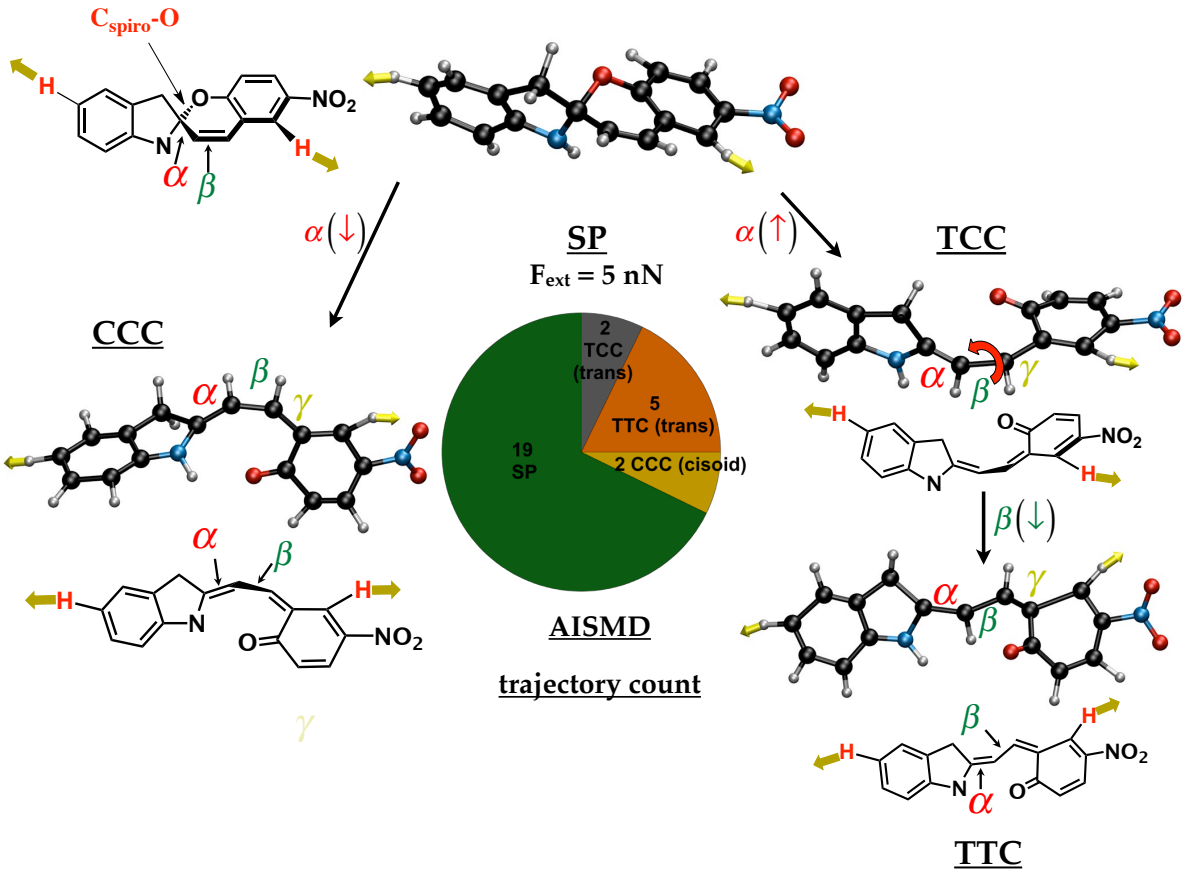

Figure 4.41: SIM3 conformer breakdown for thirty trajectories at 5 nN. Two reaction paths are shown: SP → CCC and SP → TCC → TTC. Within 1 ps, two trajectories ring open to the cis-cisoid CCC without C-C isomerization to CTC. Seven simulations follow the alternate pathway to the TCC product of which five C-C isomerize to the TCC conformer. Nineteen trajectories did not undergo C-O cleavage primarily due to C-H bond rupture at the indole ring or benzopyran ring.

4.9 References

[1] Davis, D. A.; Hamilton, A.; Yang, J.; Cremar, L. D.; Gough, D. V.; Potisek, S. L.; White, S. R.; Moore, J. S.; Sottos, N. R.; Ong, M. T.; Braun, P. V.; Martínez, T. J. *Nature* **2009**, *459*.

[2] Ben-Nun, M.; Martínez, T. J. *Adv. Chem. Phys.* **2002**, *121*, 439.

[3] Schmidt, M. W.; Baldridge, K. K.; Boatz, J. A.; Elbert, S. T.; Gordon, M. S.; Jensen, J. H.; Koseki, S.; Matsunaga, N.; Nguyen, K. A.; Shyjun, S. U.; Dupuis, M.; Montgomery, J. A. *J. Comput. Chem.* **1993**, *14*, 1347.

[4] Becke, A. D. *Phys. Rev. A* **1988**, *38*, 3098.

[5] Becke, A. D. *J. Chem. Phys.* **1993**, *98*, 5648.

[6] Kauzmann, W.; Eyring, H. *J. Am. Chem. Soc.* **1940**, *62*, 3113.

[7] Lee, C. K.; Davis, D. A.; White, S. R.; Moore, J. S.; Sottos, N. R.; Braun, P. V. *J. Am. Chem. Soc.* **2010**, *132*, 16107.

[8] Bell, G. I. *Science* **1978**, *200*, 618.

[9] Crist, B.; Oddershede, J.; Sabin, J. R.; Perram, J. W.; Ratner, M. A. *J. Polymer Sci. Polymer Phys. Ed.* **1984**, *22*, 881.

[10] Garg, A. *Phys. Rev. B* **1995**, *51*, 15592.

[11] Evans, E.; Ritchie, K. *Biophys. J.* **1997**, *72*, 1541.

[12] Evans, E. *Annu. Rev. Biophys. Biomol. Struct.* **2001**, *30*, 105.

[13] Hummer, G.; Szabo, A. *Biophys. J.* **2003**, *85*, 5.

[14] Dudko, O. K.; Hummer, G.; Szabo, A. *Phys. Rev. Lett.* **2006**, *96*, 108101.

[15] Evans, E. A.; Calderwood, D. A. *Science* **2007**, *316*, 1148.

[16] Konda, S. S. M.; Brantley, J. N.; Bielawski, C. W.; Makarov, D. E. *J. Chem. Phys.* **2011**, *135*, 164103.

[17] Makarov, D. E. *J. Chem. Phys.* **2011**, *135*, 194112.

[18] Flannery, J. B. *J. Am. Chem. Soc.* **1968**, *90*, 5660.

[19] Caruso, M. M.; Davis, D. A.; Shen, Q.; Odom, S. A.; Sottos, N. R.; White, S. R.; Moore, J. S. *Chem. Rev.* **2009**, *109*, 5755.

Chapter 5

Selective Spiropyran Reaction Pathways with Applied Force: Twist Induced Mechanophores

5.1 Introduction

Linked cis and trans benzocyclobutene polymers were shown to form the E,E isomer with the application of ultrasound, which was supported by theoretical studies.[1–3] This is in contrast to the expected E,Z product under thermal activation, indicating that mechanical forces can steer the course of a chemical reaction. Several theoretical studies outlining the thermal activation of SP have suggested a ring opening pathway from SP $\rightarrow$ CCC $\rightarrow$ CTC or one proceeding from SP $\rightarrow$ TTC, where the former is the preferred reaction route.[4–11] Additionally, these studies indicate that the cis-cisoid intermediate TCC is absent with the incorporation of methyl groups on the indole ring. The SP ($\boldsymbol{\alpha}$: 75.42°, $\boldsymbol{\beta}$: 1.81°) $\rightarrow$ CCC ($\boldsymbol{\alpha}$: -2.87°, $\boldsymbol{\beta}$: 4.09°) reaction pathway corresponds to a twisting or torsional motion about the $\boldsymbol{\alpha}$ bond. If the direction of the applied force can be coupled with the twisting motion, the C-O bond will be weakened. The twist like motion can be mimicked by pulling at the sites: (N-,8) shown in figure 1.2. However, the direction of force at each atom is assumed to be opposite in direction, so twisting (decreasing $\boldsymbol{\alpha}$) to CCC would go against the pulling direction. Instead, this would favor the following reaction: The SP ($\boldsymbol{\alpha}$: 75.42°, $\boldsymbol{\beta}$: 1.81°) $\rightarrow$ CCC ($\boldsymbol{\alpha}$: 171°, $\boldsymbol{\beta}$: -15.71°) where the C-O breaks to form TCC (increasing $\boldsymbol{\alpha}$). It is expected that barrier lowering will be facilitated. This suggests that a particular reaction reaction route can be biased, since C-O twisting to CCC would be opposite to the applied force vector. Applied force favoring a twist like motion may be referred as the Twist Induced Mechanophore (TIM) series as studied herein.

5.2 Ab Initio Steered Molecular Dynamics of TIM1

The reaction mechanism of a spiropyran molecule with applied forces at the hydrogen atoms (N-,8), called TIM1, was investigated using the AISMD method. The simulation was initially carried out for one trajectory with forces ranging from 1-4 nN to determine the breaking bond. Figure 5.1a plots the C-O distance as a function of time, which indicates dissociation

for this bond at forces low as 1.5 nN. Ten trajectories were monitored, with applied forces of 2 nN shown in figure 5.1b, to see whether C-O dissociation was reproduced. There was no indication that any other bond broke besides C-O. The reaction mechanism was further deduced by observing the $\boldsymbol{\alpha}$ and $\boldsymbol{\beta}$ dihedral angles as shown in Figure 5.2, which indicates the formation of only one trans MC conformer, TTC. After ring opening to the TCC conformer, however, only seven of the trajectories actually isomerize about the $\boldsymbol{\beta}$ C-C bond to form TTC. Figure 5.3 portrays a representative trajectory of the TIM1 reaction mechanism where the SP $\rightarrow$ TCC transition occurs within 100 fs, relatively fast compared to the TCC $\rightarrow$ TTC transition that requires over 100 fs for C-C isomerization. Indeed figure 5.2 suggests that the trajectories stay about the TCC minimum before isomerizing to the trans isomer. Twenty additional trajectories were simulated to determine the ratio of cis-cisoid and trans MC along the reaction pathway. A summary of the conformer breakdown is portrayed in figure 5.4 further verifying that mechanical force, at the TIM1 sites, biases the reaction path towards the TTC products. Only fifteen simulations form TTC within a 1 ps timescale, however, simulation at longer timescales may result in all thirteen TCC conformers isomerizing to TTC. Since many of the cis-cisoid conformers did not complete the C-C isomerization, this may suggest a relatively large barrier with respect to C-O bond breaking. Interestingly, two trajectories ring open to the CTC trans isomer, which is unexpected since the pulling direction would favor formation of the TCC cis-cisoid conformer. The discrepancy is in fact due to the initial sampling conditions, which reflect a force free equilibrated SP geometry. As a result, the initial energy is relatively high enough to surmount the SP $\rightarrow$ CTC transition, which is further explained in the following section.

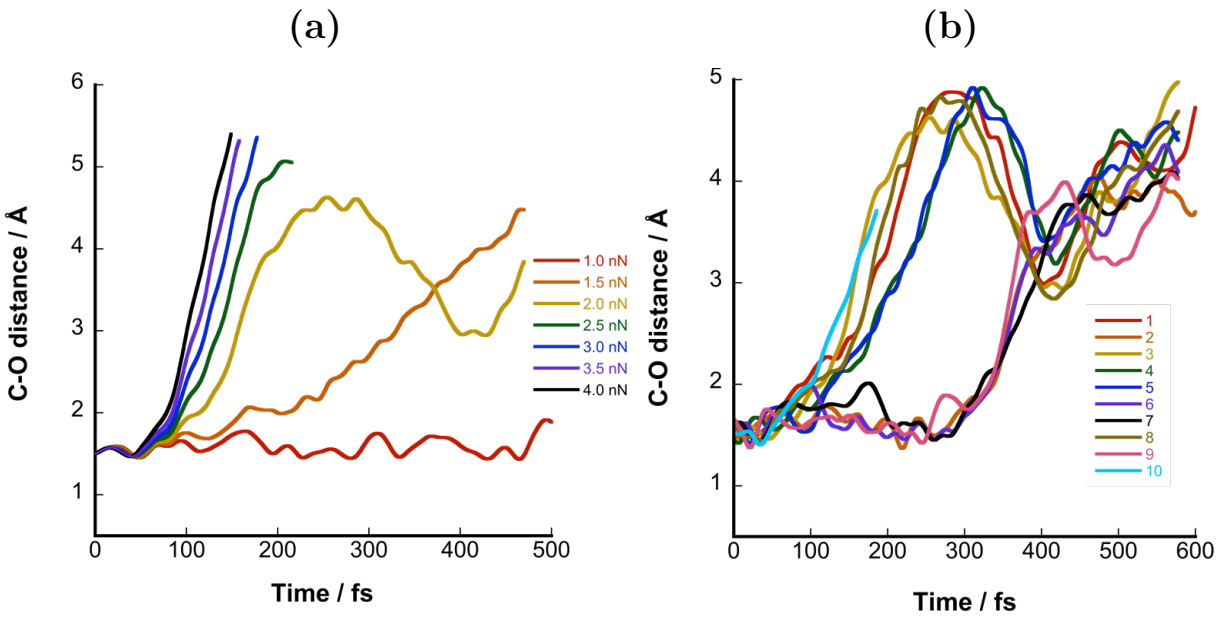

Figure 5.1: TIM1 C-O bond distance as a function of time **a**, External force between 1-4 nN (colored lines) is applied for only one trajectory which plots the C-O bond distance at each time step. The C-O bond breaks within 500 fs as indicated for TIM1, with a minimal force of 1.5 nN. **b**, The C-O distance is plotted for ten different trajectories (labeled 1-10) at an applied force of 2 nN. Most of the trajectories indicate bond rupture within 200 fs.

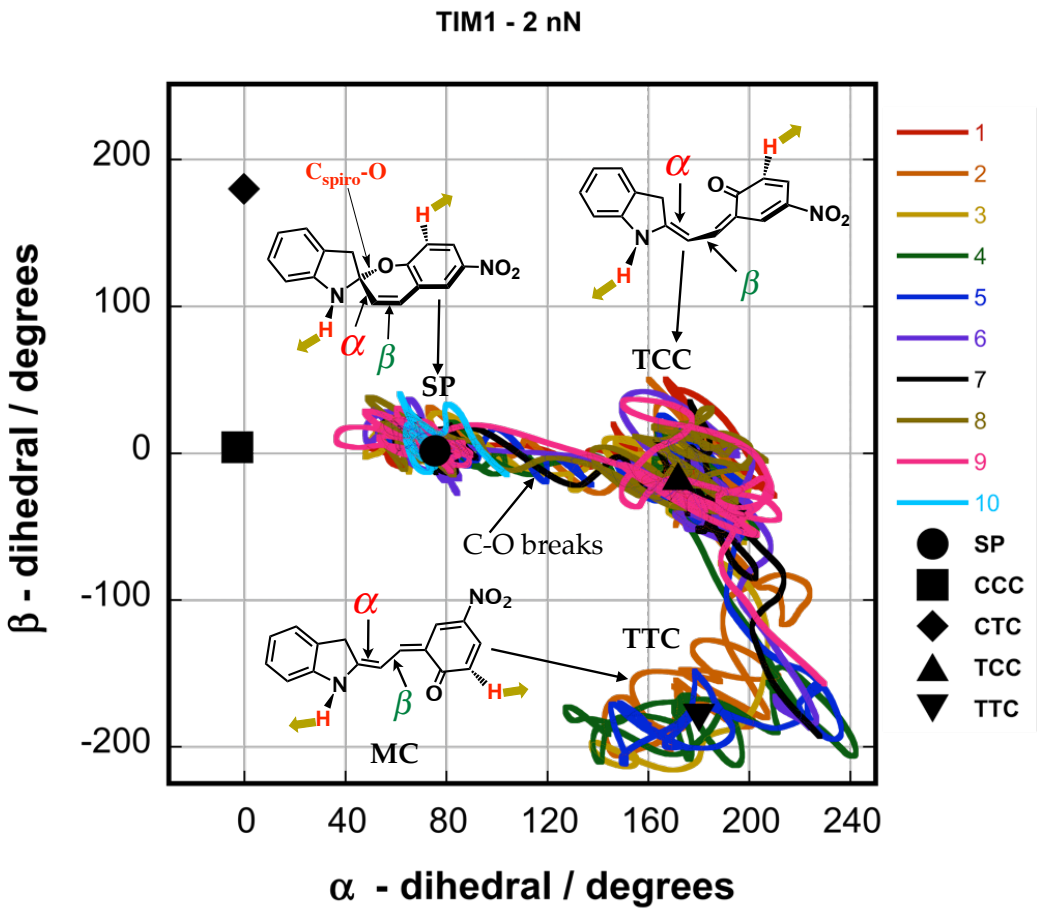

Figure 5.2: TIM1 2-D dihedral angle plot for the reaction profile: SP → TCC → TTC. The black markers are the force free angles for each designated minima (SP, CCC, CTC, TCC, TTC). For ten trajectories (colored lines), the $\boldsymbol{\alpha}$ and $\boldsymbol{\beta}$ angles throughout the course of the reaction were plotted. Starting at the SP, the $\boldsymbol{\alpha}$ angle increases, indicating C-O bond cleavage, with transition to the cis-cisoid conformer TCC. Six trajectories, shown here, complete isomerization to the TTC trans MC conformer, whereby the $\boldsymbol{\beta}$ angle changes by approximately 180 degrees. TIM1 demonstrates reaction pathway selectivity with respect to SIM1, since only one trans MC isomer is accessed.

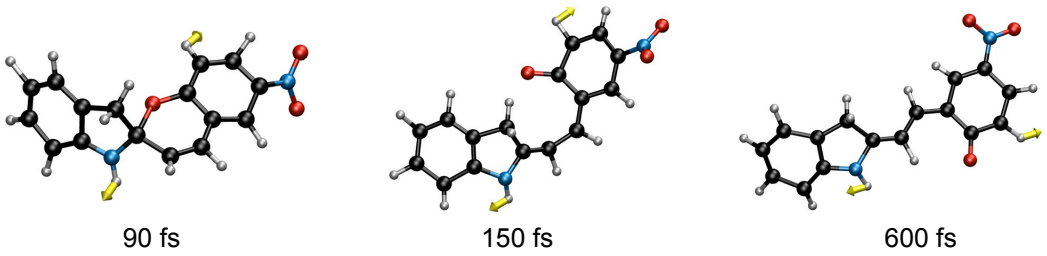

Figure 5.3: AISMD of TIM1 for one representative trajectory at 2 nN showing the following reaction mechanism: SP $\rightarrow$ TCC $\rightarrow$ TTC. The yellow arrows indicate the direction of applied force. Following C-O bond cleavage from the initial SP geometry, the TCC cis-cisoid conformer is accessed. However, there is stabilization of the TCC intermediate and C-C isomerization to TTC does not occur until about 600 fs.

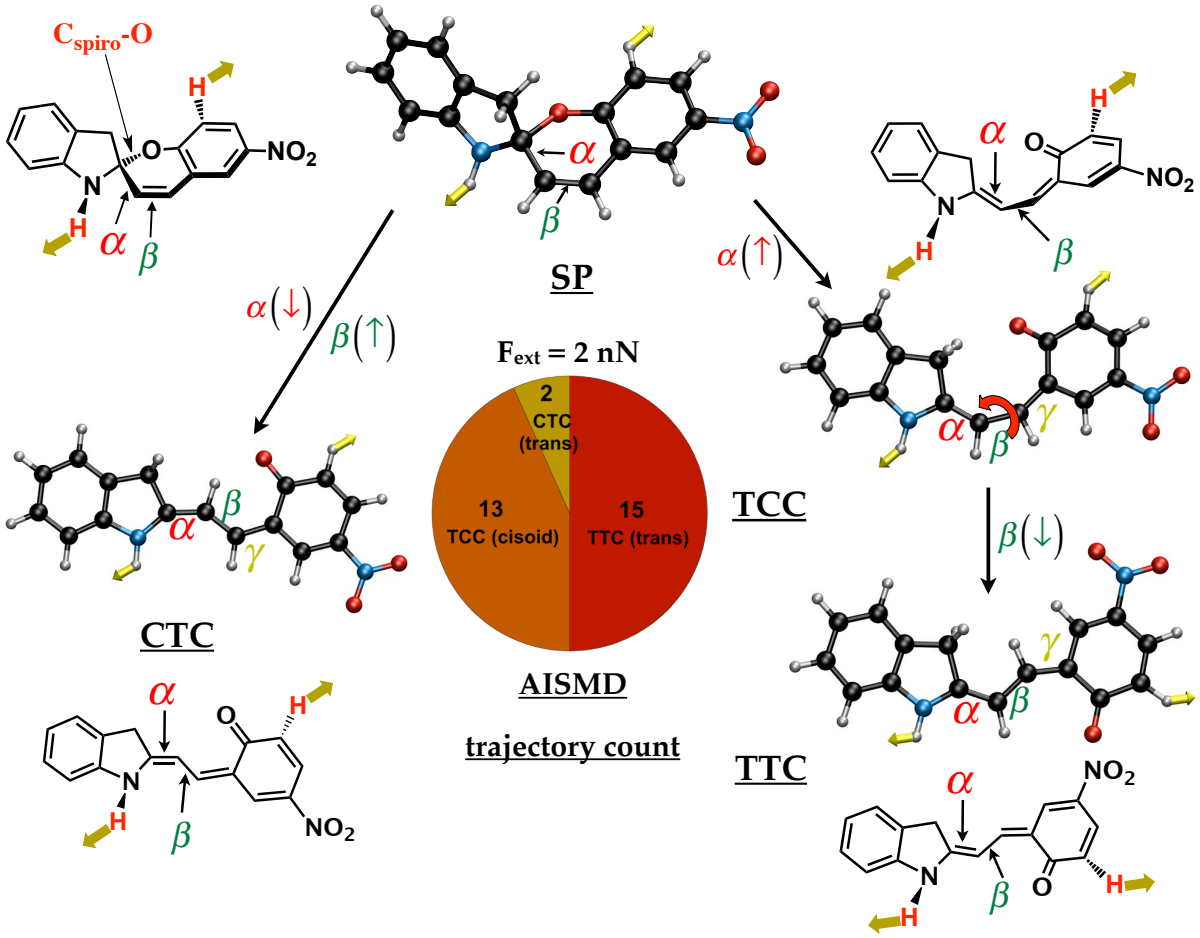

Figure 5.4: TIM1 conformer breakdown for thirty trajectories at 2 nN. One reaction pathway is primarily followed throughout: SP → TCC → TTC. Within a 1 ps timescale, fifteen trajectories result in the formation of the trans MC TTC, while thirteen of the TCC conformers do not undergo isomerization. Two simulations indicated ring-opening of SP → CTC, however, this is considered a higher energy reaction route.

5.3 TIM1 Reaction Pathways on the Force Modified Potential Energy Surface

The nature of the FMPES for TIM1 was explored under applied force and is depicted in figure 5.5 up to forces of 2 nN. There is clearly an energetic preference for the SP → TCC → TTC pathway since the TCC cis-cisoid conformer increasingly stabilizes, with respect to SP, under applied force. The C-O barrier for SP → TCC is 13.91 kcal/mol at 0 nN which lowers to 6.89 kcal/mol at 0.5 nN and becomes barrier-less at 2 nN (Table 5.2 and Figure 5.6). The

mass weighted distance (MWD) from SP to the first transition state, TS3, at 0 nN is 20.89 Å*amu$^{1/2}$ which decreases to 7.09 Å*amu$^{1/2}$ at 0.5 nN and is 1.05 Å*amu$^{1/2}$ at a force of 2 nN. Starting from the TCC minima under zero force, the C-C isomerization barrier is 21.43 kcal/mol and decreases to 16.41 kcal/mol at 2 nN, a relatively smaller change with respect to the C-O barrier.

The MWD from TCC to the next transition state, TS4, shows an opposite trend and increases with applied force. At 0 nN the MWD is 13.56 Å*amu$^{1/2}$ which increases to 22.19 Å*amu$^{1/2}$ at an applied force of 2 nN. The force perturbed reactant, transition state, and product geometries for the SP $\rightarrow$ TCC $\rightarrow$ TTC are shown in figure 5.7. The length of the C-O distance for the TS3 geometry decreases from 2.37 $\rightarrow$ 1.74 Å*amu$^{1/2}$ at 0 and 2 nN respectively. In contrast, the C-O distance at the TS4 geometry increases from 3.35 $\rightarrow$ 4.36 Å*amu$^{1/2}$ at a force of 0 and 2 nN.

Concerning the alternate reaction route towards the CTC product, the barrier heights for the C-O breaking process increases with applied force. At 0.5 nN, the SP $\rightarrow$ CCC transition increases to 22.27 kcal/mol, which decreases the stability of the CCC conformer. In contrast, the C-C isomerization from CCC $\rightarrow$ CTC decreases to 20.55 kcal/mol at 0.5 nN. This trend continues up until the force is 1.5 nN where there is only one transition barrier for the following pathway, SP $\rightarrow$ CTC. The CCC geometry becomes a transition state along the SP $\rightarrow$ CTC pathway with an energy barrier of 28.10 kcal/mol (Table 5.1). This demonstrates how applied force can convert reaction intermediates to transition states along the reaction pathway.

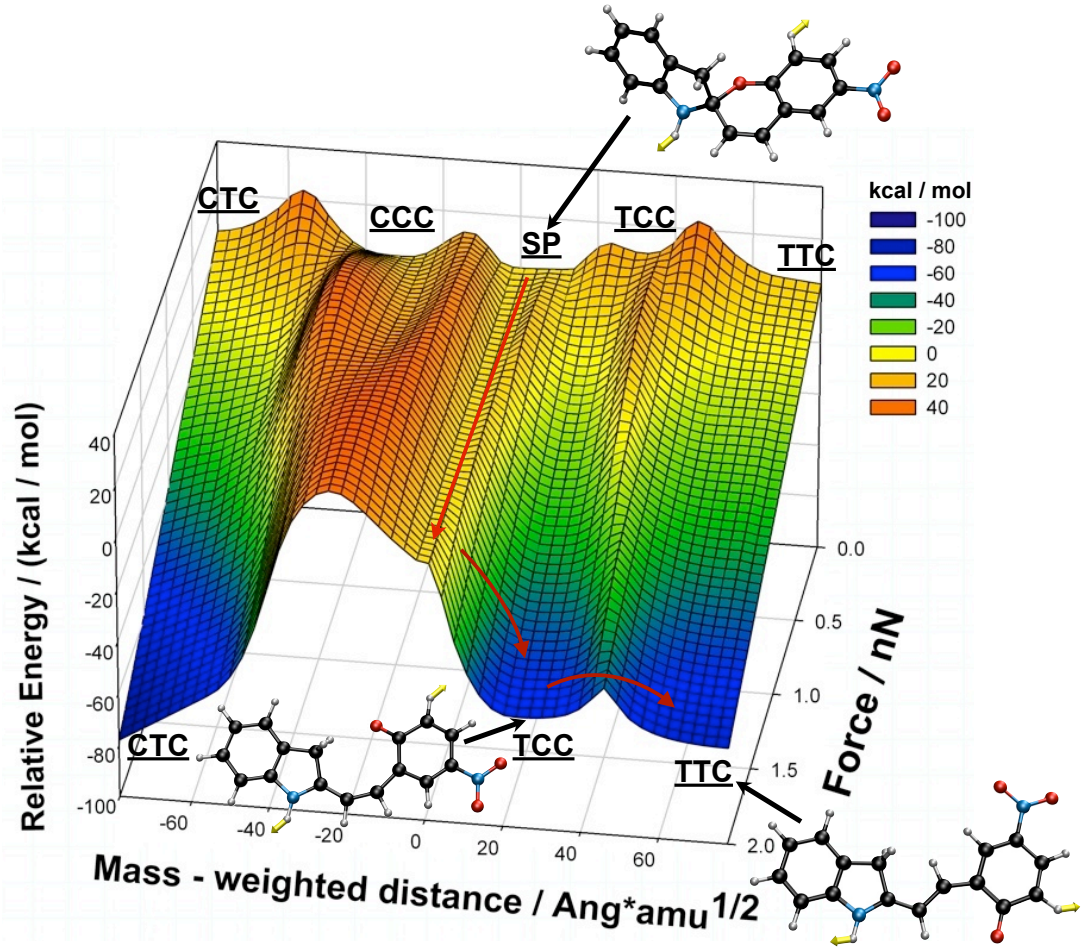

Figure 5.5: TIM1 FMPES. In the absence of force, the barriers heights for C-O cleavage and C-C isomerization to any of the respective cis-cisoid and trans isomers are approximately equal. However, at 0.5 nN differences in barrier heights for each pathway emerge whereby the SP $\rightarrow$ CCC barrier increases while transition from SP $\rightarrow$ TCC decreases respectively. At applied forces comparable to AISMD, a single barrier is shown for the SP $\rightarrow$ CTC pathway, which is relatively higher in energy with respect to the nearly barrier less transition, SP $\rightarrow$ TCC. The latter complements dynamics since the SP $\rightarrow$ CTC transition was not favorable due to relatively large barrier. A barrier from TCC $\rightarrow$ TTC is evident even at a 2 nN applied force and forces exceeding 2 nN suggest a single barrier transition.

Table 5.1: Relative energies (with respect to SP) of minima and transition states along the TIM1 SP → CCC → CTC reaction path.

Force	TS1	CCC	TS2	CTC
0	14.54	1.08	30.72	5.63
0.5	22.27	8.70	29.25	-12.75
1.0	24.08	18.45	21.07	-28.95
1.5	n/a	28.10	n/a	-44.87
2.0	n/a	26.69	n/a	-60.80

Table 5.2: Relative energies (with respect to SP) of minima and transition states along the TIM1 SP → TCC → TTC reaction path.

Force	TS3	TCC	TS4	TTC
0	13.91	9.26	30.69	3.79
0.5	6.89	-8.38	13.70	-12.23
1.0	3.26	-24.45	-3.72	-27.97
1.5	1.07	-40.58	-21.90	-44.78
2.0	0.02	-57.01	-40.60	-62.58

The vibrational modes for the TS geometries at 1 and 2 nN are shown in figures 5.9 and 5.10, which illustrate the C-O dissociation and C-C isomerization modes. Thus, the first saddle point, TS3, depicts a bond-stretching coordinate along the C-O bond while TS4 corresponds to the C-C isomerization vibrational mode. However, the relative stabilities of the conformers differ under applied force. Although the TCC (9.26 kcal/mol) conformer is less stable with respect to SP and TTC (3.79 kcal/mol), the stability of the cis-cisoid conformer increases with applied force. At 2 nN the TCC conformer is 57.01 kcal/mol lower than SP and nearly as stable as the trans TTC isomer (-62.58 kcal/mol). Thus, the difference in energy between the SP and TCC conformer increases with force and suggests trapping of the cis-cisoid product at increased force.

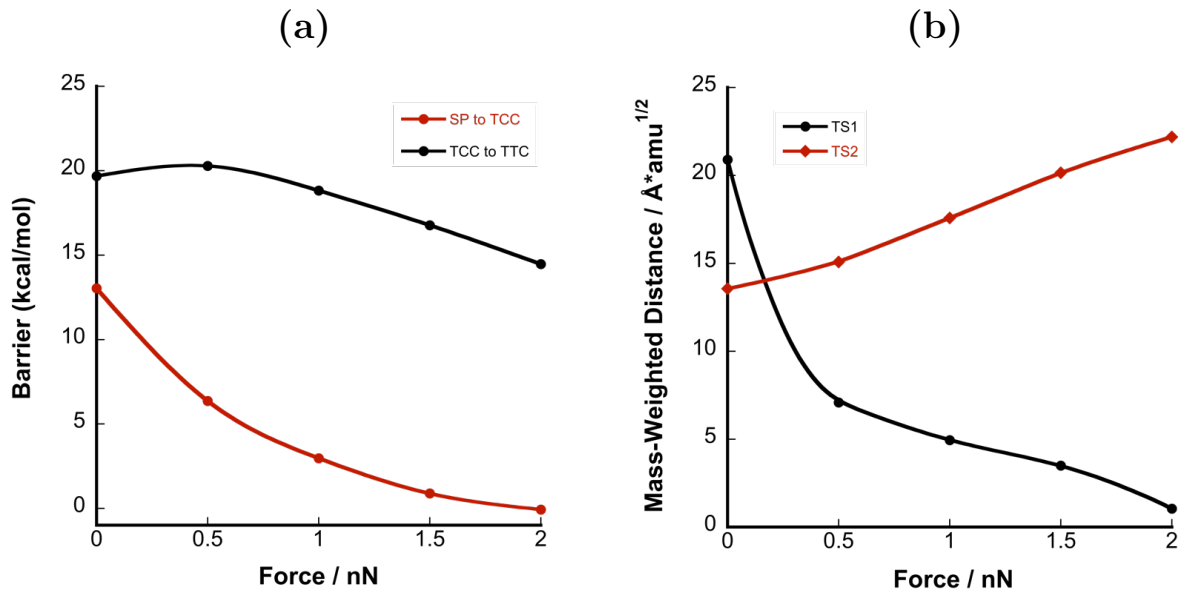

Figure 5.6: TIM1 conformer barriers and mass-weighted distance (MWD) of the MEP as a function of force for the following reaction: SP → TS3 →TCC →TS4 →TTC. **a**, The barrier height from SP → TS3 towards the TCC cisoid conformer (red line) and for the TCC → TS4 to the TTC trans isomer (black line). Increasing forces up to 2 nN indicate that the C-C isomerization barrier decreases by ∼ 5 kcal/mol compared to over 10 kcal/mol for the C-O barrier. **b**, the mass weighted distance (MWD) along the MEP for the following: SP → TS3 and TCC → TS4. The former reflects the C-O barrier and the latter the C-C isomerization barrier. The MWD for SP → TS3 decreases to nearly zero at 2 nN, indicating that applied force will remove the C-O barrier. However, the MWD from TCC → TS4 shows an opposite trend and increases with applied force.

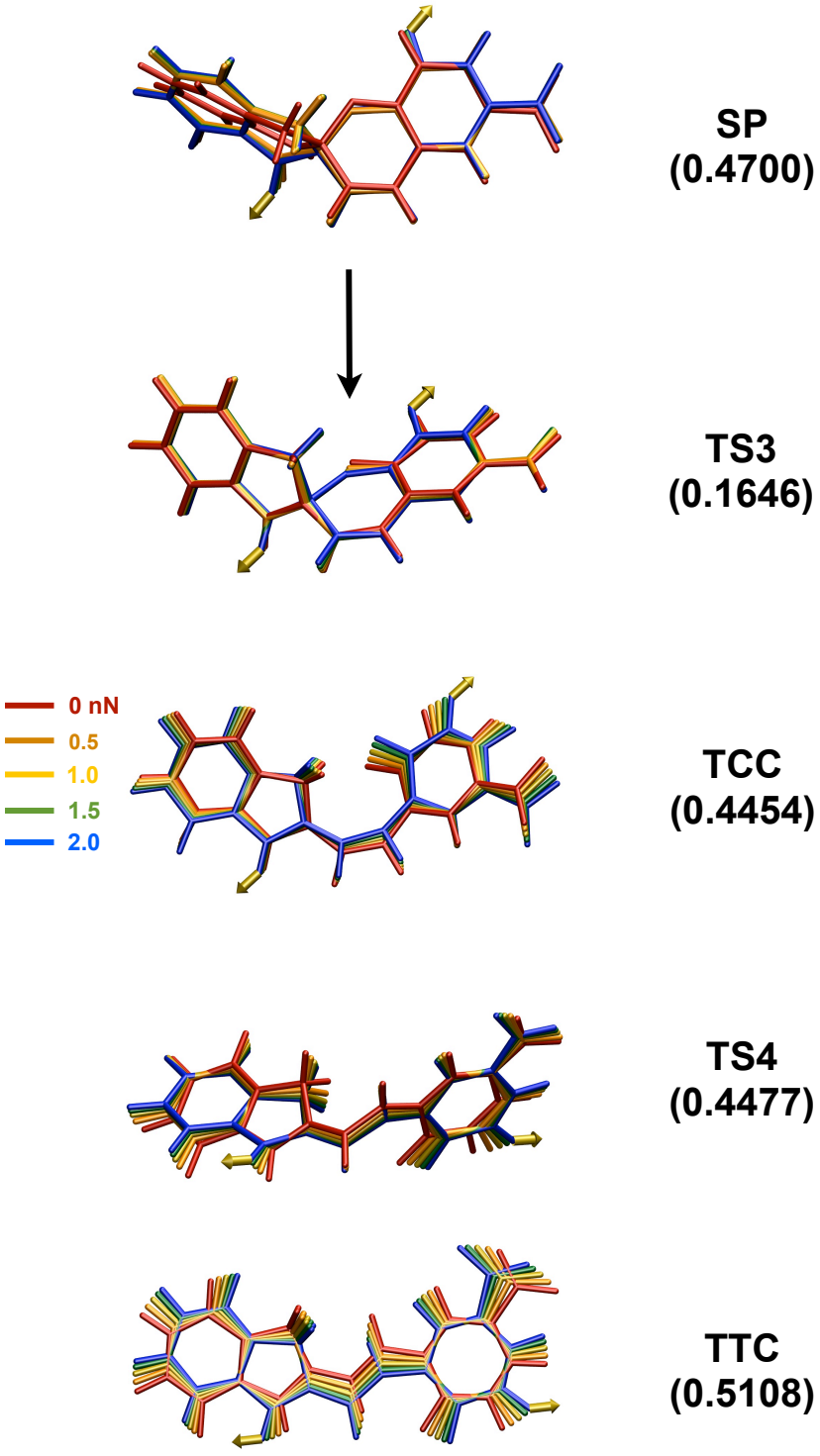

Figure 5.7: TIM1 Reactant, transition state, and product geometries at forces ranging 0-2 nN along the SP $\rightarrow$ TCC $\rightarrow$ TTC reaction route. The force free geometries are denoted in red, which are perturbed under applied force. The root mean square deviation (RMSD) with respect to the zero force geometry is indicated in parentheses.

Two - dimensional FMPES contour plots are shown in figure 5.8. The MEP is represented by the black solid line which changes with respect to the $\boldsymbol{\alpha}$ and $\boldsymbol{\beta}$ dihedral angles. There is an energetic preference for the conformers TCC and TTC with respect to SP. Mechanical forces at 0.5 nN begin to destabilize the local region near the CCC cisoid and increases the transition state energy for SP $\rightarrow$ CCC (Table 5.1). In contrast, there is a surface broadening and increased depth of the TCC minima shown in blue and the transition barrier from SP $\rightarrow$ TCC is reduced as shown by the yellow coloration. The plots indicate an angle decrease or shortening between TS3 and the SP reactant. At zero force the $\boldsymbol{\alpha}$ angle differs by 96.36° between SP ($\boldsymbol{\alpha}$: 75.42°, $\boldsymbol{\beta}$: 1.81°) and TCC ($\boldsymbol{\alpha}$: 171.78°, $\boldsymbol{\beta}$: -15.71°). However, this value reduces to 67.6° at 0.5 nN between SP ($\boldsymbol{\alpha}$: 108.17°, $\boldsymbol{\beta}$: -0.55°) and TCC ($\boldsymbol{\alpha}$: 175.77°, $\boldsymbol{\beta}$: -13.99°), indicating that the MWD decreases from SP $\rightarrow$ TS3 under applied force. Representative molecular dynamics trajectories are shown at 2.0 nN, which all proceed towards the TTC isomer and follow along the IRC pathway. The trajectories are concentrated about the TCC minima before C-C isomerization to trans TTC. For the alternate reaction pathway, SP $\rightarrow$ CCC $\rightarrow$ CTC, the CCC minima becomes destabilized. At 1 nN, the region about CCC becomes notably flat and relatively large in energy with respect to SP. At 2 nN, the CCC minima is removed indicating a single barrier pathway from SP $\rightarrow$ CTC. One trajectory is shown to pass over to the CTC product; however, this is attributed to an initial geometry that is relatively unstable.

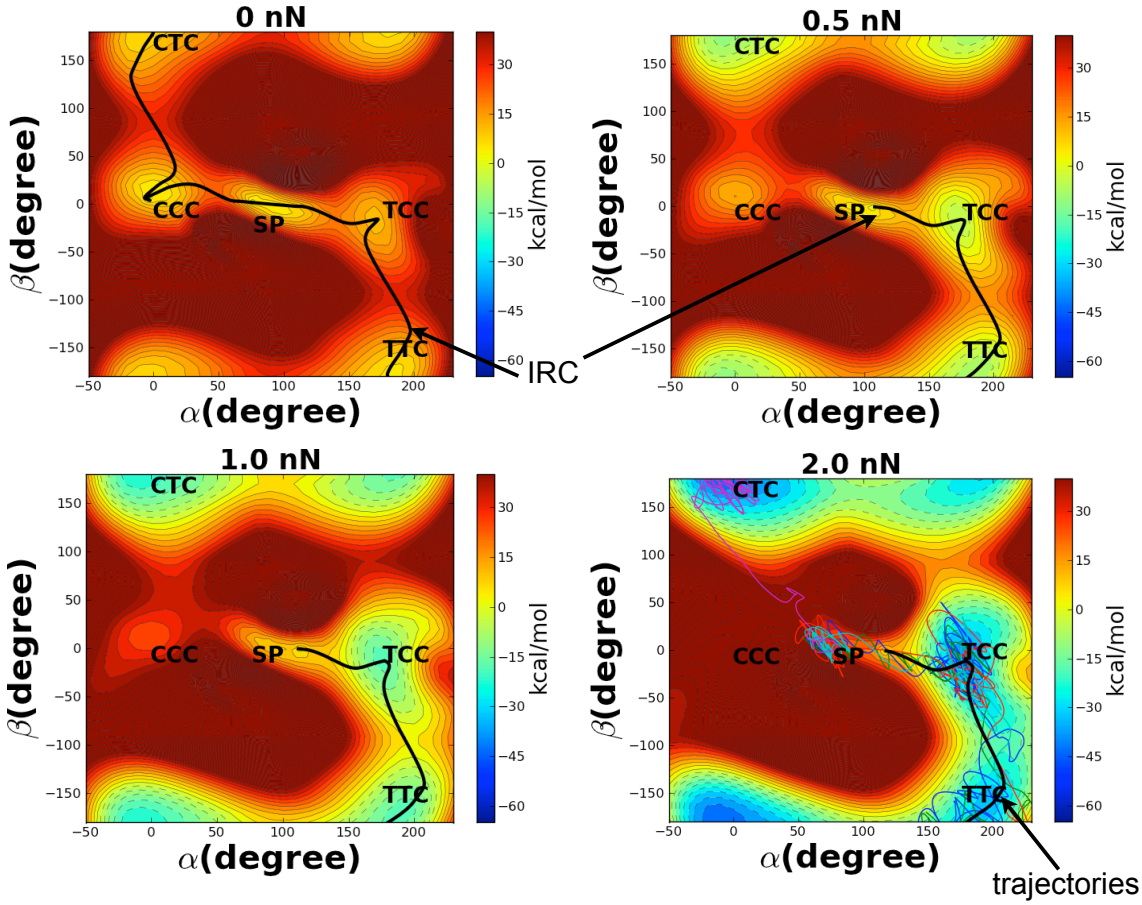

Figure 5.8: TIM1 2-D FMPES contour. The solid black line corresponds to the IRC pathway. A 0.5 nN force results in stabilization of the TCC conformer in contrast to CCC which increases in energy. Transition to the CTC isomer is highly unfavorable and the intermediate minimum, CCC, becomes energetically unstable relative to SP. The reaction path towards the TTC isomer is stabilized as shown by the blue region where the TCC and TTC isomers have similar stability. Steered molecular dynamics trajectories are shown at 2 nN on the contour plot (colored lines) which indeed follow the minimal energy path in the following order: SP $\rightarrow$ TCC $\rightarrow$ TTC. Additionally, an alternate reaction path is shown from SP $\rightarrow$ CTC at 2 nN, whereby one trajectory is shown to open to the CTC product.

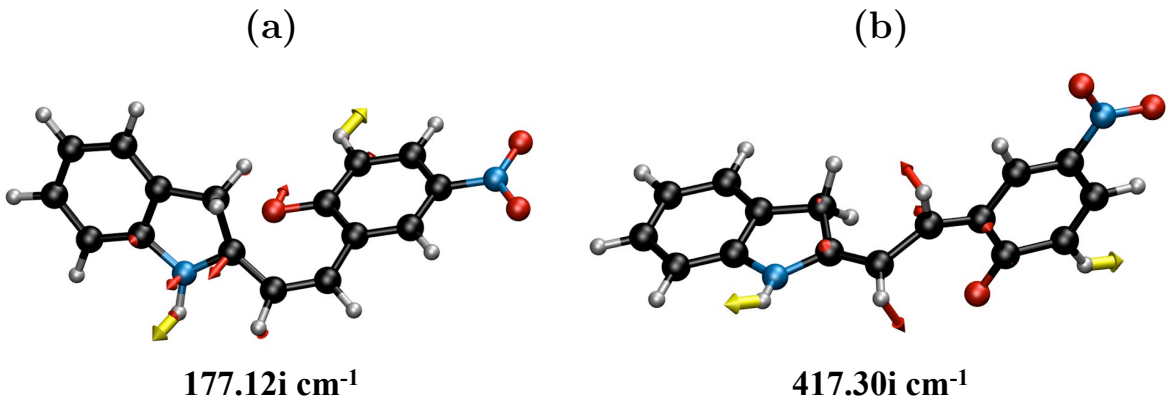

Figure 5.9: Transition states at 1 nN along the SP → TCC → TTC pathway with the normal modes shown by the red arrows. The yellow arrows are the external force vectors which are applied to the H atoms and (i) designates the imaginary frequency in cm^{-1}. **a**, TS3 reflects the Spiro C-O reaction mode while **b**, TS4 is the C-C isomerization mode.

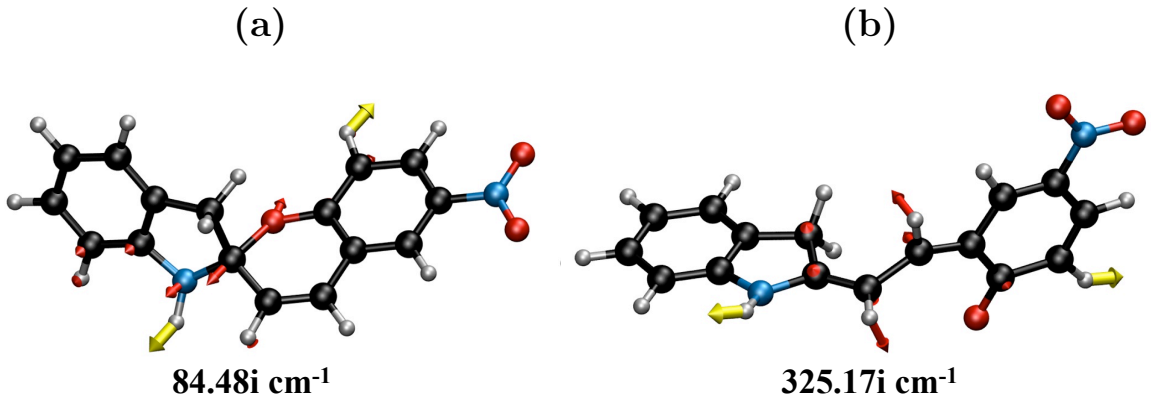

Figure 5.10: Transition states at 2 nN along the SP → TCC →TTC pathway, with the normal modes shown in red. **a**, TS3 reflects the Spiro C-O reaction mode. The imaginary frequency also decreases suggesting a negligible C-O barrier **b**, TS4 is the C-C isomerization mode.

5.4 TIM1 Reaction Rates under External Force

The activation barrier height shown in figure 5.11 represents ring opening to the TTC isomer. The barrier decreases more so compared to SIM, and is attributed to the torsional pulling motion which facilitates cleavage of the C-O bond. The relative stabilization of the TCC minima and destabilization of SP indicates that increased forces will diminish the C-O barrier while the C-C isomerization barrier will remain. The calculated activation barrier at 0 nN, with zero point energy (ZPE) correction, is 28.17 kcal/mol which is the difference in energy between SP and the TS that reflects C-C isomerization. At 0.5 nN the rate determining step

is dependent on the C-O barrier and is 11.52 kcal/mol. The C-O barrier heights decrease to 2.97 and 0.88 kcal/mol at 1 and 1.5 nN, respectively. The vibrational modes corresponding to the C-O dissociation and isomerization are shown in figures 5.9 and 5.10. At 2 nN the dissociation barrier without ZPE correction is $\sim$ 0.1 kcal/mol which is less than k_bT. As figure 5.10 suggests, the vibrational frequency for TS3 is less than 100 cm^{-1} and indicates a barrierless transition to TCC. At 2 nN, the rate-determining step is now dependent on the single barrier reflecting C-C isomerization. As a result, the activation barrier height at 2 nN increases to 14.46 kcal/mol. Thus, the activation barriers from 0-1.5 nN correspond to the SP $\rightarrow$ TCC transition and at 2 nN, the activation barrier depends on the TCC $\rightarrow$ TTC transition.

With respect to transition state theory (TST), the rate of the mechanical reaction will be dependent on the activation barrier height (Figure 5.12). The rate of reaction increases up to a force of 1.5 nN, however, at 2 nN the rate decreases which is attributed to the C-C isomerization barrier. Table 5.3 contains the lifetime of color formation to the trans MC TTC. Color formation is predicted to occur within microseconds at an applied force of 0.5 nN with a calculated wavelength of 446 nm for the TTC isomer. This is not appreciably different compared to forces at 0 nN (448 nm) and when the force is increased up to 2 nN (444 nm), as shown in figure 5.13. The absorption wavelengths of TCC at 0.5 and 2 nN are 429 and 456 nm with oscillator strengths of 0.74. The stability of the TCC or cis-cisoid conformer at the latter external forces suggests an observable absorption band. Since the wavelengths for both TCC and TTC are approximately the same, the absorbance band may be too broad to distinguish either isomer. The experimental absorption wavelength is peaked at $\sim$ 575 nm, however, the incorporation of solvent is expected to increase the absorption wavelength.[12] The rate of TTC formation at 1.0 or 1.5 nN is predicted to be on the order of picoseconds, timescales that are accessible through molecular dynamics simulations. It is expected that a distribution of forces ranging from 0.5-2 nN is sufficient to observe coloration. At a force of 2.0 nN, the rate of ring opening is calculated to occur within a millisecond, a relatively slower reaction rate with respect to forces between 0.5-1.5 nN. Table 5.2 indicates that the TCC and TTC isomers are similarly stable or within 5 kcal/mol apart. The rate for the reverse reaction must also be considered, since the barrier heights for the forward and reverse reaction are 5 kcal/mol apart. For example, at 2 nN, which reflects the C-C isomerization barrier, the rate of reaction for TTC $\rightarrow$ TCC, is calculated at $\sim$118 s, which is relatively slower than the forward rate of reaction.

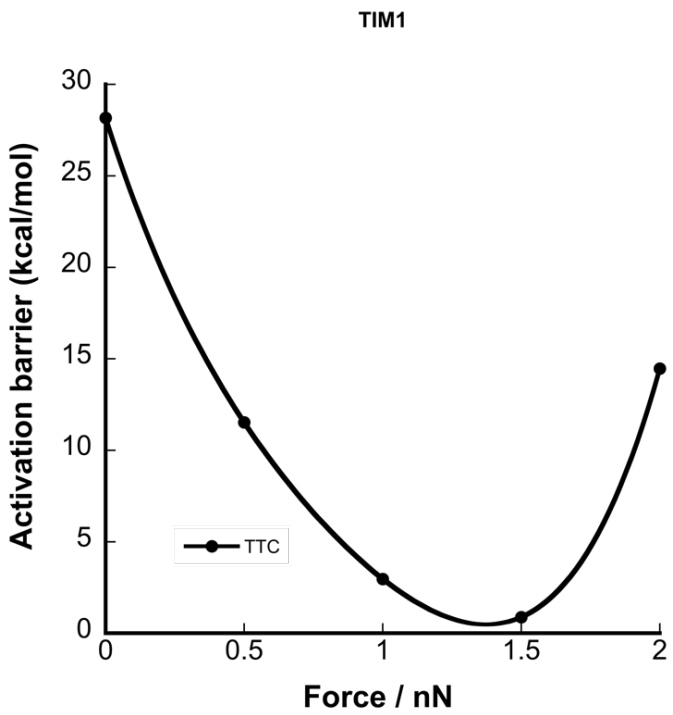

Figure 5.11: TIM1 activation barrier height as a function of applied force. The force free barrier is the energy difference between SP and TS4 for C-C isomerization. At applied forces equal to 0.5 nN the activation barrier for each process is now the difference in energy between SP and TS3 which is the C-O bond dissociation barrier. However, the C-O barrier disappears when the force reaches 2 nN and there is only one barrier, which reflects C-C isomerization from TCC $\rightarrow$ TTC.

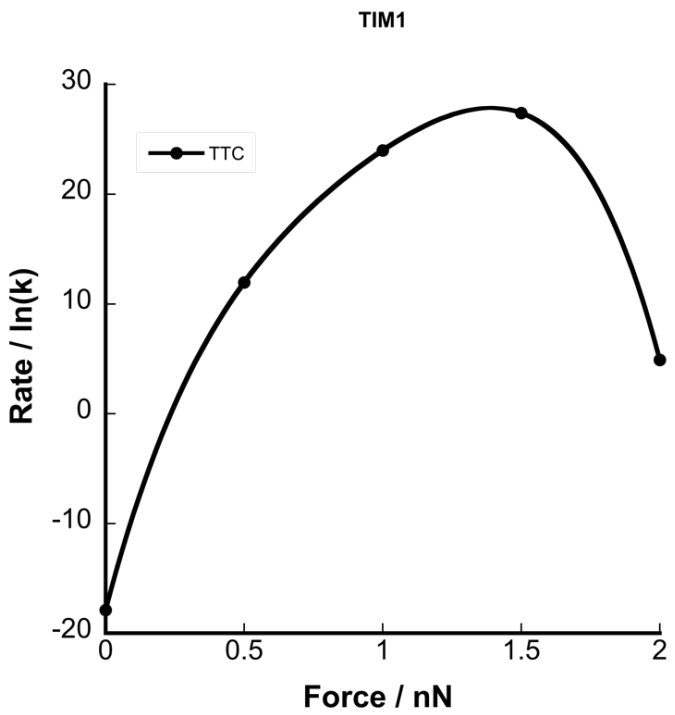

Figure 5.12: TIM1 reaction rate as a function of force. The reaction rate is dependent on the activation barrier height, shown in figure 5.11. The solid black line is the rate of ring opening towards the TTC isomer. At zero force the rate is dependent on the following barrier: SP $\rightarrow$ TS4. From 0.5-1.5 nN, the rate-determining step however reflects the SP $\rightarrow$ TS3 or C-O bond breaking barrier. At 2 nN, TCC is the stable minima and the rate is now dependent on the TCC $\rightarrow$ TS4 isomerization barrier. This leads to a decrease in the reaction rate where the isomerization barrier is greater than the C-O barrier between 0.5-1.5 nN.

Table 5.3: TIM1 lifetime of color formation in units of seconds.

Force	TTC
0	5.85e+07
0.5	6.46e-06
1.0	3.78e-11
1.5	1.27e-12
2.0	7.39e-03

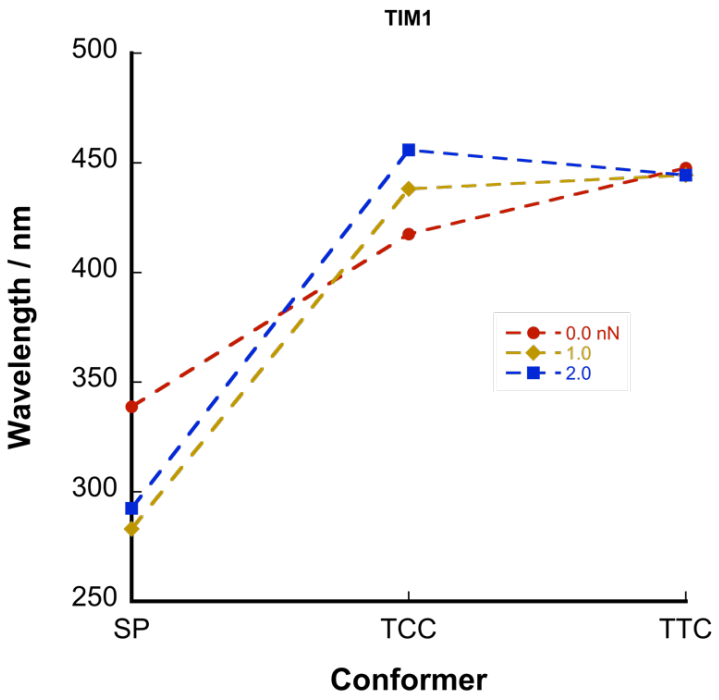

Figure 5.13: TIM1 absorption wavelength as a function of the conformer. The wavelength for SP at zero force is blue shifted at forces of 1 and 2 nN. The wavelength for the trans TTC isomer remains unchanged and reflects the $\pi \rightarrow \pi^*$ transition. The cis-cisoid conformer, TCC, is red shifted with increasing force and also reflects the $\pi \rightarrow \pi^*$ transition. The oscillator strength is similar to the trans TTC isomer (see appendix B).

5.5 Ab Initio Steered Molecular Dynamics of TIM2

The mechano-chemical outcome was investigated for attachment sites at TIM2 (N-,7) using AISMD simulations to deduce the reaction mechanism. Force scans from 1-4 nN for one trajectory is shown in figure 5.14 and the minimal force required for C-O breakage is 1.0 nN within 1 ps. Unlike TIM1, which shows a gradual bond dissociation within 500 fs at 1.5 nN, TIM2 shows sharp bond rupture at longer timescales (500-600 fs) for the same set of initial conditions. Trajectory sampling at 1.5 nN, figure 5.14b, was carried out similarly like TIM1 to quantify the number of bond rupture events. Like TIM1, all ten trajectories broke at the C-O bond within 700 fs. Figure 5.15 also indicates a selective reaction route from SP $\rightarrow$ TCC $\rightarrow$ TTC, however, only four of the trajectories actually isomerize about the β C-C bond to form the TTC isomer. Figure 5.16 shows snapshots along the bond breaking reaction route followed by isomerization to TTC, the final end product. The reaction outcome and product distribution is identical to that of TIM1, as shown in figure 5.17, although without any

evidence of the CTC isomer forming for all simulations. The percentage of TTC formation (thirty trajectories each) for TIM1 and TIM2 is 57 and 60 percent, respectively. All thirty trajectories within a 1 ps timescale ring-opened to TCC, however, only eighteen underwent subsequent C-C isomerization to TTC. Like TIM1, only one reaction pathway is followed: SP $\rightarrow$ TCC $\rightarrow$ TTC.

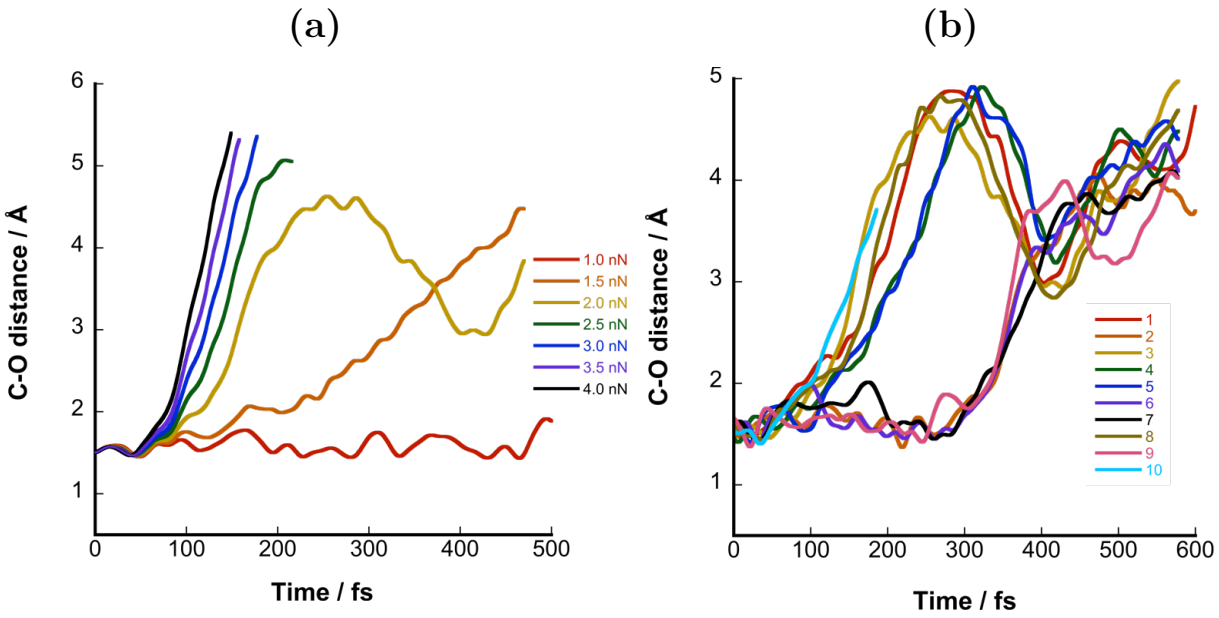

Figure 5.14: TIM2 C-O bond distance with respect to time. **a**, The C-O bond distance is monitored at applied forces between 1-4 nN (colored lines denote different force) for only one trajectory. The C-O bond breaks within 500 fs at minimal forces of 1.5 nN. **b**, The C-O bond distance was also plotted for ten trajectories (colored lines 1-10) at an applied force of 1.5 nN. All trajectories show C-O bond breakage at longer timescales (with respect to TIM1) between 400-500 fs.

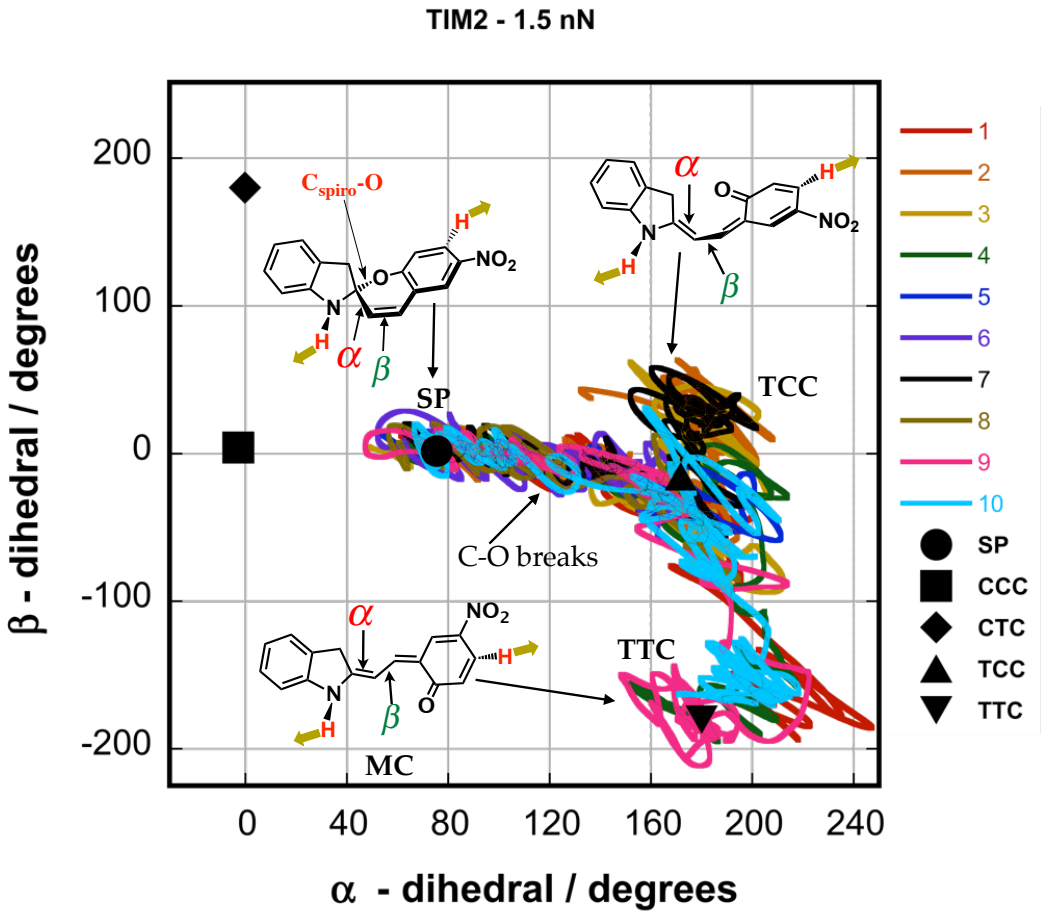

Figure 5.15: TIM2 2-D dihedral angle plot. The black markers are the force free angles for each designated minima (SP, CCC, CTC, TCC, TTC). The colored lines (1-10) correspond to individual reaction trajectories. Starting at the SP the $\boldsymbol{\alpha}$ angle increases, which corresponds to C-O bond cleavage, to form the cis-cisoid conformer TCC. Only four trajectories, shown here, complete isomerization to the trans TTC isomer, whereby the $\boldsymbol{\beta}$ angle changes approximately by 180 degrees. TIM2 also demonstrates reaction pathway selectivity, SP $\rightarrow$ TCC $\rightarrow$ TTC, since only one trans MC conformer is accessed.

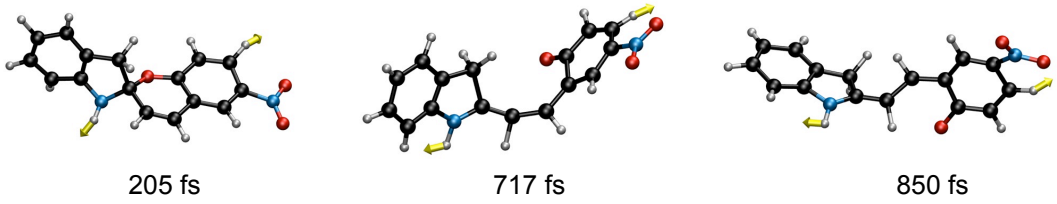

Figure 5.16: AISMD of TIM2 for a representative trajectory at 1.5 nN, SP → TCC → TTC. Following C-O bond cleavage, the cis-cisoid conformer TCC is accessed, however, at relatively longer timescales with respect to TIM1. There is subsequent isomerization to the trans TTC isomer.

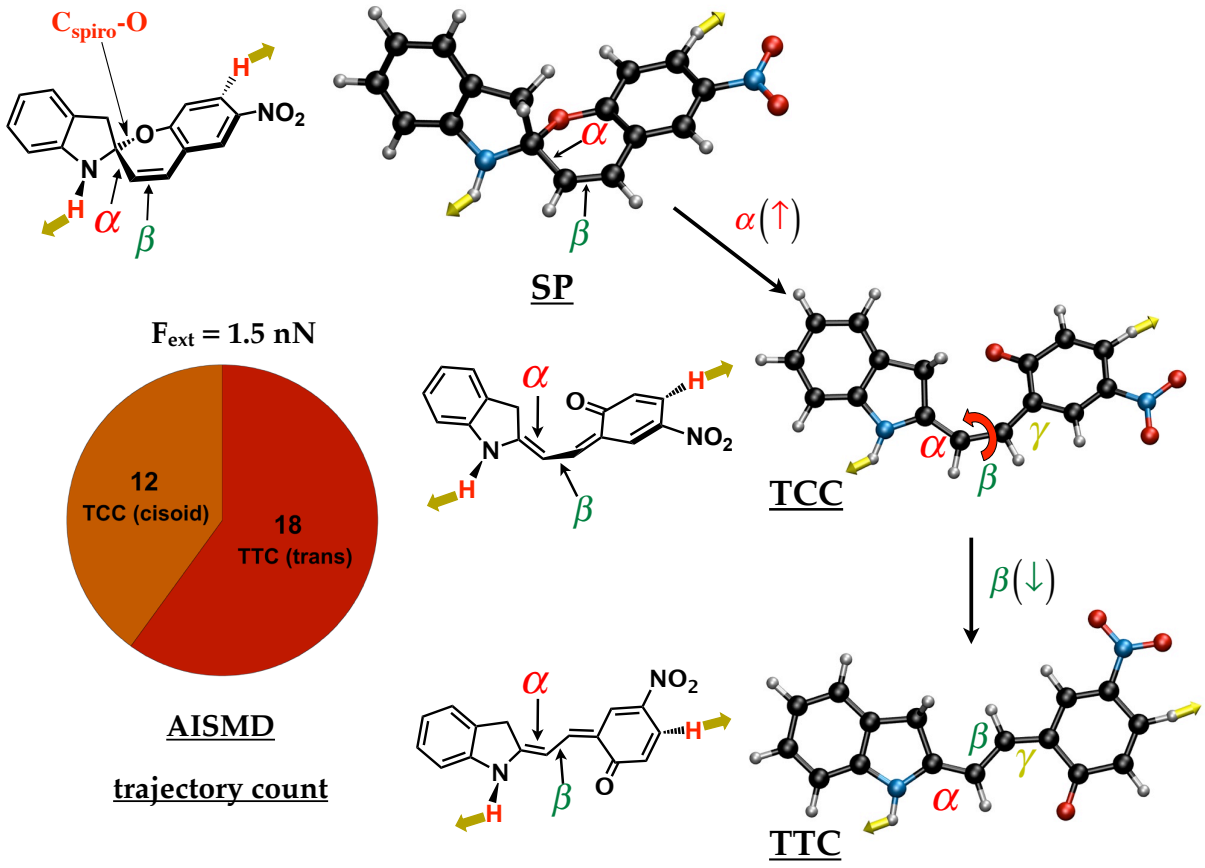

Figure 5.17: TIM2 conformer breakdown for thirty trajectories at 1.5 nN. Only one reaction pathway is followed throughout AISMD: SP → TCC → TTC. There is no indication of any CTC formation. Within a 1 ps timescale, all trajectories result in the formation of TCC, of which only eighteen isomerize to TTC.

5.6 TIM2 Reaction Pathways on the Force Modified Potential Energy Surface

The presence of the TCC and TTC isomers in AISMD simulations suggested that the energy landscape for TIM2 is qualitatively similar to that of TIM1. This was indeed verified when using modified transition state algorithms to search for stationary points on the FMPES. Globally, the surface shows the same energy trend (Figure 5.18) whereby one reaction path is energetically favored, SP → TCC → TTC. The SP → CCC → CTC pathway becomes energetically unfavorable as the force is increased to 2 nN. The CCC intermediate is no

longer a minima but rather a transition state at 2 nN. The conformer barrier height as a function of force, figure 5.19a, shows a similar trend with respect to TIM1. Table 5.4 and 5.5 contain the relative energies for all conformers and transition states with respect to SP. At 0.5 nN the SP $\rightarrow$ TCC barrier is calculated at 7.64 kcal/mol for TIM2 compared to 6.89 kcal/mol for TIM1. At 2 nN the TIM2 and TIM1 C-O barriers are 0.68 and 0.02 kcal/mol without ZPE correction. The TIM2 isomerization barriers are relatively greater than the C-O barriers. With respect to the TCC $\rightarrow$ TTC transition for TIM2 and TIM1, the barriers without the ZPE correction are 21.8 and 22.08 kcal/mol at 0.5 nN and reduce to 19.10 and 16.41 kcal/mol at 2 nN.

The MWD distance to TS3 and TS4 along the MEP also increase and decrease like TIM1, as shown in figure 5.19b. The MWD from SP $\rightarrow$ TS3 at 0.5 nN for TIM2 is 5.53 Å*amu$^{1/2}$ compared to 7.09 Å*amu$^{1/2}$ for TIM1. At 2 nN the MWD values for TIM2 and TIM1 are approximately similar and equal to 1.82 and 1.05 Å*amu$^{1/2}$. At 2 nN, The MWD for the TIM2 TCC $\rightarrow$ TS4 barrier is 16.13 Å*amu$^{1/2}$ compared to 22.19 Å*amu$^{1/2}$ for TIM1. With respect to the latter, the MWD for the TIM2 TCC $\rightarrow$ TS4 is shorter compared to TIM1, suggesting a steeper curvature on the FMPES. The TIM2 FMPES, figure 5.18, illustrates this clearly when the applied force is 2 nN (see Figure 5.5 for TIM1). The force modified reactant, intermediate, and product minima along with the transition states are shown in figure 5.20. The imaginary frequencies and vibrational modes for the transition state geometries at 1 and 2 nN are shown in figures 5.21 and 5.22. TS3 clearly depicts a bond-stretching mode (red arrows) along the C-O bond while the second transition state corresponds to the C-C isomerization vibrational mode. Increasing external forces decrease the distance of the C-O bond for TS3 from 2.37 $\rightarrow$ 1.88 Å, compared to TS4 which increases from 3.35 $\rightarrow$ 3.98 Å at forces of 0 and 2 nN, respectively. The change in C-O distance from 0-2 nN for TS3 and TS4 are 0.49 and 0.63 Å for TIM2. This difference is smaller compared to TIM1, which equal 0.63 and 1.01 Å. Therefore, applied force at the TIM2 attachment sites is slightly less effective for elongating the C-O bond compared to TIM1. As mentioned previously the relative stabilities, with respect to SP, at 0 nN is 9.26 and 3.79 kcal/mol for TCC and TTC. At 2 nN the TCC conformer is -38.46 kcal/mol (-57.01 kcal/mol for TIM1) slightly above the TTC isomer at -43.45 kcal/mol (-62.58 kcal/mol for TIM1). For TIM2, the energy difference ΔE, between the cis-cisoid and trans isomer at 0 and 2 nN is 5.47 and 4.99 kcal/mol (5.57 kcal/mol for TIM1). Therefore, there is an energy reduction between the cis-cisoid and trans isomers for TIM2 compared to TIM1. The difference is 0.48 kcal/mol indicating a reduced thermodynamic preference for the trans MC product. For TIM1, the energy gap between the cis-cisoid and trans conformer increases slightly with a difference of 0.1 kcal/mol (from 0 to 2 nN). The TIM2 MEP on the FMPES is shown in appendix D.

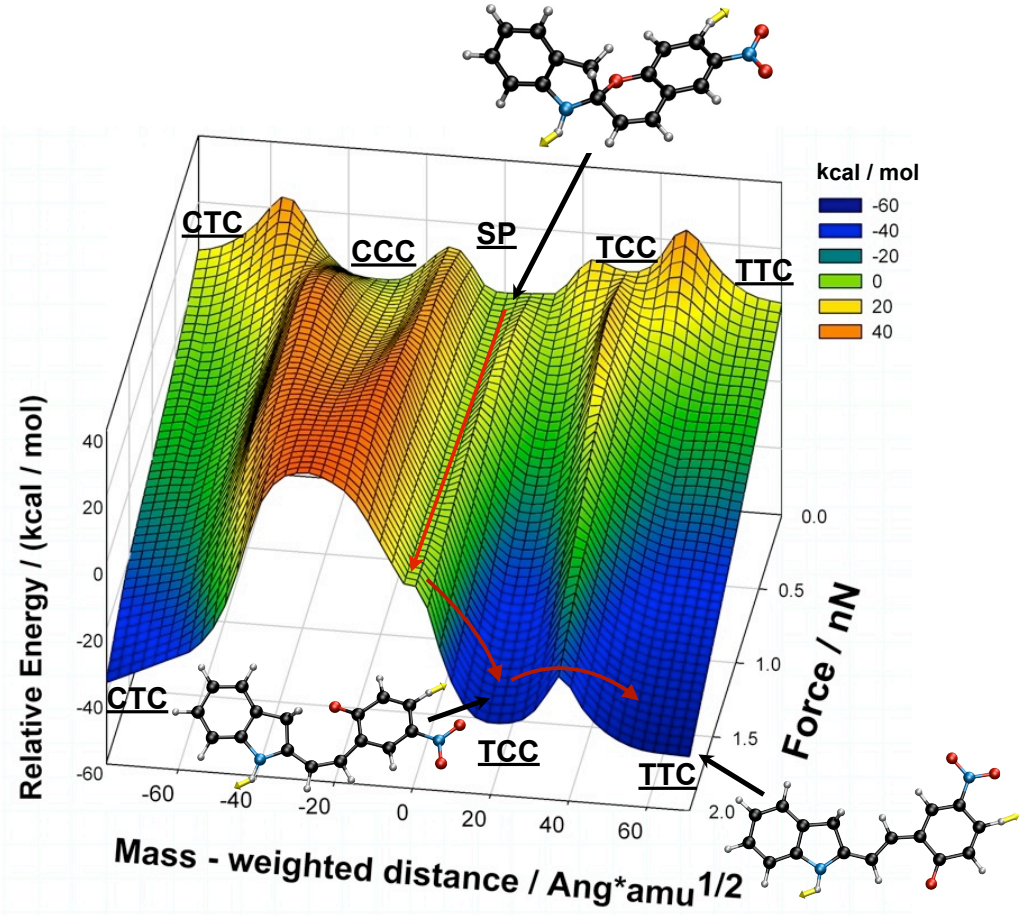

Figure 5.18: TIM2 FMPES. The barriers heights for C-O cleavage and C-C isomerization, at 0 nN, to any of the respective cisoid and trans conformers are approximately equal. Differences in barrier heights for each pathway emerge at increasing forces whereby the SP $\rightarrow$ CCC barrier increases and the transition from SP $\rightarrow$ TCC decreases, respectively. At 2 nN, a single barrier is shown for the SP $\rightarrow$ CTC pathway. The SP $\rightarrow$ CTC transition was not seen in AISMD due to large reaction barrier. The C-O barrier for SP $\rightarrow$ TCC is not negligible unlike TIM1 where only the C-C isomerization barrier is present, TCC $\rightarrow$ TTC at 2 nN.

Table 5.4: Relative energies in kcal/mol for minima and transition states (relative to SP) along the TIM2 SP → CCC → CTC reaction path.

Force	TS1	CCC	TS2	CTC
0	14.54	1.08	30.72	5.63
0.5	24.60	9.21	28.81	-2.53
1.0	27.34	19.10	29.97	-9.85
1.5	30.26	28.18	29.68	-18.15
2.0	n/a	32.66	n/a	-27.36

Table 5.5: Relative energies in kcal/mol for minima and transition states (relative to SP) along the TIM2 SP → TCC → TTC reaction path.

Force	TS3	TCC	TS4	TTC
0	13.91	9.26	30.69	3.79
0.5	7.64	-4.46	17.34	-8.99
1.0	4.37	-15.96	5.22	-20.24
1.5	2.15	-27.18	-6.99	-31.67
2.0	0.68	-38.47	-19.37	-43.45

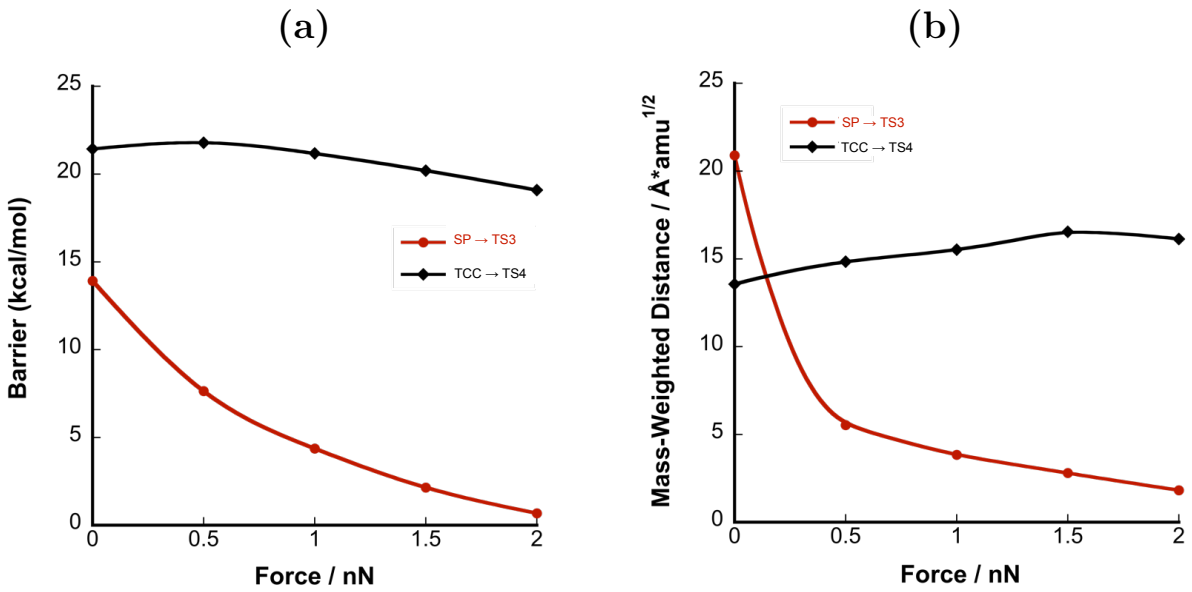

Figure 5.19: TIM2 confomer barrier and mass-weighted distance (MWD) along the MEP with respect to applied force **a**, The barrier height from SP to the TCC cisoid conformer (red line) and TCC to the TTC trans (black line). Increasing forces up to 2 nN indicate that the C-C isomerization barrier decreases by less than 5 kcal/mol compared to over 10 kcal/mol for the C-O barrier. **b**, The MWD to the transition state TS3 is the C-O barrier (red line), which decreases compared to TS4 which increases with applied force.

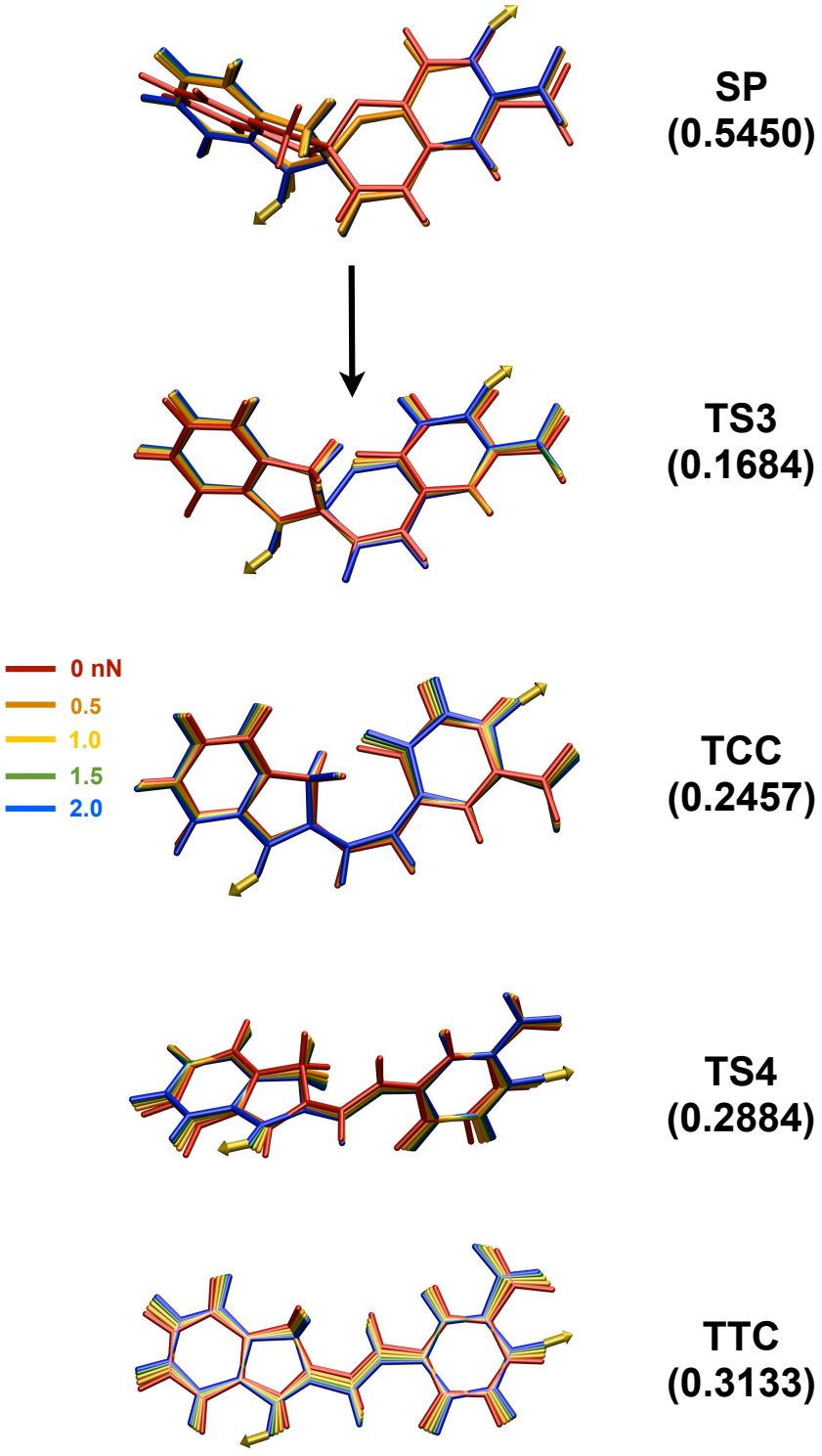

Figure 5.20: TIM2 Reactant, transition state, and product geometries at forces ranging 0-2 nN along the SP → TCC → TTC reaction route. The force free geometries are denoted in red, which are perturbed under applied force. The root mean square deviation (RMSD) with respect to the zero force geometry is indicated in parentheses.

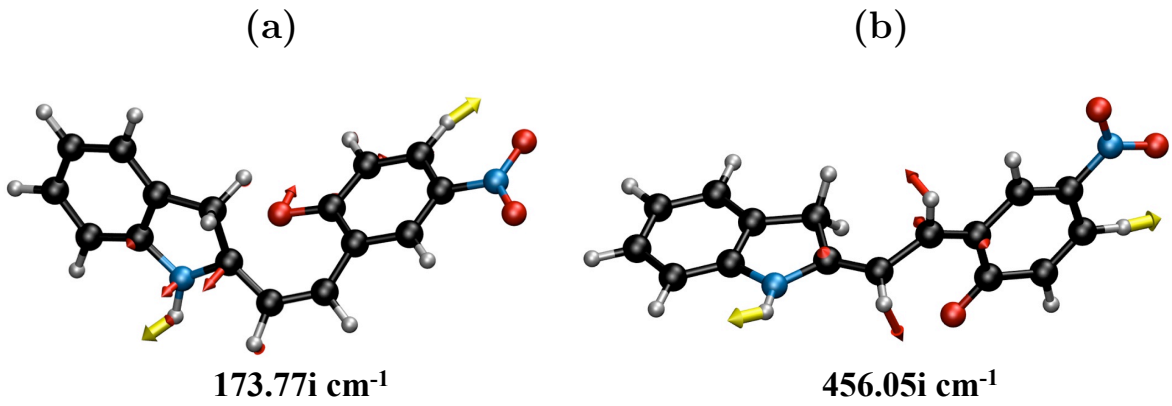

Figure 5.21: Transition states at 1 nN along the SP → TCC → TTC pathway with the normal modes shown by the red arrows. The yellow arrows are the external force vectors which indicate applied force at the H atoms and (i) designates the imaginary frequency in cm^{-1}. **a**, TS3 reflects the Spiro C-O reaction mode while **b**, TS4 is the C-C isomerization mode.

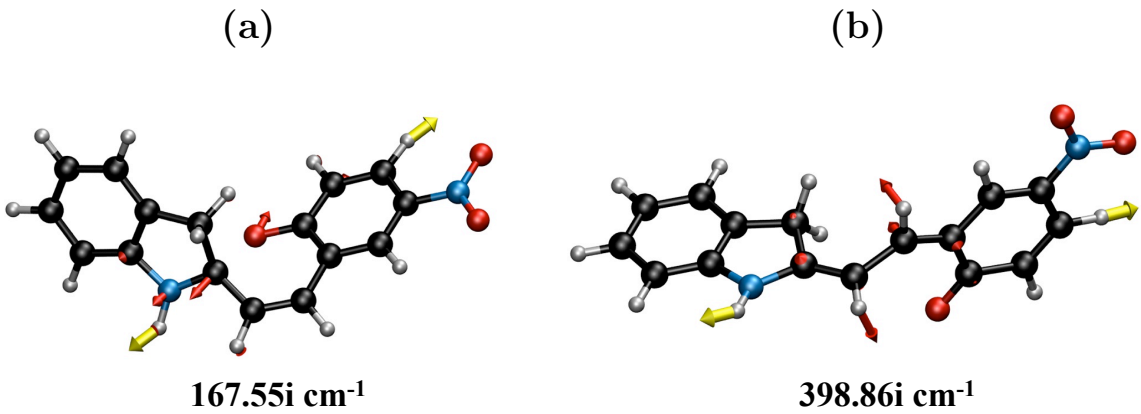

Figure 5.22: Transition states at 2 nN along the SP → TCC → TTC pathway, with the normal modes shown in red. **a**, TS3 reflects the Spiro C-O reaction mode. The imaginary frequency is greater than the TIM1 C-O mode, which would suggest a small reaction barrier. **b**, TS4 is the C-C isomerization mode.

The two dimensional FMPES contour plots are show in figure 5.23, which are similar to that of TIM1 with minor exceptions. For instance, at 0.5 nN the transition area between each minima for the SP → CCC → CTC pathway is narrower compared to TIM1. Also, the $\boldsymbol{\alpha}$ angle between SP ($\boldsymbol{\alpha}$: 115.64°, $\boldsymbol{\beta}$: -1.94°) and TCC ($\boldsymbol{\alpha}$: 173.63°, $\boldsymbol{\beta}$: -15.14°) minima is reduced to 57.99° at 0.5 nN, which is indicative of a shortened MWD from SP → TS3. With respect to the SP → CCC → CTC pathway, at 0.5 nN, the bond breaking reaction barrier towards the CCC conformer rises from 14.54 to 24.60 kcal/mol. The CCC minimum does not disappear at 1.5 nN, unlike TIM1, so a shallow well remains which is 28.18 kcal/mol

above SP. At 2 nN there is only a single barrier, 32.66 kcal/mol in height, and the pathway now proceeds from SP → CTC. This is analogous to the single barrier at 26.69 kcal/mol for TIM1 at 2 nN. Thus a single barrier forms in response to applied force and the CCC minima becomes a transition state. For TIM1 the single barrier emerges at 1.5 nN where CCC becomes a transition state, however, there is barrier lowering at 2 nN. Reaction dynamics, represented by the colored lines in figure 5.23, move along the MEP to the TTC isomer. None of the trajectories pass towards the CTC isomer unlike TIM1.

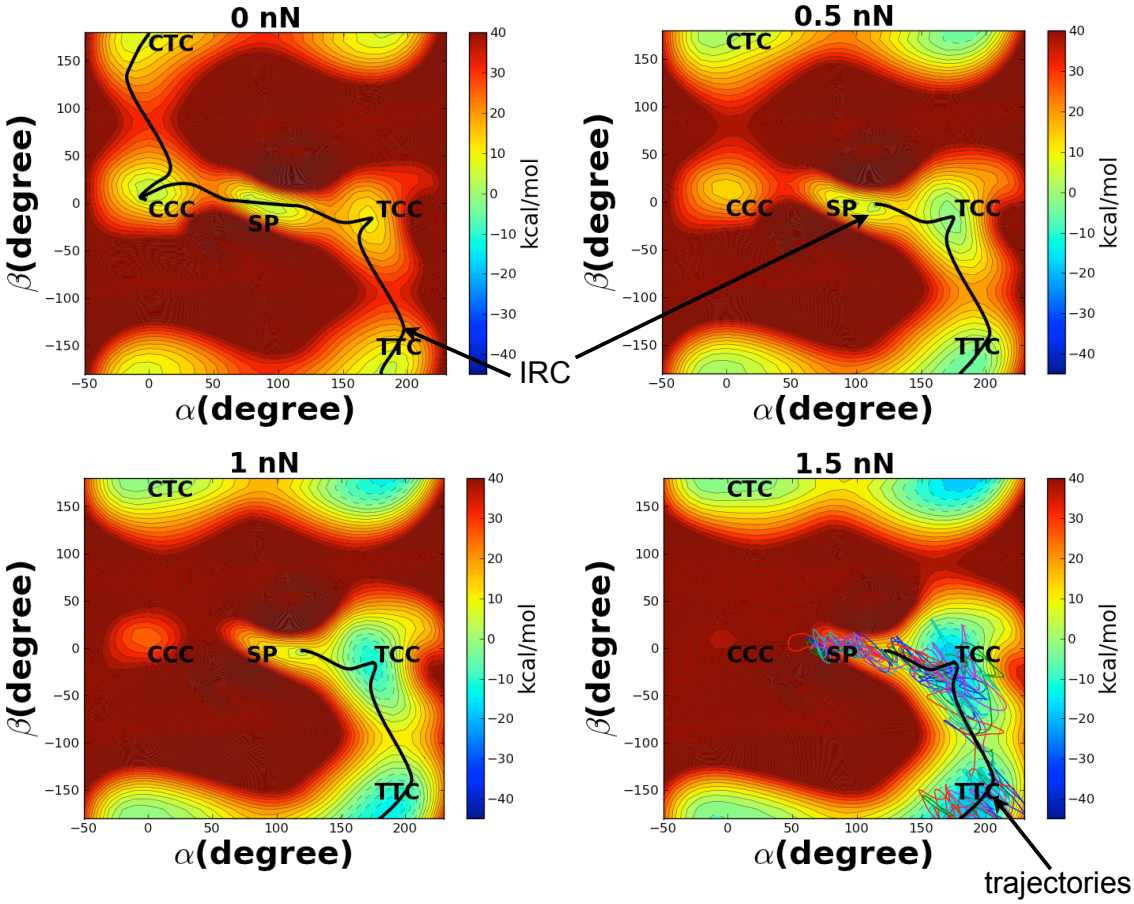

Figure 5.23: TIM2 2-D FMPES contour plot. A 0.5 nN force results in stabilization of the TCC conformer whereas the CCC conformer destabilizes. At 1 nN, transition to the CTC isomer from CCC is highly unfavorable due to a relative increase in energy. The MEP to the TTC isomer is shown by the solid black line. There is an increased stabilization about the TCC and TTC conformers as applied force is increased (blue wells). Steered molecular dynamics trajectories are shown at 1.5 nN on the contour plot. The trajectories follow along the MEP about the TCC minima before isomerization to TTC.

5.7 TIM2 Reaction Rates under External Force

There is a linear relationship between the activation barrier and the applied force as shown in figure 5.24. This relationship exists up to and after 1 nN. The activation barrier heights, with ZPE correction, represent the SP $\rightarrow$ TCC $\rightarrow$ TTC pathway. In the absence of external force 28.17 kcal/mol is required to surmount the barrier, which reflects C-C isomerization. External force makes the C-O dissociation barrier the rate-determining step. At 0.5 nN the TIM2 activation barrier is 15.13 kcal/mol in contrast to TIM1, which is 11.52 kcal/mol. For TIM2 this decreases to 3.03 kcal/mol and is approximately equal to the 2.97 kcal/mol barrier for TIM1. At 1.5 nN, the TIM2 barrier decreases to 1.88 kcal/mol, 1 kcal/mol greater than TIM1. Figure 5.22 indicates that the magnitude of the TS3 vibrational frequency would mean that the C-O barrier would remain at 2 nN, unlike TIM1. The calculated activation barrier for TIM2 at 2 nN is 0.49 kcal/mol, which is less than k_bT. Thus, the activation barrier does increase at 2 nN (with respect to TIM1) and suggests that trapping of the TCC conformer would be avoided. Figure 5.25 plots the reaction rate as a function of force. The rate increases linearly up to 1 nN, and changes marginally thereafter indicated by the flat region between 1-2 nN. The forward reaction rate at 0.5 nN, table 5.6, indicates that entropic forces required for chain elongation are enough to induce coloration within milliseconds. At the latter force, the calculated wavelength is 446 nm for the TTC isomer (figure 5.26). The wavelengths did not vary much for the TTC isomers, however, the wavelength increases with applied force for the TCC conformer. The wavelengths for the TCC conformer at 1 and 2 nN have oscillator strengths similar to the trans TTC isomers (See Appendix B), and this suggests coloration would occur after C-O bond breaking to TCC. Additionally, forces of 1 nN or greater will accelerate formation of the MC isomer on the order of pico-seconds.

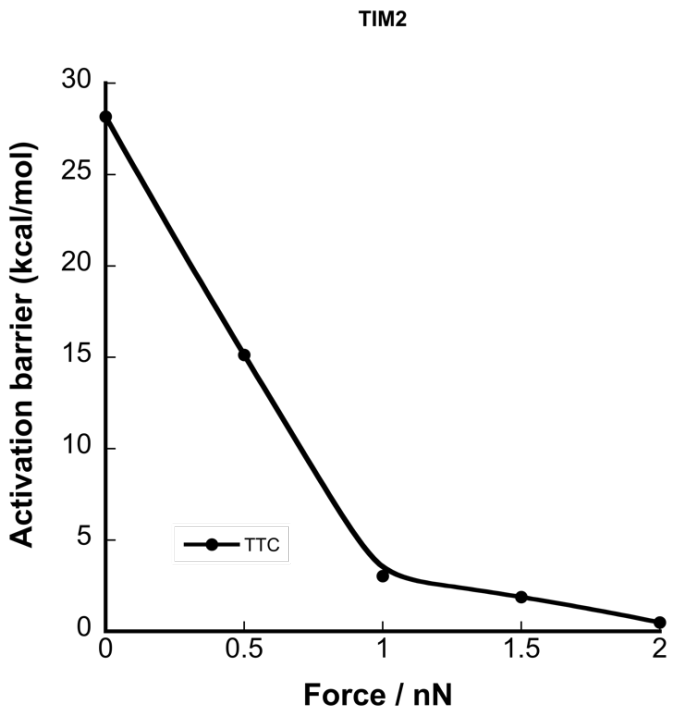

Figure 5.24: TIM2 activation barrier height as a function of applied force. The force free barrier is the energy difference between SP and TS4 for C-C isomerization. At applied forces equal to 0.5 nN, the activation barrier for each process is now the difference in energy between SP and TS3, which is the C-O bond dissociation barrier. However, unlike TIM1 the C-O barrier does not disappear at 2 nN.

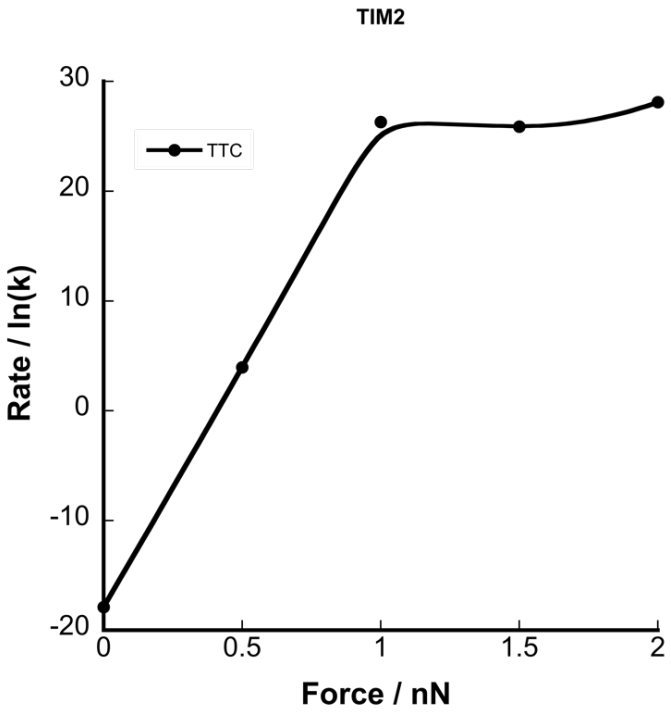

Figure 5.25: TIM2 reaction rate as a function of force. The reaction rate is dependent on the activation barrier height, shown in figure 5.24. The solid black line is the rate of ring opening towards the TTC isomer. At zero force the rate is dependent on the following barrier: SP $\rightarrow$ TS4. From 0.5-2 nN, the rate-determining step reflects the SP $\rightarrow$ TS3 or C-O bond breaking barrier. Unlike TIM1, the reaction rate does not decrease at 2 nN, since SP is a minimum at this force and the C-O barrier is therefore present.

Table 5.6: TIM2 lifetime of color formation in units of seconds.

Force	TTC
0	5.85e+07
0.5	1.90e-02
1.0	3.76e-12
1.5	5.74e-12
2.0	6.21e-13

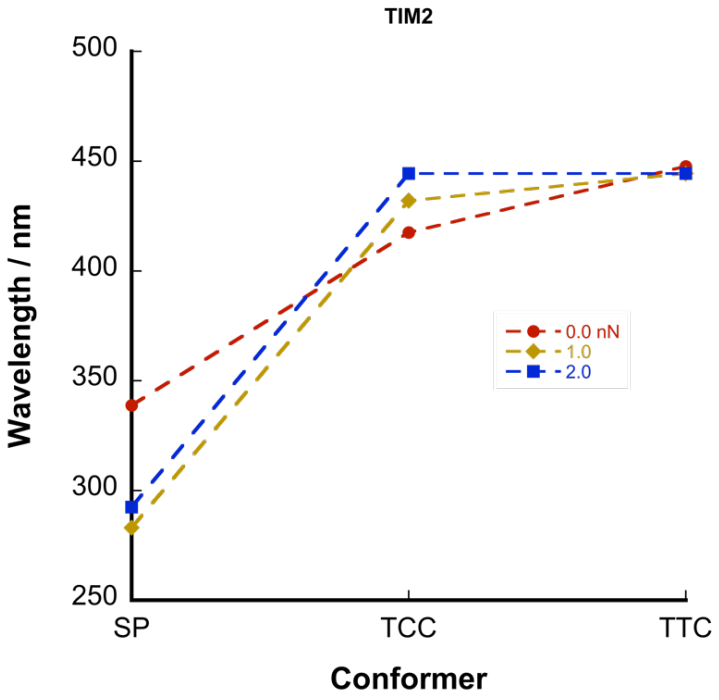

Figure 5.26: TIM2 absorption wavelengths as a function of the conformer. The wavelength for SP at zero force is blue shifted at forces of 1 and 2 nN. The wavelength for the trans TTC isomer remains unchanged and reflects the $\pi \rightarrow \pi^*$ transition. The cis-cisoid conformer, TCC, is red shifted with increasing force and also reflects the $\pi \rightarrow \pi^*$ transition, however, with an oscillator strength of approximately 0.7 at 1 and 2 nN. (See appendix B).

5.8 Ab Initio Steered Molecular Dynamics of TIM3

The mode of applied force for TIM3 (N-,C5) suggests that force transduction to the C-O would be less efficient, and therefore would result in the breaking of alternate bonds on the indole or benzopyran rings. The applied forces necessary to break a bond range from 3-5 nN, which is the largest force for all TIM pulling schemes. As figure 5.27a indicates, the C-O bond breaks for external forces ranging from 3-5 nN for one particular trajectory. Extended AISMD simulations for different starting configurations were studied to quantify the number of broken C-O bonds, shown in figure 5.27b. Only nine of the ten simulations cleaved at the C-O bond and the remaining one trajectory dissociated at the N-C on the indole ring. Snapshots for each reaction outcome are represented by figures 5.28 and 5.29.

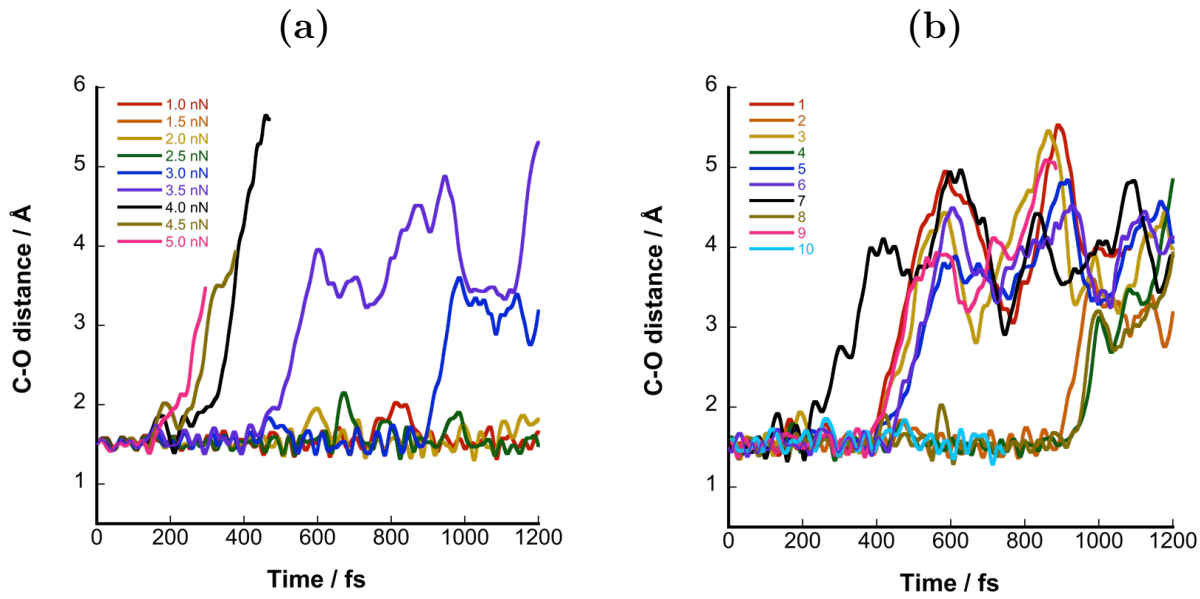

Figure 5.27: TIM3 C-O bond distance as a function of time. **a**, External force between 1-5 nN is applied for only one trajectory. The colored lines indicate different applied force. The C-O bond breaks within 1 ps with a minimal force of 3 nN. **b**, The C-O distance is plotted as a function of time for ten different initial trajectories (colored and labeled 1-10) at an applied force of 3 nN.

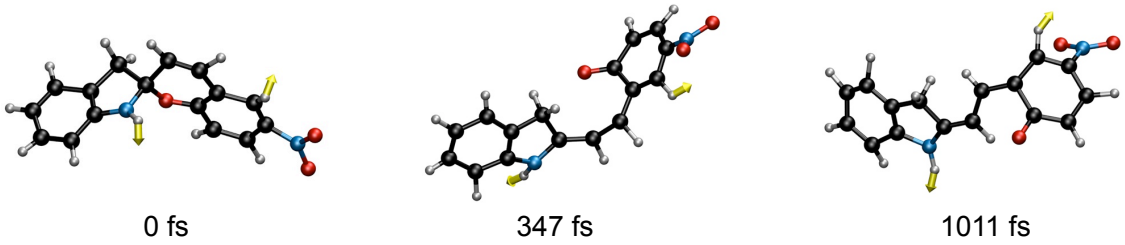

Figure 5.28: AISMD of TIM3 for one representative trajectory at 3 nN, SP → TCC → TTC. Following C-O bond cleavage near 347 fs, the cis-cisoid TCC conformer forms and undergoes subsequent C-C isomerization to the trans TTC isomer near 1 ps.

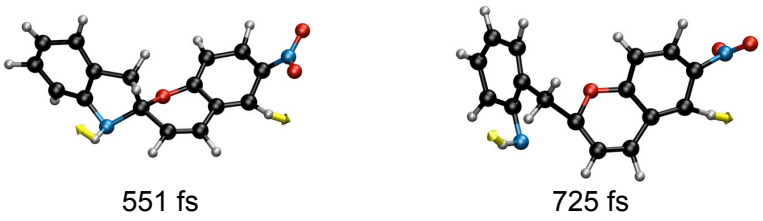

Figure 5.29: AISMD of TIM3 for one trajectory at 3 nN. There is no indication of ring-opening, instead, the N-C bond breaks at the indole ring.

Figure 5.30 plots the $\boldsymbol{\alpha}$ and $\boldsymbol{\beta}$ dihedral angles for ten reaction trajectories. Like TIM1 the trajectories follow the SP $\rightarrow$ TCC $\rightarrow$ TTC pathway. However, after C-O dissociation and formation of the cis-cisoid conformer, TCC, there is evidence of two possible routes the trajectories may follow. From TCC, the $\boldsymbol{\beta}$ angle may either decrease or increase, which either way involves isomerization of the C-C bond to form the MC isomer TTC. The isomer distribution for a total of thirty trajectories, figure 5.31, indicates a relatively larger number of trans-MC formation, with only two trapped at the cis-cisoid form, TCC. Eight trajectories do not exhibit ring opening, instead a bond on the indole ring breaks. For instance, seven trajectories cleaved at the N-C bond and one trajectory at a bond, adjacent to the N atom, connected to the benzene ring. Although nineteen of the trajectories form the trans MC product, these can undergo additional bond rupture also at the N-C bond. Due to the nature of the applied force at 3 nN, it is unclear whether forces greater than 2 nN can transduce effectively from the polymer back bone to the Spiro C-O bond, without breaking a bond along the polymer chain. Additional studies for TIM3 with extended polymer chains are required to understand the force-site and reaction barrier relationship. For instance, the dissociation energy for a C-C bond should be compared to the Spiro C-O barrier for an extended TIM3.

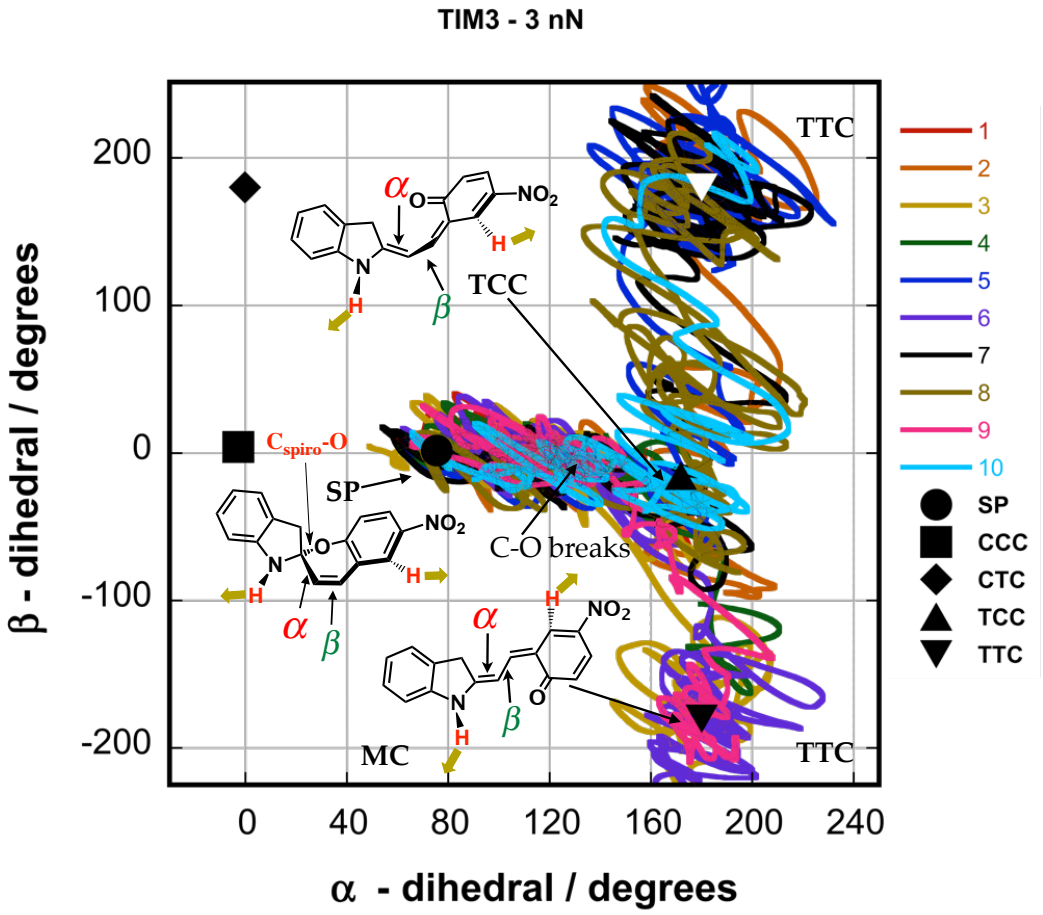

Figure 5.30: TIM3 2-D dihedral angle plot. The force free minima are shown by the black labeld markers (e.g. SP). The $\boldsymbol{\alpha}$ and $\boldsymbol{\beta}$ angles are shown for all ten trajectories which are designated by the colored lines (labeled 1-10). Starting at SP, the $\boldsymbol{\alpha}$ angle increases, which corresponds to C-O bond cleavage, and is followed by formation of the cis-cisoid conformer TCC. The cis-cisoid conformer will open to the trans isomer TTC. This is indicated by the $\boldsymbol{\beta}$ angle which may either increase or decrease by 180 degrees. Nine of ten trajectories, shown here, complete isomerization to the trans MC TTC isomer.

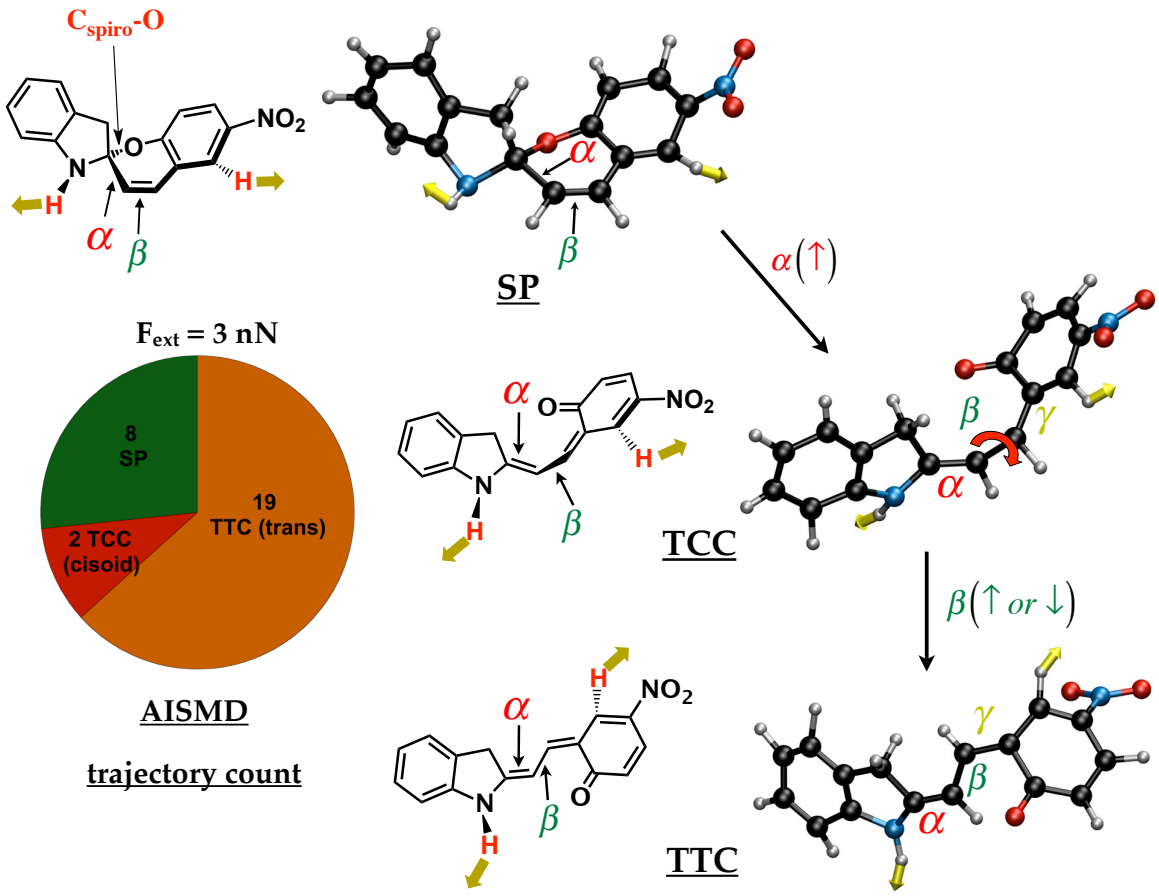

Figure 5.31: TIM3 conformer breakdown for thirty trajectories at 3 nN. Only one reaction pathway is followed throughout AISMD, SP → TCC → TTC. The presence of CTC formation is absent throughout. Within a 1 ps timescale, nineteen trajectories result in the formation of the trans MC, TTC, while two of the cis-cisoid conformers, TCC, do not undergo C-C bond isomerization. Additionally, eight trajectories do not undergo C-O bond cleavage and may break at other bonds (see figure 5.29).

5.9 References

[1] Hickenboth, C. R.; Moore, J. S.; White, S. R.; Sottos, N. R.; Baudry, J.; Wilson, S. R. *Nature* **2007**, *446*, 423.

[2] Ong, M. T.; Leiding, J.; Tao, H.; Virshup, A. M.; Martínez, T. J. *J. Am. Chem. Soc.* **2009**, *9*, 6377.

[3] Ribas-Arino, J.; Shiga, M.; Marx, D. *Chem.-Eur. J.* **2009**, *15*, 13331.

[4] Cottone, G.; Noto, R.; Manna, G. L. *Chem. Phys. Lett.* **2004**, *388*, 218.

[5] Maurel, F.; Aubard, J.; Rajzmann, M.; Guglielmetti, R.; Samat, A. *J. Chem. Soc., Perkin Trans. 2* **2002**, 1307.

[6] Wojtyk, J. T. C.; Wasey, A.; Kazmaier, P. M.; Hoz, S.; Buncel, E. *J. Phys. Chem. A* **2000**, *104*, 9046.

[7] Abe, Y.; Nakao, R.; Horii, T.; Okada, S.; Irie, M. *J. Photochem. Photobiol. A: Chem.* **1996**, *95*, 209.

[8] Horii, T.; Abe, Y.; Nakao, R. *J. Photochem. Photobiol. A: Chem.* **2001**, *144*, 119.

[9] Sheng, Y.; Leszczynski, J. *Collect. Czech. Chem. Commun.* **2004**, *69*, 47.

[10] Sheng, Y.; Leszczynski, J.; Garcia, A. A.; Rosario, R.; Gust, D.; Springer, J. *J. Phys. Chem. B* **2004**, *108*, 16233.

[11] Minkin, V. I. *Chem. Rev.* **2004**, *104*, 2751.

[12] Davis, D. A.; PhD dissertation; University of Illinois at Urbana-Champaign; 2010.

Chapter 6

Mechanotransduction Along Polymer Chains to Spiropyran Mechanophores

6.1 Introduction

Previous chapters have primarily highlighted the effect of applied force at various atom sites on spiropyran (SP), which reflected either SIM or TIM type pulling schemes. However, the SP mechanophore is incorporated at the middle of the polymer chain, which spans approximately one thousand covalent bonds.[1, 2] Thus, there is importance for studying how external force is transferred from the polymer backbone to the mechanophore itself. This will provide insight regarding the magnitude of applied forces for bond breakage at the mechanophore, which may change with respect to polymer chain length. Additionally, the relationship between the activation barrier height and polymer chain length with respect to applied force is necessary for designing mechanoresponisve polymeric architectures. The latter is tied to the reaction rate, which will be viable for predicting the timescales of mechanical activation.

6.2 Bond Cleavage Specificity and Reaction Mechanism for an Extended SIM1

Chapter 3 investigated the reaction outcome of an extended chain SIM1 using semi-empirical studies. The extended SIM1 (eSIM1) model reflects the experimentally studied SP mechanophore prior to polymerization or full chain linkage.[3] Simulations using Density Functional Theory (DFT), with B3LYP and a 6-31G basis, within the Terachem[4] software package were carried out here to validate the unchanging reaction mechanism for eSIM1. Additionally, the type of bond on the polymer chain (e.g. C-C or C-O) can determine the effectiveness of bond cleavage at the SP mechanophore. AISMD was ran for the eSIM1 mechanophore and the Spiro C-O bond was monitored for forces between 1- 4 nN. As figure 6.1a indicates, the Spiro C-O bond breaks for all forces equal to or greater than 2 nN. The results for ten simulations reflecting different starting configurations at 3 nN indicated that the Spiro C-O bond cleaved for all reaction trajectories (figure 6.1b).

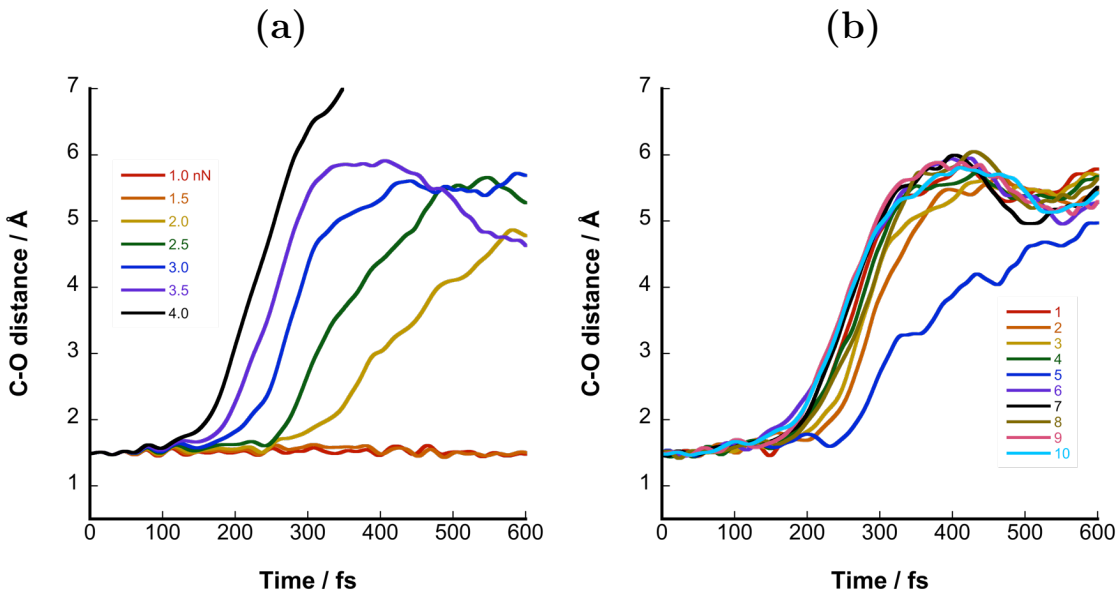

Figure 6.1: eSIM1 C-O bond length as a function of time **a**, External force between 1-4 nN is applied for only one trajectory. Each colored line indicates a different applied force. The C-O bond breaks within 500 fs with a minimal force of 2 nN. **b**, Ten different reaction trajectories (colored line labeled 1-10) at an applied force of 3 nN, which all indicate Spiro C-O bond cleavage.

The course of the reaction outcome results in either formation of the trans CTC or TTC isomer as figure 6.2 indicates. Figure 6.3 shows a representative snapshot of a trajectory opening to the CTC isomer. The snapshot at 284 fs reflects the transition after C-O bond cleavage and before C-C isomerization ($\boldsymbol{\alpha}$: 0°, $\boldsymbol{\beta}$: 80°). Figure 6.4 shows a representative snapshot for TTC formation; the image at 306 fs is the transition between SP and TTC ($\boldsymbol{\alpha}$: 160°, $\boldsymbol{\beta}$: -80°). The simulations did not indicate any rupture at the side C-O ester bonds, so ten additional simulations were carried out to confirm the frequency of bond cleavage at either the Spiro or ester C-O. Interestingly, all twenty simulations provided evidence of bond rupture at the Spiro C-O bond without any indication of the C-O ester bond breaking first. Furthermore, eighteen trajectories resulted in formation of the CTC isomer and the remaining two isomers were TTC. The latter reflects the initial starting configuration that has the polymer chain oriented such that CTC formation would be preferred.

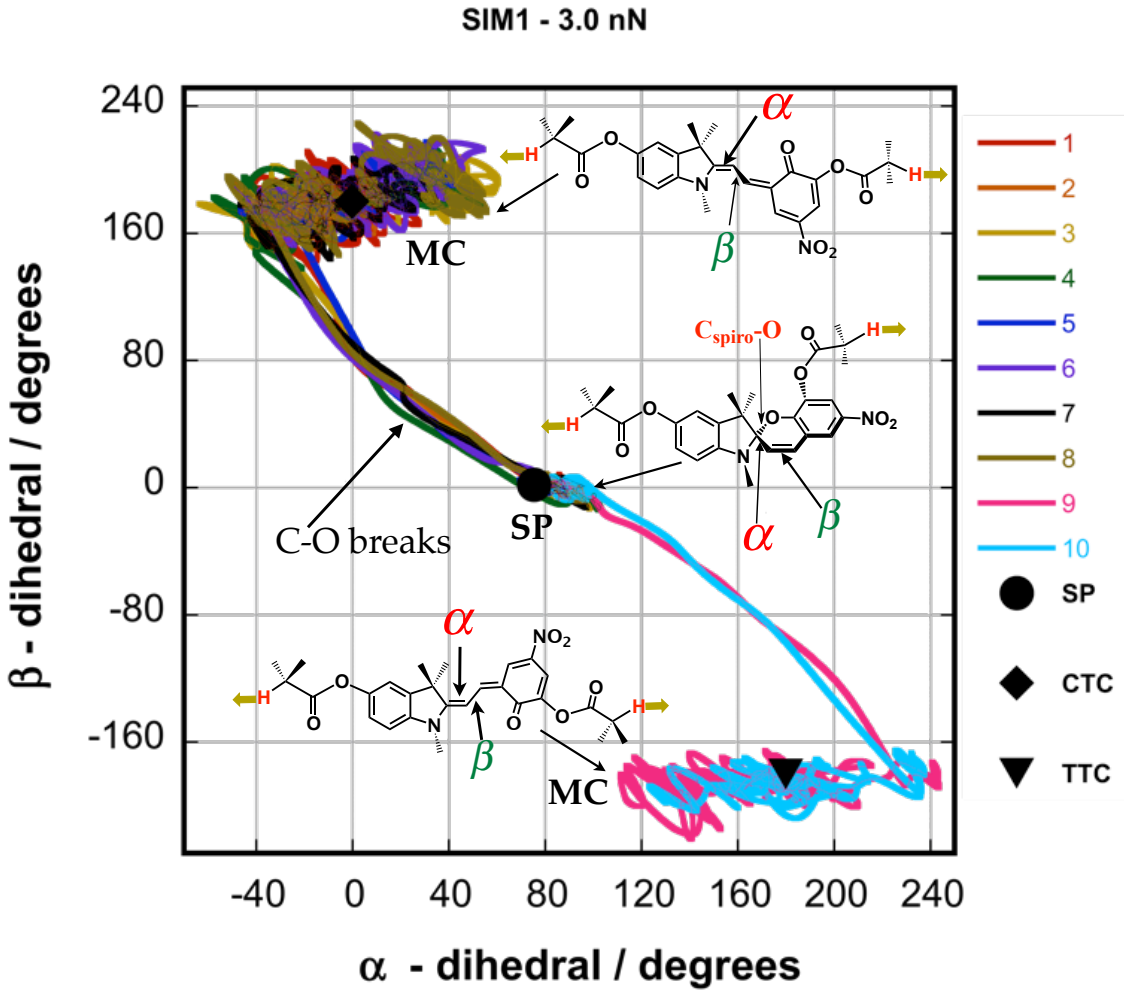

Figure 6.2: eSIM1 2-D dihedral angle plot. The force free equilibrium angles for each minimum are labeled by the black markers (e.g. SP). The $\boldsymbol{\alpha}$ and $\boldsymbol{\beta}$ angles are plotted at each timestep for all ten trajectories. Starting at SP, the $\boldsymbol{\alpha}$ angle decreases while $\boldsymbol{\beta}$ increases concurrently, which reflects C-O bond cleavage and C-C bond isomerization to trans CTC. Two trajectories shown here complete isomerization to the trans MC TTC, whereby the $\boldsymbol{\alpha}$ and $\boldsymbol{\beta}$ angle increase and decrease respectively.

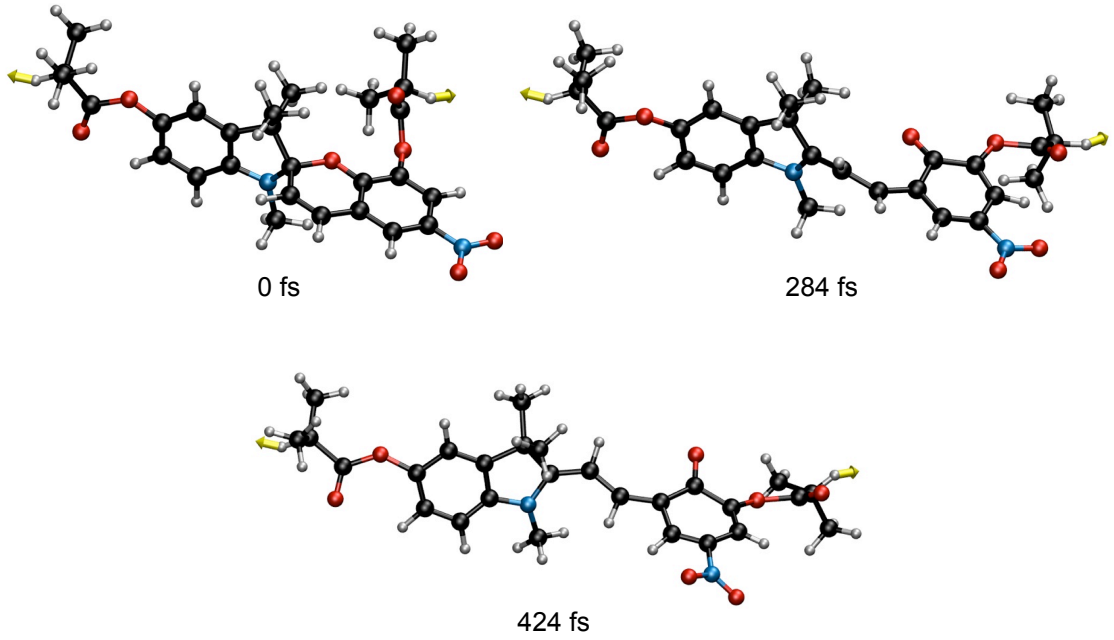

Figure 6.3: AISMD of eSIM1 for one representative trajectory at 3 nN, SP → CTC. Following Spiro C-O bond rupture, the cis-cisoid CCC conformer is bypassed (284 fs) and C-C bond isomerization to the trans CTC isomer follows.

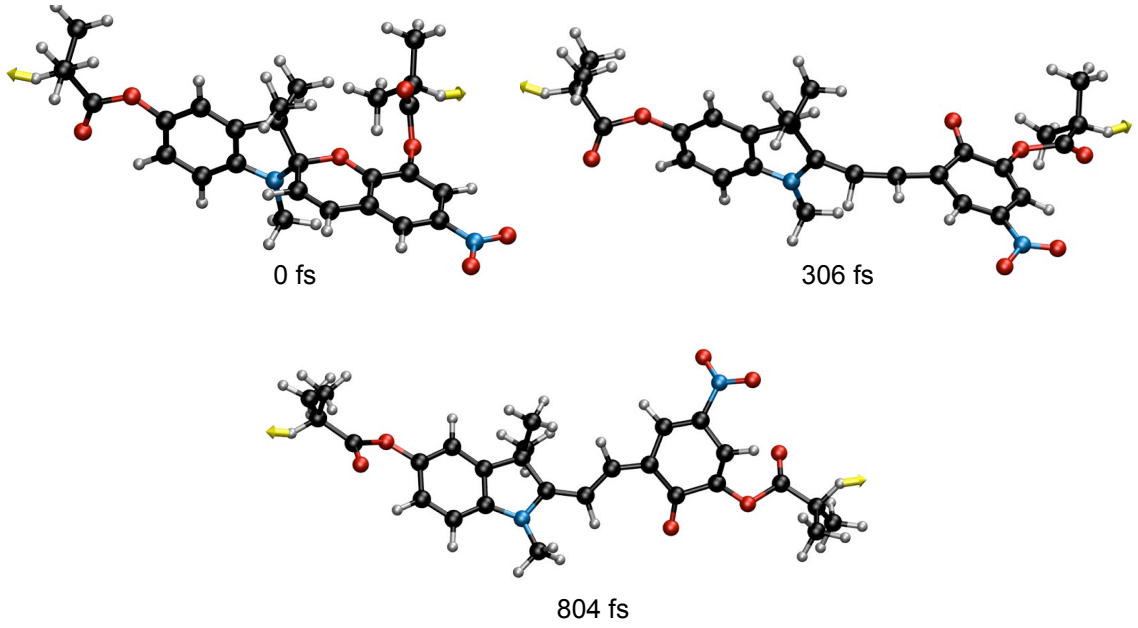

Figure 6.4: AISMD of eSIM1 for one representative trajectory at 3 nN, SP → TTC. After Spiro C-O bond rupture there is a subsequent C-C bond isomerization to the trans TTC isomer.

6.3 Extended SIM1 Energy Profile for Breakage at the Spiro Bond and Polymer Chain

AISMD for eSIM1 indicated bond rupture at the Spiro C-O bond at an applied force of 3 nN. None of the ten trajectories indicated breakage at the side chains, which may suggest that the barrier for side chain cleavage is relatively larger. The reaction profile was investigated for bond breakage at the Spiro C-O bond and at the ester C-O bond (indole side) for eSIM1. The barrier height with respect to force for bond cleavage at the Spiro and ester C-O bond is shown in figure 6.5 up to forces of 1.0 nN. The MEP for the reaction path corresponding to bond dissociation at the Spiro C-O bond in figure 6.5a indicates that the MWD from SP → TS1 increases with applied force. The force free barrier for the Spiro C-O bond to break is 10.38 kcal/mol at 8.29 Å*amu$^{1/2}$, however, the barrier and MWD increase to 12.88 kcal/mol and 16.99 Å*amu$^{1/2}$ at an applied force of 0.5 nN. The result of the barrier height increase can be described as a bond hardening effect when the magnitude of the applied forces is approximately equal to the chain entropic forces. This effect was described previously in chapter 4, whereby forces less than 1.5 nN did not show an appreciable reduction for the

Spiro C-O barrier. When the magnitude of the force is 1 nN the barrier increases to 13.11 kcal/mol at 16.91 Å*amu$^{1/2}$. Figure 6.6 shows the vibrational modes at the transition states for 0 and 1 nN respectively. The imaginary frequency, corresponding to a first order saddle point, at 1 nN increases reflecting bond hardening. It is expected that the activation barrier height will reduce linearly with respect to forces greater than 1 nN (as will be shown in the following sections), which is referred to as a bond softening effect.

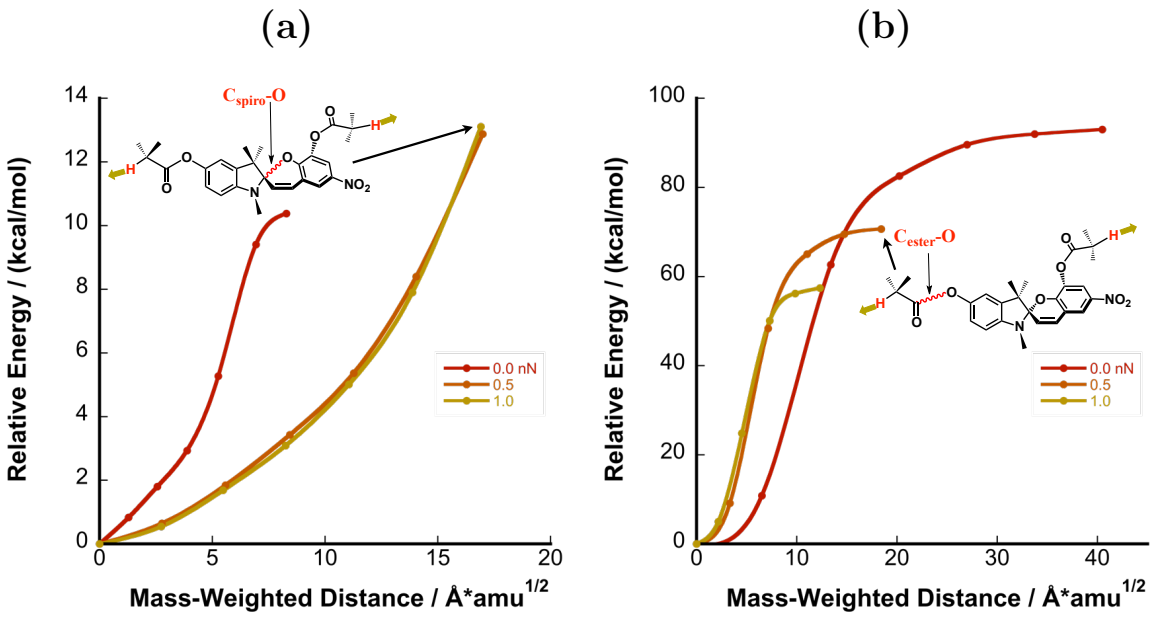

Figure 6.5: eSIM1 Minimal Energy Pathway (MEP) showing the relative Spiro C-O and ester C-O barrier heights as a function of the mass-weighted distance (MWD). **a**, MEP for bond breaking of the Spiro C-O bond up to forces of 1 nN. This can be referred to as the SP $\rightarrow$ TS1 barrier discussed in chapter 4. Interestingly, applied force will increase the Spiro C-O barrier and MWD along the reaction pathway. **b**, The reaction barrier for the ester C-O bond and MWD decreases with respect to applied force. This would suggest that C-O breakage at the side polymer chain is unfavorable and less likely which is in accord with AISMD results.

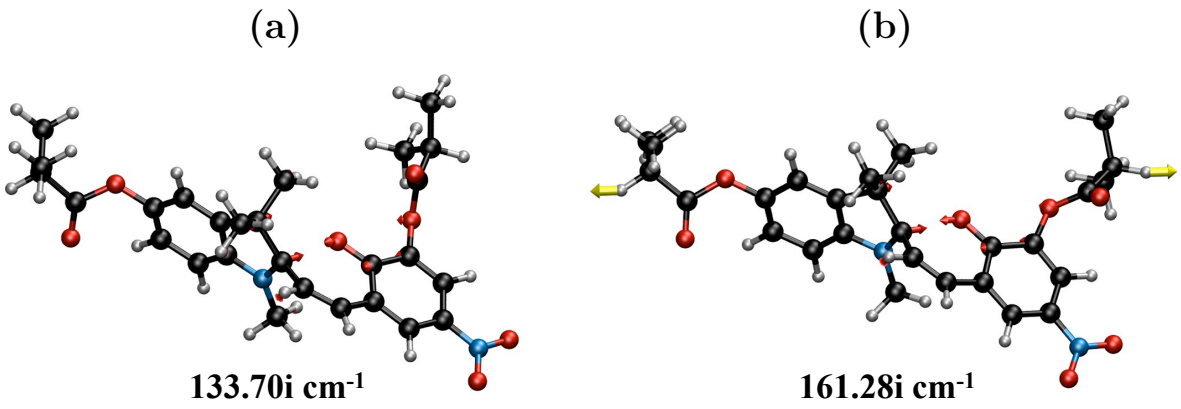

Figure 6.6: eSIM1 transition state geometries showing the imaginary frequencies designated by (i) and vibrational normal modes (red arrows) for TS1 at **a**, 0 nN and **b**, 1 nN. Both modes reflect breakage of the Spiro C-O bond. The yellow arrows indicate the location and direction of applied force.

A macroscopic load to the SP incorporated bulk polymer does not necessarily mean bond rupture will be specific to the Spiro C-O bond. The polymer chain network may involve entanglements and crosslinks, suggesting that applied force may therefore result in the cleavage of the polymer side chains.[5–7] The energy profile for dissociation at the ester C-O bond found on the polymer chain was studied, since it is the likely bond to undergo bond breakage. Figure 6.5 plots the ester C-O dissociation energy as a function of the MWD for forces up to 1 nN. A force free barrier of 93 kcal/mol at 40.48 Å*amu$^{1/2}$ was calculated for dissociation of the ester C-O bond, which is nearly nine times greater than the force free Spiro C-O barrier. An applied force of 0.5 nN results in bond softening of the ester C-O bond with a lower barrier equal to 70.68 kcal/mol at 18.43 Å*amu$^{1/2}$, almost 6 times more than the Spiro C-O bond. At 1 nN, the barrier is lowered to 57.42 kcal/mol at 12.31 Å*amu$^{1/2}$ and is 4 times greater than the Spiro C-O bond. It is unclear whether the barrier height difference will diminish at applied forces greater than 1 nN.

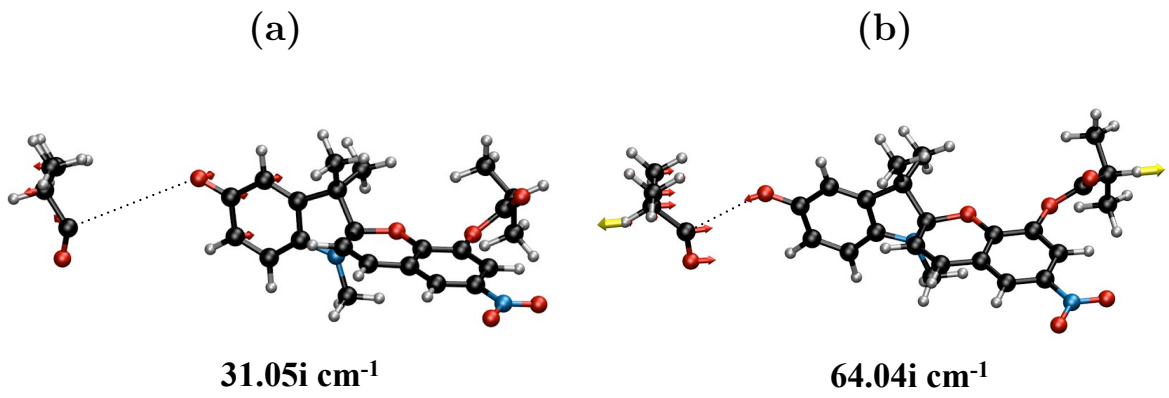

Figure 6.7: eSIM1 Transition state geometries showing the imaginary frequency (i) and vibrational normal modes (red arrows) for TS1 at **a**, 0 nN and **b**, 1 nN. The yellow arrows indicate the location and direction of applied force.

6.4 Extended SIM1 Reaction Barrier Heights under Applied Force

The change in the activation barrier height as a function of the force was studied for eSIM1 with increasing polymer chain length. The experimentally studied mechanophore incorporates ester C-O functional groups on the side chain, which is subsequently linked to a PMA or PMMA chain.[3] Replacement of the ester C-O functional groups with a hydrocarbon chain can increase the energy for bond cleavage on the polymer chain. Additionally, to determine the barrier height with increasing chain length and fixed force, it is computationally preferable and feasible to study the effect of applied force onto a simple hydrocarbon chain linked via eSIM1 attachments sites. Figure 6.8 illustrates the extended eSIM1 mechanophore incorporating a polyethylene chain, where the number of carbons atoms on the side chain is equal to three (N=3). The MEP for the eSIM1 mechanophore is shown in figure 6.9 for the SP $\rightarrow$ TS1 barrier.

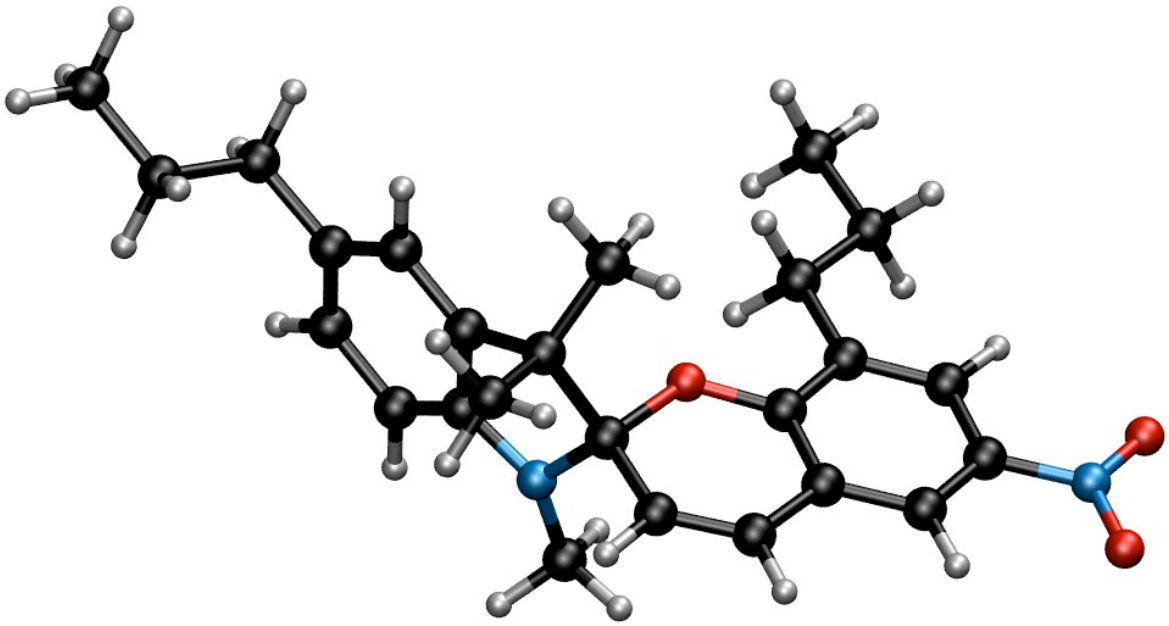

Figure 6.8: Force free SP equilibrium geometry incorporating polyethylene chains instead of the ester C-O side chains. The energy required for breakage at the side C-C polymer chain is expected to be greater than the ester C-O bond (See chapter 3).

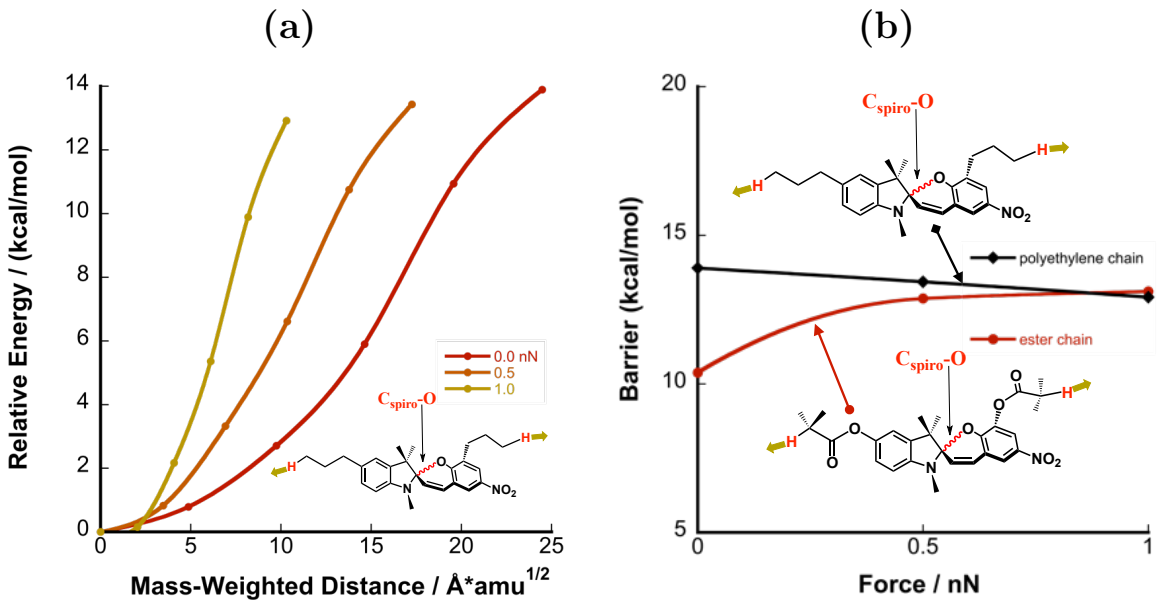

Figure 6.9: Minimal Energy Pathway (MEP) for an eSIM1 incorporating a polyethylene side chain and reaction barriers for eSIM1 with an ester or polyethylene chain. **a**, MEP for the Spiro C-O bond incorporating a polyethylene chain. The barrier height and mass-weighted distance (MWD) decreases as a function of applied force (colored lines). **b**, SP $\rightarrow$ TS1 barrier height for Spiro C-O bond breakage for the eSIM1 incorporating the ester or polyethylene chain. See appendix D for comparison to the eSIM1 ester chain MEP.

The energy profile in the absence of force is 13.90 kcal/mol at 24.48 Å*amu$^{1/2}$, which is greater with respect to the eSIM1 containing the ester side chains. Increasing the force to 0.5 nN results in a decrease of the energy barrier to 13.43 kcal/mol at 17.26 Å*amu$^{1/2}$. Thus incorporating polyethylene side chains show an opposite trend, that is a reduction in barrier height and MWD when the force is increased, unlike the eSIM1 with ester side chains which rises. This bond softening effect continues when the force is increased to 1.0 nN where the barrier height is 12.92 kcal/mol at 10.31 Å*amu$^{1/2}$. With regards to the Spiro C-O barrier height for the simplified SIM1 model discussed in chapter 4, the bond hardening effect is less pronounced. Therefore, side chains containing ester bonds, and perhaps similar polar bond connections, are responsible for the increase of the Spiro C-O barrier height up to forces of 1 nN. Figure 6.10 shows the vibrational modes for the first order saddle points at 0 and 1 nN respectively.

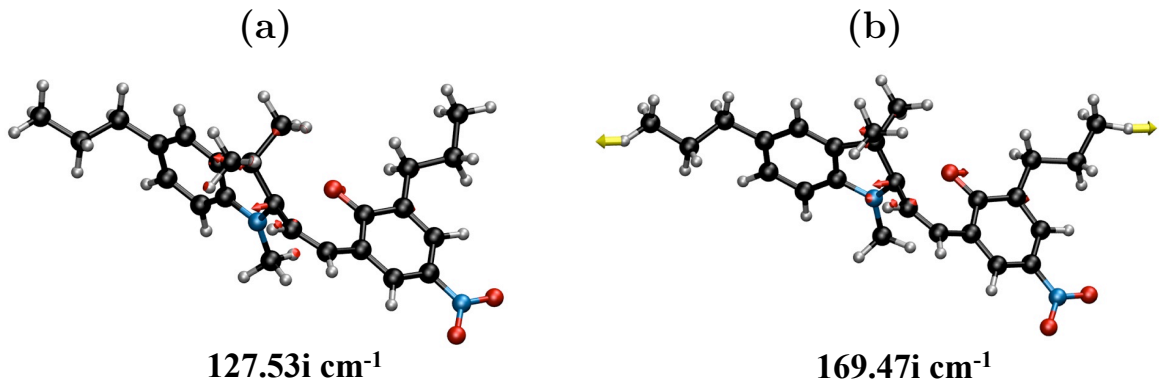

Figure 6.10: eSIM1 (polyethylene side chains) transition state geometries showing the imaginary frequencies (i) and vibrational mode (red arrows) for TS1 at **a**, 0 nN and **b**, 1 nN. The yellow arrows designate the location and direction of the applied force.

The activation barrier for the force free pathway, SP $\rightarrow$ TS1 $\rightarrow$ CCC $\rightarrow$ TS2 $\rightarrow$ CTC, is determined by the C-C isomerization barrier where TS2 has the highest absolute energy with respect to SP. However, applied force stabilizes TS2 such that the absolute energy is approximately equal to TS1 at relatively small forces or at 0.5 nN. As discussed in chapter 4, with respect to the SIM1 pathway, TS2 has an absolute energy greater than TS1 at 0 nN (See geometry coordinate appendix E). As the force is increased to 0.5 or greater, TS2 stabilizes whereby the absolute energy is less than that of TS1 and may even disappear on the FMPES. When reporting the activation barrier height, it will reflect the transition state with the highest activation energy on the PES, which is expected to affect the reaction rate the most. Transition state searches and local minima optimizations were carried out for varying polyethylene chain lengths (from N= 0,1,2,.., 20) where N is the number of C-C bonds that make up the polymer chain connected in a SIM1 fashion. The activation barrier, as a function of force shown in figure 6.11,was studied to determine the barrier dependence for varying chain lengths.

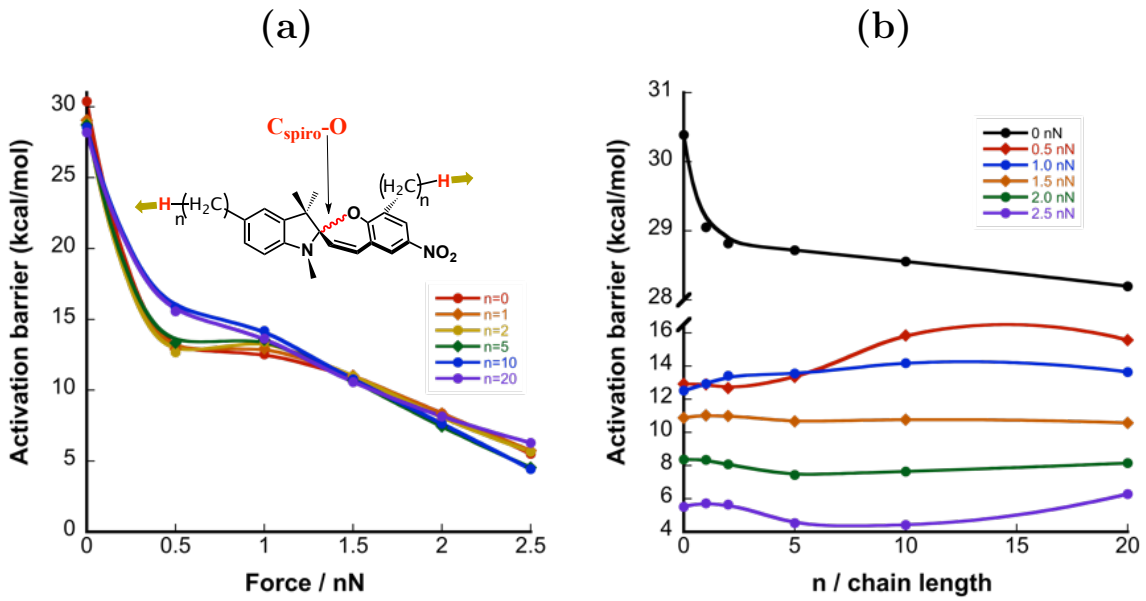

Figure 6.11: eSIM1 (extended polyethylene chains) activation barrier as a function of force and chain length. **a**, The activation barrier is plotted with respect to force, where the colored lines (labeled n=0-20) correspond to different chain lengths. The force free barrier is the difference in energy between SP and TS2 (C-C isomerization), however, at 0.5 nN and greater it is the difference between SP and TS1 (the C-O barrier). **b**, Activation barrier as a function of chain length. The applied force is indicated by the colored lines, which are labeled from 0-2.5 nN. The fluctuation in energy with increasing chain length is less than 5 kcal/mol, with respect to any force.

Figure 6.11a indicates that the barrier height fluctuates no more than 5 kcal/mol with respect to force for chain lengths up to N=20. The energy fluctuation is the energy difference between the lowest and highest barrier with respect to varying chain length and a fixed force. For example, at zero force the energy difference is 2.19 kcal/mol, where the highest barrier is N=0 and the lowest barrier N=20. The energy differences at each force is shown in Table 6.1. The change in barrier height as N increases is not necessarily systematic and with the exception of applied forces at 0.5 nN, the differences are within 2 kcal/mol (figure 6.11b). Similar studies for benzocyclobutenes with extended side chains have been reported by Marx *et. al.*[8, 9] For all chain lengths the difference in barrier heights is minimal when the applied force is 1.5 nN. The normal modes for the first order saddle point at 1.5 nN, N=5, is shown in figure 6.12. The imaginary vibrational mode corresponds to elongation of the Spiro C-O bond. Thus, the length of the chain does not necessarily influence the barrier height, and consequently the barrier and rate dependence will be intrinsic to the SIM1 mechanophore only; it is dependent on the Spiro C-O bond breaking or bond isomerization barrier.

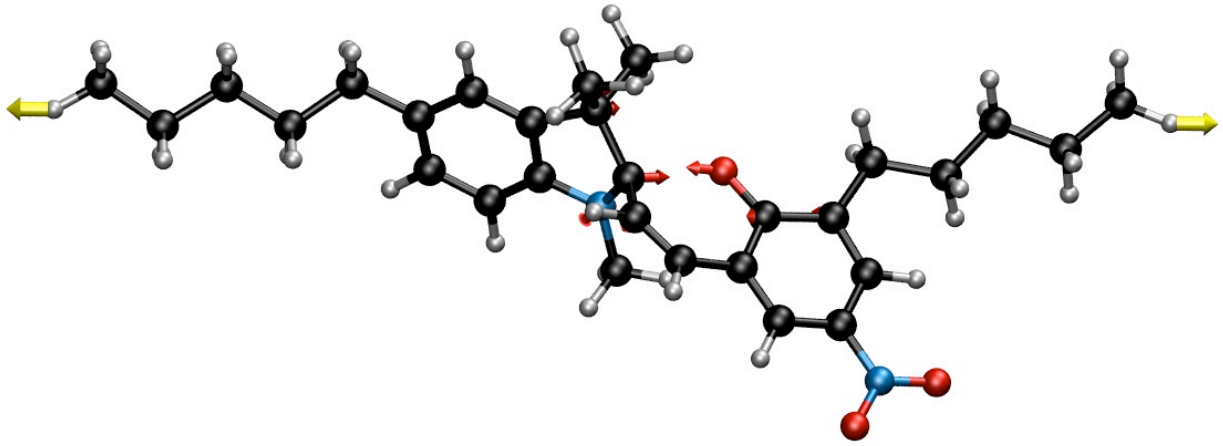

184.22i cm^{-1}

Figure 6.12: eSIM1 (N=5 with polyethylene side chains) transition state geometry showing the imaginary frequency (i) and vibrational normal modes (red arrows) for TS1. The yellow arrows, at the terminal H atoms, indicate the direction of applied force. The magnitude of the normal modes and frequency does not change significantly (See figures 4.13) with polymer chain addition.

Table 6.1: Difference in barrier height between the lowest and highest energy barrier for a particular chain length at a fixed force.

Force/nN	ΔE (kcal/mol)
0.0	2.19
0.5	3.17
1.0	1.65
1.5	0.45
2.0	0.93
2.5	1.86

6.5 Extended TIM2 Reaction Dynamics and Minimal Energy Pathways under Force

The outcome of the mechanochemical reaction will also depend on the connection of the polymer chain to the atom sites on SP, as reported in chapter 3. For example, the di-functional control was shown to be mechanically inactive since the force vector was not directed along the Spiro C-O bond. Modeling indicated that bond cleavage resulted at the terminal C-C bond instead. Of interest is channeling the force vector to facilitate bond rupture at the Spiro C-O bond. As discussed previously in chapter 5, molecular dynamics simulations indicated that applied force at TIM would result in ring-opening of SP to a cis-cisoid intermediate followed by formation of a specific MC isomer. Additionally, the MEP for TIM indicates that the barrier corresponding to bond breakage at the Spiro C-O bond is lower and decreases relatively faster compared to SIM. Applied force along the TIM coordinate also demonstrates reaction pathway bias, unlike the SIM series, which indicates the competition of two pathways or the formation of two reaction products.

Douglas Davis reported the mechanical activation of TIM1 polyurethane when subject to tensile testing.[10] The reported absorbance measurement is similar to that of SIM1, which is between 550-600 nm. The reported color change is consistent with TIM1 molecular dynamics simulations, which shows the formation of one MC isomer. Simulations were carried out for TIM2, whereby the pulling atom site is one bond further away with respect to TIM1. Since the force vector along the Spiro C-O bond is less coupled, it is expected that TIM2 may be mechanically less active than TIM1. For instance, when the applied forces are 0.5 nN the TIM1 activation barrier is 13.70 kcal/mol in contrast to TIM2, which is equal to 17.34 kcal/mol. The activation barriers for SIM1 and SIM2 towards the CTC isomer are 14.86 and 19.72 kcal/mol at 0.5 nN. Tables 4.2-4.6, show the barrier heights and rates for SIM1 and SIM2. The differences in activation barriers for both SIM1 and SIM2 diminish at forces of 1.0 nN or greater. However, the peaked absorption intensity for SIM2 is interestingly less than SIM1.[10] This implies that mechanical forces exerted on the SP mechanophores, for bulk testing, on average may be less than 1 nN. An extended TIM2 mechanophore incorporating ester functionalized side chains was studied to deduce the possible forces in bulk testing. Additionally, the role of polymer chains and its effect on reaction barriers was investigated by locating the MEPs on the FMPES in order to quantify the change in activation barriers.

AISMD simulations were first carried out for an extended TIM2 (eTIM2) for one trajectory at forces ranging from 1-3 nN, shown in figure 6.13a. The Spiro C-O bond breaks with forces as low as 2 nN within a timescale of 1 ps. Ten additional simulations were carried out with an applied force of 2 nN and the Spiro C-O bond was monitored up to 2 ps (figure

6.13b). All ten simulations indicated breaking of the Spiro C-O bond. Only one reaction pathway is accessed as figure 6.14 indicates. Following ring-opening only eight trajectories remain trapped at the TCC intermediate while two trajectories pass from TCC to TTC via C-C isomerization. However, this does not necessarily determine that TCC will not isomerize to the MC isomer. Formation of MC isomer may be seen if the simulation is allowed to run at longer timescales. In addition, the reaction outcome will depend on the pulling direction and initial starting geometry. For example, if the ester group on the polymer chain is placed closer to SP the geometry will have greater conformation energy. As a result, it will access the reaction product more easily due to excess energy.

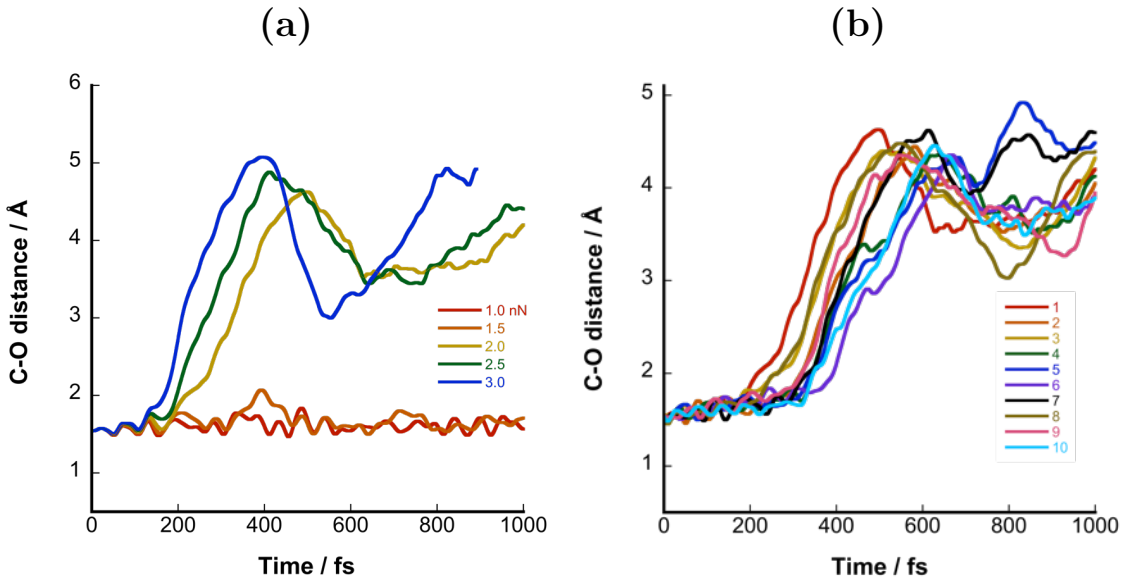

Figure 6.13: eTIM2 C-O bond distance as a function of time. **a**, External force between 1-3 nN is applied to one trajectory. Each colored line represents the same trajectory, however, pulled at a different force (1-3 nN). The C-O bond breaks within 300 fs with a minimal force of 2 nN. **b**, Ten trajectories labeled, by the colored lines 1-10, were each pulled at an applied force of 2 nN. The reaction outcome is the same for all trajectories whereby the C-O bond breaks.

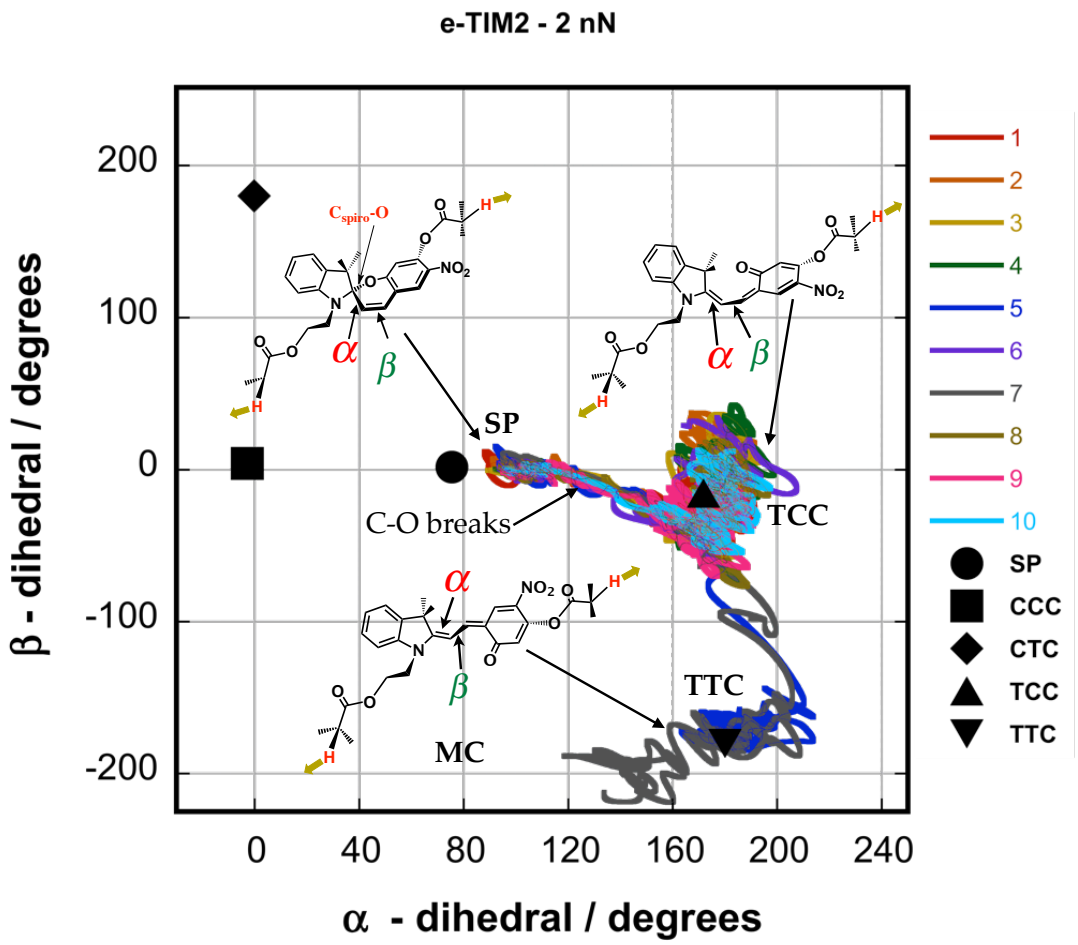

Figure 6.14: eTIM2 2-D dihedral angle plot. The force free equilibrium isomers are labeled in black. The $\boldsymbol{\alpha}$ and $\boldsymbol{\beta}$ angles were plotted throughout reaction dynamics for all ten trajectories up to 2 ps. Only two trajectories complete isomerization to the TTC trans MC conformer, whereby the $\boldsymbol{\alpha}$ angle increases first, which indicates cleavage of the Spiro C-O bond, to from the TCC intermediate. This is followed by a decrease in $\boldsymbol{\beta}$, which signifies C-C bond isomerization to the TTC isomer.

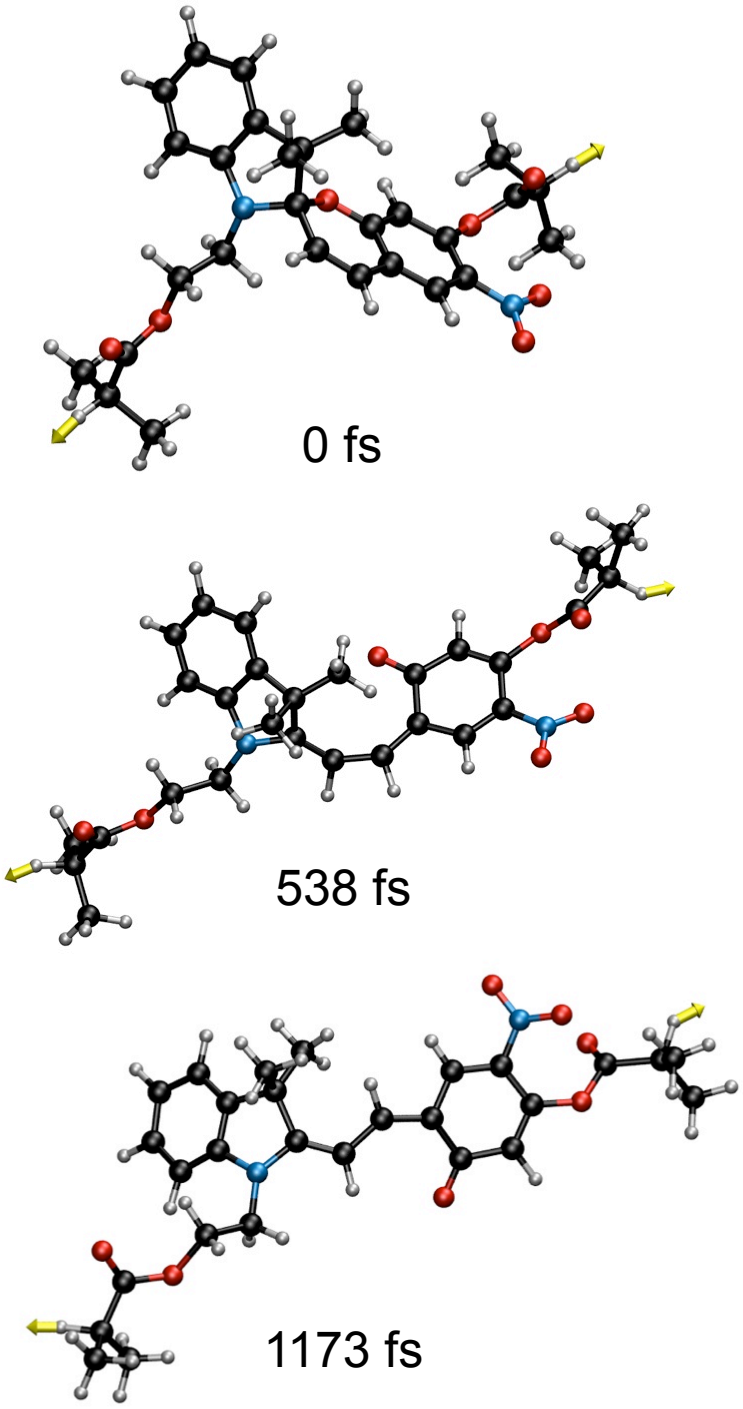

Figure 6.15: AISMD of eTIM2 for one representative trajectory at 2 nN, SP → TCC → TTC . Breakage of the Spiro C-O bond indicates formation of TCC at 538 fs, which then undergoes C-C bond isomerization to form the TTC isomer at 1173 fs.

Molecular dynamics simulation of TIM2 demonstrates reaction pathway selectivity and a two-step process where the Spiro C-O bond breaking and C-C bond isomerization steps occur separately. Therefore, two reaction barriers are expected on the MEP at 2 nN. The reaction barrier corresponding to C-C bond isomerization is likely greater than the first barrier. This is justified by figure 6.14 where most of the trajectories remain at the cis-cisoid TCC. To confirm the latter, the MEP on the FMPES was determined at forces between 0-2 nN, shown in figure 6.16. The force free pathway is a single barrier transition, from SP $\rightarrow$ TTC , equal to 30.83 kcal/mol. This is a concerted reaction process in which the Spiro C-O bond breaks and the $\boldsymbol{\beta}$ C-C bond isomerizes simultaneously. Thus, there is no TCC intermediate, which is found for the simplified TIM2 in chapter 4 which shows a double barrier on the force free reaction pathway. However, this is attributed to the methyl groups attached to the indole ring, which was not accounted for in the simplified SP model. Stabilization of the TCC conformer is not allowed, since the Spiro-oxygen atom occupies a region near two-methyl groups on the indole ring. Regarding the force free reaction pathway towards the CTC isomer, the CCC minima will be present regardless if the methyl groups are included. In the CCC conformation, the Spiro-oxygen atom occupies space near a single methyl group on the indole ring, which is attached to the nitrogen atom.

As figure 6.16 suggests, under an applied force of 0.5 nN the TCC conformer is stabilized and there are two reaction barriers as a result. The first reaction barrier corresponds to breaking of the Spiro C-O bond, which is equal to 9.53 kcal/mol (the SP $\rightarrow$ TS3 barrier). The intermediate TCC is 9.18 kcal/mol with respect to SP. Thus, the reverse reaction barrier is less than 0.5 kcal/mol. The second barrier from TCC $\rightarrow$ TTC refers to C-C bond isomerization and is equal to 18.72 kcal/mol with respect to the SP $\rightarrow$ TS4 transition. The reaction barrier from TCC $\rightarrow$ TS4 is 9.54 kcal/mol. Table 6.2 lists the relative energy barriers in kcal/mol for several transitions at forces between 0-2 nN. The transitions for SP $\rightarrow$ TS3 and SP $\rightarrow$ TS4 show a decrease in the barrier height. However, with regards to SP $\rightarrow$ TS4 at forces of 1.5 and 2.0 nN, the values are negative since TS4 lies below SP. Starting at the TCC minima, there would be two competing pathways since there are two reaction barriers: TCC $\rightarrow$ TS3 and TCC$\rightarrow$ TS4. At forces of 0.5 and 1.0 nN, the TCC $\rightarrow$ TS3 barriers are relatively lower. However, at forces of 1.5 and 2.0 nN, the TCC$\rightarrow$ TS4 barriers are lower. At 2.0 nN the SP $\rightarrow$ TS3 barrier is 0.67 kcal/mol, which is approximately equal to k_bT. A ZPE correction to the simplified TIM2 model did not remove the barrier, however, it is likely that the polymer chain will have an influence on the ZPE.

Figure 6.17 plots the activation barrier height (excluding the ZPE correction) as a function of force for the simplified TIM2 (Chapter 5) and the eTIM2, which incorporates the polymer side chains. The activation barrier is the difference in energy between the TS with

the highest absolute energy on the FMPES and SP, respectively. Differences arise primarily at forces of 0.5 and 1.0 nN, which are approximately 1-2 kcal/mol apart. Nonetheless, as reported in section 6.5, incorporation of the polymer side chains show minute energy differences as the chain length is increased. For the force free pathway, the activation barrier is dependent on a TS that describes Spiro C-O bond cleavage and C-C isomerization, unlike the SIM series. Figure 6.18-6.20 shows the normal vibrational modes at zero force and applied forces of 1 nN. At forces of 0.5 nN or greater, there are two transition states on the FMPES, which reflect Spiro C-O cleavage and C-C bond isomerization, figures 6.19-6.20. Assuming that the extended TCC conformer has a similar oscillator strength like the simplified TIM2 model (See appendix B), if color generation is not observed in bulk, this suggests that applied force to the polymer chains (on average) is no greater than 1.5 nN.

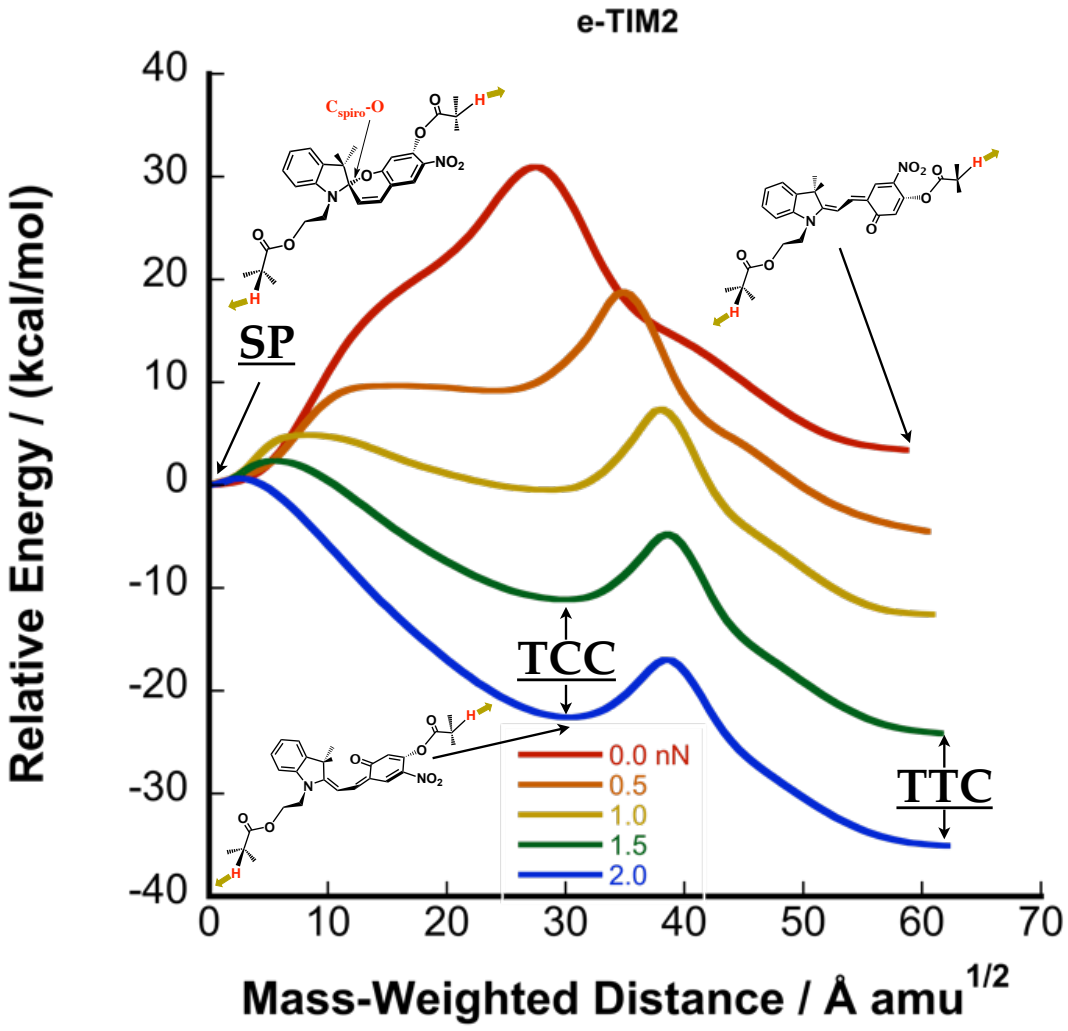

Figure 6.16: eTIM2 Minimal Energy Pathway on the FMPES, SP → TCC → TTC. The force free reaction pathway is a concerted process in which the Spiro C-O bond breaks and C-C bond isomerization occurs. Under an applied force of 0.5 nN the activation barrier height is reduced, however, the intermediate TCC is formed. Increased force stabilizes TCC with respect to SP and a two-step reaction process is evident separating the bond breaking and isomerization steps.

Table 6.2: Relative barrier heights (kcal/mol) between local minima and transition states.

Force/nN	SP → TS3	SP → TS4	TCC → TS3	TCC → TS4
0.0	n/a	30.83	n/a	n/a
0.5	9.53	18.72	0.36	9.54
1.0	4.86	7.33	5.31	7.78
1.5	2.38	-4.80	13.51	6.33
2.0	0.67	-16.97	23.24	5.60

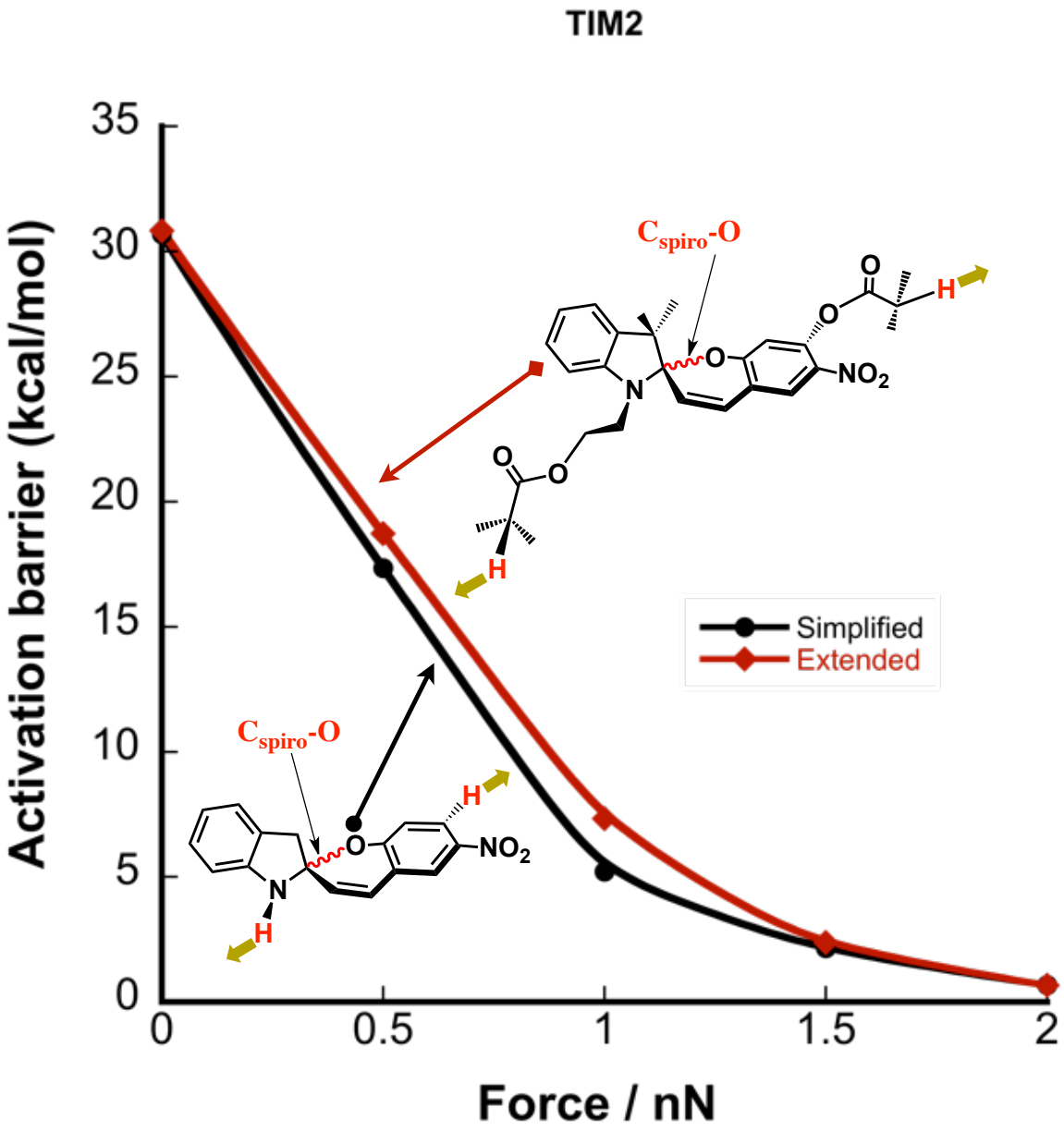

Figure 6.17: TIM2 and eTIM2 activation barrier as a function of force. The black solid line is the simplified TIM2 model studied in chapter 5. The solid red line is the eTIM2 model, which contains the C-O ester chains. The activation barrier height is based upon the transition state with the highest absolute energy on the FMPES with respect to SP.

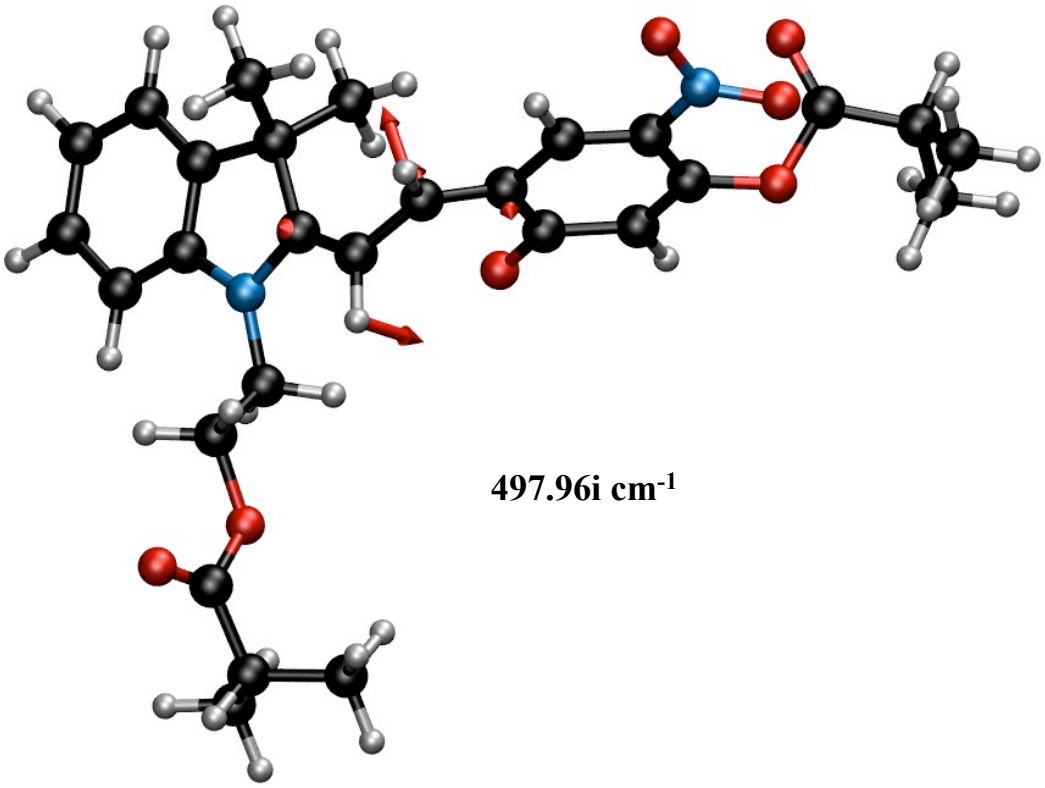

Figure 6.18: eTIM2 transition state geometry on the force free PES. The imaginary frequency (i) and normal vibrational modes (shown by the red arrows) correspond primarily to C-C bond isomerization.

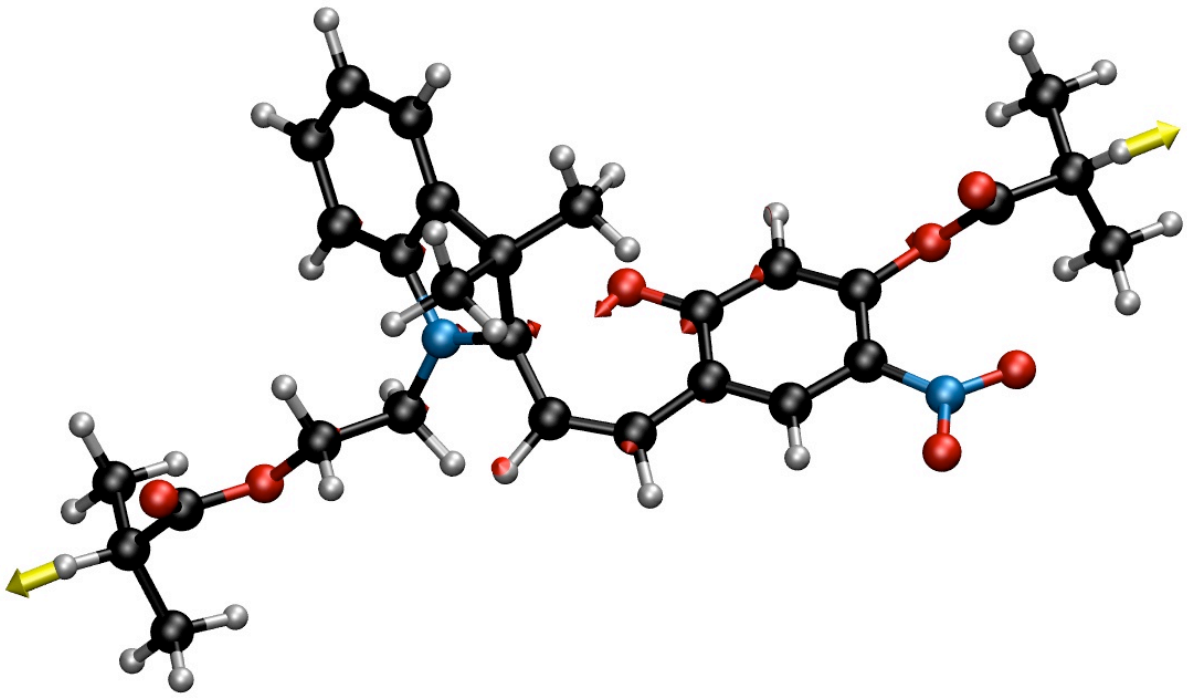

73.39i cm^{-1}

Figure 6.19: eTIM2 transition state geometry, TS3, on the FMPES at 1 nN. The normal vibrational modes indicate (red arrows) the dissociation coordinate of the Spiro C-O bond. The yellow arrows indicate the location and direction of applied force.

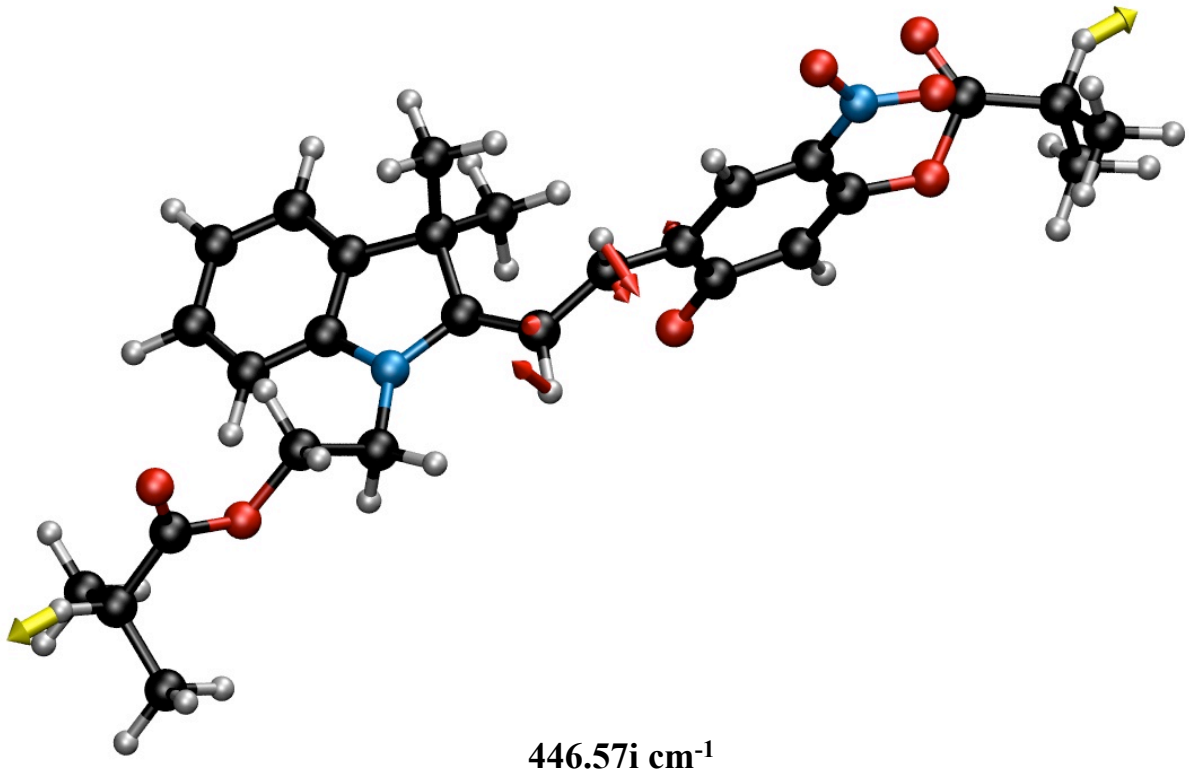

Figure 6.20: eTIM2 transition state geometry, TS4, on the FMPES at 1 nN. The normal vibrational modes (red arrows) reflect C-C bond isomerization. The value of the imaginary frequency (i) is similar to that found in simplified versions of TIM2 (see figure 5.21). External force is applied at the H atoms (yellow arrows) which indicate the direction of applied force.

6.6 Future Directions in Mechanochemistry Simulations

The computational tools developed in the Martínez group have successfully provided a framework for probing and predicting the mechanical reactivity of spiropyran and other related mechanophores.[3, 11–14] Additionally, recent innovations in computational algorithms and computer architectures, using Graphical Processing Units (GPUs), have made the study of larger molecular systems possible.[4, 15–17] The considerable achievement in high performance computing has enabled a reduction in computation time for AISMD simulations and MEPs on the FMPES for polymer linked SP mechanophores. For instance, one AISMD simulation of a spiropyran mechanophore (B3LYP 6-31G for 33 atoms or 213 basis functions) will require 168 hours using Central Processing Units (CPUs). However, using GPUs the amount of time is reduced to 6 hours. Questions regarding the effect of mechanical force on a mechanophore at various attachment points, and the change in activation barrier height with different donating and withdrawal groups can now be answered promptly. This aspect is vital since synthesizing the mechanophore-linked polymer followed by mechanical testing can be time consuming and expensive.

There are still challenges regarding the appropriate theoretical methods to use for novel mechanophore polymer architectures For example, if one undertook a computational study of a polymer chain incorporating a spiropyran and cyclopropane linked polymer. As shown, the labile bond on spiropyran is the C-O bond, which can be considered primarily ionic. Density Functional Theory would be appropriate, however, the breakage of a C-C bond (polymer chain or cyclopropane) typically requires post-Hartree Fock methods.

Furthermore, more studies are needed regarding mechanohpore reactivity and stability (e.g. barrier or equilibrium between SP and MC) in different polymers and the environment. The previous sections highlighted (figure 6.9) the barrier height differences between a polyethylene and ester chain linked SIM1. The environment is also expected to shift the equilibrium between SP and MC. Douglas Davis reported a bias towards the MC isomer for TIM1 polyurethane.[10] A quantum mechanics molecular mechanics (QMMM) simulation incorporating mechanical force would be a new direction and approach for studying mechano-chemical environmental effects.[18–20] Additionally, this type of simulation can employ random forces at the mechanophore, and would provide a more accurate picture for experiments using ultrasound to induce mechanical transformations. Simulations incorporating external effects such as chain entanglements and cross-linking is another direction and now capable using GPUs.

6.7 References

[1] Potisek, S. L.; PhD dissertation; University of Illinois at Urbana-Champaign; 2008.

[2] Potisek, S. L.; Davis, D. A.; Sottos, N. R.; White, S. R.; Moore, J. S. *J. Am. Chem. Soc.* **2007**, *129*, 13808.

[3] Davis, D. A.; Hamilton, A.; Yang, J.; Cremar, L. D.; Gough, D. V.; Potisek, S. L.; White, S. R.; Moore, J. S.; Sottos, N. R.; Ong, M. T.; Braun, P. V.; Martínez, T. J. *Nature* **2009**, *459*.

[4] Ufimtsev, I. S.; Martínez, T. J. *J. Chem. Theory Comput.* **2009**, *5*, 2619.

[5] Caruso, M. M.; Davis, D. A.; Shen, Q.; Odom, S. A.; Sottos, N. R.; White, S. R.; Moore, J. S. *Chem. Rev.* **2009**, *109*, 5755.

[6] Rubinstein, M.; Panyukov, S. *Macromolecules* **2002**, *35*, 6670.

[7] Sheiko, S. S.; Sun, F. C.; Randall, A.; Shirvanyants, D.; Rubinstein, M.; Lee, H.-i.; Matyjaszewski, K. *Nature* **2006**, *440*, 191.

[8] Dopieralski, P.; Anjukandi, P.; Rückert, M.; Shiga, M.; RibasArino, J.; Marx, D. *J. Mater. Chem.* **2011**, *21*, 8309.

[9] Ribas-Arino, J.; Shiga, M.; Marx, D. *J. Am. Chem. Soc.* **2010**, *132*, 10609.

[10] Davis, D. A.; PhD dissertation; University of Illinois at Urbana-Champaign; 2010.

[11] Ong, M. T.; Leiding, J.; Tao, H.; Virshup, A. M.; Martínez, T. J. *J. Am. Chem. Soc.* **2009**, *9*, 6377.

[12] Lenhardt, J. M.; Ong, M. T.; Choe, R.; Evenhuis, C. R.; Martínez, T. J.; Craig, S. L. *Science* **2010**, *329*, 1057.

[13] Lenhardt, J. M.; Ogle, J. W.; Ong, M. T.; Choe, R.; Martínez, T. J.; Craig, S. L. *J. Am. Chem. Soc.* **2011**, *133*, 3222.

[14] Kryger, M. J.; Ong, M. T.; Odom, S. A.; Sottos, N. R.; White, S. R.; Martínez, T. J.; Moore, J. S. *J. Am. Chem. Soc.* **2010**, *132*, 4558.

[15] Ufimtsev, I. S.; Martínez, T. J. *J. Chem. Theory Comput.* **2008**, *4*, 222.

[16] Ufimtsev, I. S.; Martínez, T. J. *Comput. Sci. Eng.* **2008**, *10*, 26.

[17] Ufimtsev, I. S.; Martínez, T. J. *J. Chem. Theory Comput.* **2009**, *5*, 1004.

[18] Warshel, A.; Levitt, M. *J. Mol. Biol.* **1976**, *103*, 227.

[19] Friesner, R. A.; Guallar, V. *Annu. Rev. Phys. Chem.* **2005**, *56*, 389.

[20] Hu, H.; Yang, W. *Annu. Rev. Phys. Chem.* **2008**, *59*, 573.

APPENDIX A

A.1 Acronym Glossary

ACM	Adiabatic connection method
AISMD	Ab initio steered molecular dynamics
AP	Attachment points
B3LYP	ACM using Beck (1988) exchange functional and LYP correlational functions
CAS	Complete active space
CAS(n,m)	Complete active space with n electrons in m orbitals
CASCI	Complete active space configuration interaction
CI	Configuration Interaction
CIS	CI including only single electronic excitations
COGEF	Constrained geometry simulates external force
DFT	Density functional theory
EFEI	External force is explicitly included
FMPES	Force modified potential energy surface
FOMO	Fractional occupation molecular orbital method
HF	Hartree-Fock
HOMO	Highest occupied molecular orbital
IR	Infrared
IRC	Intrinsic reaction coordinate
KS	Kohn-Sham
LFP	Linked functionalized polymers
LYP	Lee-Yang-Parr correlational functional
LUMO	Lowest unoccupied molecular orbital
MC	Merocyanine
MD	Molecular dynamics
MEP	Minimum energy path
MM	Molecular mechanics

MP2	Moller-Plesset perturbation theory of order 2
NDDO	Neglect of diatomic differential overlap
NEB	Nudged Elastic Band
NMR	Nuclear magnetic resonance
NVE	Constant particle N, volume V, and energy E
PBE	Perdew, Burke, and Ernzerhof functional
PES	Potential Energy Surface
PM3	Parameterized (NDDO) model 3
PP	Pulling points
QM	Quantum mechanics
QM/MM	Quantum mechanics/molecular mechanics hybrid
RHF	Restricted Hartree-Fock
RMS	Root mean square
RMSD	Root-mean square deviation
RRKM	Rice-Ramsperger-Kassel-Marcus
SCF	Self-consistent field
SIM	Stretched induced mechanophore
SMD	Steered molecular dynamics
SP	Spiropyran
STO	Slater-type orbital
TDDFT	Time-dependent density functional theory
TIM	Twist induced mechanophore
TS	Transition state
TST	Transition-state theory
UHF	Unrestricted Hartree-Fock
UV	Ultraviolet
UV/Vis	Ultraviolet/visible
VSEPR	Valence-shell electron-pair repulsion
VWN	A Vosko, Wilk, Nusair correlational functional
VWN5	A Vosko, Wilk, Nusair correlational functional
ZPVE	Zero-point vibrational energy

A.2 Abbreviations

Å	ångström, 10^{-10} m
fs	femto-second
μs	micro-second
ms	milli-second
nN	nano-newton
ps	pico-second

A.3 SI Metric prefixes

Table A.1: SI prefixes and their etymologies

Prefix	Symbol	Factor/ m	Ordinary Notation	Name
milli	m	10^{-3}	0.001	thousandth
micro	μ	10^{-6}	0.000 001	millionth
nano	n	10^{-9}	0.000 000 001	billionth
pico	p	10^{-12}	0.000 000 000 001	trillionth
femto	f	10^{-15}	0.000 000 000 000 001	quadrillionth

A.4 Physical constants

Table A.2: Values of physical constants

quantity	symbol	value
Atomic mass unit	amu	1.660 538 921(73) $\times$ 10^{-27} kg
Avogadro's number	N_A	6.022 141 29(27) $\times$ 10^{23} mol^{-1}
Bohr radius	a_0	5.291 772 1092(17) $\times$ 10^{-11} m
Boltzmann constant	k_b	1.380 6488(13) $\times$ 10^{-23} J$\cdot K^{-1}$
Hartree energy	E_h	4.359 744 34(19) $\times$ 10^{-18} J
Planck constant	h	6.626 069 57(29) $\times$ 10^{-34} J$\cdot$s
reduced Planck constant	$\hbar = h/(2\pi)$	1.054 571 726(47) $\times$ 10^{-34} J$\cdot$s

Source: P.J. Mohr, B.N. Taylor, and D.B. Newell (2011), "The 2010 CODATA Recommended Values of the Fundamental Physical Constants" (Web Version 6.0).

A.5 Energy conversion factors

Table A.3: Energy conversion factors

	eV	cm^{-1}	kcal/mol
1 eV	1	8.0657×10^{3}	2.3119×10^{1}
1 cm^{-1}	1.2398×10^{-4}	1	2.8588×10^{-3}
1 kcal/mole	4.3348×10^{-2}	3.4964×10^{2}	1
1 k_bT	2.56×10^{-2}	n/a	5.93×10^{-1}

Source: D. McQuarrie, *Statistical Mechanics* (Harper & Row, N.Y., 1976)

APPENDIX B

B.1 Conformer Excited State Transition Dipole Moment and Oscillator strengths

Table B.1: Reactant, Intermediate, and Product geometries at 0 nN.

Conformer	Transition dipole $\{ x\ y\ z \}$	Oscillator strength	Transition orbital	λ / nm
CTC	3.36994 -0.39875 -1.33941	0.90241	$73 \rightarrow 74$	448
CCC	2.28505 0.15906 -1.36532	0.44306	$73 \rightarrow 74$	488
SP	-1.27239 0.49950 0.75392	0.21842	$72 \rightarrow 74$	339
TCC	-2.80307 -0.33298 1.15317	0.67543	$73 \rightarrow 74$	417
TTC	3.17757 -0.29026 -1.64938	0.87434	$73 \rightarrow 74$	448

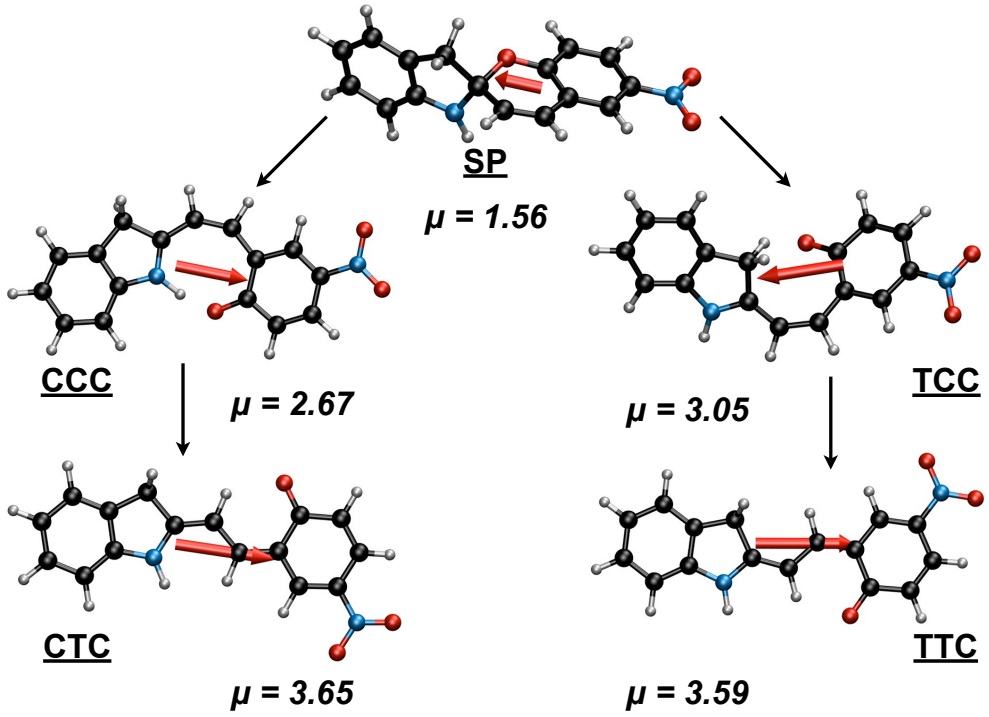

Figure B.1: Dipole moments for minima along the force free pathways.

Table B.2: SIM1 Reactant, Intermediate, and Product geometries at 1 nN.

Conformer	Transition dipole { x y z }	Oscillator strength	Transition orbital	λ / nm
CTC	3.38892 -0.39787 -1.47918	0.94037	73 → 74	446
CCC	2.56457 -0.14304 -1.72843	0.6118	73 → 74	475
SP	1.36635 0.28048 -0.74437	0.28724	72 → 75	264
TCC	-3.31157 0.16584 1.05159	0.84418	73 → 74	435
TTC	3.34195 -0.17124 -1.49654	0.91277	73 → 74	448

Table B.3: SIM1 Reactant, Intermediate, and Product geometries at 2.5 nN.

Conformer	Transition dipole { x y z }	Oscillator strength	Transition orbital	λ / nm
CTC	-3.48876 0.3272 1.48084	0.98721	73 → 74	446
SP	1.36639 0.17785 -0.71851	0.27906	72 → 75	263
TTC	3.45863 -0.1719 -1.56979	0.98341	73 → 74	446

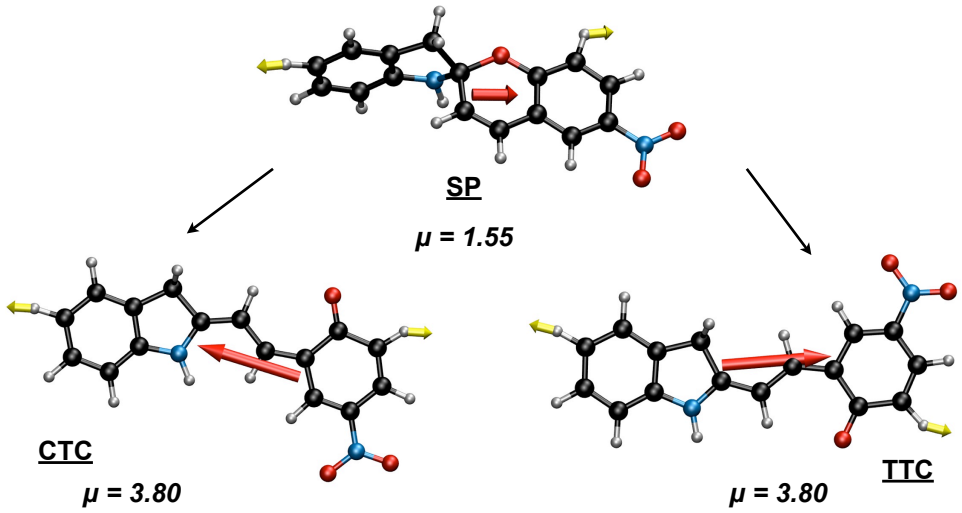

Figure B.2: Dipole moments for minima along the SIM1 2.5 nN pathway.

Table B.4: SIM2 Reactant, Intermediate, and Product geometries at 1 nN.

Conformer	Transition dipole { x y z }	Oscillator strength	Transition orbital	λ / nm
CTC	-3.39896 0.42407 1.30414	0.905	73 → 74	451
CCC	2.55529 0.06376 -1.54729	0.55765	73 → 74	486
SP	1.38007 0.3501 -0.66127	0.28094	72 → 75	267
TCC	3.09777 0.15309 -1.32755	0.77385	73 → 74	446
TTC	-3.18023 0.3036 1.7431	0.88709	73 → 74	454

Table B.5: SIM2 Reactant, Intermediate, and Product geometries at 2.5 nN.

Conformer	Transition dipole { x y z }	Oscillator strength	Transition orbital	λ / nm
CTC	-3.44667 0.42174 1.28663	0.91541	73 → 74	456
CCC	2.76802 -0.72936 -1.21212	0.8157	71 → 74	359
	3.09738 -0.07141 -1.56017	0.79604	73 → 74	459
SP	1.37652 0.29935 -0.62206	0.26912	72 → 75	268
TTC	3.06191 -0.56645 -1.20174	0.934551	71 → 74	363
	-3.20463 0.30116 1.81483	0.90209	73 → 74	459

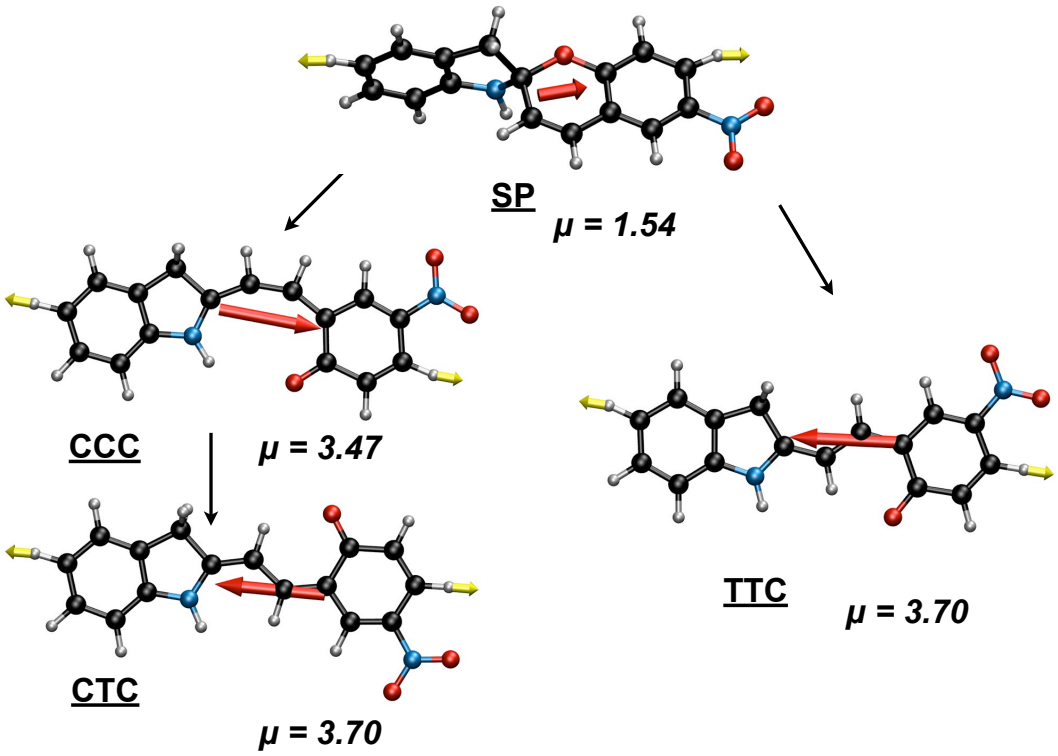

Figure B.3: Dipole moments for minima along the SIM2 2.5 nN pathway.

Table B.6: TIM1 Reactant, Intermediate, and Product geometries at 1 nN.

Conformer	Transition dipole { x y z }	Oscillator strength	Transition orbital	λ / nm
SP	1.37414 0.55342 -0.60523	0.27466	72 → 75	283
TCC	-2.98174 -0.39447 1.27876	0.74006	73 → 74	438
TTC	-3.28167 0.28073 1.50552	0.89582	73 → 74	444

Table B.7: TIM1 Reactant, Intermediate, and Product geometries at 2 nN.

Conformer	Transition dipole { x y z }	Oscillator strength	Transition orbital	λ / nm
SP	-1.59981 -0.29 0.54444	0.30524	70 → 74	292
TCC	-3.02571 -0.41635 1.32304	0.73761	73 → 74	456
TTC	-3.33757 0.2411 1.43163	0.90617	73 → 74	444

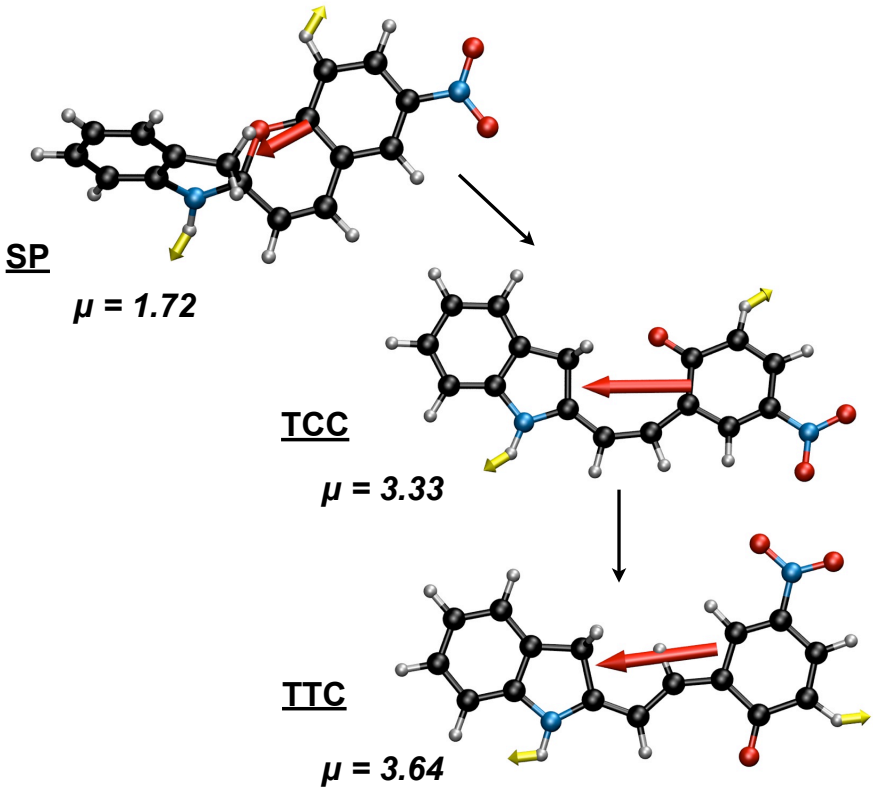

Figure B.4: Dipole moments for minima along the TIM1 2 nN pathway.

Table B.8: TIM2 Reactant, Intermediate, and Product geometries at 1 nN.

Conformer	Transition dipole { x y z }	Oscillator strength	Transition orbital	λ / nm
SP	1.37424 0.55344 -0.60521	0.27468	72 $\rightarrow$ 75	283
TCC	-2.97184 -0.40103 1.26584	0.74485	73 $\rightarrow$ 74	432
TTC	-3.28167 0.28073 1.50552	0.89582	73 $\rightarrow$ 74	444

Table B.9: TIM2 Reactant, Intermediate, and Product geometries at 2 nN.

Conformer	Transition dipole { x y z }	Oscillator strength	Transition orbital	λ / nm
SP	-1.59985 -0.29004 0.54449	0.30526	70 $\rightarrow$ 74	292
TCC	2.912 0.43073 -1.26917	0.70205	73 $\rightarrow$ 74	444
TTC	3.33753 -0.24109 -1.43166	0.90616	73 $\rightarrow$ 74	444

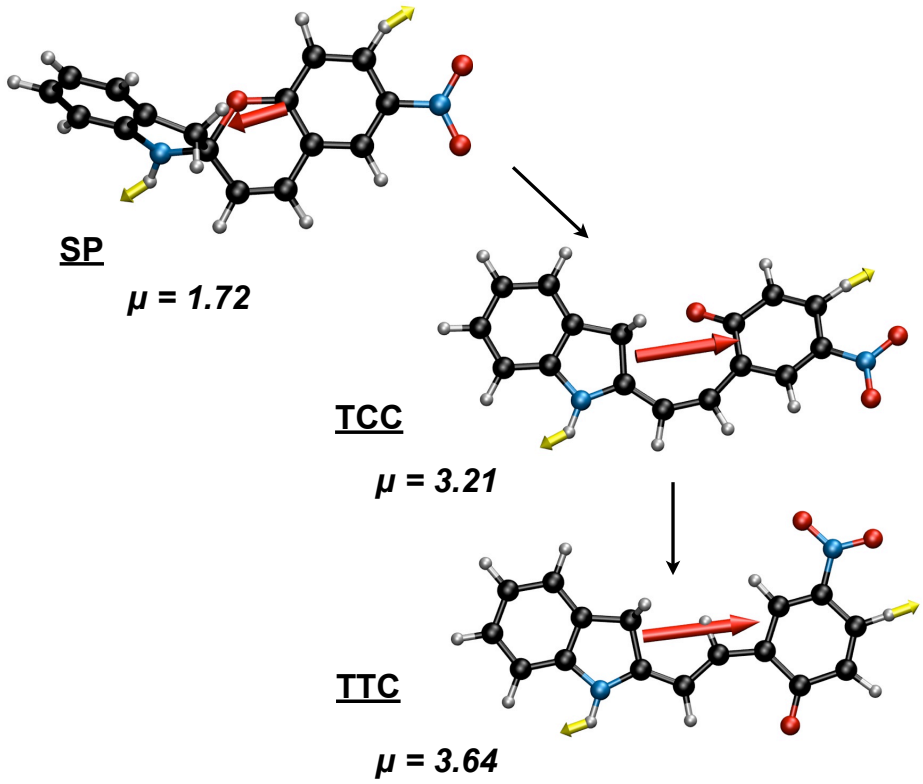

Figure B.5: Dipole moments for minima along the TIM2 2 nN pathway.

APPENDIX C[‡]

C.1 Construction of the 2-D FMPES

As shown in figure C.1, the $\boldsymbol{\alpha}$ and $\boldsymbol{\beta}$ dihedral angles show torsional motions on SP which reflect C-O bond dissociation and C-C bond isomerization. The $\boldsymbol{\alpha}$ is normally defined by N6-C2-C3-C4 and $\boldsymbol{\beta}$ by C2-C3-C4-C5. To describe a smoother reaction potential for the structural changes pertaining to C-O bond breaking and C-C bond isomerization, three dummy atoms were used to define two internal coordinates. As shown in figure C.1, the three dummy atoms (labeled in yellow) are located on the ring containing the Spiro C-O bond. The dummy atoms are each connected to a carbon atom, which is bonded to three other atoms. Each dummy atom is defined by a trisector of four atoms (A, B, C, D) where A is the central atom bonded to three other atoms: A-B, A-C, A-D defined as

$$\mathbf{X}^{tri} = (\mathbf{R}^{BA} - \mathbf{R}^{DA}) \times (\mathbf{R}^{DA} - \mathbf{R}^{CA}) \tag{C.1}$$

where $\mathbf{R}^{BA}$ is the unit vector along the bond from atom B to A. The pyramidalization angle can now be defined as the angle between each bond vector and the trisector axis. The dummy atoms are placed along the trisector axis which are each connected (yellow bond) to a specified carbon atom. For instance, dummy atom 9 lies at the trisector of carbon atom 2, whereby the angles for X9-C2-C1, X9-C2-C3, and X9-C2-C6 are all equivalent. Similarly, dummy atom 10 lies at the trisector of C3 where the angles, X10-C3-H7, X10-C3-C4, and X10-C3-C2 are the same. The trisector about C4 is defined in a similar fashion.

The ring-opening mechanism involving bond breaking and bond isomerization can now be describe by two dihedral angles. Shown in figure C.1, $\boldsymbol{\alpha}$ is defined by X9-C2-C3-X10 which is varied from -50° to +230°. The $\boldsymbol{\beta}$ angle is defined by X10-C3-C4-X11 and ranges from -180° to +180°. The force free equilibrium geometries have the following angles: SP($\boldsymbol{\alpha}$: +75.42° , $\boldsymbol{\beta}$: +1.81°), CCC($\boldsymbol{\alpha}$: -2.87° , $\boldsymbol{\beta}$: +4.07°), CTC($\boldsymbol{\alpha}$: -0.17° , $\boldsymbol{\beta}$: +179.9°), TCC($\boldsymbol{\alpha}$: +171.78° , $\boldsymbol{\beta}$: -15.71°), TTC($\boldsymbol{\alpha}$: +180.01° , $\boldsymbol{\beta}$: -180.04°).

[‡]I acknowledge Christian R. Evenhuis for code development pertaining to the 2-D interpolation scheme.

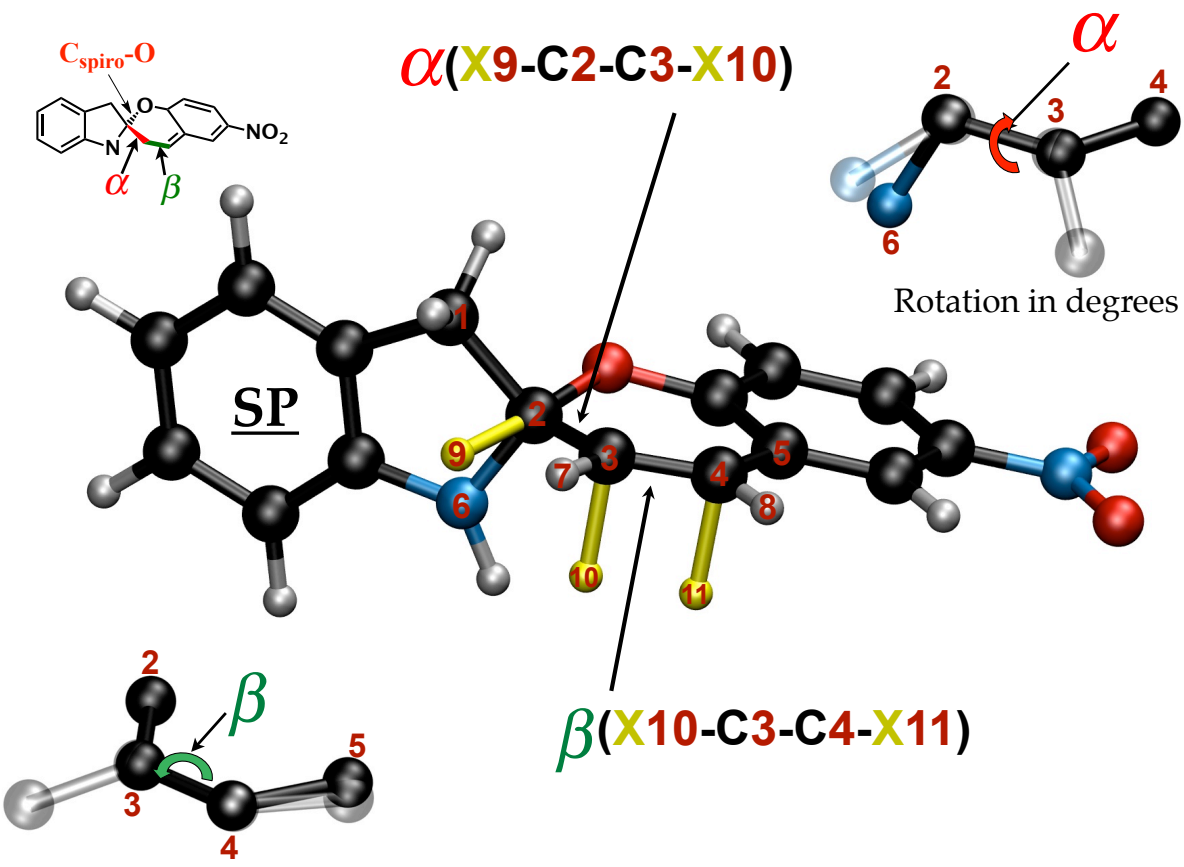

Figure C.1: Two dihedral angles labeled $\boldsymbol{\alpha}$ and $\boldsymbol{\beta}$ on the SP molecule are chosen to represent the principle reaction coordinates for construction of the 2-D FMPES. As indicated, the $\boldsymbol{\alpha}$ angle reflects torsional motion about the carbon atoms labeled 2 and 3, which reflects dissociation of the C-O bond. Additionally, the $\boldsymbol{\beta}$ angle corresponding to a torsional twist between carbon atoms labeled 3 and 4 describe C-C bond isomerization. To construct a smooth potential energy surface using both angles, $\boldsymbol{\alpha}$ and $\boldsymbol{\beta}$ are redefined with respect to the dummy atoms indicated in yellow and in parentheses. The dummy atoms are each connected to a carbon atom and were defined by a trisector or by three atoms connected to the carbon atom. For instance, dummy atom 10 is the vector perpendicular to the plane defined by the trisector about C3, C2,C4, and the H7.

The SP ring-opening reaction can now be described as a function of the $\boldsymbol{\alpha}$ and $\boldsymbol{\beta}$ angles. Construction of the 2-D plot requires a grid of stationary points on the plot which are varied with respect to $\boldsymbol{\alpha}$ and $\boldsymbol{\beta}$, however, constraint optimizations for each of these points would be costly. To minimize computational cost and to ensure that relevant stationary points (e.g transition state, minima) appear on the 2-D plot, a specified set of geometries reflecting local minima can be used to interpolate a grid of geometries that vary with respect to $\boldsymbol{\alpha}$ and $\boldsymbol{\beta}$. The remaining internal coordinates are then parameterized in terms of linear combina-

tions of functions of $\boldsymbol{\alpha}$ and $\boldsymbol{\beta}$. The set of geometries reflecting local minima or equilibrium structures are SP, CCC, CTC, TCC, and TTC, which can be referred to as the number of reference points. Additional reference points can be incorporated (e.g. transition states) to obtain better interpolated geometries. Based on these reference points, an interpolated set of geometries can be obtained by use of a Fourier-like expansion in terms of $\boldsymbol{\alpha}$ and $\boldsymbol{\beta}$ for each of the remaining 3N-8 spectator coordinates (i.e. bond length, bond angle, and dihedral angle). Both $\boldsymbol{\alpha}$ and $\boldsymbol{\beta}$ are periodic and the expansion is of the form:

$$Z^i(\boldsymbol{\alpha},\boldsymbol{\beta}) = \sum_{n=1}^{nfunc} \phi_n^i f_n(\boldsymbol{\alpha},\boldsymbol{\beta}) \tag{C.2}$$

where $Z^i(\boldsymbol{\alpha},\boldsymbol{\beta})$ is the value for the i^{th} internal coordinate, and ϕ_n^i is the n^{th} expansion coefficient for the i^{th} coordinate. The expansion consists of combinations of sine and cosine and may take the following form for 16 reference geometries:

$$\begin{aligned} Z^i(\boldsymbol{\alpha},\boldsymbol{\beta}) = \quad & \phi_1^i + \phi_2^i\cos(\alpha) + \phi_3^i\cos(\beta) + \phi_4^i\cos(\beta)\cos(\beta) \\ & \phi_5^i\sin(\alpha) + \phi_6^i\sin(\beta) + \phi_7^i\cos(2\alpha) + \phi_8^i\cos(2\beta) \\ & \phi_9^i\cos(2\alpha)\cos(\beta) + \phi_{10}^i\sin(\alpha)\cos(\beta) \\ & \phi_{11}^i\cos(\alpha)\cos(2\beta) + \phi_{12}^i\cos(\alpha)\sin(\beta) \\ & \phi_{13}^i\cos(2\alpha)\cos(2\beta) + \phi_{14}^i\cos(2\alpha)\sin(\beta) \\ & \phi_{15}^i\sin(\alpha)\cos(2\beta) + \phi_{16}^i\sin(\alpha)\sin(\beta) \end{aligned} \tag{C.3}$$

For the 16 reference geometries, the value of a given internal coordinate, $\{\mathbf{X_m}\}_{m=1}^{nref}$, gives a a set of 16 linear equations with 16 unknowns allowing for the determination of the expansion parameters for each spectator coordinate via solving a matrix equation (i.e. $\mathbf{Ax} = \mathbf{b}$) of the form:

$$\begin{pmatrix} f_1|_{\mathbf{x}_1} & \cdots & f_{nfunc}|_{\mathbf{x}_1} \\ \vdots & \ddots & \vdots \\ f_1|_{\mathbf{x}_1} & \cdots & f_{nfunc}|_{\mathbf{x}_{nref}} \end{pmatrix} \begin{pmatrix} \phi_1^i \\ \vdots \\ \phi_{nfunc}^i \end{pmatrix} = \begin{pmatrix} \mathbf{Z}^i|_{\mathbf{x}_1} \\ \vdots \\ \mathbf{Z}^i|_{\mathbf{x}_{nref}} \end{pmatrix} \tag{C.4}$$

where f are the expansion functions (combinations of the sine and cosine functions), i indexes the 3N-8 internal coordinates, n indexes the total number of expansion functions (e.g. 16), and m indexes the total number of reference geometries (e.g. 16). After the system is solved for the coefficients, ϕ_n^i, the interpolated values for the internal coordinate $\mathbf{Z_m^i}$, can be determined by substituting any value of $\boldsymbol{\alpha}$ and $\boldsymbol{\beta}$. The increment for $\boldsymbol{\alpha}$ and $\boldsymbol{\beta}$

is 10° from -50° to +230° and -180° to +180° respectively. This will provide the grid of geometries whereby single point energy calculations can be carried out to construct the force free potential energy surface. The parametrized geometries on the potential energy surface will contain the correct energy at the stationary points with a smooth set of interpolated geometries in between. The energy correction due to force (Chapter 2, equation 2.21) is then added to the each geometry on the grid to construct the 2-D force modified potential energy surface.

APPENDIX D

D.1 Minimal energy pathways for simplified and extended spiropyrans

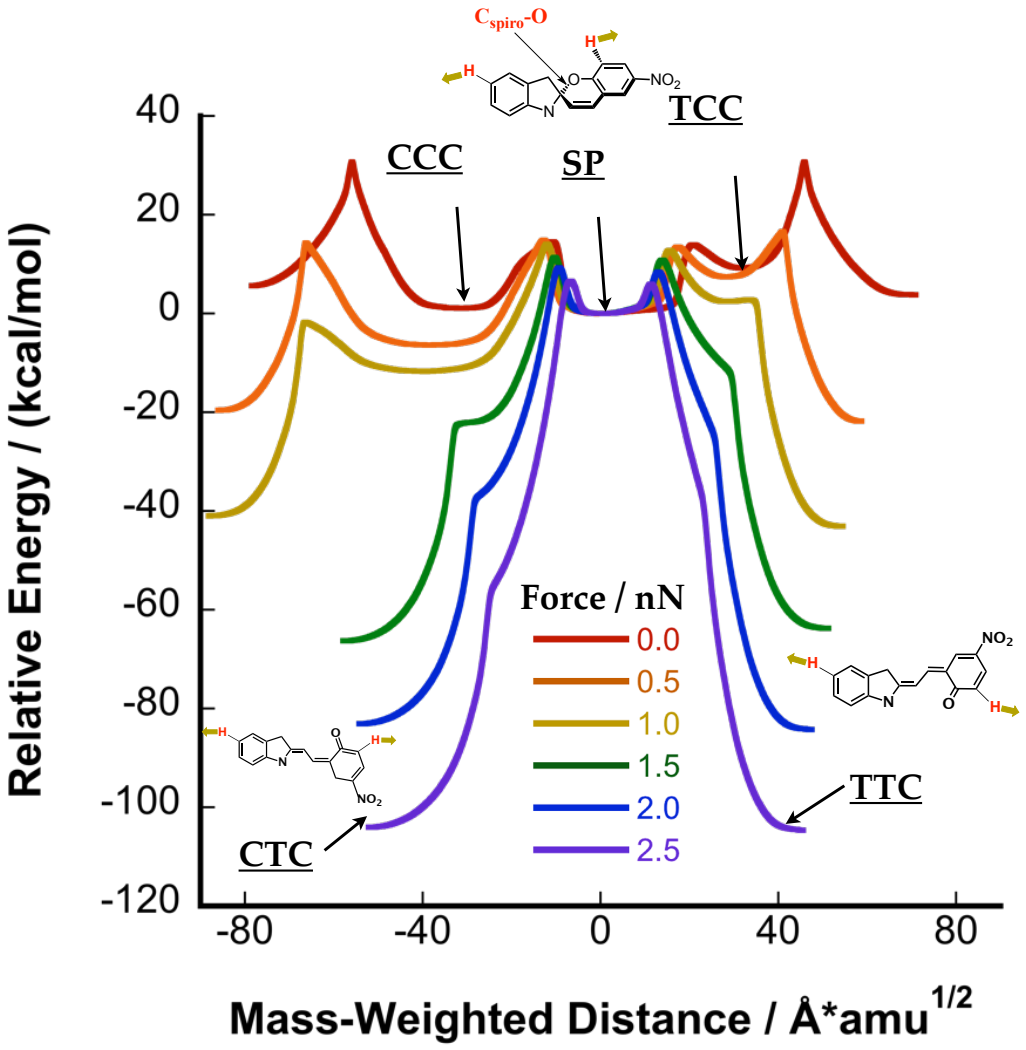

Figure D.1: Minimal energy pathway for the simplified SIM1 model.

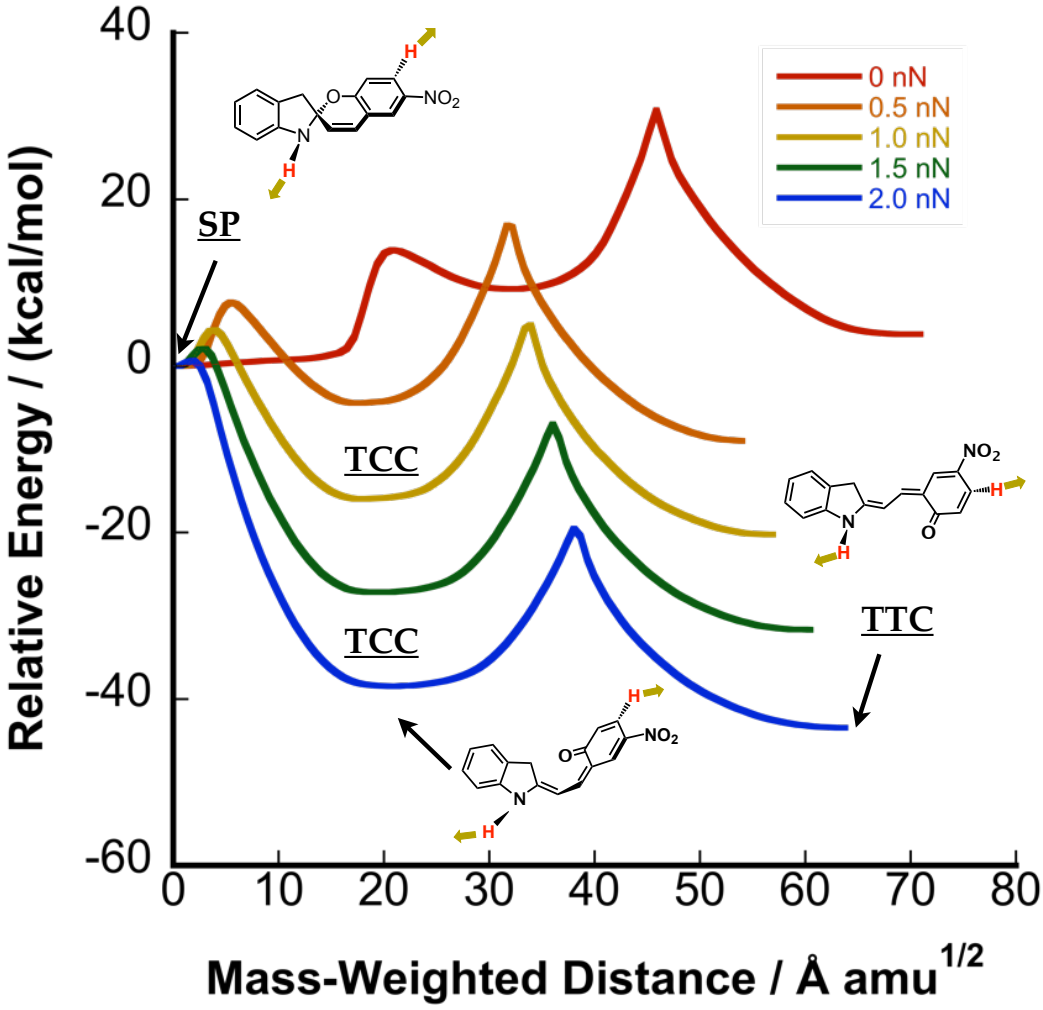

Figure D.2: Minimal energy pathway for the simplified TIM2 model.

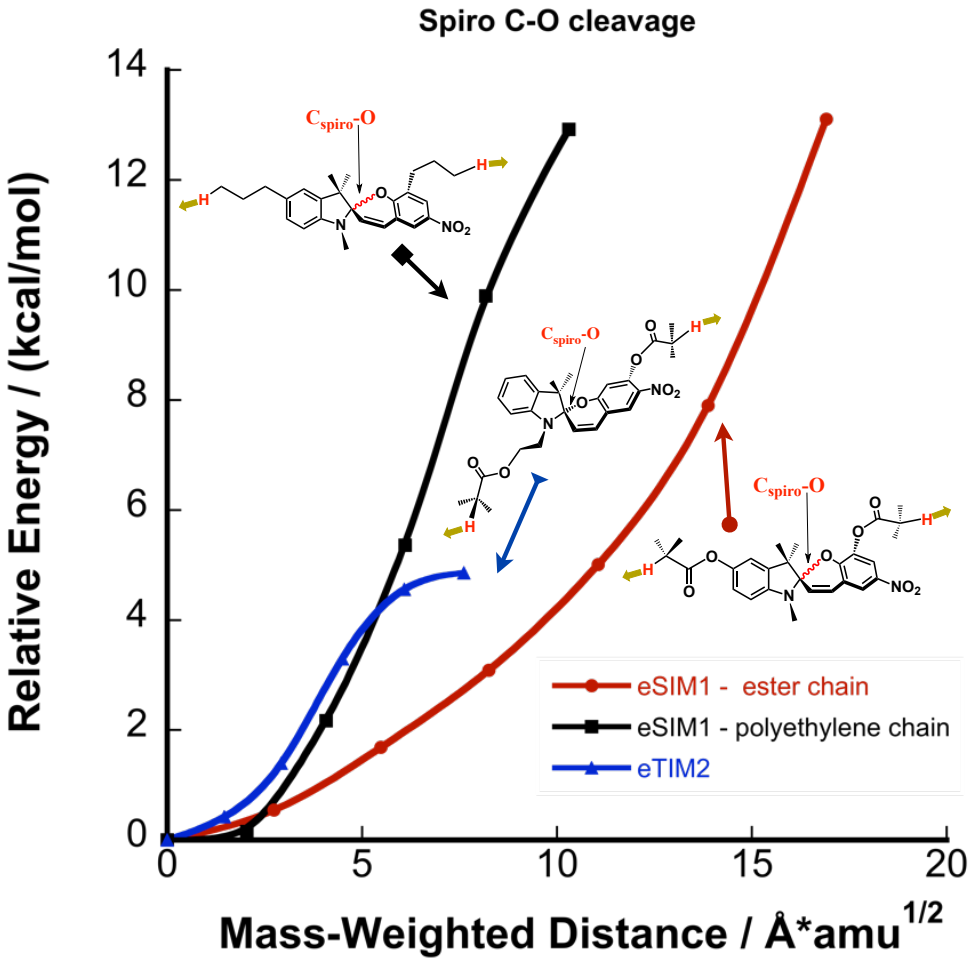

Figure D.3: Minimal energy pathway at 1 nN for breakage of the Spiro C-O bond for the extended eSIM1 with the ester functional chain, an eSIM1 incorporating a polyethylene chain, and an eTIM2.

APPENDIX E

E.1 Coordinate data for simplified spiropyrans

All computations carried out with GAMESS using a 6-31G basis and B3LYP1 density functional. Reactant geometry at 0 nN. Energy = -951.7334208562 Hartrees

C1	-3.100685	0.053871	-1.532199
C2	-1.919650	-0.378997	-0.931701
C3	-1.574909	0.003325	0.379849
C4	-2.416050	0.835068	1.106510
C5	-3.612486	1.283628	0.515873
C6	-3.945342	0.892468	-0.785805
N7	-0.918739	-1.221630	-1.441586
C8	0.250352	-1.239901	-0.604659
C9	-0.261220	-0.660740	0.747075
C10	0.912082	-2.588904	-0.566233
C11	2.021733	-2.880481	-1.269770
C12	2.715145	-1.867254	-2.053730
C13	2.281736	-0.523166	-1.933111
O14	1.247733	-0.184072	-1.098205
C15	3.800869	-2.151598	-2.887685
C16	4.428694	-1.114579	-3.579920
C17	4.004862	0.217049	-3.456802
C18	2.926888	0.510508	-2.629902
N19	5.554926	-1.423982	-4.447079
O20	5.920734	-2.634085	-4.546816
O21	6.117542	-0.469899	-5.063092
H22	4.521585	0.990838	-4.008486
H23	4.165674	-3.164632	-3.003264
H24	-2.158607	1.137795	2.117140
H25	-3.361886	-0.239734	-2.543587
H26	-4.869633	1.244206	-1.233192
H27	0.397447	-3.343998	0.018437
H28	2.433368	-3.885221	-1.257671
H29	2.569148	1.524907	-2.506450
H30	-4.277766	1.934825	1.072552
H31	-0.904217	-1.583033	-2.381401
H32	0.488426	0.022128	1.152767
H33	-0.408363	-1.474814	1.468433

SIM1 reactant geometry at 1 nN. Energy = -951.9442693381 Hartrees

C1	-3.304425	0.095029	-1.376944
C2	-1.959865	0.105250	-1.000782
C3	-1.587113	0.072999	0.360596
C4	-2.566797	0.005334	1.353237
C5	-3.934391	-0.036959	0.990986
C6	-4.280109	0.022550	-0.366380
N7	-0.808244	0.082898	-1.817210
C8	0.356340	-0.342373	-1.018222
C9	-0.060608	0.114609	0.418388
C10	0.535867	-1.834741	-1.117362
C11	1.566895	-2.421214	-1.742916
C12	2.646772	-1.633666	-2.316647
C13	2.628853	-0.222762	-2.145903
O14	1.591149	0.393553	-1.450234
C15	3.699726	-2.240343	-3.007039
C16	4.729523	-1.456974	-3.520484
C17	4.732499	-0.070088	-3.349706
C18	3.690476	0.554590	-2.665693
N19	5.822479	-2.094081	-4.239670
O20	5.792164	-3.353404	-4.379835
O21	6.750787	-1.359881	-4.691353
H22	5.550918	0.510611	-3.753887
H23	3.724363	-3.314232	-3.143537
H24	-2.280629	-0.035639	2.400370
H25	-3.596032	0.121712	-2.421963
H26	-5.326896	-0.004164	-0.653414
H27	-0.270953	-2.413655	-0.678703
H28	1.626126	-3.502036	-1.828620
H29	3.774102	1.633374	-2.571394
H30	-4.732693	-0.135684	1.743521
H31	-0.865493	-0.213159	-2.782130
H32	0.309146	1.137953	0.562858
H33	0.385201	-0.524814	1.184148

SIM1 reactant geometry at 2.5 nN. Energy = -952.2879144695 Hartrees

C1	-3.309830	0.084585	-1.390286
C2	-1.969525	0.174771	-1.001256
C3	-1.616145	0.082301	0.362932
C4	-2.615349	-0.125878	1.334707
C5	-3.987437	-0.251200	0.960449
C6	-4.296177	-0.126024	-0.405526
N7	-0.806208	0.288587	-1.808749
C8	0.371896	-0.162087	-1.030495
C9	-0.077651	0.242735	0.426080
C10	0.520167	-1.651163	-1.146727
C11	1.556336	-2.257854	-1.735252
C12	2.682815	-1.516278	-2.277732
C13	2.726712	-0.094710	-2.148138
O14	1.653241	0.557270	-1.494236
C15	3.707569	-2.227069	-2.908637
C16	4.801559	-1.547355	-3.422769
C17	4.883309	-0.161893	-3.305521
C18	3.878680	0.587605	-2.682409
N19	5.868508	-2.284554	-4.081322
O20	5.757464	-3.543928	-4.168487
O21	6.855040	-1.632755	-4.535689
H22	5.750533	0.344616	-3.708914
H23	3.651977	-3.304860	-2.995703
H24	-2.333477	-0.210849	2.380785
H25	-3.594666	0.154853	-2.435405
H26	-5.330226	-0.209831	-0.727018
H27	-0.312934	-2.215401	-0.739166
H28	1.586988	-3.339969	-1.820950
H29	4.179604	1.649067	-2.711142
H30	-4.834607	-0.459467	1.680774
H31	-0.847374	0.042990	-2.789468
H32	0.203832	1.290169	0.594349
H33	0.415163	-0.377747	1.177847

SIM1 transition state geometry 1 at 0 nN. Energy = -951.7102553768 Hartrees

C1	-2.568675	0.254401	-1.866587
C2	-1.681002	-0.377291	-1.002918
C3	-1.750664	-0.241632	0.394923
C4	-2.742024	0.552871	0.958163
C5	-3.651424	1.203292	0.105577
C6	-3.563337	1.055681	-1.285297
N7	-0.615759	-1.259852	-1.304439
C8	0.074453	-1.638380	-0.209574
C9	-0.629653	-1.057794	1.003394
C10	1.101406	-2.625891	-0.190625
C11	2.139964	-2.725708	-1.087020
C12	2.672260	-1.696781	-1.933516
C13	2.423856	-0.275606	-1.648156
O14	1.553948	0.123350	-0.783447
C15	3.620252	-2.045248	-2.918061
C16	4.297151	-1.072548	-3.635940
C17	4.101701	0.307279	-3.359684
C18	3.219338	0.682747	-2.380042
N19	5.229867	-1.467206	-4.660388
O20	5.393712	-2.708906	-4.892941
O21	5.851474	-0.555908	-5.295105
H22	4.664254	1.035497	-3.929661
H23	3.828387	-3.086961	-3.133904
H24	-2.814954	0.676313	2.033736
H25	-2.497566	0.142722	-2.942830
H26	-4.271984	1.569091	-1.926088
H27	1.043193	-3.347278	0.621295
H28	2.710459	-3.653737	-1.065115
H29	3.056006	1.726827	-2.141088
H30	-4.428279	1.829968	0.529861
H31	-0.315796	-1.489229	-2.241236
H32	0.090541	-0.441197	1.552200
H33	-0.976401	-1.846975	1.683724

SIM1 transition state geometry 1 (SP → CCC) at 1.0 nN. Energy = -951.9218725631 Hartrees

C1	-3.154947	0.037684	-1.669069
C2	-1.938017	-0.091569	-1.004452
C3	-1.824934	0.093686	0.385478
C4	-2.965461	0.366867	1.143294
C5	-4.223373	0.442059	0.502878
C6	-4.297420	0.301958	-0.891386
N7	-0.693455	-0.576608	-1.499007
C8	0.226372	-0.791039	-0.509497
C9	-0.371526	-0.174326	0.761094
C10	1.034036	-1.997310	-0.441700
C11	2.026618	-2.395590	-1.277957
C12	2.811781	-1.561920	-2.149883
C13	2.805169	-0.120174	-1.949958
O14	1.847991	0.458336	-1.252522
C15	3.739659	-2.164498	-3.012233
C16	4.692818	-1.396798	-3.665338
C17	4.798218	-0.016898	-3.394750
C18	3.915485	0.603725	-2.533011
N19	5.617913	-2.023410	-4.576434
O20	5.503853	-3.272032	-4.795179
O21	6.508606	-1.300710	-5.125177
H22	5.593737	0.543425	-3.869721
H23	3.729906	-3.237054	-3.167697
H24	-2.895254	0.477957	2.220832
H25	-3.236066	-0.099721	-2.741909
H26	-5.260704	0.371250	-1.385959
H27	0.730861	-2.667119	0.362600
H28	2.367421	-3.424909	-1.180036
H29	4.108496	1.656378	-2.342429
H30	-5.152338	0.568423	1.080890
H31	-0.563626	-0.927455	-2.436545
H32	0.178912	0.752449	0.973336
H33	-0.240203	-0.836248	1.621769

SIM1 transition state geometry 1 at 2.5 nN. Energy = -952.2774592916 Hartrees

C1	-3.373595	0.049954	-1.482488
C2	-2.073882	0.085088	-0.978249
C3	-1.831727	0.136469	0.407255
C4	-2.916194	0.104684	1.305922
C5	-4.255699	0.004511	0.824011
C6	-4.447905	0.004604	-0.569058
N7	-0.833384	-0.107228	-1.672498
C8	0.221715	-0.377484	-0.800544
C9	-0.292842	0.136340	0.578242
C10	0.776929	-1.744565	-0.831229
C11	1.833714	-2.220479	-1.509018
C12	2.840363	-1.456469	-2.213001
C13	2.897474	-0.018765	-2.078594
O14	1.868583	0.618015	-1.453599
C15	3.798290	-2.182815	-2.927886
C16	4.867601	-1.531437	-3.521219
C17	5.015890	-0.151055	-3.348645
C18	4.095928	0.613675	-2.637120
N19	5.845690	-2.278841	-4.276861
O20	5.685634	-3.534381	-4.395809
O21	6.821040	-1.648474	-4.791187
H22	5.884840	0.329234	-3.781403
H23	3.716159	-3.259557	-3.014960
H24	-2.727062	0.113879	2.375461
H25	-3.566330	0.015935	-2.549745
H26	-5.455512	-0.057892	-0.968199
H27	0.159187	-2.437872	-0.257371
H28	1.999716	-3.295141	-1.480506
H29	4.469614	1.652677	-2.604778
H30	-5.164706	-0.107651	1.487942
H31	-0.808295	-0.449171	-2.622745
H32	0.091454	1.152244	0.741392
H33	0.075740	-0.494794	1.389288

CCC geometry minimum at 0 nN. Energy = -951.7316883688 Hartrees

C1	-2.358925	1.313618	-0.755104
C2	-1.734114	0.115941	-0.418065
C3	-2.337883	-0.846998	0.414764
C4	-3.608916	-0.616332	0.927879
C5	-4.258431	0.586313	0.597661
C6	-3.640169	1.535223	-0.230124
N7	-0.459743	-0.352113	-0.810659
C8	-0.177733	-1.545269	-0.281663
C9	-1.367190	-1.998243	0.563178
C10	0.980268	-2.337227	-0.457835
C11	2.128438	-2.252133	-1.238348
C12	2.783740	-1.354076	-2.147649
C13	2.504878	0.065652	-2.384619
O14	1.606712	0.745142	-1.751322
C15	3.870320	-1.938490	-2.856135
C16	4.614832	-1.228581	-3.776354
C17	4.339483	0.140298	-4.035174
C18	3.321021	0.753088	-3.355679
N19	5.693788	-1.884882	-4.475622
O20	5.925462	-3.111134	-4.228445
O21	6.366675	-1.204584	-5.312375
H22	4.946276	0.668963	-4.758928
H23	4.128544	-2.977325	-2.686214
H24	-4.094980	-1.342303	1.571753
H25	-1.873786	2.042755	-1.393529
H26	-4.159833	2.456796	-0.469248
H27	0.916879	-3.266462	0.103342
H28	2.702075	-3.175437	-1.153976
H29	3.087665	1.799105	-3.513110
H30	-5.250374	0.783198	0.989787
H31	0.332415	0.202335	-1.289973
H32	-1.060398	-2.173074	1.603175
H33	-1.765966	-2.950020	0.188116

SIM1 CCC geometry minimum at 1.0 nN. Energy = -951.9628718028 Hartrees

C1	-2.721384	1.410866	-0.908515
C2	-1.888711	0.354747	-0.535457
C3	-2.250313	-0.505790	0.520940
C4	-3.442621	-0.326320	1.217113
C5	-4.298676	0.731665	0.858923
C6	-3.926411	1.583675	-0.196781
N7	-0.623838	-0.069812	-1.058754
C8	-0.150183	-1.151158	-0.403109
C9	-1.159828	-1.531531	0.679800
C10	1.016900	-1.919871	-0.540357
C11	2.180823	-1.998687	-1.316337
C12	2.878274	-1.382413	-2.392121
C13	2.477502	-0.198603	-3.184933
O14	1.382569	0.428517	-2.965865
C15	4.112284	-2.030538	-2.697949
C16	4.940576	-1.591387	-3.701995
C17	4.585404	-0.455807	-4.479636
C18	3.415197	0.210500	-4.237925
N19	6.176269	-2.285964	-3.966913
O20	6.472674	-3.298927	-3.256130
O21	6.917614	-1.851928	-4.904266
H22	5.260931	-0.134829	-5.262503
H23	4.418973	-2.899304	-2.127188
H24	-3.709797	-0.996103	2.028667
H25	-2.459142	2.082388	-1.718213
H26	-4.580324	2.402032	-0.479546
H27	1.003452	-2.714325	0.203810
H28	2.763587	-2.847866	-0.958828
H29	3.222634	1.067309	-4.879400
H30	-5.242777	0.875407	1.408426
H31	-0.067967	0.334070	-1.833263
H32	-0.684864	-1.504512	1.669449
H33	-1.511647	-2.560489	0.527829

Transition state geometry 2 at 0 nN. Energy = -951.6844607148 Hartrees

C1	-2.939333	0.109462	-1.779506
C2	-1.938177	-0.319429	-0.909511
C3	-2.089992	-0.245042	0.490358
C4	-3.262352	0.261893	1.034186
C5	-4.286162	0.697879	0.171885
C6	-4.119550	0.621286	-1.215626
N7	-0.682332	-0.871907	-1.205626
C8	0.042621	-1.186189	-0.046554
C9	-0.826076	-0.775369	1.146359
C10	1.266896	-1.746672	0.005269
C11	2.060048	-2.166050	-1.159165
C12	2.959083	-1.434788	-1.893110
C13	3.319034	-0.005333	-1.590823
O14	2.842396	0.626323	-0.617635
C15	3.608252	-2.083131	-3.015315
C16	4.494685	-1.406937	-3.792783
C17	4.844927	-0.027188	-3.542632
C18	4.284573	0.630231	-2.497210
N19	5.114515	-2.090384	-4.922468
O20	4.806616	-3.299280	-5.141308
O21	5.932581	-1.431982	-5.630965
H22	5.557217	0.445144	-4.206802
H23	3.378356	-3.118421	-3.241134
H24	-3.391377	0.325110	2.110663
H25	-2.817396	0.051393	-2.856216
H26	-4.913968	0.961969	-1.872125
H27	1.715299	-1.922604	0.980827
H28	1.940148	-3.208468	-1.478685
H29	4.529567	1.662845	-2.278844
H30	-5.206653	1.095659	0.585543
H31	-0.311620	-0.962295	-2.136267
H32	-0.317866	-0.009065	1.745748
H33	-1.020945	-1.627528	1.808985

Transition state geometry 2 (CCC → CTC) at 1.0 nN. Energy = -951.9471113282 Hartrees

C1	-3.394797	-0.098596	-1.570227
C2	-2.216114	-0.129712	-0.824126
C3	-2.248882	-0.222513	0.581692
C4	-3.468837	-0.306666	1.252399
C5	-4.675280	-0.302668	0.516776
C6	-4.619255	-0.187973	-0.880711
N7	-0.868099	-0.139652	-1.259803
C8	0.021627	-0.358614	-0.205743
C9	-0.811701	-0.228040	1.084302
C10	1.315028	-0.790866	-0.222831
C11	2.161014	-1.354737	-1.278835
C12	3.088889	-0.909732	-2.207166
C13	3.639035	0.490789	-2.333270
O14	3.078830	1.473141	-1.790170
C15	3.705188	-1.950676	-3.004925
C16	4.788520	-1.700050	-3.788801
C17	5.420440	-0.407088	-3.818013
C18	4.903273	0.625685	-3.102224
N19	5.360252	-2.779514	-4.578954
O20	4.813324	-3.922539	-4.531596
O21	6.381533	-2.517888	-5.283080
H22	6.318053	-0.293688	-4.412470
H23	3.301521	-2.956355	-2.972917
H24	-3.492128	-0.390739	2.335066
H25	-3.378612	-0.024772	-2.652690
H26	-5.540374	-0.178411	-1.454962
H27	1.667551	-1.105361	0.762472
H28	2.141615	-2.451143	-1.227872
H29	5.441841	1.577572	-3.131918
H30	-5.649622	-0.402001	1.021944
H31	-0.590093	-0.125835	-2.227526
H32	-0.564542	0.712717	1.597635
H33	-0.599356	-1.043111	1.782995

CTC geometry at 0 nN. Energy = -951.7244556167 Hartrees

C1	-3.765675	-0.983770	-1.286880
C2	-2.527080	-0.605483	-0.777299
C3	-2.384848	0.052944	0.458083
C4	-3.513409	0.345678	1.214405
C5	-4.776090	-0.027105	0.720083
C6	-4.896740	-0.681920	-0.512800
N7	-1.241017	-0.783022	-1.339189
C8	-0.243824	-0.277757	-0.544665
C9	-0.910605	0.309701	0.693604
C10	1.121933	-0.280359	-0.784620
C11	1.731028	-0.825759	-1.924269
C12	3.101749	-0.859223	-2.225942
C13	4.141190	-0.289520	-1.330474
O14	3.865137	0.269950	-0.224040
C15	3.503790	-1.469115	-3.448332
C16	4.829032	-1.536283	-3.806439
C17	5.857097	-0.995989	-2.965855
C18	5.521890	-0.402449	-1.785914
N19	5.194001	-2.163607	-5.054776
O20	4.272340	-2.639241	-5.792599
O21	6.426301	-2.213030	-5.362692
H22	6.884621	-1.075852	-3.296657
H23	2.760893	-1.891181	-4.116212
H24	-3.427333	0.852725	2.170028
H25	-3.860779	-1.490744	-2.241032
H26	-5.878731	-0.961946	-0.878609
H27	1.772431	0.168380	-0.044085
H28	1.089989	-1.284710	-2.680996
H29	6.275284	0.015318	-1.128575
H30	-5.665482	0.194886	1.299447
H31	-1.082085	-1.232203	-2.227506
H32	-0.670675	1.376892	0.788588
H33	-0.529895	-0.176630	1.601328

SIM1 CTC geometry at 1.0 nN. Energy = -952.0095862656 Hartrees

C1	-3.478084	-1.572377	-0.980043
C2	-2.356297	-0.816334	-0.647064
C3	-2.398285	0.207674	0.315761
C4	-3.603132	0.486283	0.968956
C5	-4.758016	-0.265078	0.651058
C6	-4.680226	-1.280209	-0.315290
N7	-1.039138	-0.905301	-1.161247
C8	-0.174176	0.004774	-0.601451
C9	-0.997669	0.808840	0.413785
C10	1.184192	0.170806	-0.892907
C11	1.872526	-0.609827	-1.843174
C12	3.213104	-0.611783	-2.284161
C13	4.293958	0.298598	-1.792747
O14	4.065883	1.172941	-0.905506
C15	3.535355	-1.576358	-3.285030
C16	4.803618	-1.682355	-3.798508
C17	5.862025	-0.826932	-3.351509
C18	5.629415	0.119116	-2.397213
N19	5.076167	-2.676434	-4.809610
O20	4.126410	-3.429318	-5.199335
O21	6.259019	-2.756053	-5.268186
H22	6.841660	-0.957184	-3.793587
H23	2.770035	-2.248219	-3.657953
H24	-3.654862	1.273003	1.715185
H25	-3.433684	-2.360032	-1.724636
H26	-5.566803	-1.856253	-0.558568
H27	1.735316	0.937732	-0.362156
H28	1.274405	-1.369534	-2.352972
H29	6.471360	0.749046	-2.088522
H30	-5.725590	-0.077377	1.142129
H31	-0.773251	-1.573854	-1.867367
H32	-0.975160	1.877448	0.163154
H33	-0.563842	0.714562	1.417852

SIM1 CTC geometry at 2.5 nN. Energy = -952.4537181088 Hartrees

C1	-3.399954	-1.784155	-0.998601
C2	-2.348763	-0.935392	-0.646814
C3	-2.522312	0.100817	0.286628
C4	-3.787129	0.289643	0.883198
C5	-4.882388	-0.558185	0.547473
C6	-4.654806	-1.580939	-0.393262
N7	-1.000630	-0.931410	-1.109727
C8	-0.217398	0.055358	-0.548808
C9	-1.162177	0.814904	0.418250
C10	1.150777	0.329838	-0.790711
C11	1.973597	-0.402307	-1.690440
C12	3.329213	-0.391798	-2.150350
C13	4.485396	0.527011	-1.778987
O14	4.318369	1.455586	-0.942355
C15	3.600072	-1.420492	-3.107938
C16	4.834571	-1.591621	-3.678927
C17	5.941777	-0.745259	-3.350931
C18	5.811065	0.271980	-2.451306
N19	5.021324	-2.656062	-4.637808
O20	4.031932	-3.405268	-4.923190
O21	6.172375	-2.799034	-5.157889
H22	6.886275	-0.942015	-3.842692
H23	2.810821	-2.101466	-3.406693
H24	-3.926777	1.088868	1.605111
H25	-3.265756	-2.584093	-1.719266
H26	-5.470386	-2.241951	-0.668404
H27	1.585734	1.158980	-0.243431
H28	1.432382	-1.214038	-2.184753
H29	6.753241	0.859220	-2.283772
H30	-5.920496	-0.463339	0.986535
H31	-0.662184	-1.596642	-1.788486
H32	-1.215270	1.875381	0.140039
H33	-0.765358	0.778441	1.441011

Transition state geometry 3 at 0 nN. Energy = -951.7112525362 Hartrees

C1	-3.749358	-0.244409	-0.685861
C2	-2.403879	-0.586108	-0.606019
C3	-1.511291	0.026549	0.288836
C4	-1.973663	1.024712	1.139141
C5	-3.330880	1.386502	1.081684
C6	-4.204125	0.760944	0.181703
N7	-1.678064	-1.555769	-1.344922
C8	-0.354853	-1.567387	-1.052094
C9	-0.138073	-0.578326	0.089398
C10	0.477871	-2.655608	-1.459878
C11	1.821895	-2.632394	-1.746880
C12	2.652274	-1.528436	-2.122598
C13	2.069174	-0.255070	-2.541727
O14	0.827087	0.042709	-2.336239
C15	4.034461	-1.744735	-2.303351
C16	4.839248	-0.771547	-2.873795
C17	4.286877	0.449557	-3.343779
C18	2.941194	0.679312	-3.210427
N19	6.252029	-1.015204	-3.021264
O20	6.730484	-2.114874	-2.593498
O21	6.964618	-0.117544	-3.573773
H22	4.945922	1.174798	-3.803654
H23	4.487533	-2.680341	-1.996370
H24	-1.303062	1.518978	1.834163
H25	-4.423163	-0.725569	-1.386456
H26	-5.247185	1.056865	0.150298
H27	-0.029417	-3.616441	-1.539171
H28	2.297194	-3.608890	-1.835768
H29	2.490691	1.600252	-3.560861
H30	-3.705921	2.161960	1.740786
H31	-2.079405	-2.112730	-2.085104
H32	0.605871	0.167009	-0.201041
H33	0.229547	-1.112603	0.974793

SIM1 transition state geometry 3 at 1.0 nN. Energy = -951.9239181327 Hartrees

C1	-3.747962	0.227986	-0.888324
C2	-2.377526	0.006818	-0.802334
C3	-1.686341	0.003615	0.422194
C4	-2.402689	0.179386	1.609851
C5	-3.807751	0.341708	1.558107
C6	-4.456012	0.389730	0.315629
N7	-1.478243	-0.410739	-1.824307
C8	-0.240464	-0.753302	-1.352784
C9	-0.214097	-0.293301	0.120511
C10	0.348012	-1.987474	-1.849661
C11	1.655928	-2.297667	-2.054007
C12	2.763172	-1.400670	-2.235967
C13	2.508249	0.016615	-2.424426
O14	1.360524	0.542516	-2.046457
C15	4.038824	-1.938282	-2.468139
C16	5.065547	-1.128592	-2.931095
C17	4.813845	0.220076	-3.258182
C18	3.565034	0.775233	-3.058650
N19	6.378631	-1.686709	-3.142682
O20	6.568113	-2.912971	-2.861423
O21	7.290901	-0.928711	-3.600193
H22	5.617456	0.809459	-3.681496
H23	4.230912	-2.992759	-2.306469
H24	-1.894237	0.149282	2.568334
H25	-4.265286	0.234006	-1.841781
H26	-5.531531	0.527441	0.277299
H27	-0.389750	-2.771032	-2.023436
H28	1.874457	-3.345509	-2.254113
H29	3.449997	1.804049	-3.390971
H30	-4.418643	0.392959	2.472641
H31	-1.772345	-0.632686	-2.763995
H32	0.408055	0.609078	0.183064
H33	0.231875	-1.057244	0.761237

SIM1 transition state geometry 3 at 2.5 nN. Energy = -952.2784370258 Hartrees

C1	-3.711386	0.312256	-0.963258
C2	-2.333303	0.205413	-0.779987
C3	-1.781751	-0.020387	0.495155
C4	-2.637526	-0.187544	1.601975
C5	-4.055253	-0.144852	1.438091
C6	-4.554533	0.130291	0.153100
N7	-1.299333	0.115590	-1.768619
C8	-0.096113	-0.353296	-1.236504
C9	-0.245194	-0.089158	0.300234
C10	0.305669	-1.710221	-1.653981
C11	1.540339	-2.161835	-1.938023
C12	2.714929	-1.362752	-2.210132
C13	2.587109	0.065559	-2.386117
O14	1.451473	0.673413	-1.944839
C15	3.912466	-2.041235	-2.459594
C16	5.013920	-1.350925	-2.940638
C17	4.894058	0.006194	-3.261178
C18	3.718495	0.720717	-3.045174
N19	6.259317	-2.044961	-3.175960
O20	6.322158	-3.283065	-2.895978
O21	7.236559	-1.387325	-3.650896
H22	5.746854	0.505976	-3.703452
H23	3.980937	-3.109925	-2.295560
H24	-2.214530	-0.389785	2.581683
H25	-4.138683	0.490891	-1.944558
H26	-5.627791	0.182158	-0.001559
H27	-0.525154	-2.415796	-1.626216
H28	1.660520	-3.232682	-2.086361
H29	3.852440	1.741051	-3.449876
H30	-4.800695	-0.347952	2.264288
H31	-1.511578	-0.018382	-2.746698
H32	0.228260	0.873016	0.538088
H33	0.252570	-0.868443	0.879077

TCC geometry minimum at 0 nN. Energy = -951.7186699419 Hartrees

C1	-3.822371	-0.800390	0.236152
C2	-2.505407	-0.857215	-0.213949
C3	-1.584892	0.190606	-0.017761
C4	-1.991333	1.338729	0.656652
C5	-3.312581	1.415916	1.125557
C6	-4.214308	0.361143	0.915523
N7	-1.840162	-1.890557	-0.908649
C8	-0.533695	-1.582291	-1.179458
C9	-0.282576	-0.196195	-0.664967
C10	0.334568	-2.517638	-1.753275
C11	1.672855	-2.425853	-2.138122
C12	2.572210	-1.371873	-2.454668
C13	2.189599	-0.012390	-2.870047
O14	0.969400	0.352302	-3.016704
C15	3.953979	-1.719022	-2.480580
C16	4.923663	-0.789068	-2.782326
C17	4.582172	0.553271	-3.124429
C18	3.265964	0.914911	-3.167627
N19	6.314795	-1.183208	-2.761806
O20	6.605499	-2.383159	-2.457442
O21	7.188872	-0.306948	-3.049704
H22	5.378517	1.248844	-3.355519
H23	4.263509	-2.728777	-2.235942
H24	-1.302707	2.161743	0.816512
H25	-4.519520	-1.615092	0.071823
H26	-5.231491	0.443268	1.283244
H27	-0.075776	-3.525831	-1.811848
H28	2.139998	-3.407933	-2.227459
H29	2.965849	1.917982	-3.447423
H30	-3.642049	2.303287	1.655084
H31	-2.280080	-2.752435	-1.195471
H32	-0.003356	0.421410	-1.555481
H33	0.596429	-0.148472	-0.010595

SIM1 TCC geometry minimum at 1.0 nN. Energy = -951.9403573466 Hartrees

C1	-4.133330	-0.375703	-0.535272
C2	-2.751849	-0.288601	-0.682361
C3	-1.887391	0.050437	0.376574
C4	-2.435391	0.269094	1.646033
C5	-3.834346	0.143812	1.834460
C6	-4.662886	-0.156924	0.744376
N7	-1.976198	-0.591494	-1.817095
C8	-0.617084	-0.577746	-1.567814
C9	-0.448141	0.034085	-0.174566
C10	0.227719	-1.293509	-2.403371
C11	1.608202	-1.625125	-2.445018
C12	2.850754	-0.971854	-2.415859
C13	3.043361	0.500027	-2.569736
O14	2.108873	1.317750	-2.331530
C15	3.997143	-1.828900	-2.487685
C16	5.239952	-1.334060	-2.779316
C17	5.422775	0.044256	-3.122004
C18	4.373391	0.913193	-3.070540
N19	6.372338	-2.232693	-2.825668
O20	6.190142	-3.459248	-2.545490
O21	7.503869	-1.750430	-3.143999
H22	6.406920	0.364336	-3.439981
H23	3.885359	-2.894641	-2.323160
H24	-1.794343	0.508952	2.488661
H25	-4.777770	-0.631805	-1.369647
H26	-5.734186	-0.241807	0.893988
H27	-0.339137	-1.938964	-3.080193
H28	1.725883	-2.681875	-2.702217
H29	4.566402	1.935318	-3.401935
H30	-4.311667	0.248270	2.819375
H31	-2.367026	-0.928685	-2.683812
H32	-0.015312	1.041512	-0.268465
H33	0.248395	-0.552206	0.431823

Transition state geometry 4 at 0 nN. Energy = -951.6845234193 Hartrees

C1	-3.979455	-0.276544	-0.306350
C2	-2.631543	-0.576759	-0.498779
C3	-1.627860	-0.047647	0.338644
C4	-1.971719	0.796068	1.385988
C5	-3.327530	1.111083	1.595861
C6	-4.312939	0.578147	0.756799
N7	-2.034845	-1.391890	-1.470859
C8	-0.640693	-1.444633	-1.333418
C9	-0.277853	-0.553963	-0.141471
C10	0.195688	-2.145835	-2.122922
C11	1.652396	-2.213936	-1.939515
C12	2.620439	-1.400606	-2.470575
C13	2.327145	-0.233005	-3.371406
O14	1.163767	0.080810	-3.723095
C15	4.003782	-1.689469	-2.149502
C16	5.007902	-0.913076	-2.636073
C17	4.757754	0.223900	-3.492407
C18	3.484835	0.539630	-3.837915
N19	6.387965	-1.231544	-2.288127
O20	6.608835	-2.227593	-1.537703
O21	7.299191	-0.488052	-2.758998
H22	5.608384	0.796464	-3.838675
H23	4.239751	-2.533646	-1.511035
H24	-1.208136	1.213530	2.035750
H25	-4.748340	-0.685990	-0.953406
H26	-5.355678	0.827867	0.926274
H27	-0.202734	-2.719462	-2.960135
H28	2.028564	-3.040284	-1.323980
H29	3.263364	1.383207	-4.480786
H30	-3.607986	1.770261	2.410365
H31	-2.534833	-1.834485	-2.223191
H32	0.380923	0.264204	-0.460318
H33	0.260708	-1.118196	0.631438

SIM1 transition state geometry 4 at 1.0 nN. Energy = -951.9398866398 Hartrees

C1	-4.173045	-0.323685	-0.529369
C2	-2.786146	-0.245543	-0.633859
C3	-1.950759	-0.110531	0.492649
C4	-2.527105	-0.086822	1.766945
C5	-3.932786	-0.200932	1.902833
C6	-4.733835	-0.302578	0.757048
N7	-1.987215	-0.349559	-1.785247
C8	-0.623527	-0.418503	-1.496631
C9	-0.495620	-0.051566	-0.009553
C10	0.246125	-0.979811	-2.397928
C11	1.627624	-1.407415	-2.354440
C12	2.886827	-0.821770	-2.455453
C13	3.155419	0.599772	-2.867484
O14	2.274624	1.493255	-2.787073
C15	4.002357	-1.733922	-2.393583
C16	5.253837	-1.355572	-2.782480
C17	5.504468	-0.058596	-3.348089
C18	4.503549	0.858960	-3.431713
N19	6.345255	-2.308121	-2.691580
O20	6.109384	-3.459858	-2.213167
O21	7.489803	-1.938555	-3.095934
H22	6.500290	0.152138	-3.716742
H23	3.847724	-2.748110	-2.042998
H24	-1.902376	-0.001428	2.651033
H25	-4.801853	-0.421814	-1.408120
H26	-5.810897	-0.382324	0.862491
H27	-0.274245	-1.483518	-3.219461
H28	1.686212	-2.500842	-2.414243
H29	4.737370	1.812827	-3.913020
H30	-4.430190	-0.232892	2.883632
H31	-2.356785	-0.521016	-2.706982
H32	-0.071367	0.957487	0.096773
H33	0.175590	-0.739068	0.512806

TTC geometry minimum at 0 nN. Energy = -951.7273821196 Hartrees

C1	-4.188259	-0.032619	-0.280822
C2	-2.808875	-0.208196	-0.341072
C3	-2.020388	-0.403930	0.807970
C4	-2.621884	-0.426148	2.060091
C5	-4.014917	-0.250907	2.145515
C6	-4.783291	-0.057295	0.990082
N7	-1.959355	-0.229010	-1.469029
C8	-0.644173	-0.428277	-1.141551
C9	-0.572692	-0.559094	0.378585
C10	0.373226	-0.488043	-2.077997
C11	1.714665	-0.693730	-1.727152
C12	2.816588	-0.771703	-2.594232
C13	2.695563	-0.639394	-4.068131
O14	1.583712	-0.445305	-4.653420
C15	4.102784	-0.988135	-2.023917
C16	5.224333	-1.075398	-2.814390
C17	5.142561	-0.952104	-4.239974
C18	3.932567	-0.744020	-4.832044
N19	6.510745	-1.295823	-2.197160
O20	6.570859	-1.404690	-0.930494
O21	7.531919	-1.371823	-2.950704
H22	6.056720	-1.028846	-4.814514
H23	4.211646	-1.087447	-0.949518
H24	-2.032931	-0.575715	2.959307
H25	-4.784336	0.117357	-1.174358
H26	-5.856398	0.076186	1.074746
H27	0.148982	-0.374664	-3.133467
H28	1.947112	-0.808377	-0.667183
H29	3.838274	-0.646815	-5.907194
H30	-4.498548	-0.265886	3.115976
H31	-2.274498	-0.111805	-2.420705
H32	0.077771	0.212838	0.808890
H33	-0.150067	-1.529037	0.669624

SIM1 TTC geometry minimum at 1.0 nN. Energy = -952.0129068440 Hartrees

C1	-4.018242	0.551230	-0.176826
C2	-2.712188	0.094215	-0.340741
C3	-2.165085	-0.915534	0.471535
C4	-2.945940	-1.487630	1.479883
C5	-4.274696	-1.042850	1.668608
C6	-4.790584	-0.033397	0.840720
N7	-1.730796	0.504314	-1.274988
C8	-0.540887	-0.169057	-1.147831
C9	-0.727436	-1.160086	0.012364
C10	0.565172	0.072033	-1.962720
C11	1.783559	-0.618651	-1.832312
C12	2.987672	-0.504313	-2.561278
C13	3.222847	0.441093	-3.696831
O14	2.318145	1.235488	-4.095159
C15	4.047570	-1.370411	-2.162999
C16	5.265428	-1.350968	-2.797680
C17	5.524146	-0.459178	-3.888201
C18	4.557205	0.398869	-4.324101
N19	6.307197	-2.248094	-2.356801
O20	6.066082	-3.036448	-1.386900
O21	7.425700	-2.210822	-2.960251
H22	6.503618	-0.490688	-4.348367
H23	3.901981	-2.064453	-1.342495
H24	-2.538435	-2.267933	2.115135
H25	-4.431837	1.330438	-0.807967
H26	-5.810195	0.307927	0.985392
H27	0.498579	0.826598	-2.740735
H28	1.821566	-1.370994	-1.041982
H29	4.798265	1.064455	-5.161738
H30	-4.920969	-1.468747	2.452072
H31	-1.881033	1.220603	-1.970363
H32	0.003465	-0.970138	0.808492
H33	-0.566867	-2.191387	-0.326392

SIM1 TTC geometry minimum at 2.5 nN. Energy = -952.4546205791 Hartrees

C1	-4.035838	0.604019	0.041473
C2	-2.755610	0.099247	-0.193450
C3	-2.281305	-1.045765	0.470206
C4	-3.119546	-1.701696	1.397198
C5	-4.433188	-1.212931	1.661222
C6	-4.857379	-0.063024	0.968883
N7	-1.747448	0.582984	-1.068959
C8	-0.584073	-0.157351	-1.062103
C9	-0.842117	-1.298450	-0.040837
C10	0.525086	0.176798	-1.870299
C11	1.752568	-0.529613	-1.922027
C12	2.983699	-0.390169	-2.637932
C13	3.391468	0.659273	-3.660590
O14	2.588333	1.578705	-3.984306
C15	3.943525	-1.400342	-2.319853
C16	5.185898	-1.440322	-2.900860
C17	5.600200	-0.468001	-3.866746
C18	4.771382	0.545830	-4.252047
N19	6.101416	-2.493450	-2.526979
O20	5.727084	-3.355647	-1.668199
O21	7.248516	-2.513777	-3.075260
H22	6.596076	-0.566899	-4.280371
H23	3.698377	-2.169989	-1.596294
H24	-2.761345	-2.586858	1.914541
H25	-4.398404	1.487908	-0.472773
H26	-5.852355	0.330422	1.150688
H27	0.426660	1.052570	-2.507592
H28	1.781077	-1.396488	-1.257415
H29	5.214067	1.241491	-5.014951
H30	-5.159130	-1.684771	2.388688
H31	-1.866475	1.400082	-1.650529
H32	-0.102474	-1.265155	0.769001
H33	-0.739631	-2.278329	-0.523918

SIM2 SP geometry minimum at 1.0 nN. Energy = -951.9930271529 Hartrees

C1	-3.337423	0.162095	-1.412397
C2	-2.001382	0.054442	-1.020414
C3	-1.644844	0.043033	0.344468
C4	-2.633386	0.126135	1.327102
C5	-3.995026	0.211947	0.951201
C6	-4.322875	0.238224	-0.411699
N7	-0.852658	-0.103119	-1.820645
C8	0.302498	-0.508500	-1.015324
C9	-0.123670	-0.057999	0.425545
C10	0.544075	-1.992204	-1.135554
C11	1.616285	-2.536282	-1.735075
C12	2.688025	-1.706836	-2.265417
C13	2.602894	-0.304062	-2.088140
O14	1.526582	0.271453	-1.422318
C15	3.800551	-2.241733	-2.921314
C16	4.806631	-1.394024	-3.384499
C17	4.746059	-0.003027	-3.213383
C18	3.630738	0.540017	-2.562352
N19	5.958652	-1.973490	-4.062712
O20	5.994748	-3.231212	-4.214414
O21	6.870345	-1.193006	-4.469674
H22	5.587925	0.582119	-3.604014
H23	3.894633	-3.310019	-3.071224
H24	-2.360350	0.108078	2.378421
H25	-3.616592	0.173384	-2.461061
H26	-5.364452	0.307840	-0.710246
H27	-0.253243	-2.608423	-0.730794
H28	1.712158	-3.613905	-1.828657
H29	3.538105	1.607809	-2.406724
H30	-4.803519	0.243812	1.698779
H31	-0.912956	-0.395754	-2.784928
H32	0.336784	0.920572	0.611010
H33	0.244180	-0.755848	1.182368

SIM2 SP geometry minimum at 2.5 nN. Energy = -952.4003903099 Hartrees

C1	-3.364683	0.163892	-1.402082
C2	-2.022138	0.101750	-1.014027
C3	-1.677635	0.059972	0.353337
C4	-2.690192	0.067720	1.333509
C5	-4.068516	0.107101	0.964192
C6	-4.364950	0.164758	-0.409032
N7	-0.860969	0.022767	-1.821154
C8	0.309775	-0.396508	-1.038779
C9	-0.134109	0.033633	0.418349
C10	0.541210	-1.879995	-1.164581
C11	1.627481	-2.446009	-1.716542
C12	2.740774	-1.655260	-2.220396
C13	2.683505	-0.244528	-2.100809
O14	1.571595	0.367749	-1.487913
C15	3.862673	-2.248006	-2.808248
C16	4.913326	-1.457672	-3.273916
C17	4.904801	-0.055798	-3.186340
C18	3.767747	0.544996	-2.590767
N19	6.070108	-2.116047	-3.872775
O20	6.073716	-3.381101	-3.938844
O21	7.019120	-1.391394	-4.298231
H22	5.824314	0.439192	-3.608564
H23	3.928751	-3.324565	-2.905197
H24	-2.416299	0.028222	2.384443
H25	-3.642892	0.198713	-2.450741
H26	-5.402419	0.201098	-0.728296
H27	-0.277564	-2.487362	-0.789014
H28	1.701195	-3.526768	-1.795930
H29	3.702206	1.622023	-2.491176
H30	-4.931631	0.084034	1.695286
H31	-0.918136	-0.234419	-2.796205
H32	0.272145	1.036200	0.603610
H33	0.276493	-0.646704	1.168493

SIM2 transition state geometry 1 (SP → CCC) at 1.0 nN. Energy = -951.9704632620 Hartrees

C1	-3.292645	0.343801	-1.501274
C2	-2.072797	-0.021761	-0.937490
C3	-1.867477	-0.028495	0.453889
C4	-2.920065	0.296229	1.312281
C5	-4.183779	0.618768	0.769440
C6	-4.346628	0.659311	-0.624593
N7	-0.920186	-0.577190	-1.565790
C8	0.031598	-0.980893	-0.682812
C9	-0.447010	-0.516567	0.698454
C10	0.823862	-2.195788	-0.814164
C11	1.899600	-2.503844	-1.587679
C12	2.794367	-1.624946	-2.289565
C13	2.687250	-0.192706	-2.114052
O14	1.644884	0.331631	-1.507125
C15	3.882683	-2.169785	-2.988441
C16	4.877107	-1.346428	-3.501181
C17	4.844377	0.055858	-3.304890
C18	3.778474	0.613525	-2.615703
N19	5.983195	-1.936506	-4.215379
O20	5.996973	-3.198397	-4.383401
O21	6.902189	-1.171083	-4.649759
H22	5.694410	0.619935	-3.710410
H23	3.970114	-3.241551	-3.124534
H24	-2.780819	0.266204	2.388356
H25	-3.444465	0.354543	-2.575126
H26	-5.313583	0.918106	-1.042972
H27	0.455245	-2.979527	-0.149029
H28	2.207491	-3.548312	-1.566215
H29	3.721883	1.682585	-2.446532
H30	-5.052141	0.806490	1.420632
H31	-0.846207	-0.754039	-2.556773
H32	0.222301	0.290245	1.027402
H33	-0.365493	-1.323506	1.433647

SIM2 transition state geometry 1 (SP → CCC) at 2.5 nN. Energy = -952.3903223759 Hartrees

C1	-3.488119	0.320361	-1.362970
C2	-2.191215	0.072861	-0.920529
C3	-1.881695	0.016233	0.449463
C4	-2.905221	0.170611	1.401629
C5	-4.251518	0.369327	0.985390
C6	-4.504097	0.462286	-0.395866
N7	-1.037540	-0.329740	-1.671569
C8	0.008216	-0.719063	-0.891169
C9	-0.385621	-0.312256	0.546495
C10	0.695555	-2.002576	-1.108622
C11	1.855217	-2.362317	-1.701888
C12	2.894851	-1.548885	-2.283258
C13	2.807004	-0.114448	-2.245830
O14	1.730128	0.468355	-1.719972
C15	4.017109	-2.172785	-2.839136
C16	5.063239	-1.421996	-3.369103
C17	5.048031	-0.007465	-3.361539
C18	3.931418	0.625348	-2.800230
N19	6.198547	-2.103832	-3.937848
O20	6.209042	-3.376245	-3.937334
O21	7.147131	-1.404182	-4.419193
H22	5.965526	0.457925	-3.818051
H23	4.087482	-3.253626	-2.863485
H24	-2.669527	0.098990	2.458321
H25	-3.724390	0.367487	-2.420077
H26	-5.519700	0.627605	-0.737689
H27	0.101709	-2.801546	-0.654721
H28	2.060204	-3.431104	-1.707137
H29	3.866465	1.705884	-2.765456
H30	-5.127357	0.424293	1.696807
H31	-1.056323	-0.524189	-2.662961
H32	0.214386	0.565446	0.823071
H33	-0.140132	-1.115078	1.246116

SIM2 CCC geometry minimum 1.0 nN. Energy = -952.0101157415 Hartrees

C1	-2.629764	1.402673	-0.728903
C2	-1.886888	0.249467	-0.473025
C3	-2.368169	-0.740585	0.407583
C4	-3.598517	-0.591713	1.044549
C5	-4.366513	0.563910	0.802077
C6	-3.872188	1.542376	-0.079238
N7	-0.613845	-0.163431	-0.976099
C8	-0.239872	-1.358030	-0.477347
C9	-1.341505	-1.844702	0.466342
C10	0.906984	-2.151908	-0.675984
C11	2.111425	-2.143122	-1.391611
C12	2.873501	-1.364972	-2.310460
C13	2.526764	-0.060211	-2.893609
O14	1.434339	0.554740	-2.620201
C15	4.115264	-1.956156	-2.686082
C16	4.983765	-1.348441	-3.565369
C17	4.682826	-0.082951	-4.152108
C18	3.496269	0.526035	-3.819780
N19	6.224632	-2.007047	-3.899835
O20	6.481376	-3.135275	-3.370765
O21	7.010891	-1.426482	-4.713679
H22	5.432257	0.327668	-4.842396
H23	4.400222	-2.917400	-2.273847
H24	-3.962820	-1.358342	1.721451
H25	-2.269938	2.170753	-1.404067
H26	-4.458887	2.434886	-0.270153
H27	0.820659	-3.058119	-0.079116
H28	2.656157	-3.059187	-1.160638
H29	3.222273	1.487329	-4.238723
H30	-5.340891	0.690748	1.301109
H31	0.022711	0.320696	-1.643994
H32	-0.937087	-2.002818	1.474923
H33	-1.732115	-2.813831	0.128747

SIM2 CCC geometry minimum 2.5 nN. Energy = -952.4546668375 Hartrees

C1	-2.975579	1.632714	-0.221618
C2	-2.182559	0.484503	-0.317861
C3	-2.634764	-0.726712	0.238217
C4	-3.876126	-0.803380	0.892187
C5	-4.703706	0.342651	1.006716
C6	-4.222719	1.541822	0.439260
N7	-0.887117	0.271032	-0.920787
C8	-0.451186	-1.019554	-0.795282
C9	-1.567426	-1.771160	-0.025528
C10	0.688670	-1.763581	-1.173750
C11	1.977547	-1.827120	-1.811445
C12	3.038978	-1.192631	-2.525360
C13	3.181460	0.209220	-2.982634
O14	2.278943	1.073932	-2.759300
C15	4.134352	-2.070725	-2.842201
C16	5.260749	-1.670369	-3.526226
C17	5.451726	-0.320500	-3.995177
C18	4.432698	0.562669	-3.718327
N19	6.296062	-2.649555	-3.783904
O20	6.135124	-3.842480	-3.373083
O21	7.331353	-2.268120	-4.416417
H22	6.415011	-0.109042	-4.544886
H23	4.089829	-3.109518	-2.533994
H24	-4.200644	-1.750909	1.312282
H25	-2.655571	2.581082	-0.639562
H26	-4.826036	2.441605	0.505448
H27	0.493848	-2.769591	-0.802179
H28	2.285012	-2.865889	-1.683682
H29	4.488011	1.599478	-4.031765
H30	-5.708702	0.312845	1.527565
H31	-0.335903	0.979657	-1.392589
H32	-1.159189	-2.201870	0.897813
H33	-1.936599	-2.610195	-0.629347

SIM2 transition state geometry 2 (CCC → CTC) at 1.0 nN. Energy = -951.9788858045 Hartrees

C1	-3.463523	0.375813	-1.465353
C2	-2.297433	-0.005459	-0.799728
C3	-2.310769	-0.289157	0.580959
C4	-3.501066	-0.208505	1.303693
C5	-4.697985	0.158824	0.647841
C6	-4.657934	0.452232	-0.723753
N7	-0.993546	-0.210485	-1.306632
C8	-0.116965	-0.702872	-0.332521
C9	-0.893172	-0.655376	1.000244
C10	1.123590	-1.239890	-0.462145
C11	1.939380	-1.669527	-1.615974
C12	3.000836	-1.124235	-2.310017
C13	3.568404	0.247388	-2.097077
O14	2.942220	1.137015	-1.471240
C15	3.725968	-2.004675	-3.208937
C16	4.936630	-1.654456	-3.727260
C17	5.583917	-0.392643	-3.429102
C18	4.919090	0.500992	-2.645662
N19	5.628688	-2.598082	-4.598491
O20	5.069584	-3.703363	-4.864928
O21	6.762918	-2.257211	-5.049695
H22	6.585197	-0.221040	-3.848548
H23	3.314947	-2.979832	-3.446781
H24	-3.511640	-0.434941	2.366163
H25	-3.461303	0.598923	-2.527410
H26	-5.570497	0.739544	-1.236828
H27	1.505745	-1.687384	0.459241
H28	1.782619	-2.729103	-1.856436
H29	5.343374	1.468654	-2.403579
H30	-5.654010	0.209677	1.193827
H31	-0.731898	-0.062328	-2.267180
H32	-0.461476	0.106224	1.664851
H33	-0.836877	-1.613590	1.527975

SIM2 transition state geometry 2 (CCC → CTC) at 2.5 nN. Energy = -952.4459850186 Hartrees

C1	-3.719451	0.585770	-1.248508
C2	-2.510652	0.116587	-0.723763
C3	-2.462941	-0.399045	0.585248
C4	-3.628615	-0.454711	1.371396
C5	-4.875249	0.005969	0.861796
C6	-4.881192	0.522736	-0.447851
N7	-1.218304	0.033763	-1.322157
C8	-0.268667	-0.579463	-0.496639
C9	-1.013322	-0.813197	0.856051
C10	1.010006	-1.049824	-0.703249
C11	1.994847	-1.414617	-1.769553
C12	3.151256	-0.959475	-2.417374
C13	3.793479	0.397021	-2.372211
O14	3.206763	1.392794	-1.881664
C15	3.921739	-1.971000	-3.130926
C16	5.171877	-1.745846	-3.644963
C17	5.870817	-0.474207	-3.544570
C18	5.180152	0.529593	-2.922713
N19	5.850294	-2.853259	-4.309141
O20	5.254262	-3.968075	-4.409248
O21	7.017020	-2.641119	-4.758471
H22	6.913419	-0.394141	-3.971277
H23	3.505685	-2.966425	-3.243879
H24	-3.573607	-0.859658	2.378120
H25	-3.779871	0.989573	-2.253988
H26	-5.811760	0.886984	-0.872534
H27	1.308069	-1.655007	0.162256
H28	1.905395	-2.498452	-1.921860
H29	5.605691	1.520266	-2.806907
H30	-5.842014	-0.027704	1.450043
H31	-1.020323	0.351314	-2.257418
H32	-0.557859	-0.197687	1.643706
H33	-0.923925	-1.858326	1.171764

SIM2 CTC geometry minimum at 1.0 nN. Energy = -952.0344499070 Hartrees

C1	-3.740427	-1.186215	-1.135650
C2	-2.515079	-0.648603	-0.746354
C3	-2.401159	0.242538	0.336017
C4	-3.543942	0.608849	1.052469
C5	-4.799662	0.078964	0.679852
C6	-4.880377	-0.808248	-0.405436
N7	-1.225000	-0.858321	-1.301806
C8	-0.238822	-0.155152	-0.652759
C9	-0.932363	0.622294	0.472849
C10	1.131031	-0.119510	-0.921999
C11	1.800188	-0.821939	-1.945819
C12	3.177081	-0.824083	-2.264412
C13	4.201311	-0.038485	-1.527036
O14	3.906053	0.704080	-0.540711
C15	3.620058	-1.626122	-3.358929
C16	4.946011	-1.681588	-3.731622
C17	5.967082	-0.936444	-3.043211
C18	5.590592	-0.154099	-1.988437
N19	5.321648	-2.515895	-4.850711
O20	4.416671	-3.172647	-5.458740
O21	6.548848	-2.556619	-5.180205
H22	7.007967	-1.021702	-3.387449
H23	2.905341	-2.214846	-3.923865
H24	-3.469863	1.295674	1.889847
H25	-3.822063	-1.873003	-1.971387
H26	-5.843860	-1.215933	-0.692799
H27	1.744084	0.507610	-0.284837
H28	1.196129	-1.459858	-2.596763
H29	6.314188	0.430001	-1.431521
H30	-5.720154	0.346397	1.222643
H31	-1.057746	-1.462471	-2.091837
H32	-0.757615	1.699757	0.355412
H33	-0.508380	0.342554	1.446121

SIM2 CTC geometry minimum at 2.5 nN. Energy = -952.5075401111 Hartrees

C1	-3.767074	-1.289648	-0.973049
C2	-2.548449	-0.673673	-0.679804
C3	-2.458865	0.340768	0.289578
C4	-3.618847	0.747012	0.981139
C5	-4.877771	0.140247	0.707117
C6	-4.915721	-0.871228	-0.272429
N7	-1.253934	-0.907719	-1.237067
C8	-0.266376	-0.106781	-0.704292
C9	-0.986286	0.778702	0.344343
C10	1.114437	-0.049749	-0.998900
C11	1.862948	-0.816083	-1.938161
C12	3.252413	-0.797187	-2.272210
C13	4.279491	0.093023	-1.662081
O14	3.981852	0.935641	-0.762721
C15	3.735421	-1.698822	-3.276616
C16	5.062608	-1.755423	-3.668689
C17	6.096491	-0.911193	-3.104991
C18	5.680686	-0.031285	-2.138803
N19	5.431069	-2.708522	-4.694410
O20	4.532149	-3.456875	-5.196302
O21	6.650384	-2.755775	-5.051952
H22	7.160538	-1.008949	-3.470334
H23	3.045657	-2.378403	-3.766199
H24	-3.549927	1.530605	1.729907
H25	-3.841533	-2.072962	-1.720163
H26	-5.860379	-1.352851	-0.503783
H27	1.681823	0.679737	-0.429640
H28	1.301720	-1.554872	-2.518106
H29	6.376379	0.644614	-1.653929
H30	-5.842447	0.421683	1.227058
H31	-1.087732	-1.597912	-1.954290
H32	-0.851870	1.839737	0.097455
H33	-0.537979	0.629315	1.335067

SIM2 transition state geometry 3 (SP → TCC) at 1.0 nN. Energy = -951.9717018575 Hartrees

C1	-3.795968	-0.260985	-0.875267
C2	-2.415394	-0.292010	-0.710076
C3	-1.771229	0.226666	0.426789
C4	-2.547673	0.759584	1.461365
C5	-3.958361	0.752868	1.347331
C6	-4.561401	0.266784	0.177921
N7	-1.438039	-0.939877	-1.515295
C8	-0.183879	-0.916941	-0.983592
C9	-0.266530	-0.003436	0.252186
C10	0.628150	-2.113980	-1.148124
C11	1.945469	-2.294126	-1.450337
C12	2.891158	-1.382341	-2.026470
C13	2.474225	-0.054378	-2.418584
O14	1.329256	0.430896	-1.998767
C15	4.159634	-1.858448	-2.397866
C16	5.001867	-1.083538	-3.183403
C17	4.600743	0.188008	-3.663992
C18	3.359076	0.681602	-3.296372
N19	6.298081	-1.605440	-3.549405
O20	6.644956	-2.744839	-3.101260
O21	7.041594	-0.903624	-4.306217
H22	5.313460	0.701530	-4.322768
H23	4.487978	-2.845628	-2.094256
H24	-2.076927	1.142444	2.361287
H25	-4.273424	-0.660020	-1.763839
H26	-5.642684	0.275352	0.089352
H27	0.040873	-3.022384	-1.001848
H28	2.296214	-3.323626	-1.386029
H29	3.020704	1.652516	-3.639397
H30	-4.610211	1.089851	2.167798
H31	-1.664778	-1.490165	-2.331133
H32	0.275908	0.923499	0.022818
H33	0.218781	-0.469651	1.113722

SIM2 transition state geometry 3 (SP → TCC) at 2.5 nN. Energy = -952.3902391216 Hartrees

C1	-3.682051	-0.269510	-1.016165
C2	-2.321751	-0.147237	-0.736836
C3	-1.863094	0.284420	0.520018
C4	-2.798934	0.560620	1.538286
C5	-4.196080	0.389780	1.305426
C6	-4.602857	-0.002172	0.017036
N7	-1.200708	-0.575361	-1.520707
C8	-0.002532	-0.535585	-0.846886
C9	-0.317555	0.263979	0.453197
C10	0.782425	-1.791225	-0.784459
C11	1.987858	-2.138817	-1.282756
C12	2.894813	-1.359835	-2.095944
C13	2.571155	-0.006046	-2.439859
O14	1.445743	0.555147	-1.952691
C15	4.074097	-1.947088	-2.567985
C16	4.948267	-1.237037	-3.388388
C17	4.686194	0.094136	-3.784512
C18	3.504323	0.692276	-3.310850
N19	6.155647	-1.885530	-3.850804
O20	6.379031	-3.084467	-3.490363
O21	6.946270	-1.229443	-4.600806
H22	5.478730	0.532712	-4.455763
H23	4.323618	-2.967878	-2.302557
H24	-2.450277	0.868546	2.519548
H25	-4.033904	-0.596787	-1.988903
H26	-5.660362	-0.128200	-0.192276
H27	0.233870	-2.549071	-0.218765
H28	2.315628	-3.154938	-1.070812
H29	3.258141	1.712485	-3.583324
H30	-4.995299	0.519740	2.095235
H31	-1.304962	-1.112572	-2.369693
H32	0.101221	1.273704	0.344304
H33	0.164965	-0.202580	1.315325

SIM2 TCC geometry minimum at 1.0 nN. Energy = -951.9830004735 Hartrees

C1	-4.061136	-0.947106	-0.124498
C2	-2.708151	-0.717426	-0.356101
C3	-1.982809	0.328063	0.245445
C4	-2.652232	1.165349	1.148323
C5	-4.022923	0.938315	1.426675
C6	-4.710459	-0.100466	0.782514
N7	-1.826325	-1.473565	-1.147199
C8	-0.522764	-1.039667	-1.100819
C9	-0.528742	0.233384	-0.252506
C10	0.450267	-1.899299	-1.626651
C11	1.829842	-1.954858	-1.912330
C12	2.904178	-1.111528	-2.266494
C13	2.815510	0.341851	-2.501685
O14	1.772001	1.001889	-2.196323
C15	4.127055	-1.778012	-2.586795
C16	5.185120	-1.113246	-3.158332
C17	5.113324	0.281936	-3.481460
C18	3.973920	0.970829	-3.156071
N19	6.388105	-1.848317	-3.478938
O20	6.446153	-3.085494	-3.189231
O21	7.341176	-1.220585	-4.039750
H22	5.986796	0.709978	-3.991709
H23	4.226700	-2.841945	-2.403624
H24	-2.125066	1.973755	1.645130
H25	-4.590930	-1.759653	-0.610449
H26	-5.761522	-0.260911	0.998130
H27	0.003141	-2.877171	-1.824987
H28	2.131600	-3.000911	-1.993333
H29	3.873890	2.027935	-3.374839
H30	-4.590945	1.537480	2.152062
H31	-2.107262	-2.295844	-1.660838
H32	-0.190415	1.082271	-0.862618
H33	0.198589	0.149320	0.562859

SIM2 transition state geometry 4 (TCC → TTC) at 1.0 nN. Energy = -951.9719884014 Hartrees

C1	-4.151616	-0.655496	-0.305811
C2	-2.770970	-0.494772	-0.418369
C3	-2.019335	0.212511	0.541863
C4	-2.669816	0.752516	1.655638
C5	-4.068898	0.582628	1.804287
C6	-4.787563	-0.108551	0.819443
N7	-1.908945	-0.997034	-1.401873
C8	-0.553844	-0.748462	-1.124441
C9	-0.547507	0.197175	0.090487
C10	0.427751	-1.403244	-1.800318
C11	1.886028	-1.542495	-1.664180
C12	2.960321	-0.943207	-2.292719
C13	2.858331	0.186908	-3.268829
O14	1.842275	0.922269	-3.334813
C15	4.254118	-1.585054	-2.157989
C16	5.285922	-1.287276	-2.999514
C17	5.171926	-0.315760	-4.066436
C18	4.005116	0.377446	-4.183067
N19	6.547484	-2.001193	-2.842164
O20	6.652180	-2.854265	-1.910702
O21	7.483161	-1.727674	-3.652132
H22	6.032672	-0.186910	-4.738179
H23	4.397319	-2.351748	-1.404926
H24	-2.106911	1.292112	2.411828
H25	-4.719065	-1.198838	-1.054387
H26	-5.860117	-0.234708	0.929382
H27	0.054187	-2.190539	-2.466528
H28	2.168125	-2.453652	-1.121465
H29	3.868712	1.133749	-4.947362
H30	-4.622191	0.965012	2.675237
H31	-2.213381	-1.561881	-2.177713
H32	-0.203287	1.196248	-0.211986
H33	0.137073	-0.157258	0.868216

SIM2 TTC geometry minimum at 1.0 nN. Energy = -952.0343682702 Hartrees

C1	-4.044121	0.427816	-0.306053
C2	-2.705451	0.041945	-0.296615
C3	-2.092341	-0.526063	0.835397
C4	-2.845211	-0.714722	1.998944
C5	-4.207105	-0.331953	2.017281
C6	-4.785604	0.231708	0.869555
N7	-1.749837	0.128093	-1.332217
C8	-0.510534	-0.348320	-0.979399
C9	-0.630994	-0.819614	0.478279
C10	0.550606	-0.338065	-1.883887
C11	1.863678	-0.790613	-1.656991
C12	2.941787	-0.780794	-2.574924
C13	2.836446	-0.270880	-3.967900
O14	1.755680	0.200576	-4.443830
C15	4.206986	-1.286162	-2.152147
C16	5.301445	-1.307914	-2.992212
C17	5.237816	-0.823739	-4.345619
C18	4.045875	-0.330102	-4.794915
N19	6.552296	-1.834456	-2.495270
O20	6.606884	-2.263053	-1.298133
O21	7.550645	-1.846112	-3.282722
H22	6.140585	-0.864699	-4.972068
H23	4.328549	-1.667860	-1.144164
H24	-2.391968	-1.151207	2.883574
H25	-4.503368	0.864527	-1.186326
H26	-5.830113	0.524496	0.886017
H27	0.360534	0.059756	-2.877460
H28	2.098346	-1.197631	-0.671270
H29	3.935793	0.048825	-5.804476
H30	-4.837266	-0.461892	2.910554
H31	-1.944830	0.502074	-2.249734
H32	0.074463	-0.278705	1.121840
H33	-0.384604	-1.885588	0.564180

SIM2 TTC geometry minimum at 2.5 nN. Energy = -952.3902391216 Hartrees

C1	-3.992044	0.617044	-0.291577
C2	-2.683013	0.134210	-0.245131
C3	-2.190798	-0.570023	0.868110
C4	-3.044705	-0.789690	1.971338
C5	-4.387910	-0.307610	1.958177
C6	-4.827368	0.387066	0.815700
N7	-1.661382	0.237934	-1.220156
C8	-0.466885	-0.356936	-0.868612
C9	-0.719204	-0.942933	0.547403
C10	0.627930	-0.315151	-1.761243
C11	1.933588	-0.864321	-1.661956
C12	3.013751	-0.797342	-2.600085
C13	2.975130	-0.083650	-3.907250
O14	1.941010	0.540232	-4.300837
C15	4.246779	-1.459798	-2.296528
C16	5.341382	-1.450494	-3.147703
C17	5.352173	-0.765214	-4.423414
C18	4.190943	-0.115289	-4.755626
N19	6.530874	-2.166432	-2.737916
O20	6.533502	-2.775207	-1.620256
O21	7.531389	-2.156378	-3.523047
H22	6.277203	-0.790511	-5.070621
H23	4.349891	-2.004341	-1.363747
H24	-2.676761	-1.330469	2.838336
H25	-4.364249	1.157498	-1.155467
H26	-5.845023	0.762279	0.780378
H27	0.446150	0.223002	-2.690425
H28	2.169306	-1.427562	-0.756004
H29	4.095360	0.427338	-5.689634
H30	-5.130480	-0.441736	2.800049
H31	-1.786327	0.706347	-2.106563
H32	-0.014335	-0.513936	1.270517
H33	-0.555450	-2.027930	0.550734

TIM1 SP geometry minimum at 1.0 nN. Energy = -951.8570432589 Hartrees

C1	-3.592533	-0.117427	-0.960702
C2	-2.259811	-0.481572	-0.784085
C3	-1.473723	0.066304	0.247351
C4	-2.018544	1.005156	1.113985
C5	-3.362512	1.388391	0.948480
C6	-4.136210	0.826513	-0.073431
N7	-1.487670	-1.399857	-1.525477
C8	-0.103755	-1.332286	-1.169349
C9	-0.107503	-0.589562	0.208684
C10	0.585503	-2.663603	-1.225596
C11	1.844133	-2.818395	-1.665795
C12	2.638591	-1.699546	-2.156262
C13	1.997821	-0.442065	-2.354270
O14	0.640762	-0.323039	-2.137968
C15	3.998494	-1.845305	-2.435638
C16	4.730172	-0.749197	-2.889914
C17	4.124161	0.499029	-3.064016
C18	2.765652	0.664298	-2.799225
N19	6.146137	-0.905178	-3.174756
O20	6.669652	-2.047630	-3.002141
O21	6.792068	0.106626	-3.582275
H22	4.726363	1.334214	-3.396796
H23	4.494454	-2.798522	-2.300476
H24	-1.422142	1.434396	1.913439
H25	-4.190898	-0.535443	-1.763429
H26	-5.171699	1.129236	-0.192352
H27	0.015727	-3.504071	-0.840787
H28	2.310591	-3.799075	-1.655137
H29	2.375372	1.672459	-2.929772
H30	-3.799838	2.122390	1.616813
H31	-1.910442	-2.168899	-2.037544
H32	0.731673	0.106447	0.267118
H33	0.004364	-1.322704	1.019973

TIM1 SP geometry minimum at 2.0 nN. Energy = -951.9960257248 Hartrees

C1	-3.628772	-0.177115	-0.864371
C2	-2.288520	-0.529274	-0.737909
C3	-1.445750	0.079417	0.208916
C4	-1.942870	1.072528	1.044249
C5	-3.294643	1.444953	0.929276
C6	-4.124794	0.821427	-0.009599
N7	-1.558405	-1.504679	-1.467843
C8	-0.157994	-1.386405	-1.201049
C9	-0.083671	-0.580277	0.132421
C10	0.568200	-2.684748	-1.308451
C11	1.825697	-2.788799	-1.763352
C12	2.609290	-1.653719	-2.232207
C13	1.966762	-0.389489	-2.442015
O14	0.601349	-0.303308	-2.243258
C15	3.972036	-1.825255	-2.479703
C16	4.736089	-0.747661	-2.914889
C17	4.148843	0.505810	-3.097871
C18	2.786675	0.712607	-2.871146
N19	6.153409	-0.925737	-3.166231
O20	6.654533	-2.077315	-2.983491
O21	6.826103	0.076153	-3.556427
H22	4.773955	1.331446	-3.413005
H23	4.443121	-2.789121	-2.331420
H24	-1.304276	1.551317	1.780184
H25	-4.267953	-0.643473	-1.606650
H26	-5.165445	1.118747	-0.089111
H27	0.029862	-3.560375	-0.956313
H28	2.309988	-3.760964	-1.783909
H29	2.516743	1.766467	-3.037187
H30	-3.695290	2.221249	1.572406
H31	-2.034710	-2.375232	-1.750121
H32	0.757905	0.112980	0.126677
H33	0.060708	-1.282017	0.967422

TIM1 transition state geometry 1 (SP → TCC) at 1.0 nN. Energy = -951.8518413610 Hartrees

C1	-3.670362	-0.205604	-0.738465
C2	-2.332031	-0.571076	-0.652824
C3	-1.429386	0.053117	0.223471
C4	-1.869552	1.086484	1.041853
C5	-3.218925	1.476613	0.972337
C6	-4.105165	0.836489	0.097007
N7	-1.630934	-1.580854	-1.366455
C8	-0.277632	-1.535519	-1.144519
C9	-0.082160	-0.622994	0.081481
C10	0.506775	-2.739825	-1.424507
C11	1.804496	-2.750783	-1.807500
C12	2.601316	-1.609824	-2.207943
C13	1.959115	-0.355126	-2.540176
O14	0.650943	-0.196849	-2.360391
C15	3.980024	-1.772768	-2.383721
C16	4.758359	-0.722972	-2.860095
C17	4.164961	0.507517	-3.193749
C18	2.799791	0.693911	-3.058742
N19	6.180264	-0.902245	-3.020222
O20	6.688583	-2.027222	-2.711183
O21	6.866913	0.072087	-3.462863
H22	4.798742	1.307926	-3.554091
H23	4.458643	-2.716169	-2.148149
H24	-1.188597	1.585488	1.723530
H25	-4.353790	-0.691619	-1.426453
H26	-5.142169	1.152071	0.055217
H27	-0.012788	-3.683935	-1.274283
H28	2.293691	-3.719148	-1.889741
H29	2.428113	1.682918	-3.326446
H30	-3.576091	2.283573	1.603002
H31	-2.115143	-2.305737	-1.892463
H32	0.752820	0.062583	-0.046743
H33	0.132809	-1.264344	0.950097

TIM1 transition state geometry 1 (SP → TCC) at 2.0 nN. Energy = -951.9959869255 Hartrees

C1	-3.637137	-0.185023	-0.812070
C2	-2.295851	-0.540747	-0.713372
C3	-1.425393	0.076855	0.201348
C4	-1.896032	1.084425	1.034674
C5	-3.248642	1.461413	0.948403
C6	-4.105872	0.829005	0.040452
N7	-1.584529	-1.530567	-1.444487
C8	-0.187384	-1.419289	-1.216667
C9	-0.068198	-0.587993	0.094567
C10	0.548389	-2.704699	-1.357073
C11	1.813920	-2.786908	-1.796552
C12	2.597386	-1.645535	-2.247452
C13	1.948079	-0.387502	-2.490657
O14	0.587304	-0.301975	-2.303730
C15	3.966260	-1.811528	-2.463187
C16	4.733589	-0.738423	-2.902629
C17	4.140809	0.505881	-3.128481
C18	2.773569	0.708257	-2.935549
N19	6.155755	-0.914258	-3.119485
O20	6.660385	-2.056902	-2.892793
O21	6.831355	0.080449	-3.524128
H22	4.767707	1.327173	-3.451665
H23	4.440896	-2.769650	-2.289537
H24	-1.236348	1.571705	1.745872
H25	-4.297947	-0.658953	-1.530243
H26	-5.146650	1.130723	-0.016868
H27	0.013994	-3.596401	-1.040042
H28	2.302985	-3.756639	-1.829303
H29	2.501071	1.754974	-3.138559
H30	-3.628404	2.249243	1.590304
H31	-2.076711	-2.386756	-1.741808
H32	0.773833	0.102412	0.050791
H33	0.099443	-1.276601	0.936199

TIM1 TCC geometry minimum at 1.0 nN. Energy = -951.8960133636 Hartrees

C1	-3.871480	-1.045398	0.447054
C2	-2.584649	-0.986382	-0.082369
C3	-1.831104	0.201524	-0.122393
C4	-2.378929	1.375848	0.384499
C5	-3.675671	1.340877	0.923936
C6	-4.409603	0.145981	0.954099
N7	-1.812074	-2.025100	-0.656185
C8	-0.585037	-1.566863	-1.092949
C9	-0.494268	-0.102315	-0.748838
C10	0.378499	-2.396561	-1.664824
C11	1.701030	-2.195936	-2.106416
C12	2.625800	-1.168839	-2.463308
C13	2.357099	0.245408	-2.844372
O14	1.173617	0.711015	-2.932753
C15	3.975727	-1.633929	-2.541882
C16	5.019585	-0.802642	-2.866578
C17	4.795302	0.566229	-3.196904
C18	3.526438	1.070485	-3.191310
N19	6.364250	-1.330563	-2.896123
O20	6.547214	-2.555897	-2.607617
O21	7.309662	-0.540862	-3.209362
H22	5.647614	1.176947	-3.466188
H23	4.201075	-2.671230	-2.322008
H24	-1.817965	2.304214	0.361907
H25	-4.441000	-1.968690	0.466573
H26	-5.409969	0.140113	1.373505
H27	0.092909	-3.448564	-1.674990
H28	2.190760	-3.167503	-2.190126
H29	3.403154	2.115563	-3.492065
H30	-4.115648	2.249404	1.320577
H31	-2.159492	-2.983748	-0.696799
H32	-0.220160	0.474363	-1.654337
H33	0.346923	0.072597	-0.062394

TIM1 TCC geometry minimum at 2.0 nN. Energy = -952.0868741992 Hartrees

C1	-3.962333	-1.220359	0.504182
C2	-2.678054	-1.071188	-0.013241
C3	-2.068317	0.184702	-0.178018
C4	-2.759934	1.335695	0.183527
C5	-4.059182	1.210363	0.705018
C6	-4.649312	-0.051265	0.863527
N7	-1.785611	-2.082224	-0.458716
C8	-0.603050	-1.525712	-0.946276
C9	-0.679917	-0.027936	-0.729111
C10	0.462464	-2.248114	-1.476948
C11	1.769879	-1.958249	-1.971721
C12	2.726695	-0.973232	-2.395761
C13	2.598725	0.499487	-2.705405
O14	1.483405	1.096772	-2.627203
C15	4.017918	-1.566066	-2.601888
C16	5.114655	-0.850422	-3.005559
C17	5.024183	0.544485	-3.289598
C18	3.837816	1.205508	-3.157783
N19	6.380869	-1.526784	-3.166227
O20	6.447195	-2.772826	-2.917189
O21	7.379617	-0.840586	-3.550674
H22	5.918104	1.055564	-3.624378
H23	4.155719	-2.626267	-2.423490
H24	-2.307861	2.314648	0.063574
H25	-4.421823	-2.196214	0.623536
H26	-5.652954	-0.128696	1.267722
H27	0.293776	-3.324645	-1.444932
H28	2.263392	-2.926801	-2.055486
H29	3.885981	2.279013	-3.436883
H30	-4.611637	2.099964	0.987212
H31	-2.080413	-3.068340	-0.370830
H32	-0.418525	0.520722	-1.644292
H33	0.094359	0.271405	-0.007518

TIM1 transition state geometry 2 (TCC → TTC) at 1.0 nN. Energy = -951.8629723930 Hartrees

C1	-4.074566	-0.711484	0.107386
C2	-2.750681	-0.738390	-0.329098
C3	-1.765392	0.089391	0.241328
C4	-2.103261	0.965442	1.265087
C5	-3.434853	1.008992	1.717845
C6	-4.403314	0.177124	1.143155
N7	-2.175559	-1.540360	-1.333718
C8	-0.795435	-1.265643	-1.483595
C9	-0.443752	-0.191014	-0.445777
C10	0.078398	-1.809660	-2.363531
C11	1.551369	-1.801504	-2.174869
C12	2.642462	-1.107861	-2.656791
C13	2.653089	0.068524	-3.612596
O14	1.591399	0.586136	-4.030263
C15	3.927567	-1.594998	-2.179910
C16	5.096609	-1.042950	-2.593075
C17	5.138249	0.054711	-3.526614
C18	3.988165	0.581720	-4.018242
N19	6.354968	-1.577918	-2.086476
O20	6.317522	-2.547315	-1.271942
O21	7.427635	-1.039550	-2.491690
H22	6.108662	0.437636	-3.815340
H23	3.955498	-2.424631	-1.482447
H24	-1.352665	1.609187	1.713782
H25	-4.830837	-1.349510	-0.338547
H26	-5.427749	0.218475	1.499314
H27	-0.275270	-2.533359	-3.099476
H28	1.860333	-2.612943	-1.501918
H29	4.075030	1.415497	-4.722074
H30	-3.712146	1.690423	2.514797
H31	-2.686004	-2.339357	-1.696178
H32	-0.032891	0.691372	-0.950921
H33	0.326673	-0.547628	0.252873

TIM1 transition state geometry 2 (TCC → TTC) at 2.0 nN. Energy = -952.0607230848 Hartrees

C1	-4.059206	-0.885416	0.311013
C2	-2.776010	-0.824588	-0.231793
C3	-1.834190	0.123897	0.201716
C4	-2.172146	1.035373	1.194545
C5	-3.462852	0.992252	1.752685
C6	-4.390323	0.039637	1.313137
N7	-2.216541	-1.653463	-1.228675
C8	-0.876401	-1.248027	-1.527839
C9	-0.548753	-0.093177	-0.566738
C10	0.005509	-1.720150	-2.450891
C11	1.501937	-1.621626	-2.329308
C12	2.639833	-0.957827	-2.785936
C13	2.821527	0.219154	-3.755928
O14	1.835103	0.809739	-4.247571
C15	3.866626	-1.528688	-2.239047
C16	5.099535	-1.073922	-2.574899
C17	5.295987	0.004404	-3.507826
C18	4.235362	0.625994	-4.084054
N19	6.272196	-1.703726	-1.977764
O20	6.100489	-2.650434	-1.153598
O21	7.411030	-1.265269	-2.317761
H22	6.313623	0.298540	-3.730980
H23	3.797328	-2.351469	-1.536979
H24	-1.452966	1.772315	1.539493
H25	-4.783987	-1.618013	-0.030336
H26	-5.383748	0.014510	1.749677
H27	-0.301900	-2.538460	-3.105234
H28	1.814705	-2.446995	-1.675828
H29	4.500717	1.444125	-4.787931
H30	-3.740557	1.700280	2.525976
H31	-2.735784	-2.511258	-1.449677
H32	-0.236185	0.789958	-1.135845
H33	0.289295	-0.359113	0.094675

TIM1 TTC geometry minimum at 1.0 nN. Energy = -951.9016210846 Hartrees

C1	-4.160863	-0.092671	-0.014575
C2	-2.808160	-0.241557	-0.308920
C3	-1.842236	-0.474682	0.679428
C4	-2.224426	-0.564635	2.012576
C5	-3.585018	-0.417701	2.336096
C6	-4.536874	-0.185198	1.334227
N7	-2.169445	-0.193305	-1.572090
C8	-0.803757	-0.384288	-1.490059
C9	-0.493767	-0.583404	0.004900
C10	0.146698	-0.402600	-2.515135
C11	1.501577	-0.622263	-2.171590
C12	2.716337	-0.708725	-2.882093
C13	2.896997	-0.571227	-4.358808
O14	1.910831	-0.354888	-5.122105
C15	3.868056	-0.953253	-2.071834
C16	5.122200	-1.063069	-2.615443
C17	5.331959	-0.936084	-4.025927
C18	4.281043	-0.702271	-4.862469
N19	6.250635	-1.310881	-1.749727
O20	6.049057	-1.421581	-0.497674
O21	7.401996	-1.408074	-2.279694
H22	6.343167	-1.031012	-4.400869
H23	3.762399	-1.056906	-0.997608
H24	-1.491929	-0.744644	2.792802
H25	-4.899119	0.087387	-0.788890
H26	-5.582227	-0.074307	1.601520
H27	-0.130742	-0.254225	-3.552356
H28	1.664673	-0.760596	-1.103724
H29	4.504746	-0.614951	-5.929934
H30	-3.900384	-0.485021	3.371414
H31	-2.737041	-0.031477	-2.393377
H32	0.209000	0.179185	0.361996
H33	-0.022987	-1.558665	0.178733

TIM1 TTC geometry minimum at 2.0 nN. Energy = -952.0957539631 Hartrees

C1	-4.097176	-0.201892	0.187902
C2	-2.783443	-0.311230	-0.262275
C3	-1.710552	-0.549190	0.600445
C4	-1.933858	-0.686225	1.965758
C5	-3.250632	-0.580132	2.446505
C6	-4.315451	-0.341210	1.566746
N7	-2.307844	-0.209211	-1.596192
C8	-0.921691	-0.370911	-1.684383
C9	-0.452995	-0.605832	-0.227611
C10	-0.024784	-0.349980	-2.774301
C11	1.361779	-0.557716	-2.490413
C12	2.643700	-0.641277	-3.109118
C13	3.057192	-0.514564	-4.559717
O14	2.199274	-0.297897	-5.457709
C15	3.685279	-0.888098	-2.152356
C16	5.002979	-1.008291	-2.503566
C17	5.424933	-0.893458	-3.865465
C18	4.521428	-0.659570	-4.858675
N19	5.986306	-1.256330	-1.475034
O20	5.598511	-1.356415	-0.266386
O21	7.203386	-1.364324	-1.824956
H22	6.481221	-0.998193	-4.079299
H23	3.438912	-0.986658	-1.101119
H24	-1.112779	-0.871272	2.650781
H25	-4.923151	-0.016917	-0.491309
H26	-5.325404	-0.262170	1.954394
H27	-0.371910	-0.183058	-3.787516
H28	1.508362	-0.707118	-1.424874
H29	4.968812	-0.590720	-5.873030
H30	-3.444264	-0.684159	3.508362
H31	-3.044938	-0.035195	-2.280549
H32	0.268240	0.162376	0.075718
H33	0.051325	-1.575083	-0.134816

TIM2 SP geometry minimum at 1.0 nN. Energy = -951.9016900257 Hartrees

C1	-3.561755	-0.050871	-0.857715
C2	-2.239604	-0.479574	-0.766508
C3	-1.355977	0.046604	0.194439
C4	-1.790320	1.026758	1.077165
C5	-3.121708	1.476332	0.997182
C6	-3.992698	0.936683	0.043969
N7	-1.569804	-1.451571	-1.535966
C8	-0.161322	-1.437285	-1.294213
C9	-0.033315	-0.682526	0.072662
C10	0.513199	-2.777371	-1.381225
C11	1.802616	-2.903103	-1.742994
C12	2.592913	-1.753864	-2.174232
C13	1.906036	-0.547159	-2.476662
O14	0.532819	-0.479609	-2.341086
C15	3.978962	-1.807326	-2.338615
C16	4.670468	-0.676134	-2.778771
C17	4.014154	0.525620	-3.086553
C18	2.621921	0.578399	-2.944795
N19	6.117006	-0.748352	-2.922188
O20	6.694643	-1.841600	-2.640834
O21	6.733464	0.285059	-3.321430
H22	4.637073	1.369774	-3.410242
H23	4.530732	-2.714545	-2.125776
H24	-1.117894	1.439178	1.823396
H25	-4.236788	-0.453242	-1.605933
H26	-5.017424	1.290449	-0.009369
H27	-0.073163	-3.634385	-1.064922
H28	2.284164	-3.876418	-1.734440
H29	2.071132	1.483089	-3.171498
H30	-3.473186	2.244052	1.678134
H31	-2.075753	-2.139879	-2.083135
H32	0.846313	-0.035539	0.073739
H33	0.088761	-1.416989	0.881022

TIM2 SP geometry minimum at 2.0 nN. Energy = -952.0817938620 Hartrees

C1	-3.575411	-0.074284	-0.801600
C2	-2.254971	-0.512091	-0.746951
C3	-1.327393	0.041912	0.152728
C4	-1.714885	1.062992	1.011486
C5	-3.044119	1.522506	0.967537
C6	-3.960345	0.953576	0.075355
N7	-1.633094	-1.530680	-1.511497
C8	-0.206743	-1.494252	-1.331637
C9	-0.020939	-0.709763	0.009085
C10	0.494328	-2.813136	-1.452504
C11	1.791185	-2.900526	-1.802371
C12	2.572354	-1.733984	-2.206561
C13	1.876821	-0.534366	-2.526339
O14	0.493584	-0.497413	-2.414718
C15	3.962549	-1.774911	-2.339867
C16	4.661389	-0.643066	-2.767908
C17	4.016394	0.560829	-3.099340
C18	2.611558	0.597992	-2.984766
N19	6.111544	-0.717477	-2.876355
O20	6.682552	-1.808901	-2.575107
O21	6.738854	0.313355	-3.266760
H22	4.686736	1.395600	-3.417307
H23	4.515123	-2.678299	-2.112720
H24	-1.008644	1.498104	1.712045
H25	-4.282752	-0.498299	-1.506790
H26	-4.982763	1.316721	0.049872
H27	-0.072212	-3.696410	-1.173088
H28	2.288290	-3.866213	-1.811670
H29	2.060623	1.498448	-3.229224
H30	-3.359458	2.322285	1.629092
H31	-2.209702	-2.321574	-1.829086
H32	0.869056	-0.079546	-0.023490
H33	0.107513	-1.430685	0.829619

TIM2 transition state geometry 1 (SP → TCC) at 1.0 nN. Energy = -951.8947312024 Hartrees

C1	-3.662237	-0.177922	-0.689946
C2	-2.331842	-0.577452	-0.641785
C3	-1.385342	0.029812	0.198022
C4	-1.771855	1.081705	1.020026
C5	-3.111902	1.507003	0.988510
C6	-4.042364	0.883358	0.147336
N7	-1.682546	-1.612202	-1.369305
C8	-0.325402	-1.608004	-1.186068
C9	-0.064291	-0.685317	0.017401
C10	0.462973	-2.790446	-1.510972
C11	1.783476	-2.779026	-1.833545
C12	2.580419	-1.625115	-2.192440
C13	1.923853	-0.401308	-2.598732
O14	0.617931	-0.242971	-2.462185
C15	3.973324	-1.732841	-2.305146
C16	4.734167	-0.669114	-2.785167
C17	4.127574	0.532173	-3.218904
C18	2.745665	0.643121	-3.153163
N19	6.168899	-0.804447	-2.857652
O20	6.698434	-1.896312	-2.473885
O21	6.847308	0.175446	-3.302460
H22	4.794504	1.325141	-3.584941
H23	4.481220	-2.644755	-2.013277
H24	-1.056539	1.568791	1.674458
H25	-4.379929	-0.652675	-1.350433
H26	-5.071203	1.226737	0.134770
H27	-0.057845	-3.743166	-1.442098
H28	2.280753	-3.743063	-1.923116
H29	2.243312	1.545559	-3.481045
H30	-3.428095	2.328975	1.621498
H31	-2.216331	-2.285844	-1.914313
H32	0.785599	-0.025216	-0.140770
H33	0.159941	-1.324462	0.885598

TIM2 transition state geometry 1 (SP → TCC) at 2.0 nN. Energy = -952.0807101197 Hartrees

C1	-3.631068	-0.144981	-0.720862
C2	-2.304194	-0.558509	-0.682642
C3	-1.353302	0.039448	0.159296
C4	-1.728549	1.089646	0.988304
C5	-3.065073	1.527946	0.964269
C6	-4.001908	0.914520	0.123755
N7	-1.679056	-1.603179	-1.418439
C8	-0.286408	-1.564688	-1.274981
C9	-0.041914	-0.695700	-0.013871
C10	0.474194	-2.811532	-1.507335
C11	1.782802	-2.836240	-1.843764
C12	2.571479	-1.670404	-2.217803
C13	1.892724	-0.462327	-2.586214
O14	0.543506	-0.374706	-2.471964
C15	3.963775	-1.741690	-2.328116
C16	4.700108	-0.642507	-2.775233
C17	4.082244	0.564437	-3.161798
C18	2.682377	0.634092	-3.080474
N19	6.143024	-0.752498	-2.854016
O20	6.687694	-1.847287	-2.508796
O21	6.803683	0.251795	-3.265601
H22	4.774292	1.375313	-3.496941
H23	4.493010	-2.649950	-2.065326
H24	-1.007389	1.564702	1.645616
H25	-4.353837	-0.607957	-1.384517
H26	-5.028448	1.265505	0.115087
H27	-0.059937	-3.742020	-1.331566
H28	2.284430	-3.799411	-1.898802
H29	2.157214	1.536904	-3.369851
H30	-3.372063	2.350094	1.601701
H31	-2.269258	-2.356386	-1.798252
H32	0.829519	-0.052355	-0.119029
H33	0.137957	-1.373912	0.834437

TIM2 TCC geometry minimum at 1.0 nN. Energy = -951.9271159654 Hartrees

C1	-3.903795	-0.946353	0.325705
C2	-2.592280	-0.943941	-0.144064
C3	-1.773161	0.199192	-0.110792
C4	-2.277378	1.386657	0.412115
C5	-3.596115	1.407810	0.894499
C6	-4.396739	0.256340	0.850447
N7	-1.852628	-2.007524	-0.714267
C8	-0.578496	-1.610510	-1.071968
C9	-0.437546	-0.158479	-0.703380
C10	0.391546	-2.474580	-1.590224
C11	1.732126	-2.294015	-1.985219
C12	2.630045	-1.253058	-2.369547
C13	2.287030	0.109017	-2.822004
O14	1.079193	0.507244	-2.954704
C15	4.009008	-1.627537	-2.431201
C16	4.997700	-0.746984	-2.815083
C17	4.703788	0.597858	-3.211115
C18	3.392779	0.993066	-3.198470
N19	6.371690	-1.201183	-2.832167
O20	6.627792	-2.395776	-2.479493
O21	7.267263	-0.378271	-3.201005
H22	5.535971	1.245179	-3.523100
H23	4.305391	-2.634099	-2.157927
H24	-1.665680	2.282086	0.444893
H25	-4.524177	-1.835775	0.288390
H26	-5.413686	0.294391	1.226017
H27	0.089665	-3.522010	-1.590964
H28	2.240254	-3.259766	-2.014291
H29	3.102337	1.990949	-3.506571
H30	-4.002107	2.326212	1.304465
H31	-2.269586	-2.931999	-0.815831
H32	-0.137200	0.404431	-1.616434
H33	0.404980	-0.010982	-0.013793

TIM2 TCC geometry minimum at 2.0 nN. Energy = -952.1430738053 Hartrees

C1	-3.975011	-1.035766	0.368216
C2	-2.662424	-1.000343	-0.097626
C3	-1.911183	0.184983	-0.161300
C4	-2.484498	1.383147	0.254111
C5	-3.806871	1.372587	0.727761
C6	-4.540217	0.178113	0.783636
N7	-1.870877	-2.077798	-0.574509
C8	-0.611073	-1.633163	-0.979172
C9	-0.546226	-0.150396	-0.696462
C10	0.432498	-2.425828	-1.472918
C11	1.771300	-2.175172	-1.894209
C12	2.682993	-1.152925	-2.323832
C13	2.401392	0.235730	-2.755066
O14	1.217561	0.703788	-2.825985
C15	4.050079	-1.573991	-2.448514
C16	5.065367	-0.743137	-2.879725
C17	4.839145	0.623350	-3.269643
C18	3.543963	1.069982	-3.185091
N19	6.409867	-1.276740	-2.953872
O20	6.614918	-2.483419	-2.608661
O21	7.333699	-0.505868	-3.364090
H22	5.708885	1.229514	-3.627063
H23	4.320579	-2.591916	-2.189897
H24	-1.923243	2.310586	0.210733
H25	-4.544489	-1.958799	0.407736
H26	-5.560774	0.190468	1.151036
H27	0.215131	-3.493540	-1.446232
H28	2.298072	-3.131549	-1.904839
H29	3.277010	2.080786	-3.472507
H30	-4.267388	2.299267	1.052598
H31	-2.297418	-3.016414	-0.559657
H32	-0.217023	0.389784	-1.606090
H33	0.252239	0.052353	0.032208

TIM2 transition state geometry 2 (TCC → TTC) at 1.0 nN. Energy = -951.8933783107 Hartrees

C1	-4.085609	-0.560546	-0.036606
C2	-2.742430	-0.680183	-0.391871
C3	-1.733653	0.040952	0.274204
C4	-2.065816	0.902076	1.312083
C5	-3.416250	1.038409	1.683758
C6	-4.408568	0.312000	1.014702
N7	-2.169181	-1.483505	-1.394556
C8	-0.763450	-1.325659	-1.443443
C9	-0.397600	-0.318045	-0.344967
C10	0.124114	-1.912627	-2.279411
C11	1.594201	-1.931932	-2.062546
C12	2.654666	-1.203588	-2.556584
C13	2.561727	-0.027251	-3.486901
O14	1.461101	0.455541	-3.846595
C15	3.989483	-1.618173	-2.154793
C16	5.105938	-0.998135	-2.628005
C17	5.057074	0.111784	-3.559124
C18	3.836210	0.557314	-3.961702
N19	6.413805	-1.471879	-2.184020
O20	6.465495	-2.437981	-1.366652
O21	7.437432	-0.884322	-2.644377
H22	6.010222	0.544622	-3.895141
H23	4.104140	-2.447150	-1.465253
H24	-1.296776	1.464762	1.832902
H25	-4.860103	-1.117378	-0.554326
H26	-5.447393	0.423771	1.308804
H27	-0.227115	-2.584569	-3.063577
H28	1.914387	-2.750259	-1.403630
H29	3.733739	1.387302	-4.651116
H30	-3.688885	1.709211	2.491350
H31	-2.738234	-2.164722	-1.885796
H32	0.108357	0.548077	-0.789058
H33	0.298225	-0.759361	0.382727

TIM2 transition state geometry 2 (TCC → TTC) at 2.0 nN. Energy = -952.1126588453 Hartrees

C1	-4.117507	-0.667724	0.090656
C2	-2.789577	-0.739327	-0.330118
C3	-1.788509	0.061367	0.245251
C4	-2.109877	0.954483	1.259853
C5	-3.444167	1.042815	1.697097
C6	-4.431442	0.237847	1.115830
N7	-2.240473	-1.574264	-1.326128
C8	-0.835928	-1.334095	-1.470984
C9	-0.473888	-0.262230	-0.428660
C10	0.081224	-1.864247	-2.323519
C11	1.572869	-1.821950	-2.128515
C12	2.667853	-1.118818	-2.611488
C13	2.674058	0.067967	-3.537775
O14	1.612806	0.613052	-3.923592
C15	3.986071	-1.583884	-2.190817
C16	5.147328	-1.017109	-2.632662
C17	5.198507	0.104178	-3.558660
C18	3.997883	0.596918	-3.979077
N19	6.413114	-1.570534	-2.154789
O20	6.388068	-2.549613	-1.351811
O21	7.481208	-1.033864	-2.574803
H22	6.199651	0.495923	-3.867932
H23	4.055704	-2.421665	-1.505420
H24	-1.344634	1.578342	1.712059
H25	-4.888318	-1.285692	-0.359256
H26	-5.458349	0.313459	1.459066
H27	-0.231502	-2.597285	-3.068970
H28	1.892234	-2.642089	-1.470711
H29	3.937110	1.434658	-4.664453
H30	-3.709038	1.738074	2.486270
H31	-2.860210	-2.301721	-1.699380
H32	-0.032269	0.605412	-0.933647
H33	0.279253	-0.639823	0.277562

TIM2 TTC geometry minimum at 1.0 nN. Energy = -951.9339386807 Hartrees

C1	-4.190275	-0.061543	-0.097619
C2	-2.825683	-0.223992	-0.321303
C3	-1.911821	-0.445800	0.719148
C4	-2.361936	-0.509866	2.032453
C5	-3.736022	-0.348698	2.284353
C6	-4.634492	-0.127865	1.231858
N7	-2.124331	-0.201190	-1.551306
C8	-0.765573	-0.398468	-1.392800
C9	-0.530789	-0.574139	0.115967
C10	0.225760	-0.437170	-2.373743
C11	1.574251	-0.653424	-2.002635
C12	2.760494	-0.738301	-2.758629
C13	2.833854	-0.604760	-4.234064
O14	1.799827	-0.398374	-4.939099
C15	3.977566	-0.969193	-2.046992
C16	5.188987	-1.067517	-2.692758
C17	5.304806	-0.944592	-4.121704
C18	4.166602	-0.722958	-4.845958
N19	6.381721	-1.301608	-1.910506
O20	6.276276	-1.409881	-0.646832
O21	7.491539	-1.389487	-2.524559
H22	6.306618	-1.035054	-4.565875
H23	3.962520	-1.071964	-0.967365
H24	-1.671074	-0.680644	2.851784
H25	-4.887317	0.109563	-0.911136
H26	-5.691164	-0.005805	1.444161
H27	-0.011027	-0.304365	-3.423202
H28	1.748405	-0.780508	-0.933919
H29	4.194689	-0.622145	-5.924906
H30	-4.103660	-0.395886	3.303431
H31	-2.644505	-0.049963	-2.407861
H32	0.159562	0.189980	0.493832
H33	-0.074716	-1.548998	0.327920

TIM2 TTC geometry minimum at 2.0 nN. Energy = -952.1510351053 Hartrees

C1	-4.182449	-0.117627	0.038716
C2	-2.836089	-0.256291	-0.290796
C3	-1.845941	-0.480191	0.671553
C4	-2.192041	-0.571814	2.014858
C5	-3.544467	-0.435354	2.373706
C6	-4.523714	-0.211416	1.396280
N7	-2.243862	-0.201879	-1.579686
C8	-0.857956	-0.384368	-1.532850
C9	-0.519614	-0.578144	-0.039154
C10	0.121818	-0.408566	-2.541338
C11	1.489234	-0.620694	-2.183173
C12	2.722768	-0.709074	-2.878836
C13	2.926605	-0.586737	-4.345296
O14	1.956321	-0.382207	-5.132633
C15	3.898147	-0.940509	-2.089676
C16	5.158913	-1.047202	-2.638927
C17	5.407427	-0.935185	-4.057839
C18	4.314722	-0.713667	-4.854971
N19	6.279231	-1.281436	-1.752917
O20	6.066941	-1.381082	-0.502106
O21	7.436950	-1.378124	-2.269350
H22	6.461065	-1.033881	-4.421176
H23	3.812350	-1.038668	-1.012713
H24	-1.437667	-0.745142	2.775521
H25	-4.942458	0.055816	-0.716284
H26	-5.562755	-0.108342	1.690015
H27	-0.136888	-0.270108	-3.584865
H28	1.645880	-0.749260	-1.112872
H29	4.411707	-0.617068	-5.930609
H30	-3.832394	-0.504062	3.416899
H31	-2.907835	-0.039831	-2.341216
H32	0.185509	0.190628	0.299301
H33	-0.036880	-1.549291	0.123917

E.2 Coordinate data for extended spiropyrans

All computations carried out with Terachem using a 6-31G basis and B3LYP1 density functional. eSIM1-ester chain SP geometry minimum at 0 nN. Energy = -1682.4375197650 Hartrees

C1	18.131286	13.999259	12.648514
C2	18.295727	12.638211	12.285442
C3	19.345910	12.261852	11.442830
C4	20.228770	13.232936	10.974288
C5	20.109503	14.573230	11.355393
C6	19.071760	14.946504	12.196505
C7	17.347172	11.681853	12.832217
C8	16.270352	12.082019	13.531030
C9	15.879504	13.525128	13.709264
N10	14.827644	13.896393	12.785151
C11	13.739861	14.500946	13.425376
C12	13.938857	14.513124	14.816569
C13	15.310943	13.932698	15.159069
C14	12.934940	14.970608	15.657544
C15	11.729429	15.415073	15.088184
C16	11.543571	15.450325	13.705076
C17	12.563259	14.990661	12.856323
O18	10.747081	15.838925	16.028926
C19	9.377670	15.658077	15.845256
O20	8.880834	15.222558	14.805636
C21	14.920147	13.740832	11.341503
C22	16.204329	14.991649	15.848929
C23	15.168321	12.710458	16.098129
N24	21.307845	12.847201	10.078204
O25	22.096887	13.749123	9.667515
O26	18.978544	16.312375	12.532720
C27	19.378041	16.736604	13.819369
O28	19.614283	15.942308	14.723113
O29	17.100439	14.412440	13.446707
C30	19.524346	18.245332	13.852298
O31	21.403779	11.626974	9.750118
C32	8.606185	16.050927	17.090387
H33	20.813640	15.310766	10.996825
H34	19.480585	11.229222	11.147332
H35	13.040420	14.976971	16.736515
H36	12.415700	15.009261	11.783295
H37	10.610551	15.797288	13.287939
H38	15.568004	11.357314	13.922351

H39	17.537243	10.625834	12.666782
H40	17.206564	14.601461	16.044220
H41	16.308553	15.886585	15.234480
H42	15.743192	15.272217	16.802826
H43	16.134217	12.219842	16.260014
H44	14.795343	13.048275	17.070652
H45	14.455978	11.973915	15.713653
H46	15.616374	12.935349	11.100169
H47	13.940987	13.466463	10.935242
H48	15.259095	14.661110	10.848210
H49	20.312718	18.471204	13.116581
C50	18.236871	18.960657	13.381692
C51	19.986668	18.717832	15.238269
H52	7.553229	15.915857	16.818004
C53	8.947490	15.101855	18.261561
C54	8.846628	17.527941	17.467099
H55	18.411673	20.041761	13.345968
H56	17.938656	18.620461	12.387681
H57	17.410559	18.772472	14.076941
H58	20.198421	19.792123	15.213520
H59	19.213075	18.535730	15.991361
H60	20.890905	18.192425	15.558087
H61	8.226828	17.794428	18.330378
H62	9.896195	17.695540	17.726246
H63	8.584013	18.198156	16.641466
H64	8.330031	15.347794	19.132728
H65	8.756873	14.056246	17.995122
H66	10.000821	15.201263	18.541962

eSIM1-ester chain transition state geometry 1 at 0 nN. Energy = -1682.42097361500 Hartrees

C1	18.648408	14.922398	13.094692
C2	18.740642	13.517604	12.764054
C3	19.710269	13.050398	11.868134
C4	20.611964	13.934229	11.286119
C5	20.610940	15.295718	11.645889
C6	19.680376	15.758518	12.547875
C7	17.908973	12.572719	13.468137
C8	16.849667	12.843956	14.268133
C9	16.097514	14.089704	14.416169
N10	15.217861	14.522254	13.473447
C11	14.129044	15.239464	14.044910
C12	14.259422	15.218333	15.440514
C13	15.584879	14.560643	15.810367
C14	13.220676	15.678859	16.236570
C15	12.057065	16.147786	15.604895
C16	11.957225	16.238473	14.212734
C17	13.013751	15.777793	13.410780
O18	11.004683	16.501585	16.488860
C19	9.660944	16.198780	16.225238
O20	9.264743	15.795696	15.133171
C21	15.356095	14.312929	12.035184
C22	16.561856	15.586465	16.451625
C23	15.380937	13.372985	16.784010
N24	21.575910	13.450468	10.331414
O25	22.397416	14.280402	9.828605
O26	19.734430	17.140614	12.855286
C27	20.200923	17.547045	14.113654
O28	20.383120	16.759458	15.038176
O29	17.689700	15.399176	13.848395
C30	20.525161	19.031765	14.112400
O31	21.561881	12.214353	10.029991
C32	8.804091	16.406971	17.457303
H33	21.340878	15.969245	11.217781
H34	19.767622	11.997891	11.618034
H35	13.256082	15.644774	17.319176
H36	12.929223	15.821803	12.331787
H37	11.055682	16.614968	13.754345
H38	16.452489	12.031414	14.872408
H39	18.232921	11.534703	13.418819
H40	17.538141	15.126097	16.621285
H41	16.713370	16.443615	15.797035
H42	16.144969	15.918843	17.408696

H43	16.335859	12.891195	17.014190
H44	14.961694	13.748697	17.722787
H45	14.689464	12.625455	16.381331
H46	15.984295	13.440962	11.856282
H47	14.370829	14.141370	11.595617
H48	15.820997	15.188326	11.571403
H49	21.443233	19.114513	13.506128
C50	19.439816	19.880554	13.418628
C51	20.839793	19.520080	15.534850
H52	7.779565	16.217146	17.117426
C53	9.167458	15.370364	18.546636
C54	8.901601	17.850500	17.992099
H55	19.753683	20.930159	13.394978
H56	19.270983	19.541256	12.394333
H57	18.489993	19.820676	13.962025
H58	21.197638	20.555005	15.504692
H59	19.945159	19.484266	16.166584
H60	21.605061	18.898348	16.007588
H61	8.232968	17.969422	18.851796
H62	9.922740	18.078196	18.311307
H63	8.606542	18.580029	17.230178
H64	8.488040	15.478865	19.398802
H65	9.077889	14.345450	18.169902
H66	10.192259	15.523730	18.898903

eSIM1-ester chain SP geometry minimum at 1 nN. Energy = -1682.8003829617 Hartrees
Force is applied at H49 and H52.

C1	19.517405	15.236844	15.265607
C2	19.204281	13.923554	14.813425
C3	20.166763	13.117812	14.203195
C4	21.450369	13.617111	14.025328
C5	21.794999	14.886541	14.475528
C6	20.853976	15.693840	15.119001
C7	17.854375	13.423158	15.009209
C8	16.891609	14.203482	15.514107
C9	17.086685	15.665354	15.815519
N10	16.352194	16.469227	14.797096
C11	15.004923	16.519561	15.214044
C12	14.914172	16.240728	16.598327
C13	16.349880	16.103597	17.152285
C14	13.667326	16.129576	17.206692
C15	12.499511	16.294496	16.424517
C16	12.590181	16.607044	15.064925
C17	13.853674	16.715738	14.451160
O18	11.270795	16.102979	17.140594
C19	9.987821	15.990655	16.590748
O20	9.751601	16.090916	15.385395
C21	16.741860	16.457048	13.393577
C22	16.871750	17.488713	17.611960
C23	16.509206	15.083428	18.289021
N24	22.456085	12.803926	13.354787
O25	23.610318	13.295910	13.187768
O26	21.288007	16.982847	15.523499
C27	22.589309	17.098927	16.118794
O28	23.097388	16.164640	16.726791
O29	18.531599	16.041467	15.835093
C30	23.227507	18.471973	15.941247
O31	22.120648	11.645573	12.968781
C32	8.937101	15.741082	17.677219
H33	22.808400	15.229845	14.332177
H34	19.919464	12.119480	13.866543
H35	13.563729	15.894910	18.260173
H36	13.907827	16.920674	13.388114
H37	11.693675	16.727304	14.476341
H38	15.880222	13.837400	15.649272
H39	17.654252	12.392052	14.734872
H40	17.920759	17.419844	17.914508
H41	16.796499	18.225665	16.808471

H42	16.278861	17.836776	18.464605
H43	17.565706	14.974028	18.557950
H44	15.974164	15.431479	19.179977
H45	16.116360	14.097217	18.025097
H46	17.824428	16.578982	13.325132
H47	16.450100	15.537411	12.862409
H48	16.280535	17.310817	12.889443
H49	24.329360	18.308581	15.987630
C50	22.875166	19.131079	14.595803
C51	22.824921	19.371465	17.139385
H52	7.951229	15.629765	17.176058
C53	9.245397	14.436118	18.445556
C54	8.861930	16.950662	18.637850
H55	23.413927	20.080153	14.501264
H56	23.157577	18.496419	13.748731
H57	21.802113	19.330558	14.527940
H58	23.337211	20.336229	17.063908
H59	21.744784	19.554230	17.138663
H60	23.101140	18.907417	18.091549
H61	8.077864	16.783164	19.384814
H62	9.813963	17.088526	19.159302
H63	8.625802	17.874795	18.099242
H64	8.473690	14.260078	19.203347
H65	9.264644	13.571365	17.773306
H66	10.215033	14.504986	18.947450

eSIM1-ester chain transition state geometry 1 at 1 nN. Energy = -1682.77983015980 Hartrees
Force is applied at H49 and H52.

C1	19.053392	15.977590	14.302317
C2	18.887730	14.635514	13.784878
C3	19.725744	14.107337	12.798292
C4	20.766374	14.876741	12.297199
C5	21.046712	16.126265	12.860909
C6	20.267320	16.640999	13.883745
C7	17.913513	13.767232	14.406763
C8	16.914105	14.153443	15.223379
C9	16.375591	15.507454	15.420374
N10	15.511850	16.024327	14.473229
C11	14.262814	16.401885	15.052232
C12	14.326390	16.237139	16.444278
C13	15.785144	15.915184	16.820412
C14	13.162014	16.318769	17.205133
C15	11.934139	16.546598	16.544965
C16	11.888354	16.766706	15.164976
C17	13.068128	16.697467	14.400875
O18	10.771362	16.571195	17.375080
C19	9.509492	16.059427	16.990541
O20	9.310101	15.542856	15.893879
C21	15.660730	15.878749	13.026298
C22	16.492554	17.208361	17.325678
C23	15.910906	14.814092	17.889139
N24	21.592830	14.372623	11.226534
O25	22.533013	15.108308	10.792588
O26	20.720633	17.878533	14.435780
C27	22.078757	17.925468	14.875195
O28	22.682661	16.914225	15.216314
O29	18.133715	16.515690	15.101574
C30	22.681470	19.328842	14.903211
O31	21.336844	13.217808	10.761558
C32	8.472354	16.255909	18.096463
H33	21.905697	16.675816	12.500325
H34	19.570325	13.104522	12.420046
H35	13.162019	16.166284	18.278328
H36	13.019811	16.831385	13.326814
H37	10.942705	16.942720	14.673263
H38	16.343129	13.389206	15.746269
H39	18.063953	12.700338	14.257184
H40	17.542721	17.001349	17.540351
H41	16.457335	17.996326	16.571053

H42	15.990682	17.555056	18.234990
H43	16.957592	14.526954	18.029480
H44	15.535317	15.194414	18.844971
H45	15.330770	13.920612	17.637749
H46	16.650180	15.494300	12.793188
H47	14.903440	15.194055	12.626281
H48	15.546826	16.856667	12.548827
H49	23.764894	19.204049	14.666596
C50	22.048803	20.286746	13.880251
C51	22.581009	19.885732	16.348166
H52	7.520036	15.795485	17.755792
C53	8.917806	15.555753	19.401136
C54	8.226323	17.766723	18.326747
H55	22.556967	21.256892	13.917239
H56	22.132805	19.899309	12.859116
H57	20.987109	20.440406	14.094431
H58	23.085293	20.856166	16.406235
H59	21.532831	20.025002	16.636592
H60	23.053645	19.205178	17.063817
H61	7.454567	17.902469	19.092187
H62	9.142445	18.260004	18.664736
H63	7.885515	18.259066	17.409435
H64	8.138864	15.664052	20.164124
H65	9.089924	14.484931	19.242438
H66	9.841182	16.002504	19.780918

eSIM1-side ester C-O transition state geometry at 0 nN. Energy = -1682.289383125 Hartrees

C1	9.4349174	4.6669265	4.7084147
C2	9.1054320	3.3283447	4.3934396
C3	10.0960050	2.4697101	3.9080326
C4	11.3924696	2.9512818	3.7393930
C5	11.7380522	4.2692494	4.0496532
C6	10.7540018	5.1239316	4.5375285
C7	7.7292466	2.9036174	4.6022829
C8	6.8001589	3.7638099	5.0495964
C9	7.0681578	5.2284359	5.2966025
N10	6.3092050	6.0271210	4.2958611
C11	5.0702980	6.3583136	4.8256077
C12	5.0696319	6.1443167	6.2371173
C13	6.4906506	5.7671416	6.6703510
C14	3.9302636	6.3360994	6.9740763
C15	2.6925929	6.7580909	6.3267436
C16	2.7543803	6.9877700	4.8917129
C17	3.9091980	6.7895377	4.1528949
O18	1.6047716	6.9181340	6.9881782
C19	-2.7811719	4.7345717	5.8292236
O20	-3.0589577	5.0167983	4.6953698
C21	6.6327693	6.0123027	2.8771097
C22	7.2442474	7.0559624	7.0982742
C23	6.5631510	4.7309858	7.8027969
N24	12.4211577	2.0571826	3.2200754
O25	13.5877220	2.5196563	3.0573663
O26	11.0310200	6.4753031	4.8122524
C27	12.1433424	6.8270289	5.6094975
O28	12.8336249	5.9869633	6.1771226
O29	8.4968826	5.5573892	5.1937028
C30	12.3199613	8.3275385	5.6769002
O31	12.0926416	0.8634831	2.9526718
C32	-3.5510879	4.9085787	7.1433351
H33	12.7568533	4.6009839	3.9177786
H34	9.8680080	1.4403373	3.6628440
H35	3.8984818	6.1808901	8.0474840
H36	3.9122997	6.9434980	3.0786386
H37	1.8354617	7.3067319	4.4127102
H38	5.7702451	3.4601817	5.2016167
H39	7.4776640	1.8691864	4.3901204
H40	8.2806198	6.8301725	7.3634650
H41	7.2465311	7.7989233	6.2962130
H42	6.7380418	7.4851086	7.9690525

H43	7.6030030	4.4459211	7.9994850
H44	6.1571453	5.1641396	8.7234157
H45	5.9909585	3.8258352	7.5801397
H46	7.7181463	6.0238019	2.7569421
H47	6.2217682	5.1367074	2.3533883
H48	6.2341362	6.9173669	2.4109644
H49	13.3405062	8.4645821	6.0549676
C50	12.1877626	9.0027906	4.2980803
C51	11.3342214	8.9308995	6.7086798
H52	-4.6211989	4.8279147	6.8851102
C53	-3.1658863	3.8153770	8.1500520
C54	-3.2543212	6.3341893	7.6714365
H55	12.4359564	10.0656407	4.3853317
H56	12.8661650	8.5558776	3.5630478
H57	11.1662163	8.9145454	3.9170570
H58	11.5212037	10.0052278	6.8062559
H59	10.2974757	8.7871728	6.3867785
H60	11.4632347	8.4714941	7.6947060
H61	-3.7726480	6.4726314	8.6268360
H62	-2.1800667	6.4748123	7.8337774
H63	-3.6046771	7.0996401	6.9723612
H64	-3.7410446	3.9440275	9.0729013
H65	-3.3719463	2.8149179	7.7553615
H66	-2.1000474	3.8753138	8.3925532

eSIM1-side ester C-O transition state geometry at 1 nN. Energy = -1682.7088906394 Hartrees
Force is applied at H49 and H52.

C1	12.4199687	8.1287236	8.1228677
C2	12.1031387	6.8174732	7.6677457
C3	13.0646732	6.0113701	7.0563185
C4	14.3495049	6.5087789	6.8806033
C5	14.6965002	7.7775056	7.3315691
C6	13.7566048	8.5857005	7.9755906
C7	10.7512504	6.3201194	7.8599281
C8	9.7911681	7.0976365	8.3747862
C9	9.9931176	8.5527808	8.6996238
N10	9.2396946	9.3639738	7.6984482
C11	7.9154309	9.4661634	8.1394587
C12	7.8354838	9.1505103	9.5265396
C13	9.2784271	8.9725736	10.0521086
C14	6.6094486	9.0719858	10.1567566
C15	5.3757354	9.3634577	9.4342051
C16	5.5213791	9.7095116	8.0396439
C17	6.7546704	9.7486981	7.3969609
O18	4.2092998	9.3692780	10.0195013
C19	1.3884182	8.2622527	9.2662666
O20	1.3442858	8.4270719	8.0858823
C21	9.6431413	9.4311822	6.3013560
C22	9.8298267	10.3375524	10.5380253
C23	9.4336814	7.9246744	11.1638584
N24	15.3546863	5.6939524	6.2111073
O25	16.5088996	6.1854396	6.0420971
O26	14.1901648	9.8753509	8.3799622
C27	15.4924499	9.9958589	8.9730259
O28	16.0086663	9.0608191	9.5729912
O29	11.4360257	8.9340860	8.6952861
C30	16.1208746	11.3748013	8.8025923
O31	15.0190308	4.5347726	5.8276491
C32	0.3528208	8.1404519	10.3921851
H33	15.7106942	8.1185273	7.1886118
H34	12.8156964	5.0144153	6.7169086
H35	6.5216033	8.8170180	11.2081747
H36	6.8118061	9.9791351	6.3379046
H37	4.6090844	9.9189665	7.4916858
H38	8.7780736	6.7364058	8.5113942
H39	10.5475873	5.2923663	7.5755894
H40	10.8798305	10.2445979	10.8308895
H41	9.7596079	11.0958047	9.7537153

H42	9.2477453	10.6754499	11.4018520
H43	10.4903241	7.7913753	11.4218794
H44	8.9105174	8.2625100	12.0652814
H45	9.0203793	6.9516351	10.8830558
H46	10.7198755	9.6026252	6.2496612
H47	9.3961914	8.5209792	5.7339169
H48	9.1457544	10.2819311	5.8284518
H49	17.2235344	11.2215086	8.8608838
C50	15.7781708	12.0293379	7.4521939
C51	15.6976442	12.2734661	9.9941525
H52	-0.6620143	7.9500251	9.9560189
C53	0.7493293	6.9703645	11.3137672
C54	0.3474670	9.4934283	11.1477733
H55	16.3079760	12.9839285	7.3632520
H56	16.0777874	11.3972427	6.6091295
H57	14.7041040	12.2178269	7.3709639
H58	16.2059859	13.2408214	9.9238988
H59	14.6167099	12.4504330	9.9794005
H60	15.9637013	11.8124142	10.9507110
H61	-0.3370655	9.4210135	11.9995426
H62	1.3516255	9.7269359	11.5142518
H63	0.0139324	10.3129521	10.5032569
H64	0.0356126	6.8960175	12.1411008
H65	0.7498808	6.0162919	10.7757591
H66	1.7505697	7.1371148	11.7230081

eSIM1 (polyethylene chain N=3) SP geometry minimum at 0 nN. Energy = -1305.47117982000 Hartrees

C1	36.7141964	39.3743705	37.3916522
C2	37.7109961	38.9028421	38.2440451
C3	37.7735953	39.3125215	39.5869245
C4	36.8257865	40.1884104	40.0951611
C5	35.7957273	40.6788190	39.2605105
C6	35.7619704	40.2610472	37.9209582
N7	38.7624578	38.0043562	37.9659432
C8	39.7480840	38.0587251	39.0214341
C9	38.9238886	38.5825972	40.2781232
C10	40.5041323	36.7748191	39.1989075
C11	41.8098726	36.6243088	38.9072611
C12	42.6240417	37.7168115	38.3977177
C13	43.9601368	37.5566096	38.0198914
C14	44.6597816	38.6576746	37.5315423
C15	44.0622465	39.9211900	37.4100045
C16	42.7316984	40.1122216	37.7803012
C17	42.0230236	38.9900976	38.2759291
O18	40.7229510	39.1972944	38.6608994
C19	42.0229272	41.4489875	37.6829674
C20	42.8648459	42.6171562	37.1443199
N21	46.0500391	38.4922050	37.1387196
O22	46.5806380	37.3480833	37.2729629
C23	39.7618306	39.4590211	41.2206428
C24	38.3377041	37.3823738	41.0728126
C25	39.1034812	37.6090886	36.6052371
C26	34.7238185	41.5976505	39.8136365
C27	33.5008141	40.8369549	40.3848059
O28	46.6700157	39.4982684	36.6781670
H29	44.6596964	40.7356009	37.0260303
H30	44.4546649	36.5970324	38.1000403
H31	36.8684346	40.5081559	41.1333650
H32	36.6704795	39.0800146	36.3491386
H33	34.9802123	40.6413759	37.2689183
H34	39.9186337	35.9335824	39.5480438
H35	42.2888145	35.6586729	39.0397420
H36	40.5976954	38.8882323	41.6417745
H37	40.1621561	40.3309828	40.7026423
H38	39.1385326	39.8014359	42.0546746
H39	39.1280347	36.8141040	41.5757348
H40	37.6524951	37.7617812	41.8373856
H41	37.7723089	36.7084477	40.4208868

H42	39.8804492	36.8425922	36.6359407
H43	38.2244411	37.1821211	36.1125731
H44	39.4643807	38.4566122	36.0042666
H45	41.1259014	41.3250819	37.0590244
H46	41.6351562	41.7111809	38.6783527
H47	35.1453746	42.2306759	40.6071661
H48	34.3756292	42.2792467	39.0252341
C49	42.0608977	43.9254505	37.0799952
H50	43.7472081	42.7633283	37.7820375
H51	43.2417403	42.3735504	36.1410376
C52	32.4158708	41.7786533	40.9275970
H53	33.0816340	40.1978216	39.5952517
H54	33.8417312	40.1589683	41.1795195
H55	42.6744634	44.7466540	36.6936362
H56	41.1882206	43.8203094	36.4243891
H57	41.6984507	44.2165303	38.0736867
H58	31.5578149	41.2177312	41.3152147
H59	32.8037804	42.4024699	41.7430377
H60	32.0493697	42.4509099	40.1416725

eSIM1 (polyethylene chain N=3) transition state geometry 1 at 0 nN. Energy = -1305.44871296400 Hartrees

C1	25.8226980	28.7883425	26.6690214
C2	26.8813254	28.3377370	27.4524085
C3	26.8641530	28.4262685	28.8494213
C4	25.7389837	28.9233454	29.4962290
C5	24.6168039	29.3283313	28.7405731
C6	24.6913065	29.2802053	27.3366953
N7	28.0541270	27.6370750	27.0499305
C8	28.8493345	27.3218429	28.1061754
C9	28.1687207	27.8572289	29.3994004
C10	29.7101761	26.1462685	28.1208448
C11	30.8350862	25.9024391	27.3982486
C12	31.6444373	26.8568051	26.6841726
C13	32.7048988	26.4110245	25.8823224
C14	33.5952766	27.3289420	25.3430226
C15	33.5021192	28.7034435	25.6596440
C16	32.4877739	29.1823767	26.4680155
C17	31.4656143	28.2691850	26.9322859
O18	30.4234187	28.7231248	27.5896362
C19	32.4016987	30.6341700	26.8964102
C20	33.6954036	31.4463345	26.7041926
N21	34.6548869	26.8668705	24.4829185
O22	34.7230502	25.6233599	24.2143411
C23	29.0279194	28.9719396	30.0581842
C24	27.9147800	26.7312253	30.4330092
C25	28.3469995	27.3371754	25.6521324
C26	23.3172937	29.7068571	29.4251458
C27	22.3383364	28.5066587	29.5247585
O28	35.4791964	27.7195270	24.0212460
H29	34.2587156	29.3642396	25.2591158
H30	32.8416134	25.3556946	25.6780416
H31	25.6994242	28.9750371	30.5809300
H32	25.8488200	28.7492046	25.5863500
H33	23.8391505	29.6136076	26.7517149
H34	29.3540784	25.3590028	28.7815774
H35	31.2373033	24.8917550	27.4489884
H36	29.9949162	28.5683370	30.3710266
H37	29.2183731	29.7819732	29.3549585
H38	28.4974985	29.3580119	30.9357451
H39	28.8601863	26.3255849	30.8066111
H40	27.3679251	27.1478870	31.2846880
H41	27.3165352	25.9158377	30.0132506

H42	29.0291225	26.4889416	25.6004452
H43	27.4193659	27.0868898	25.1314091
H44	28.8196426	28.2013319	25.1736754
H45	31.5725420	31.1320492	26.3695176
H46	32.1111528	30.6529286	27.9562555
H47	23.5207486	30.0862469	30.4354414
H48	22.8238501	30.5202144	28.8760648
C49	33.6187056	32.8472425	27.3297858
H50	34.5359368	30.8965798	27.1502489
H51	33.9242597	31.5421144	25.6337080
C52	21.0112747	28.8640247	30.2108976
H53	22.1421385	28.1255984	28.5127698
H54	22.8319301	27.6895271	30.0690428
H55	34.5532682	33.3975801	27.1743420
H56	32.8052308	33.4378277	26.8912496
H57	33.4418917	32.7857322	28.4110025
H58	20.3436714	27.9953832	30.2534669
H59	21.1758056	29.2098038	31.2391001
H60	20.4874525	29.6616210	29.6692992

eSIM1 (polyethylene chain N=3) SP geometry minimum at 1 nN. Energy = -1305.7983585449 Hartrees. Force is applied at H55 and H58

C1	13.7982232	17.1307800	14.8574199
C2	15.0403174	17.1438648	15.4951609
C3	15.1245703	17.0598776	16.9012939
C4	13.9620460	16.9562325	17.6641208
C5	12.6809686	16.9323081	17.0460011
C6	12.6364052	17.0358443	15.6453689
N7	16.3340829	17.1638267	14.9247473
C8	17.2656937	16.6038815	15.9465690
C9	16.6160817	17.1341134	17.2947195
C10	17.2417484	15.1019013	15.8493886
C11	18.2274904	14.3959935	15.2817200
C12	19.4543541	15.0387325	14.8392535
C13	20.4266716	14.3027063	14.1596159
C14	21.6008377	14.9379904	13.7835061
C15	21.8389347	16.2720421	14.1161650
C16	20.9012479	17.0489317	14.8124365
C17	19.6608543	16.4148864	15.1308673
O18	18.6444554	17.1454135	15.7607811
C19	21.2819339	18.4875520	15.1994832
C20	22.7627687	18.8472081	14.8568748
N21	22.6143709	14.1977126	13.0450537
O22	22.3776988	12.9856321	12.7591731
C23	17.0181703	18.6127295	17.5320827
C24	17.0061547	16.2920442	18.5189469
C25	16.5506473	16.9356256	13.5010161
C26	11.3988455	16.8838454	17.8918069
C27	10.2682177	15.8975781	17.4604156
O28	23.6821740	14.7975436	12.7191171
H29	22.7862828	16.6889369	13.8148538
H30	20.2700173	13.2572155	13.9275071
H31	14.0252486	16.8831657	18.7473002
H32	13.7178714	17.1795618	13.7769305
H33	11.6740557	17.0324135	15.1420392
H34	16.3220797	14.6313743	16.1777736
H35	18.1449557	13.3216399	15.1470286
H36	18.0888786	18.6893028	17.7434714
H37	16.7947126	19.2266869	16.6559542
H38	16.4601350	19.0067877	18.3882983
H39	18.0917069	16.3139282	18.6678179
H40	16.5387029	16.7055444	19.4197009
H41	16.6924063	15.2482073	18.4283414

H42	17.6000425	17.1198882	13.2631844
H43	16.2867582	15.9170321	13.1764431
H44	15.9514639	17.6509078	12.9300548
H45	20.6016007	19.1951904	14.7037265
H46	21.1081240	18.6196100	16.2771362
H47	11.6761952	16.6560427	18.9304940
H48	10.9617911	17.8956049	17.9178342
C49	23.2706675	20.2379318	15.2998765
H50	23.4161817	18.0894919	15.3103091
H51	22.9019655	18.7660733	13.7701354
C52	9.0030436	16.0269519	18.3519478
H53	9.9942703	16.0875946	16.4139410
H54	10.6517867	14.8691631	17.4991520
H55	24.3348377	20.3926501	15.0074890
H56	22.6827123	21.0457307	14.8463310
H57	23.2088859	20.3549433	16.3891204
H58	8.1588982	15.3582758	18.0757774
H59	9.2508955	15.8119435	19.3998107
H60	8.6182487	17.0549149	18.3149395

eSIM1 (polyethylene chain N=3) transition state geometry 1 at 1 nN. Energy = -1305.82464274469 Hartrees. Force is applied at H55 and H58

C1	19.0302508	22.5163041	20.3353732
C2	20.2342526	22.3073874	21.0041902
C3	20.2953356	22.2389918	22.4022238
C4	19.1227003	22.3325535	23.1513882
C5	17.8651399	22.4825992	22.5072088
C6	17.8561246	22.6017345	21.1053453
N7	21.5028264	21.9494472	20.4545461
C8	22.3845570	21.5382908	21.4365804
C9	21.7637800	22.0049697	22.8044299
C10	22.9850623	20.2007616	21.3366904
C11	24.0135316	19.8055251	20.5614764
C12	24.9576651	20.6699656	19.8931382
C13	25.8439160	20.1058569	18.9704100
C14	26.8554320	20.8885119	18.4392550
C15	27.0622191	22.1948303	18.9117305
C16	26.2416436	22.7894101	19.8655827
C17	25.0567072	22.0561115	20.2891732
O18	24.0928596	22.6094514	21.0345341
C19	26.6493510	24.1569413	20.4355271
C20	28.1073437	24.5652899	20.0511008
N21	27.7447086	20.3389700	17.4451663
O22	27.5506310	19.1434068	17.0548018
C23	22.4099282	23.3555702	23.2351617
C24	21.9268229	20.9785276	23.9409262
C25	21.6771643	21.7291742	19.0210206
C26	16.5623816	22.5532198	23.3150860
C27	15.4401448	21.5258238	22.9570618
O28	28.6828052	21.0713916	16.9972013
H29	27.9141235	22.7217426	18.5105624
H30	25.7482210	19.0692949	18.6710683
H31	19.1558099	22.2551547	24.2347684
H32	18.9810566	22.5809141	19.2543940
H33	16.9109643	22.7461292	20.5907418
H34	22.4423231	19.4489648	21.9056779
H35	24.2120366	18.7381074	20.4889203
H36	23.4667699	23.2095144	23.4681942
H37	22.3459688	24.0951922	22.4346460
H38	21.8862228	23.7337154	24.1193277
H39	22.9831748	20.7466886	24.1092818
H40	21.5221128	21.4001212	24.8671023
H41	21.3891860	20.0469883	23.7388655

H42	22.6721486	21.3370990	18.8267811
H43	20.9298943	21.0201099	18.6454342
H44	21.5665343	22.6793258	18.4895905
H45	25.9439039	24.9343897	20.1063297
H46	26.5502780	24.1171687	21.5299531
H47	16.8054444	22.4416527	24.3801791
H48	16.1362762	23.5627502	23.2079233
C49	28.6957841	25.8317207	20.7132352
H50	28.7699577	23.7211731	20.2848872
H51	28.1579535	24.7028423	18.9626794
C52	14.1628447	21.7212955	23.8173078
H53	15.1833756	21.6242174	21.8937879
H54	15.8298992	20.5077734	23.0890755
H55	29.7437100	26.0125605	20.3781327
H56	28.1102568	26.7259860	20.4647512
H57	28.7118713	25.7397067	21.8067827
H58	13.3260366	21.0282528	23.5817217
H59	14.3962668	21.5895554	24.8822061
H60	13.7735800	22.7411385	23.6947832

eSIM1 (polyethylene chain N=5) transition state geometry 1 at 1.5 nN. Energy = -1463.42175381362 Hartrees. Force is applied at H67 and H70

C1	-6.2485771	-2.8712733	-4.9547656
C2	-5.0039517	-2.9485577	-4.3344704
C3	-4.8934352	-3.0782724	-2.9408418
C4	-6.0479047	-3.1738480	-2.1604538
C5	-7.3422139	-3.1566890	-2.7602386
C6	-7.4035298	-2.9739554	-4.1525450
N7	-3.7137753	-3.1120814	-4.9381057
C8	-2.7882825	-3.5565471	-3.9942398
C9	-3.3852564	-3.1438218	-2.5967770
C10	-2.2494999	-4.9147190	-4.1483031
C11	-1.2557977	-5.3231114	-4.9569282
C12	-0.2874839	-4.4742888	-5.6106954
C13	0.5583115	-5.0656779	-6.5531028
C14	1.5938028	-4.3205948	-7.0856784
C15	1.8588665	-3.0342170	-6.5962268
C16	1.0897607	-2.4079934	-5.6151669
C17	-0.1286285	-3.1005364	-5.1863944
O18	-1.0877274	-2.5324169	-4.4264195
C19	1.6202051	-1.0614389	-5.0567005
C20	3.0789719	-0.7408766	-5.5518228
N21	2.4532178	-4.8924071	-8.0955885
O22	2.2065134	-6.0734349	-8.4991894
C23	-2.8659531	-1.7232680	-2.2270737
C24	-3.0467420	-4.1246023	-1.4616077
C25	-3.5598155	-3.3026545	-6.3779460
C26	-8.6136323	-3.2853057	-1.8905378
C27	-9.8208858	-4.1241291	-2.4350506
O28	3.4179873	-4.1941520	-8.5401643
H29	2.7252601	-2.5457404	-7.0106169
H30	0.4115435	-6.0930524	-6.8633983
H31	-5.9680214	-3.3053495	-1.0842835
H32	-6.3450135	-2.7767332	-6.0305054
H33	-8.3709439	-2.9373183	-4.6430669
H34	-2.8192283	-5.6600726	-3.5967353
H35	-1.1017590	-6.3938542	-5.0737687
H36	-1.9635550	-4.2554299	-1.3730057
H37	-3.4174049	-3.7235912	-0.5122585
H38	-3.5066527	-5.1066018	-1.6073774
H39	-1.7867788	-1.7520907	-2.0600129
H40	-3.0604484	-1.0124909	-3.0334763
H41	-3.3701084	-1.3807784	-1.3175378

H42	-2.5078886	-3.2083294	-6.6414157
H43	-3.9309608	-4.2843988	-6.7020675
H44	-4.1167679	-2.5197382	-6.8998389
H45	0.9408558	-0.2417469	-5.3316434
H46	1.5987336	-1.1109052	-3.9586844
H47	-8.3162643	-3.7041871	-0.9191788
H48	-8.9852663	-2.2707232	-1.6734849
C49	3.8848801	0.4807596	-5.0087250
H50	3.6945142	-1.6307562	-5.3588421
H51	3.0457467	-0.6241185	-6.6441062
C52	-11.0428577	-4.1640426	-1.4575323
H53	-10.1536245	-3.7065168	-3.3959706
H54	-9.4834030	-5.1494998	-2.6410613
C55	5.3171180	0.5190078	-5.6570158
H56	3.3562486	1.4195359	-5.2298669
H57	3.9791889	0.4205340	-3.9146541
C58	-12.2987534	-4.9569310	-1.9548462
H59	-10.7137956	-4.5957428	-0.4998583
H60	-11.3485102	-3.1295995	-1.2369237
C61	6.2511924	1.6881727	-5.2272668
H62	5.8149241	-0.4357000	-5.4326302
H63	5.1940482	0.5456811	-6.7496153
C64	-13.4819717	-4.9589314	-0.9365513
H65	-12.6366630	-4.5242164	-2.9074685
H66	-12.0023258	-5.9928814	-2.1732730
H67	7.2686838	1.6804559	-5.7025045
H68	5.7929757	2.6550484	-5.4746126
H69	6.4099008	1.6743458	-4.1406467
H70	-14.4077518	-5.5124195	-1.2428343
H71	-13.1563482	-5.4003638	0.0150774
H72	-13.7924883	-3.9275910	-0.7217679

eTIM2 SP geometry minimum at 0 nN. Energy = -1721.7443553800 Hartrees.

H1	-10.0096044	2.4566118	2.0188545
H2	-0.6465862	-7.5002700	8.3243802
C3	-4.3527560	-1.8613586	-0.5245931
C4	-3.5192195	-1.4268987	0.5057872
C5	-2.1261563	-1.6119850	0.4516009
C6	-1.5481170	-2.2430040	-0.6415602
C7	-2.3737851	-2.6949574	-1.6885962
C8	-3.7571033	-2.5009734	-1.6255853
N9	-3.8691862	-0.7770843	1.7118009
C10	-2.7574532	-0.8205740	2.6312476
C11	-1.4884718	-0.9728072	1.6819799
C12	-2.7228203	0.3203926	3.6080102
C13	-2.5924335	0.1709823	4.9393664
C14	-2.5307032	-1.1423889	5.5641684
C15	-2.7173039	-2.2752507	4.7360845
O16	-2.9169802	-2.1539229	3.3880567
C17	-2.3356813	-1.3423392	6.9286200
C18	-2.3096903	-2.6297402	7.4813964
C19	-2.4955733	-3.7521779	6.6404153
C20	-2.7105532	-3.5632019	5.2785840
C21	-0.9454043	0.4312343	1.2982076
N22	-2.1182618	-2.7274517	8.9179975
O23	-2.0388730	-1.6463712	9.5787176
C24	-0.3628403	-1.8000193	2.3225651
C25	-5.2514745	-0.6546450	2.1725195
O26	-2.0480526	-3.8687228	9.4625187
H27	-2.8554131	-4.4212533	4.6364687
H28	-2.2004900	-0.5025805	7.5980815
H29	-0.4737664	-2.3925725	-0.6924228
H30	-5.4275395	-1.7229791	-0.4865374
H31	-4.3875553	-2.8522156	-2.4363099
C32	-5.9029292	0.6097486	1.6172388
H33	-5.8325664	-1.5355370	1.8730739
H34	-5.2575741	-0.6212618	3.2648985
H35	-2.7849387	1.3081157	3.1663999
H36	-2.5461640	1.0431572	5.5844147
H37	-0.6845488	-2.8213167	2.5334434
H38	0.4962546	-1.8430065	1.6438781
H39	-0.0221236	-1.3368044	3.2560421
H40	-0.5125598	0.9378276	2.1677265
H41	-0.1610177	0.3171646	0.5430714
H42	-1.7313895	1.0637343	0.8724907

O43	-2.5305500	-5.0759191	7.0917242
O44	-7.3061661	0.5759105	2.0649702
C45	-8.0738829	1.7008170	1.8225737
C46	-9.4911409	1.5453196	2.3376596
O47	-7.6103998	2.6987765	1.2620069
C48	-9.5021912	1.4742300	3.8817745
C49	-10.1893215	0.3169218	1.7153335
H50	-10.2052749	0.3752602	0.6214918
H51	-9.6763853	-0.6057953	2.0034387
H52	-11.2256161	0.2617283	2.0668510
H53	-9.0169642	2.3499431	4.3264497
H54	-10.5354902	1.4387300	4.2445573
H55	-8.9829493	0.5754533	4.2293180
H56	-5.4235996	1.5163064	1.9958442
H57	-5.8763874	0.6417133	0.5240229
C58	-1.3321576	-5.7152532	7.5093826
O59	-0.2426214	-5.1742611	7.3820713
C60	-1.6249148	-7.1000404	8.0348664
C61	-2.5416533	-7.0545590	9.2771729
C62	-2.2251856	-7.9901299	6.9211327
H63	-2.3815239	-9.0033175	7.3066400
H64	-3.1894143	-7.5923343	6.5905848
H65	-1.5587996	-8.0557093	6.0537272
H66	-2.6654386	-8.0687662	9.6727212
H67	-2.1200454	-6.4200389	10.0607863
H68	-3.5270475	-6.6586968	9.0152459
H69	-1.9347405	-3.1940938	-2.5456379

eTIM2 transition state geometry at 0 nN. Energy = -1721.69521177800 Hartrees.

H1	-10.5409473	2.1090281	2.4694990
H2	-1.1260642	-7.9964568	9.0937618
C3	-4.2138647	-0.2882622	-1.4427805
C4	-3.6174429	-0.4706943	-0.1945587
C5	-2.2404514	-0.7210446	-0.0625824
C6	-1.4373564	-0.7930744	-1.1934008
C7	-2.0187519	-0.6106895	-2.4624581
C8	-3.3911033	-0.3644130	-2.5785314
N9	-4.2165391	-0.4526926	1.0813731
C10	-3.2538196	-0.6369455	2.0924276
C11	-1.8873914	-0.9047108	1.4157812
C12	-3.5430147	-0.5289175	3.4085363
C13	-2.6973648	-0.8414508	4.5663961
C14	-2.6109680	-2.0435400	5.2270396
C15	-3.4052906	-3.2560456	4.8441323
O16	-4.0540359	-3.3503589	3.7719692
C17	-1.8181199	-2.1094717	6.4330924
C18	-1.8326126	-3.1873690	7.2665711
C19	-2.6643973	-4.3438519	6.9457870
C20	-3.4018660	-4.3518620	5.8058601
C21	-0.8237619	0.1215238	1.8747316
N22	-1.0438850	-3.0846157	8.4906887
O23	-0.1640414	-2.1760131	8.5533420
C24	-1.3871299	-2.3504509	1.6800006
C25	-5.6533722	-0.5249630	1.3098016
O26	-1.2904071	-3.8788022	9.4434899
H27	-3.9993289	-5.2199461	5.5606980
H28	-1.1998196	-1.2619172	6.7071965
H29	-0.3729748	-0.9914630	-1.1077199
H30	-5.2740466	-0.0842918	-1.5437342
H31	-3.8318121	-0.2239802	-3.5605082
C32	-6.2918856	0.8445136	1.5474118
H33	-6.1265139	-1.0002966	0.4443420
H34	-5.8354562	-1.1729178	2.1738001
H35	-4.5385677	-0.1872549	3.6962212
H36	-2.1704875	-0.0065269	5.0406347
H37	-2.1540212	-3.0860855	1.4265581
H38	-0.4990457	-2.5475751	1.0691598
H39	-1.1146657	-2.4836547	2.7310417
H40	-0.5933660	-0.0013005	2.9396195
H41	0.1062189	-0.0239613	1.3140009
H42	-1.1678101	1.1471818	1.7090009

O43	-2.7856693	-5.4529140	7.7895750
O44	-7.7078121	0.5597798	1.8312965
C45	-8.5435725	1.6350452	2.0716968
C46	-9.9606492	1.1848884	2.3703812
O47	-8.1343106	2.7995053	2.0527652
C48	-10.0089061	0.4137850	3.7101633
C49	-10.5368590	0.3387015	1.2144958
H50	-10.5371280	0.8963443	0.2711128
H51	-9.9472816	-0.5728194	1.0764657
H52	-11.5705386	0.0541934	1.4407501
H53	-9.6180233	1.0204011	4.5345115
H54	-11.0444269	0.1464433	3.9476691
H55	-9.4194710	-0.5062977	3.6462884
H56	-5.8479543	1.3683963	2.3989551
H57	-6.2197851	1.4974132	0.6727607
C58	-1.6661579	-6.2845776	8.0431149
O59	-0.5993870	-6.1055099	7.4679254
C60	-2.0186426	-7.3629212	9.0393282
C61	-2.2941516	-6.7547624	10.4345623
C62	-3.2142710	-8.2104276	8.5477654
H63	-3.3968531	-9.0277580	9.2535923
H64	-4.1195335	-7.5993705	8.4833848
H65	-3.0217919	-8.6497835	7.5626411
H66	-2.4959429	-7.5616603	11.1473991
H67	-1.4396379	-6.1745666	10.7928426
H68	-3.1619901	-6.0896015	10.3999456
H69	-1.4002916	-0.6607944	-3.3521322

eTIM2 TTC trans geometry minimum at 0 nN. Energy = -1721.7389157610 Hartrees.

H1	-10.0838169	1.5258750	2.8978269
H2	-2.2552810	-7.7849760	10.1023960
C3	-4.1243989	0.5504910	-1.4642610
C4	-3.3831559	0.0041000	-0.4178030
C5	-1.9815789	0.0255700	-0.3992420
C6	-1.2854719	0.6017620	-1.4557680
C7	-2.0106439	1.1558990	-2.5251790
C8	-3.4111519	1.1287790	-2.5253100
N9	-3.8468499	-0.6410160	0.7600270
C10	-2.8053129	-1.0361720	1.5668080
C11	-1.4778219	-0.6446320	0.8771320
C12	-3.0224759	-1.6712080	2.7854600
C13	-2.0321589	-2.1529580	3.6490760
C14	-2.2537679	-2.8278900	4.8661840
C15	-3.6018760	-3.1033270	5.4122810
O16	-4.6760229	-2.7284830	4.8412930
C17	-1.1215790	-3.2714650	5.5947430
C18	-1.2138670	-3.9692170	6.7818390
C19	-2.5252590	-4.2650390	7.3150340
C20	-3.6433590	-3.8431490	6.6585100
C21	-0.6700469	0.3664440	1.7373900
N22	0.0235630	-4.3410880	7.4259980
O23	1.1152810	-3.9327420	6.9108130
C24	-0.6193439	-1.8923350	0.5269420
C25	-5.2733719	-0.8293240	1.0498680
O26	-0.0038990	-5.0503110	8.4785260
H27	-4.6193840	-4.0607760	7.0721129
H28	-0.1263579	-3.0641430	5.2190540
H29	-0.2003779	0.6260321	-1.4624850
H30	-5.2079649	0.5408970	-1.4698030
H31	-3.9575749	1.5622940	-3.3559370
C32	-5.8550879	0.3632460	1.8117439
H33	-5.8028259	-0.9520060	0.1017409
H34	-5.4120529	-1.7473510	1.6228759
H35	-4.0377779	-1.8345230	3.1273430
H36	-0.9872259	-2.0200620	3.3797850
H37	-1.1952919	-2.6094120	-0.0656120
H38	0.2499111	-1.5817060	-0.0622450
H39	-0.2574699	-2.4000280	1.4244360
H40	-0.3307069	-0.0846110	2.6730830
H41	0.2106171	0.7017120	1.1794440
H42	-1.2756389	1.2451080	1.9790990

O43	-2.7072350	-4.9069010	8.5505070
O44	-7.2930889	0.0882860	1.8965699
C45	-8.0993209	1.0838970	2.4303379
C46	-9.5466799	0.6493570	2.5183279
O47	-7.6356739	2.1705260	2.7856649
C48	-9.6965709	-0.5133870	3.5269189
C49	-10.1087889	0.2715030	1.1306139
H50	-10.0151549	1.1010530	0.4209529
H51	-9.5802579	-0.5952200	0.7223819
H52	-11.1711299	0.0193980	1.2185349
H53	-9.3240330	-0.2327880	4.5177719
H54	-10.7528999	-0.7857310	3.6252699
H55	-9.1396759	-1.3918010	3.1872369
H56	-5.4367419	0.4475360	2.8184570
H57	-5.6923179	1.3074670	1.2842300
C58	-2.4551480	-6.2921490	8.6695940
O59	-2.2167770	-6.9899540	7.6909290
C60	-2.6067480	-6.7466230	10.1027250
C61	-1.7470410	-5.9164330	11.0770660
C62	-4.1009210	-6.7273980	10.5078699
H63	-4.2107190	-7.1229150	11.5235389
H64	-4.4902850	-5.7043990	10.4912869
H65	-4.7074650	-7.3431140	9.8346479
H66	-1.8161700	-6.3477010	12.0822450
H67	-0.6983050	-5.9032390	10.7704340
H68	-2.0999450	-4.8816050	11.1176440
H69	-1.4812969	1.6095661	-3.3557630

eTIM2 SP geometry minimum at 1 nN. Energy = -1722.1273810938 Hartrees. Force is applied at H1 and H2.

H1	-9.3572911	3.5720919	-0.0354914
H2	0.8228945	-7.6439708	8.4068271
C3	-5.1948614	-2.0885728	0.1748664
C4	-4.3580656	-1.6589846	1.2037538
C5	-2.9613447	-1.7907109	1.1193982
C6	-2.3815949	-2.3849871	0.0075449
C7	-3.2115243	-2.8465924	-1.0327111
C8	-4.5981287	-2.6891023	-0.9480398
N9	-4.7045676	-1.0538628	2.4372568
C10	-3.5792124	-1.1136700	3.3345839
C11	-2.3302082	-1.1292355	2.3422199
C12	-3.5713837	-0.0796569	4.4216905
C13	-3.1419053	-0.3340993	5.6721690
C14	-2.7093074	-1.6615068	6.0906198
C15	-2.9503898	-2.7505404	5.2140358
O16	-3.5931841	-2.5446974	4.0144497
C17	-2.0954447	-1.9119029	7.3134547
C18	-1.6863080	-3.2009867	7.6859506
C19	-1.8796259	-4.2843277	6.7915141
C20	-2.5329368	-4.0455171	5.5732469
C21	-1.9545828	0.3376759	1.9844524
N22	-1.1422257	-3.3415745	9.0244145
O23	-0.8694183	-2.2839937	9.6696651
C24	-1.0849734	-1.8513681	2.8779345
C25	-6.0132293	-0.4114378	2.6382252
O26	-0.9958238	-4.4999969	9.5194617
H27	-2.6919818	-4.8721007	4.8937645
H28	-1.9247032	-1.1087013	8.0187263
H29	-1.3038240	-2.4923527	-0.0655571
H30	-6.2723297	-1.9799559	0.2317792
H31	-5.2309360	-3.0396694	-1.7573312
C32	-6.1076152	0.8734326	1.7774231
H33	-6.8146608	-1.1010676	2.3495055
H34	-6.1424299	-0.1914253	3.6996896
H35	-3.8740209	0.9228971	4.1384385
H36	-3.1061466	0.4638405	6.4081749
H37	-1.2692130	-2.9131655	3.0460072
H38	-0.2732884	-1.7623319	2.1468683
H39	-0.7316666	-1.3991215	3.8104812
H40	-1.5425959	0.8599050	2.8548926
H41	-1.1962613	0.3325428	1.1954617

H42	-2.8188934	0.8975783	1.6122733
O43	-1.5156070	-5.6108709	7.0629470
O44	-7.5288584	1.2745650	1.6137684
C45	-7.7722903	2.3937713	0.8094728
C46	-9.2610797	2.7014343	0.6486367
O47	-6.8474894	3.0333587	0.3021862
C48	-9.8752223	3.0829219	2.0154596
C49	-9.9996305	1.4999613	0.0150314
H50	-9.5802091	1.2448412	-0.9646934
H51	-9.9304599	0.6186329	0.6595481
H52	-11.0580713	1.7460212	-0.1237814
H53	-9.3834488	3.9655704	2.4390502
H54	-10.9398174	3.3118081	1.8952624
H55	-9.7763666	2.2559656	2.7253074
H56	-5.5590466	1.7042127	2.2312486
H57	-5.6897466	0.6941973	0.7834282
C58	-0.1903742	-6.0015864	7.4684381
O59	0.7616129	-5.2513459	7.3199860
C60	-0.1732106	-7.4450754	7.9561102
C61	-1.2524605	-7.7049888	9.0270992
C62	-0.3507684	-8.3859216	6.7363387
H63	-0.3089804	-9.4283469	7.0688249
H64	-1.3204526	-8.2138215	6.2587649
H65	0.4376907	-8.2325117	5.9912737
H66	-1.1769482	-8.7406324	9.3766791
H67	-1.1281347	-7.0361055	9.8820128
H68	-2.2530802	-7.5490946	8.6146606
H69	-2.7716135	-3.3202476	-1.9039467

eTIM2 transition state geometry 3 at 1 nN. Energy = -1722.11961812550 Hartrees. Force is applied at H1 and H2.

H1	-9.5840520	3.6138592	-0.0071464
H2	0.9377391	-7.8369332	8.5651201
C3	-5.3398690	-1.6942682	-0.0803776
C4	-4.4673646	-1.4210081	0.9692340
C5	-3.0900893	-1.6563976	0.8888365
C6	-2.5505458	-2.1982966	-0.2721515
C7	-3.4110917	-2.4936188	-1.3438266
C8	-4.7853195	-2.2406389	-1.2486428
N9	-4.7666281	-0.8941938	2.2667294
C10	-3.6838885	-0.9746355	3.0955634
C11	-2.4346304	-1.1807101	2.1757346
C12	-3.6669103	-0.2689225	4.3698788
C13	-3.0900086	-0.6755725	5.5367758
C14	-2.5944101	-1.9809083	5.9048224
C15	-2.9343818	-3.1487662	5.1165855
O16	-3.5708924	-3.0375312	3.9773619
C17	-1.9033344	-2.1483163	7.1076376
C18	-1.4880262	-3.3971117	7.5791540
C19	-1.7785074	-4.5599457	6.7980040
C20	-2.5068783	-4.4240869	5.6251940
C21	-1.8724094	0.2693961	1.9403665
N22	-0.8660954	-3.4245197	8.8767818
O23	-0.5324326	-2.3174081	9.4105018
C24	-1.2802297	-2.0695026	2.6589296
C25	-6.0977226	-0.3067262	2.5433614
O26	-0.6984406	-4.5374805	9.4710011
H27	-2.7287677	-5.3089719	5.0431059
H28	-1.6716410	-1.2902916	7.7272046
H29	-1.4872424	-2.3969963	-0.3536749
H30	-6.4052729	-1.5070293	-0.0115399
H31	-5.4354163	-2.4740076	-2.0848797
C32	-6.2361608	1.0607523	1.8281471
H33	-6.8647900	-0.9933289	2.1746303
H34	-6.2209655	-0.2191991	3.6231315
H35	-4.1308145	0.7165105	4.3599057
H36	-3.0702245	0.0627356	6.3372675
H37	-1.5821253	-3.1132317	2.7132813
H38	-0.4450456	-1.9728946	1.9553899
H39	-0.9232356	-1.7528952	3.6421535
H40	-1.4507897	0.6643308	2.8694152
H41	-1.0829661	0.2213588	1.1847419

H42	-2.6454535	0.9566993	1.5807483
O43	-1.4247843	-5.8685063	7.1817404
O44	-7.6710184	1.3279301	1.5665533
C45	-7.9589362	2.4941351	0.8387293
C46	-9.4530575	2.6779914	0.5779888
O47	-7.0601600	3.2540158	0.4717044
C48	-10.2199765	2.8216607	1.9134029
C49	-10.0042039	1.5002853	-0.2601185
H50	-9.4787840	1.4118869	-1.2177863
H51	-9.8986712	0.5559516	0.2827591
H52	-11.0670040	1.6617914	-0.4712785
H53	-9.8500936	3.6709957	2.4986383
H54	-11.2843231	2.9868780	1.7123875
H55	-10.1183186	1.9152324	2.5183662
H56	-5.8298602	1.8778789	2.4310766
H57	-5.7102598	1.0560490	0.8694323
C58	-0.0954091	-6.2577266	7.5386367
O59	0.8732060	-5.5727865	7.2424146
C60	-0.0882771	-7.6392862	8.1872337
C61	-1.0702448	-7.7260065	9.3736617
C62	-0.4154231	-8.7034910	7.1077647
H63	-0.3758142	-9.7036260	7.5529321
H64	-1.4198350	-8.5429420	6.7035169
H65	0.3030418	-8.6678798	6.2815752
H66	-0.9909064	-8.7150091	9.8393452
H67	-0.8506808	-6.9631370	10.1242799
H68	-2.0999585	-7.5804188	9.0347234
H69	-3.0064588	-2.9230609	-2.2538274

eTIM2 TCC cisoid geometry minimum at 1 nN. Energy = -1722.1280998020 Hartrees. Force is applied at H1 and H2.

H1	-9.5321270	4.1246830	-0.1689960
H2	1.7115690	-7.8229970	8.9845540
C3	-5.4268500	-0.2667710	-0.3183350
C4	-4.6926950	-0.6523300	0.8044680
C5	-3.4375700	-1.2601930	0.7087060
C6	-2.8749760	-1.4908650	-0.5420670
C7	-3.5873030	-1.1031560	-1.6891130
C8	-4.8476880	-0.5021910	-1.5745810
N9	-5.0483230	-0.5332900	2.1779450
C10	-4.0867790	-1.1017920	3.0045570
C11	-2.9044120	-1.5631200	2.1021590
C12	-4.1038010	-0.9507670	4.3959740
C13	-3.2978890	-1.4197680	5.4633230
C14	-2.6344350	-2.6104550	5.8615220
C15	-2.9478230	-3.9831680	5.3907520
O16	-3.8253350	-4.2192470	4.5099440
C17	-1.7563160	-2.4959370	6.9789460
C18	-1.1275270	-3.5632120	7.5910020
C19	-1.3673740	-4.9077040	7.0996610
C20	-2.2314130	-5.0745430	6.0524130
C21	-1.6779740	-0.6502710	2.4118370
N22	-0.3346300	-3.2634920	8.7609400
O23	-0.0734550	-2.0446410	9.0190840
C24	-2.4821560	-3.0466040	2.2124160
C25	-6.3530520	0.0619340	2.5391960
O26	0.0507410	-4.2147770	9.5091570
H27	-2.4400870	-6.0740980	5.6930880
H28	-1.5587500	-1.5165850	7.3998460
H29	-1.9030330	-1.9638980	-0.6380340
H30	-6.4015090	0.1990510	-0.2372410
H31	-5.3877160	-0.2119920	-2.4696020
C32	-6.4834210	1.5655270	2.1704630
H33	-7.1336630	-0.4876550	2.0010160
H34	-6.5223900	-0.1010840	3.6033410
H35	-4.7714170	-0.1554800	4.7300540
H36	-3.2311570	-0.6577690	6.2448940
H37	-3.3377660	-3.7211050	2.2304270
H38	-1.8483380	-3.2866200	1.3517440
H39	-1.9011200	-3.2219600	3.1177550
H40	-1.3343230	-0.8131440	3.4371170
H41	-0.8622960	-0.8994500	1.7252880

H42	-1.9249980	0.4085560	2.2839190
O43	-0.8754150	-6.0721220	7.7218500
O44	-7.7211770	1.7290710	1.3570930
C45	-8.0651700	3.0316970	0.9624550
C46	-9.3882380	3.0858580	0.1976140
O47	-7.3577540	3.9955360	1.2607570
C48	-10.5547770	2.7525190	1.1615960
C49	-9.3791400	2.1327220	-1.0172710
H50	-8.5502520	2.3571340	-1.6978390
H51	-9.2904870	1.0908400	-0.6943950
H52	-10.3136570	2.2414880	-1.5779720
H53	-10.5764310	3.4423280	2.0120990
H54	-11.5093400	2.8383790	0.6312730
H55	-10.4609070	1.7310440	1.5440080
H56	-6.5721580	2.2021040	3.0539180
H57	-5.6310240	1.9139940	1.5826630
C58	0.5025450	-6.3784820	7.9314940
O59	1.3935040	-5.7452100	7.3840310
C60	0.6335720	-7.6104940	8.8266580
C61	-0.0130770	-7.3633910	10.2088260
C62	-0.0011660	-8.8381060	8.1278160
H63	0.1292500	-9.7252060	8.7575100
H64	-1.0719490	-8.6787940	7.9702300
H65	0.4664740	-9.0369900	7.1568970
H66	0.1232030	-8.2515240	10.8366470
H67	0.4381950	-6.5038720	10.7108330
H68	-1.0841710	-7.1695820	10.1034420
H69	-3.1581510	-1.2730720	-2.6705690

eTIM2 transition state geometry 4 at 1 nN. Energy = -1722.11573205005 Hartrees. Force is applied at H1 and H2.

H1	-11.4196350	2.5118801	-1.9317613
H2	-0.1716701	-9.8542090	7.3199657
C3	-7.2555968	-1.6891286	-2.0476010
C4	-6.5088174	-2.0935966	-0.9377814
C5	-5.2009657	-2.5817863	-1.0714236
C6	-4.6079486	-2.6573108	-2.3249219
C7	-5.3377505	-2.2462824	-3.4553567
C8	-6.6457271	-1.7724637	-3.3105328
N9	-6.8896204	-2.0930047	0.4255048
C10	-5.8792577	-2.7112741	1.2224048
C11	-4.6533068	-2.9654977	0.2987582
C12	-5.9520050	-3.0272972	2.5417566
C13	-4.8314228	-3.3741354	3.4607725
C14	-4.3011481	-4.5413456	3.9792741
C15	-4.7290735	-5.9452759	3.6701530
O16	-5.6054079	-6.2085104	2.8115668
C17	-3.2403287	-4.3985324	4.9599068
C18	-2.6637002	-5.4439729	5.6233142
C19	-3.1012134	-6.8208783	5.3674197
C20	-4.0718603	-7.0204336	4.4312645
C21	-3.4696783	-2.0407651	0.6913835
N22	-1.6596015	-5.0976024	6.6277542
O23	-1.1926008	-3.9200629	6.6242261
C24	-4.2072479	-4.4468811	0.3146522
C25	-8.1816898	-1.5168850	0.8313350
O26	-1.3181288	-5.9726078	7.4740531
H27	-4.4106799	-8.0272476	4.2219248
H28	-2.8829764	-3.4036964	5.2011025
H29	-3.5960327	-3.0349973	-2.4381715
H30	-8.2708375	-1.3237306	-1.9507083
H31	-7.2062150	-1.4636962	-4.1872847
C32	-8.3520825	-0.0184884	0.4326747
H33	-9.0046560	-2.0854437	0.3783211
H34	-8.2717367	-1.6226037	1.9145550
H35	-6.8751086	-2.8113574	3.0847304
H36	-4.3734175	-2.4819652	3.9069844
H37	-5.0559415	-5.1169354	0.1604589
H38	-3.4733636	-4.6181144	-0.4811131
H39	-3.7387832	-4.7084670	1.2656939
H40	-3.0985850	-2.2802576	1.6941919
H41	-2.6413579	-2.1759240	-0.0130601

H42	-3.7675840	-0.9874921	0.6713081
O43	-2.6757326	-7.9257577	6.1231990
O44	-9.5923773	0.1338237	-0.3903636
C45	-9.9446435	1.4256443	-0.8001033
C46	-11.2308528	1.4584128	-1.6328752
O47	-9.2608092	2.4065404	-0.4985730
C48	-12.4325825	0.9715451	-0.7891410
C49	-11.0742303	0.6119994	-2.9168368
H50	-10.2290401	0.9566179	-3.5231365
H51	-10.9178243	-0.4420312	-2.6687476
H52	-11.9816502	0.6918844	-3.5265749
H53	-12.5744888	1.5952932	0.1001758
H54	-13.3495316	1.0211814	-1.3875180
H55	-12.2835403	-0.0637255	-0.4679231
H56	-8.4573271	0.6286928	1.3068592
H57	-7.5055220	0.3386138	-0.1573209
C58	-1.3259286	-8.4135104	6.2080628
O59	-0.4584138	-8.0099470	5.4498886
C60	-1.2187045	-9.4847058	7.2923035
C61	-1.5536769	-8.8945271	8.6824114
C62	-2.1401991	-10.6835545	6.9600313
H63	-2.0210889	-11.4559619	7.7279442
H64	-3.1886370	-10.3724046	6.9418608
H65	-1.8910963	-11.1278809	5.9902297
H66	-1.4338509	-9.6740124	9.4433724
H67	-0.8948766	-8.0583618	8.9297151
H68	-2.5856509	-8.5333728	8.7101696
H69	-4.8862374	-2.3020247	-4.4399991

eTIM2 TTC trans geometry minimum at 1 nN. Energy = -1722.1474098577 Hartrees. Force is applied at H1 and H2.

H1	-9.6805130	3.8854040	-0.1398300
H2	0.9467600	-8.6985520	9.5105380
C3	-5.4981740	0.3963410	-0.2451130
C4	-4.6818980	-0.0991090	0.7730240
C5	-3.3079610	-0.2765070	0.5987340
C6	-2.7036130	0.0754060	-0.6033600
C7	-3.5011970	0.5894590	-1.6386980
C8	-4.8813500	0.7399260	-1.4577010
N9	-5.0529950	-0.5280940	2.0852150
C10	-3.9772370	-1.1326750	2.7380550
C11	-2.7082580	-0.8911260	1.8540390
C12	-4.0083750	-1.9264220	3.9004450
C13	-2.8115340	-2.3788560	4.5192260
C14	-2.5058750	-3.3570410	5.4970460
C15	-3.4649250	-4.2888660	6.1303280
O16	-4.7055630	-4.2400450	5.8770630
C17	-1.1358620	-3.4810880	5.8748350
C18	-0.6592110	-4.4062340	6.7846390
C19	-1.5737770	-5.3643250	7.3849020
C20	-2.9009210	-5.2867290	7.0500650
C21	-1.7391290	0.1399850	2.5099330
N22	0.7389660	-4.3052860	7.1356680
O23	1.4963820	-3.5849450	6.4094530
C24	-1.9783630	-2.2059730	1.4707790
C25	-6.4348730	-0.2696260	2.5657190
O26	1.1596510	-4.9033880	8.1741670
H27	-3.5993410	-5.9877190	7.4890850
H28	-0.4027590	-2.8036610	5.4514760
H29	-1.6364460	-0.0553250	-0.7518760
H30	-6.5653470	0.5163620	-0.1177800
H31	-5.4908340	1.1259030	-2.2680660
C32	-6.8682160	1.2294200	2.4765280
H33	-7.1429330	-0.8788950	1.9919480
H34	-6.4804800	-0.5970510	3.6059990
H35	-4.9550380	-2.2611850	4.3114400
H36	-1.9130690	-1.8800820	4.1733070
H37	-2.6774150	-2.9156670	1.0185660
H38	-1.1965040	-1.9836270	0.7371610
H39	-1.5068070	-2.6914920	2.3263310
H40	-1.2583010	-0.2483200	3.4107030
H41	-0.9523470	0.3981690	1.7932490

H42	-2.2716530	1.0590450	2.7744660
O43	-1.1947900	-6.3028080	8.3738580
O44	-7.9347710	1.4195410	1.4387730
C45	-8.3093400	2.7451720	1.1245100
C46	-9.4626220	2.8158820	0.1089950
O47	-7.7494000	3.7061900	1.6525880
C48	-10.7408970	2.2055580	0.7342210
C49	-9.0836340	2.0902210	-1.2025560
H50	-8.1804260	2.5199290	-1.6503160
H51	-8.9125520	1.0243890	-1.0226420
H52	-9.8988500	2.1882000	-1.9275070
H53	-11.0380660	2.7465770	1.6391200
H54	-11.5671540	2.2636010	0.0174750
H55	-10.5806750	1.1548490	0.9945590
H56	-7.2944210	1.5574550	3.4276890
H57	-6.0265130	1.8810230	2.2339270
C58	-0.1487980	-7.2795610	8.2534190
O59	0.3556750	-7.5477050	7.1737560
C60	0.1361440	-7.9346880	9.6141510
C61	0.6166250	-6.8783840	10.6356870
C62	-1.1341170	-8.6622230	10.1203590
H63	-0.9140680	-9.1660140	11.0681480
H64	-1.9461330	-7.9488020	10.2866140
H65	-1.4761390	-9.4183040	9.4049750
H66	0.8240440	-7.3690770	11.5935210
H67	1.5261450	-6.3793420	10.2919310
H68	-0.1506260	-6.1147160	10.7894360
H69	-3.0465770	0.8610150	-2.5851950